

Design and Synthesis of Fluorescent Opioids for Bioimaging

Raymond Lam, BPharmSc(Hons), AMRSC

April 2018

This thesis is submitted as a requirement for the degree of
Doctor of Philosophy at Monash University (2018).

Supervisors

Prof. Peter J. Scammells
A/Prof. Bim Graham
Prof. Barrie Kellam

Panel Members

Dr David Chalmers
Dr Meritxell Canals
A/Prof. Paul Donnelly



MONASH University

Medicinal Chemistry Theme
Monash Institute of Pharmaceutical Sciences
Monash University (Parkville)
Melbourne, Australia



**The University of
Nottingham**

Centre for Biomolecular Sciences
University of Nottingham
Nottingham, United Kingdom

"We are like dwarfs sitting on the shoulders of giants. We see more, and things that are more distant, than they did, not because our sight is superior or because we are taller than they, but because they raise us up, and by their great stature add to ours."

- John of Salisbury, 1159

Copyright Notice

©Raymond Lam (2018)

I certify that I have made all reasonable efforts to secure copyright permissions for third-party content included in this thesis and have not knowingly added copyright content to my work without the owner's permission.



Raymond Lam

October 12, 2018

Contents

Thesis Including Published Works Declaration	VII
The Monash-Nottingham Joint Doctoral Training Program	X
Acknowledgements	XI
Abstract	XIV
Acronyms and Abbreviations	XVI
1 Introduction	1
1.1 Opioid Receptors, Structure, Function, Use and Abuse	2
1.1.1 μ -Opioid Receptor Pharmacology	8
1.1.2 μ -Opioid Receptor Heterodimers	10
1.1.3 Bivalent μ -Opioid Receptor Ligands	12
1.1.4 Monovalent μ -Opioid Receptor Biased Ligands	14
1.2 Opioid-Fluorophore Conjugates	17
1.2.1 Peptide-Fluorophore Conjugates	17
1.2.2 Small Molecule-Fluorophore Conjugates	19
1.3 Nanoparticles, an Overview	21
1.3.1 Overview of Commonly Used Nanoparticle Probes in Bioimaging	21
1.3.2 Advantages of Nanoparticle Conjugates in Bioimaging	24
1.3.3 Gold Nanorods	25
1.3.4 Synthesis of Gold Nanorods	28
1.3.5 Gold Nanorods in Bioimaging	31
1.3.6 Functionalization of Gold Nanorods for Biocompatibility	33
1.4 Need for Pharmacological Tools	35
1.4.1 Aims	35
1.4.2 Hypothesis	36
1.5 The Monash-Nottingham Joint Doctoral Training Program Rotations	36
2 Molecular Modelling of the Opioid Receptors	50
2.1 Receptor Subtype Selectivity based on Docking Methods	51
2.2 Molecular Dynamics Simulations Attempting to Generate An Agonist Homology Structure	53
2.2.1 Comparison of Generated Agonist Model with Published Structures	58
2.3 Conclusion	59
2.4 Experimental	62
3 Fluorescent Opioid Partial Agonist Probes for the μ-Opioid Receptor	65
3.1 Morphine-based Fluorescent Probes, Paper Context	66
3.2 Fluorescently Labelled Morphine Derivatives for Bioimaging (Paper)	67
3.2.1 Additional Notes	82

4	Development of Gold Nanorod-based Imaging Systems	87
4.1	Synthesis of Gold Nanorods	88
4.1.1	Characterization of Gold Nanorods	90
4.1.2	Attempted Alternative Synthesis via Radical Reduction Method	94
4.1.3	Optimization of Cleaning Protocol	95
4.2	Synthesis of a Biocompatible Zwitterionic Surface Coat	96
4.2.1	Attempts at Further Optimizing Synthesis of Surface Coat	97
4.3	Synthesis of a Opiate Congener for Conjugation to Gold Nanorods	99
4.3.1	Problematic 7'-Nitro Naltrindole Reduction	106
4.3.2	Attempted Alternate Pathways to 7'-aminonaltrindole	108
4.4	Development of Coating Procedures	110
4.4.1	Initial Attempts and Development of the "2 Step Method"	110
4.4.2	Addition of Targeting Ligand to Gold Nanorod Surface	113
4.5	Validation of Coating Success	114
4.5.1	Changes in UV-Vis Absorbance Spectra	114
4.5.2	pERK1/2 Assay to Determine Biological Activity of Coated Gold Nanorods	114
4.5.3	Other Attempts at Validating Coating Methods	117
4.6	Coating of Multiple Ligands onto AuNRs	118
4.7	Synthesis of a Control System for Comparison	119
4.8	Conclusions	122
4.9	Experimental	123
4.9.1	2 Step Method for Coating Gold Nanorods	144
5	Alternative Catalysts for Non-Classical Polonovski <i>N</i>-Demethylation of Alkaloids	152
5.1	<i>N</i> -Demethylation of Alkaloids, a History	153
5.2	Green Chemistry, Starting with Solvents	155
5.3	Fe ₃ (CO) ₁₂ as a Solution-Phase Catalyst for <i>N</i> -Demethylations, Paper Context .	156
5.4	Utility of Iron Species for <i>N</i> -Demethylation of Alkaloids (Paper)	157
5.4.1	Additional Notes	166
6	Industrial Placement at Sun Pharmaceutical Industries	170
6.1	Reaction Overview and Immediate Issues	171
6.1.1	Project Aims and Objectives	173
6.2	Optimization of the Diels Alder Reaction	174
6.3	One-Pot Feasibility and Boc-Deprotection Optimization	175
6.4	Extraction Workup of Compound E	177
6.5	20 L Pilot Scale-Up	178
6.6	Final 20 L Scale Procedure	182
6.7	Conclusion	183
7	Thesis Outcomes and Future Directions	187
8	Appendix	197
8.1	Molecular Modelling Compounds	198
8.1.1	Subtype Selectivity Ligands	202
8.1.2	Training Set Compounds	204

8.1.3	Test Set compounds	205
8.2	Characterization of Nitro vs Nitroso Derivatives of Naltrindole	206
8.3	Characterization of Attempted 2-Aminophenylhydrazine Synthesis	208
8.4	Zwitterionic Modification of Ultrasmall Iron Oxide Nanoparticles for Reduced Protein Corona Formation (Paper)	210
8.5	Curriculum Vitae	221

Thesis Including Published Works Declaration

This thesis contains three original papers published in peer reviewed journals. These three papers cover the themes explored in this thesis; namely medicinal chemistry, cell biology, green chemistry, catalyst development and nanoparticle chemistry. Where the candidate was the primary or co-author, the ideas, development and work were primarily the responsibility of myself, the student, working with the supervision Prof. Peter J. Scammells and A/Prof. Bim Graham at the Medicinal Chemistry Theme at the Monash Institute of Pharmaceutical Sciences, as well as with Prof. Barrie Kellam at the Centre for Biomolecular Sciences at the University of Nottingham.

Additional contributors and supervisors are noted in the author list for each paper, reflecting the collaborative nature of any scientific work, especially here where the work was conducted at a variety of international institutions with a multi-disciplinary team of researchers.

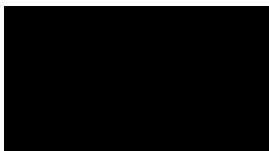
Thesis Chapter	Publication Title	Status	Nature and % of student contribution	Co-author name(s) Nature and % of Co-authors' contribution	Co-author(s) Monash student Y/N	
3.2	Fluorescently Labelled Morphine Derivatives for Bioimaging	Published	Primary author of manuscript. Preparation of figures and final manuscript. 60%	1	Arisbel B. Gondin: Performed confocal microscopy studies, 10%	Y
				2	Meritxell Canals: Performed CAMYEL assay, 10%	N
				3	Barrie Kellam: Manuscript co-author, 5%	N
				4	Stephen J. Briddon: Manuscript co-author, 5%	N
				5	Bim Graham: Manuscript co-author, 5%	N
				6	Peter J. Scammells: Manuscript co-author, 5%	N
5.4	Utility of Iron Nanoparticles and a Solution-Phase Iron Species for the <i>N</i> -Demethylation of Alkaloids	Published	Co-primary author of manuscript. Preparation of figures and final manuscript. 40%	1	Jon Kyle Awalt: Performed half the work published in paper, 40%	N
				2	Barrie Kellam: Manuscript co-author, 5%	N
				3	Bim Graham: Manuscript co-author, 5%	N
				4	Peter J. Scammells: Manuscript co-author, 5%	N
				4	Robert D. Singer: Manuscript co-author, 5%	N

The candidate was a contributing author on the paper shown in Appendix 8.4.

The sections of published papers have not been renumbered in order to generate a consistent presentation within the thesis. Throughout the thesis, compound numbers are carried throughout due to the overlapping nature of the work. Where referencing compounds that have been published, these will be clearly indicated with a reference to the paper and the chapter in which these papers are located. References to literature throughout this thesis are chapter

specific, and hence numbering of references commences from 1 in each chapter.

Student signature:

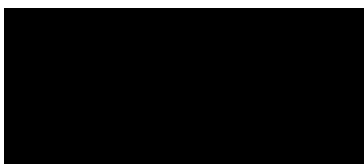


Raymond Lam

October 12, 2018

The undersigned hereby certify that the above declaration correctly reflects the nature and extent of the student's and co-author's contribution to this work. In instances where I am not the responsible author I have consulted with the responsible author to agree on the respective contributions of the authors.

Main supervisor signature:



Peter J. Scammells

October 12, 2018

The Monash-Nottingham Joint Doctoral Training Program

This PhD was completed as part of the newly established Monash-Nottingham Joint Doctoral Training Program. This program consists of a four year course, which is commenced by performing three rotations in different labs, each of which is required to be summarized in a different method of scientific presentation. These are a poster, a scientific report, and an oral presentation. The student is then to work in their primary lab until the conclusion of their second year. The third year is spent at the secondary institution (the University of Nottingham) working on complementary projects designed to be completed within the time-frame of the exchange. The fourth year is then spent at the home institution, during which an industrial placement is required to be completed. In addition to completing all the hurdle requirements of the home institution, some of the requirements of the secondary institution also need to be completed.

Acknowledgements

A PhD is never a simple project one accomplishes on one's own, especially on a project of this complexity and novelty. Furthermore, a chemist is not someone who acquires skills simply by reading them in a book. The various mentors I've had over the years have made me who I am today. Simply saying I am indebted to these people is an understatement. Throughout the last four years and beyond, many people have helped enable the work that has been done either by giving advice, maintaining the equipment vitally important to every chemist, or simply for just being a friend there to bounce various ludicrous ideas off. This list is extensive in my case, so it remains for me to thank those who have helped me along the way.

Prof. Peter J. Scammells, A/Prof. Bim Graham and Prof. Barrie Kellam, my supervisors, have all been great mentors throughout my time as a PhD student. Peter in particular has been a great mentor since my undergraduate days when I started working in the lab for a Summer Research project. They have all given me great advice over the years, solved countless issues and have given me great ideas of what to do not only for this project, but for the rest of my research career. Their tutelage is in no small part responsible for the chemist I am today.

Dr Meritxell Canals, A/Prof. Paul Donnelly and Dr David Chalmers have been great panel members. Aside from their expertise in their respective subject matters, all of which have aided me greatly during my project, they have been extremely approachable and helpful with matters that my primary supervisors may not have been able to assist me with. All the questions with non-obvious answers I've asked over the years have almost always been answered by them. Much of the work done here would not have been possible without their advice and suggestions on how to approach the matter.

Dr Gaik Orbell and Dr Luke S. Schembri have been generous with their knowledge of opiate chemistry during my time in the lab with them. Even simple things would have been rendered difficult without their input. Through their tutelage, I have learned some lab techniques which I otherwise wouldn't have been able to find in literature. Nothing in opiate chemistry is ever straightforward, and much like the non-linear and winding roads of England,

having someone there to help you navigate is crucial.

A/Prof. Shailesh Mistry and Dr Sarah Mistry, both of whom I met when I was just starting out in research during my undergraduate years, have been very understanding mentors to me. Both in our professional and private lives, they have been a significant influence. Their assistance during my time at the University of Nottingham has changed my mentality and methodology when going about chemical synthesis.

Dr Daniel Malone, our resident S8/9 chemicals controller, has been very understanding of my opiate work, especially my constant need for more morphine. Our safety rules prevented me from obtaining more than 400 mg of morphine at any one time, and definitely did not permit storing any in the lab for any practical length of time. The constant failures and difficulties I experienced during the first 2 years in dealing with morphine chemistry necessitated a constant stream of this restricted alkaloid, which Dan had to weigh, log and arrange for a pick-up time every 2 weeks or so. His patience and understanding of this has been immense, and I dare say I've paid Dan more visits than any other opiate chemist at the faculty before me.

Dr Jason Dang at the Monash Institute of Pharmaceutical Sciences and Lee Hibbett at the University of Nottingham have both been instrumental in my work, primarily for their maintenance of the instruments we require. Without them, work would have crawled to a halt and nothing would ever get done. Their constant attention to the equipment we use on a daily basis has allowed the work to proceed without interruption. Jason, in particular, has been a great help over the last few years with the characterization of some of my larger and more complex compounds.

Stefan Tomlins, Jisook Lee, Cassandra Yong and Anthony Lai are some of the fellow PhD students that I've interacted with the most throughout my time at Monash. More often than not, bouncing my ideas off them have allowed me to assess the lunacy of some of my ideas. While they have been helpful academically, they are also been there for all the laughs, all the rough times, and all the crazy things that happen in the lab.

Sean Conroy, Elliott Lumb, Emanuel Sousa, Sebastian Dekkers, Max Ziemann and Aimie Garces were some of the PhD students I met during my stint at the University of Nottingham.

They made my time there enjoyable, enlightening and were people I could turn to whenever I needed help with something, or just needed someone to hang out with while I was in England.

Finally, I need to thank my girlfriend, Lih En Tiah, who completed her Masters on δ -opioid receptors pharmacology recently. Even before we dated, we had great discussions about opioid receptor pharmacology, cell biology and the field of opioids in general. Without her, my knowledge-base in the field would not be what it is today, and certainly the discussions I've had with the various biology collaborators I've worked with over the years would have been far more stunted and less productive. Her support has enabled me to excel beyond what I would be able to achieve on my own.

Abstract

Opioids are a class of alkaloid that have been used since pre-history for the treatment and control of pain. Morphine and codeine, the active ingredients in the opium latex from the plant *Papaver somniferum*, have been known since the 19th century. Although their use in the clinic is widespread, they suffer from various adverse effects, including euphoria, constipation, respiratory depression, tolerance, dependence. These last two side effects are of note, as they are responsible for increasing opioid addiction and related deaths in the United States, as well as in other parts of the world.

These drugs act at the μ -opioid receptor (MOR), a G protein-coupled receptor (GPCR) thought to be the primary target of all opioid analgesics. Classically, it was viewed that GPCRs acted as single units, with an active and inactive state. This simplistic view of GPCR activation fails to explain the varying pharmacological profiles of different opioid drugs. More recently, a new paradigm has emerged in which GPCRs may act as heterodimers, forming functional units with different GPCRs. The MOR has been demonstrated to form heterodimers with various receptors. These include the δ -opioid receptor (DOR), the neurokinin 1 receptor and the cannabinoid 1 receptor just to name a few. Knock-out animal models demonstrate the therapeutic possibilities of targeting these heterodimers.

Studying the MOR has historically been hindered by a lack of useful tool compounds. Previous attempts utilized peptide agonists conjugated to fluorescent tags. Attempts at producing small molecule probes have typically resulted in antagonists, and therefore there is a need to develop novel small molecule opioid agonist probes for the MOR. Furthermore, there is a need to develop new systems in order to study GPCR heterodimers. Of particular interest here is the MOR-DOR heterodimer, as various literature has shown the therapeutic potential of this dimer. For this purpose, we envisioned a nanoparticle-based system to allow for conjugation of multiple congeners to produce a multidentate system.

During the synthesis of these probes, the *N*-demethylation of alkaloids was of particular importance. Opioids, like many other alkaloids, contain *N*-methyl moieties. Replacement of

this methyl group allows for attachment of other alkyl groups that may give varying and clinically useful pharmacologies. Several historical methods are available, including the von Braun reaction, the Polonovski reaction and the use of chloroformates. These all suffer from various drawbacks that limit their use. The more recent development of a non-classical Polonovski reaction enables direct access to the *N*-nor product from the *N*-oxide, which is advantageous compared to the historical methods. These reactions utilize various iron species, from iron salts to organometallic complexes. During this work, new conditions for the non-classical Polonovski reaction were found and optimized. Here, we explored the use of $\text{Fe}_3(\text{CO})_{12}$, a metallo-carbonyl complex that has previously not been described as a catalyst. In addition, we explored the effect of its catalytic activity in various solvents, as well as on a variety of biologically interesting alkaloids.

Acronyms and Abbreviations

5-HT _{1A}	Serotonin 1A receptor
AR	Aspect ratio
AuNP	Gold nanoparticle
AuNR	Gold nanorod
BAIB	Bis(acetoxy)iodobenzene
BCE	Before common era
β -FNA	β -Funaltrexamine
BODIPY	Boron-dipyrromethene
BRET	Bioluminescence resonance energy transfer
cAMP	Cyclic adenosine monophosphate
CAMYEL	cAMP sensor using YFP-Epac-RLuc
CB ₁ R	Cannabinoid receptor type 1
CHO	Chinese hamster ovary
CMC	Critical micellar concentration
CTAB	Cetyltrimethylammonium bromide
CXCR ₄	C-X-C chemokine receptor type 4
Cy5	Cyanin 5
DADLE	[D-Ala ² , D-Leu ⁵]-Enkephalin
DALDA	[D-Arg ² , Lys ⁴]-dermorphin-(1-4)-amide
DAMGO	[D-Ala ² , N-MePhe ⁴ , Gly-ol]-enkephalin
dansyl	5-(Dimethylamino)naphthalene-1-sulfonyl
DCM	Dichloromethane
DIPEA	Diisopropylethylamine
DMF	Dimethylformamide
DMSO	Dimethylsulfoxide
DOR	δ -Opioid receptor
EDC · HCl	1-Ethyl-3-(3-dimethylaminopropyl)carbodiimide hydrochloride
EDTA	Ethylenediaminetetraacetic acid
EGFR	Epidermal growth factor receptor
ELISA	Enzyme-linked immunosorbent assay
FRET	Fluorescence resonance energy transfer
GFP	Green fluorescent protein
GM	Goeppert-Mayer units
GPCR	G protein-coupled receptor
GRK	GPCR receptor kinase
HCTU	2-(6-Chloro-1- <i>H</i> -benzotriazole-1-yl)-1,1,3,3-tetramethylammonium hexafluorophosphate
HOBt	1-Hydroxybenzotriazole
HEK-293	Human embryonic kidney 293 cells
ICP-MS	Inductively coupled plasma - mass spectrometry
IL	Intracellular loop
K_D	Dissociation constant
KOR	κ -Opioid receptor

LC-MS	Liquid chromatography - mass spectrometry
LiHMDS	Lithium bis(trimethylsilyl)amide
LSPR	Longitudinal surface plasmon resonance
MD	Molecular dynamics
mGluR5	Metabotropic glutamate receptor 5
MOR	μ -Opioid receptor
MPL	Multi-photon luminescence
MW	Molecular weight
NBD	7-Nitrobenzo-2-oxa-1,3-diazole
NECA	5'-(<i>N</i> -Ethylcarboxamido)adenosine
NK ₁ R	Neurokinin-1 receptor
N/OFG	Nociception/orphanin FQ peptide
NMR	Nuclear magnetic resonance
NOPr	Nociception/orphanin FQ receptor
PDB	Protein database
PEG	Polyethylene glycol
pERK1/2	Phospho-extracellular signal-regulated kinase 1/2
PSI	Pounds per square inch
PSS	Poly(sodium 4-styrenesulfonate)
Pya	<i>L</i> -1-Pyrenylalanine
PyBOP	Benzotriazol-1-yl-oxytripyrrolidinophosphonium hexafluorophosphate
QD	Quantum dot
Quant.	Quantitative
RT	Room temperature
SAR	Structure-activity relationship
SERS	Surface-enhanced Raman spectroscopy
SPR	Surface plasmon resonance
TEA	Triethylamine
TEM	Transmission electron microscopy
TEMPO	(2,2,6,6-Tetramethylpiperidin-1-yl)oxyl
TFA	Trifluoroacetic acid
THC	Tetrahydrocannabinol
THF	Tetrahydrofuran
TIRFM	Total internal reflection fluorescence microscopy
TM	Transmembrane
TMDS	Tetramethyldisiloxane
TOPO	Trioctylphosphine oxide
TPL	Two-photon luminescence
TSPR	Transverse surface plasmon resonance
Tris	Trisaminomethane
UV	Ultraviolet
Vis	Visible
XAC	Xanthine amine congener
XPS	X-ray photoelectron spectroscopy

1 Introduction

1.1 Opioid Receptors, Structure, Function, Use and Abuse

G protein-coupled receptors (GPCRs) are a superfamily of membrane-bound proteins involved in cell signalling, and are an important class of therapeutic target.¹ About 670 genes have been found to encode for GPCRs. Typically, these bind to small molecule neurotransmitters such as dopamine or acetylcholine, or small peptides such as substance P.² GPCRs are characterized by their seven transmembrane (7TM) α -helix domain, featuring an extracellular N-terminus and intracellular C-terminus. Coupling of various G_α , G_β and G_γ subunits at the intracellular domain forms the functional unit. Binding of an agonist to GPCRs typically results in dissociation of this complex, with the G protein subunits binding to secondary messenger proteins, giving rise to the observed pharmacological outcomes.

Within the GPCR superfamily, the opioid receptors are of particular interest, as they are the primary target of many analgesic drugs such as morphine and codeine.^{2,3} Three classical opioid receptors are known. These are the μ , δ and κ opioid receptors (MOR, DOR and KOR respectively). More recently, a fourth opioid receptor has been discovered, the nociception/orphanin FQ receptor (NOPr).⁴ Although this receptor is known to not bind to the commonly used opiate drugs, it is thought to modulate many of the same functions as the classical opioid receptors, including pain, anxiety, food intake, intestinal motility, learning and memory.^{4,5} These functions may be modified upon binding of the native nociception/orphanin FQ peptide (N/OFQ).

The three classical opioid receptors are highly conserved, sharing 65 - 70% sequence homology. Endogenously, opioid peptides activate these receptors and have varying roles in homeostasis and normal signalling processes. Endorphins and endomorphins targeting the MOR, dynorphins targeting the DOR and enkephalins targeting the KOR have all been studied for their roles in regulation of stress, eating and drinking, self-administration, as well as cardiovascular, respiratory, digestive and hepatic function.⁶ Opioid receptors are found throughout the body, with their function dictated by the tissue in which they are found. Receptors found in the brain and CNS are typically associated with euphoria and analgesia, whilst those found in the

gastro-intestinal tract are thought to play a role in gastric motility. Receptors in the airways play a major role in breathing and respiratory function. Clearly, this family of receptors plays a significant role in maintenance of normal function. Modulation of these functions by external drug administration will obviously interfere with homeostatic functions, and therefore lead to the observed side effects.

More recently the x-ray crystal structures of all opioid receptors have been solved, enabling in-depth study of their structural properties and binding pockets. The MOR has been solved by the Kobilka group bound to both an antagonist,⁷ as well as to an agonist.⁸ Similarly, the DOR has been crystallized by Granier *et al.*,¹ the KOR by Wu *et al.*⁹ and the NOPr by Thompson *et al.*⁵ Although all opioid receptors are structurally similar, they differ in some important aspects from other GPCRs. Compared to small-molecule binding GPCRs such as the muscarinic receptors, the opioid receptors have large, solvent-exposed binding pockets.⁷ In the case of the M₃ muscarinic acetylcholine receptors, the ligand binds in a buried pocket, with the transmembrane helices and extracellular loops folding over the binding pocket (Figure 1). In comparison, the MOR was not found to have this folded structure upon ligand binding. This has been hypothesized to be responsible for the fast k_{off} rate observed for opioid drugs.⁷ Even more interestingly, compared to other peptide-binding GPCRs such as the C-X-C chemokine receptor 4 (CXCR₄), the opioid receptors have deeper binding pockets.⁷

Producing subtype selective drugs has proven to be difficult, but has been achieved. The prototypical natural product morphine (Figure 2), extracted from the poppy plant *Papaver somniferum*, selectively binds to the MOR. This drug has formed the backbone of clinically used treatments for pain, with an estimated 8700 tons of opium and poppy straw concentrate being produced worldwide in the year 2000.¹⁰ Despite their wide usage, morphine and other opioids suffer from various side effects such as respiratory depression, sedation, constipation, tolerance and dependence. These last two side effects are of particular interest, as they are thought to be mediated by signal transduction mechanisms.^{11,12}

The use of opiates as analgesics has been known since early history, with some of the earliest written records coming from the Greek poet Homer. Even in those early days, its "lethal

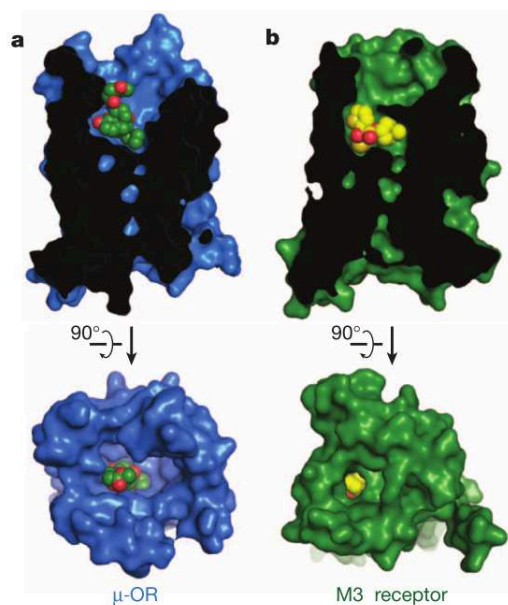


Figure 1. A comparison of the MOR bound to the antagonist β -FNA with the M₃ muscarinic acetylcholine receptor bound to the antagonist tiotropium. Note the larger, more solvent-exposed binding pocket of the opioid receptor, as compared to the M₃ receptor, where the transmembrane helices and extracellular loops fold over the binding pocket upon ligand binding. Adapted from Manglik et al.⁷

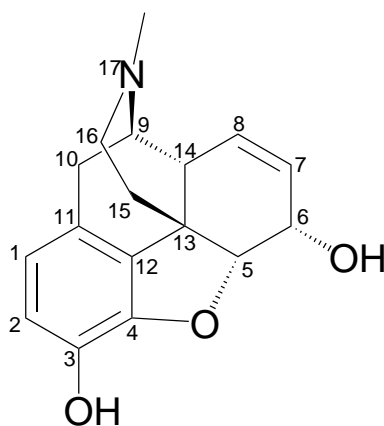


Figure 2. The prototypical opiate morphine, with the numbering positioning numbering convention. The analgesic effects of this drug have been known since early history, and its use documented by various civilizations.

slumber" was noted in his epic *The Odyssey* around the 8th century BCE. Even further back, archaeological evidence suggests the ancient Sumerians cultivated the poppy plant around 3000 BCE, and its use has been documented throughout history by various cultures and civilizations.¹⁰ The analgesic properties of morphine, historically used as the plant extract opium, or as the 16th century concoction Laudanum, has widely been exploited for the treatment of pain. Identification of morphine as the active ingredient was not achieved until 1806, when it was isolated from opium by Sertürner.¹⁰ This has allowed for more effective treatment of pain, and its use proliferated with the invention of the hypodermic needle in 1853.¹⁰

However, the addictive property of opiates have led to them being abused, both by individuals and by empires. The Chinese addiction to opium during the 19th century was exploited by the British Empire, who fought two wars with the Qing Dynasty in order to maintain the opium trade in China despite the objections of the Chinese monarchy, as well as to grant extraterritoriality in of the British Empire in China. This enabled the British trade of Chinese goods, effectively in exchange for opium instead of gold or silver, and hence maintain control over the Chinese economy. Even today, conflicts over opiates continue. Prior to the United States led invasion of Afghanistan, the Taliban had banned the cultivation of the poppy plant in 2000. However, since the overthrow of the regime, Afghanistan has become the world's leading supplier of illegal opiates, with some 6,400 tons of opium thought to be produced in 2014.¹³ Former Afghan President Hamid Karzai recognized that the illegal trade in opium represented a significant portion of the gross domestic product, and refused to allow the United States Drug Enforcement Agency to destroy the poppy fields. Consequently, the number of opium poppy fields being eradicated has dropped significantly, with a 90% drop in the number of eradications between 2015 and 2016.¹⁴

The ready availability of Afghan-produced opium, and the relative ease of smuggling these drugs through the "Balkans" route (Figure 3), has led to a direct rise in opioid addiction and related deaths in Europe.¹⁵ In 2017, it was reported that 38% of all requests for illicit drug-related treatments in this region were due to heroin or other opioid use, numbering around 630,000. It is noteworthy that 79% of patients requesting opioid substitution treatment are

repeat patients, highlighting the difficulty patients have with fully abstaining from opioid use. Furthermore, 81% of drug-related deaths in this region, numbering around 8,500, are due to opioids, giving a perspective on the magnitude of issues associated with this single class of drug. This is in spite of the fact that opioids are not the most readily available or common illicit drugs available in Europe, a title which is shared by amphetamines and cocaine. This is, perhaps, perpetuated by the relatively low cost of heroin compared to other illicit drugs. Again, this highlights the danger associated with illicit opioid use.

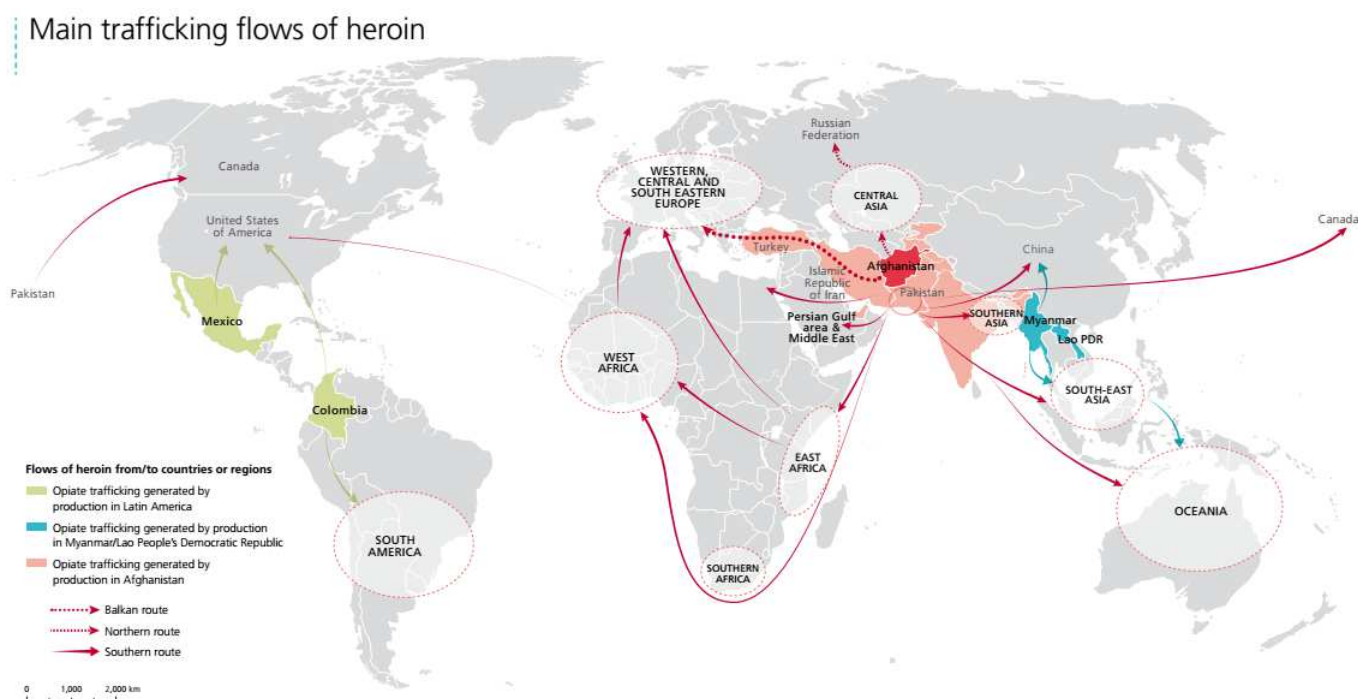


Figure 3. Trafficking routes of Afghan-produced opium to the global black market. The ease of trafficking drugs through the "Balkans" route has led to a direct rise in heroin addiction in Europe. Adapted from United Nations World Drug Report 2016.¹⁶

In the United States, opioid addiction and related deaths are also becoming more frequent. The picture here is more complex, as it seems to be driven primarily by the over-prescription of opioid analgesics, but also by an increase in heroin usage.¹⁷ Between 2014 and 2015, the Center for Disease Prevention reported that death rates from semi-synthetic and synthetic opioids other than methadone increased by 72.2%.¹⁷ Heroin related deaths alone increased by 20.6%. Furthermore, amongst the 47,055 drug related deaths in 2014, 61% involved an opi-

oid, with the majority being prescription opioids given for the control of pain. Despite this, opioids continue to be widely prescribed. Although overprescription of these drugs continues to be one of the leading issues in the United States, changes in legislation and the increasing availability of naloxone, a drug used to assist in opioid detoxification, may enable better control of opioid addiction levels. Still, there is a need to monitor the situation closely, as the rate of opioid prescription has not slowed.

In Australia, the numbers are far lower, but data suggests that opioid addiction and related deaths are increasing.¹⁸ The Victorian Coronor's Office reported that of the 420 drug-related deaths reported in Victoria in 2015, more than 40% were due to legally prescribed opioids.¹⁹ Furthermore, most of these involved over-the-counter opioids, primarily codeine, methadone, oxycodone and tramadol. In addition to this, 40% of the drug-related deaths were due to heroin. In all, this means that in the state of Victoria alone, more than 80% of drug-related deaths were due in part to opioids.

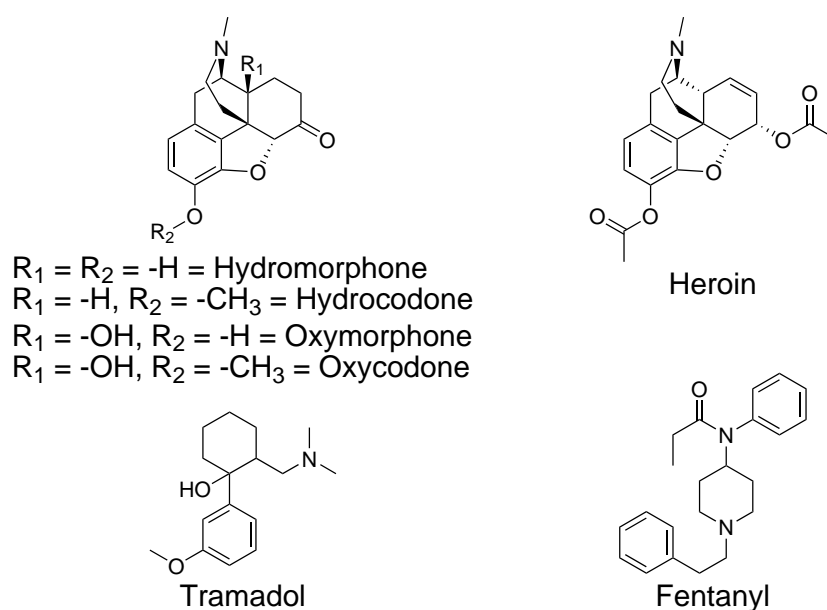


Figure 4. Some of the synthetic and semi-synthetic opioids responsible for the increasing rates of opioid-related deaths worldwide. Drugs such as oxycodone are widely prescribed for the control and treatment of pain.

Treatment options for opioid dependence is generally limited to two drugs; methadone

and buprenorphine.²⁰ While both have shown success in the clinic, issues have arisen with both drugs in patients. Methadone, the front-line in opioid-dependence treatment in Australia, allows patients to function at a basal level. Its long half-life enables patients to take a once-daily dose, and is typically administered by a pharmacist. However, patients report that the withdrawal symptoms of methadone are often worse than those of heroin. To combat this, buprenorphine is often given to assist with the withdrawal of methadone, or used as the primary treatment for opioid dependence. The initial dose can be gradually lowered to reduce the patient's reliance on the drug.

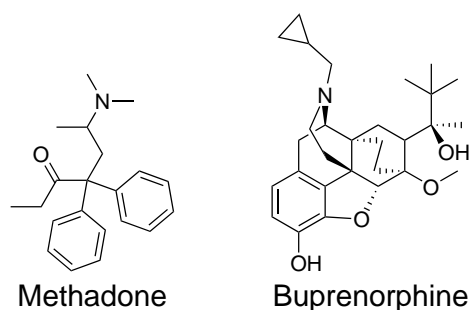


Figure 5. Methadone and buprenorphine, the two primary drugs used in the treatment opioid dependence.

1.1.1 μ -Opioid Receptor Pharmacology

The MOR is thought to be the primary opioid receptor responsible for the analgesic effects of opioids.³ Knockout animal models have shown that loss of the MOR results in a complete loss of morphine-induced analgesia. Analgesics are therefore typically designed to act at this receptor. Because of this, great interest in MOR pharmacology has historically fuelled study into this receptor.

Classically, it was thought that activation of MOR by an agonist resulted in dissociation of the $G_{i/o}$ protein complex. The G_α subunit then binds to and inhibits the activity of adenylate cyclase (AC).¹⁰ The resulting drop in cyclic adenosine monophosphate (cAMP) enables influx of K^+ via G protein mediated K^+ channels, causing hyperpolarization and blockade of voltage-

gated Ca^{2+} .¹⁰ This increased membrane potential reduces firing potential, and therefore inhibits signalling. This cascade gives opioids their analgesic effects, blocking pain signalling. Following MOR activation, GPCR kinases (GRKs) phosphorylate the receptor, promoting β -arrestin recruitment, resulting in signal termination and inducing internalization of the receptor via clathrin-coated pits.²¹

Recently, this classical view of MOR pharmacology has been disputed, as it assumes equilibrium between only the active and inactive states. This two-state model fails to explain various agonist-specific side effects and observed pharmacologies. Agonists such as DAMGO, fentanyl, etorphine and methadone are able to strongly induce receptor internalization.^{22,23} However, other agonists such as morphine and oxycodone do not promote receptor internalization. The ability of a drug to induce internalization is not enough to explain the development of tolerance and dependence in patients. Herkinorin, a semi-synthetic derivative of the natural product KOR agonist Salvinorin A, fails to demonstrate robust internalization of the MOR while able to provide analgesia without the tolerance or dependence liabilities in rats.²² On the other hand, it is well known that morphine similarly does not induce internalization of the receptor, but does suffer from causing tolerance and dependence in patients.²²

As discussed, GPCR deactivation is typically mediated by phosphorylation of the C-terminal tail, allowing β -arrestin recruitment and internalization into endosomes for recycling. However, for morphine the situation is rather perplexing. It is known that morphine only results in weak phosphorylation of the receptor population, and therefore only very weakly promotes β -arrestin 2 recruitment to the cell membrane.¹² This effect may be reversed by overexpression of GRK2, where an enhanced response to both morphine and DAMGO are observed in genetic mouse models. This would lead one to think that natively expressed β -arrestin 2 plays little part in morphine-induced receptor pharmacology, but this is not the case. As Bohn *et al.* have demonstrated, β -arrestin 2 knock-out mice show significantly different pharmacologies to native mice. These mice can still develop a dependence towards morphine, but lack the usual tolerance (i.e. the same dose may be given repeatedly to provide analgesia).¹¹ This is counter-intuitive, as one would think that a lack of association would lead to a lack of pharmacological significance,

but this is clearly not the case and warrants further investigation. However, what this does suggest is that the tolerance and dependence pathways are not linked, but are induced via two separate signalling pathways.

Further mystifying the mechanism is what happens when the MOR does get phosphorylated in the presence of morphine. Yu *et al.* have demonstrated that the low levels of receptor phosphorylation observed with morphine may be reversed by addition of the inverse agonist naloxone.²⁴ Exactly how this occurs is a mystery, as it clearly does not undergo the typical recycling pathway of internalization, dephosphorylation, followed by recycling back to the cell surface.

1.1.2 μ -Opioid Receptor Heterodimers

A more recent paradigm in GPCR pharmacology is the ability of these receptors to operate as dimers or oligomers rather than as single units. Homodimers are known, as well as the more interesting heterodimers. These functional units exhibit unique pharmacologies that may assist in explaining the various MOR pharmacologies observed. For clarity, it is known that these receptors tend to form oligomers, rather than discreet dimers. However, for the purposes of this discussion, we will herein refer to them as heterodimers, and generally to the association between two different GPCR units, rather than between two discreet receptors.

Various MOR heterodimers have been described in literature. These have all been reviewed by Lee *et al.*²⁵ KOR, DOR, NOPr, cannabinoid 1 (CB₁R), neurokinin 1 (NK₁R) and metabotropic glutamate receptor 5 (mGluR5) have all been shown to form heterodimers with MOR. Association of MOR with these receptors modulates its phosphorylation, internalization and recycling, therefore altering the pharmacological outcomes in terms of tolerance and dependence.

MOR-NK₁R dimers have been shown to form via a proximity assay known as bioluminescence resonance energy transfer (BRET).²⁶ Being co-expressed in the nucleus accubens, knock-out of NK₁R in mice demonstrate a loss of MOR associated tolerance and dependence. This lack of addictive behaviour is strictly limited to morphine, as these NK₁R knock-out mice

can still develop a dependence for cocaine. Cross phosphorylation of these receptors has also been observed. Stimulation of the heterodimer with DAMGO induces NK₁R phosphorylation, while stimulation of NK₁R with substance P (Figure 6) does the same to the MOR. This indicates significant cross-talk between the two monomeric units, and therefore the potential to use this heterodimer as a therapeutic target.

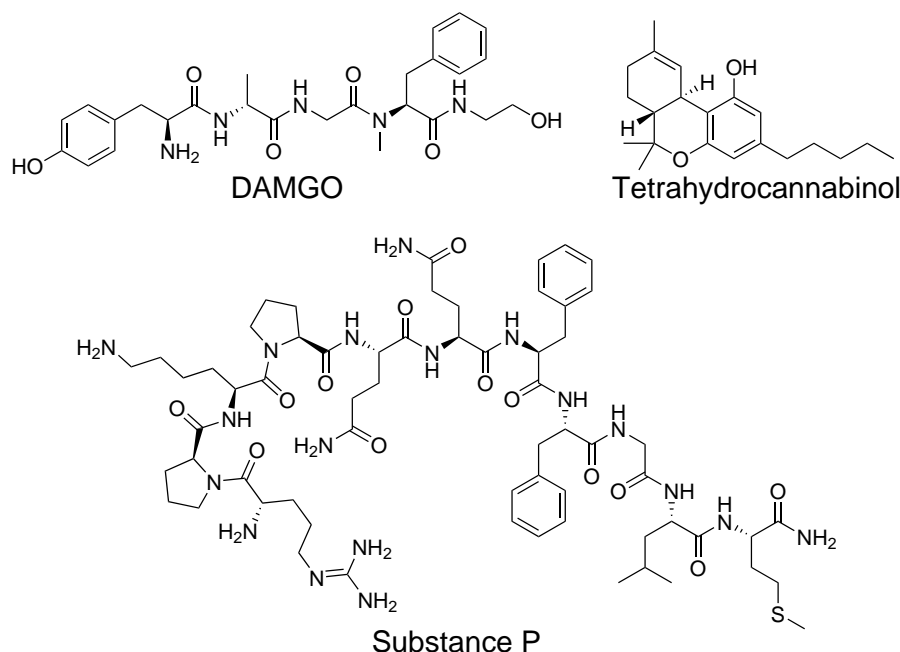


Figure 6. DAMGO, substance P and tetrahydrocannabinol (THC) are some of the ligands that have been assessed for their ability to activate various MOR heterodimers. When administered with a MOR agonist such as DAMGO or morphine, substance P and THC give differing pharmacologies compared to when a MOR agonist is administered by itself. These give some insight into the potential of targeting MOR heterodimers as drug targets for more specific treatment of various conditions.

In the presence of CB₁R, morphine shows increased affinity for MOR when co-administered with the selective CB₁R agonist tetrahydrocannabinol (THC) (Figure 6).²⁵ Again, BRET and fluorescence resonance energy transfer (FRET) experiments suggest close association of these receptors, and are known to be co-expressed in the caudate putamen and dorsal horn of the spinal cord. This effect is particularly interesting, as it suggests the possible synergistic effects of administering two drugs rather than a single active agent for the treatment of pain.

The MOR-DOR heterodimer is of particular interest and has been extensively studied.²⁷

These receptors are expressed together in dorsal root ganglion neurons, and have been shown to associate using a number of techniques including BRET and co-immunoprecipitation. Furthermore, knock-out of DOR in mice enable morphine induced analgesia without the associated tolerance and dependence. This same effect is also observed on co-administration of DOR antagonists with morphine. More importantly, many clinically and experimentally used agents for the MOR such as morphine, methadone, fentanyl and DAMGO have all been shown to target this heterodimer.²⁷ This bias in both the clinic and in the lab may be due to the search for agents that behave similarly to the prototypical opiate morphine. This will be further discussed in Chapter 1.1.4.

Further evidence of MOR heterodimerization was described by Manglik *et al.* following the crystallization of the MOR (Figure 7).⁷ Crystal packing of the MOR revealed close association between TM1, TM2 and helix 8 of the receptor, with a buried surface area of 615 Å. An even more significant association interface was found to form between TM5 and TM6, with a surface area of 1492 Å, again highlighting the potential of close interplay between two monomeric receptors. However, a more recent crystallographic study where the MOR was crystallized bound to an agonist suggested that displacement of TM6 helix may preclude the association between two GPCR subunits at this interface.⁸ The significance of this has yet to be understood, but may suggest changes in dimer formation upon binding of an agonist.

1.1.3 Bivalent μ -Opioid Receptor Ligands

In order to target these MOR heterodimers, various bivalent ligands containing two separate pharmacophores have been synthesized, separated by an appropriately sized linker. One of the most notable examples was described by the Portuguese group.^{28,29} They describe a ligand containing a MOR agonist pharmacophore oxymorphone, conjugated to the DOR antagonist pharmacophore naltrindole. These were separated by a spacer of 21 heavy atoms, hence the designation MDAN-21 (Figure 8). Their results show that administration of this molecule to morphine dependent Rhesus monkeys suppressed withdrawal symptoms, even at low doses.³⁰ They suggest that such a approach could be useful in the treatment of opioid dependence.

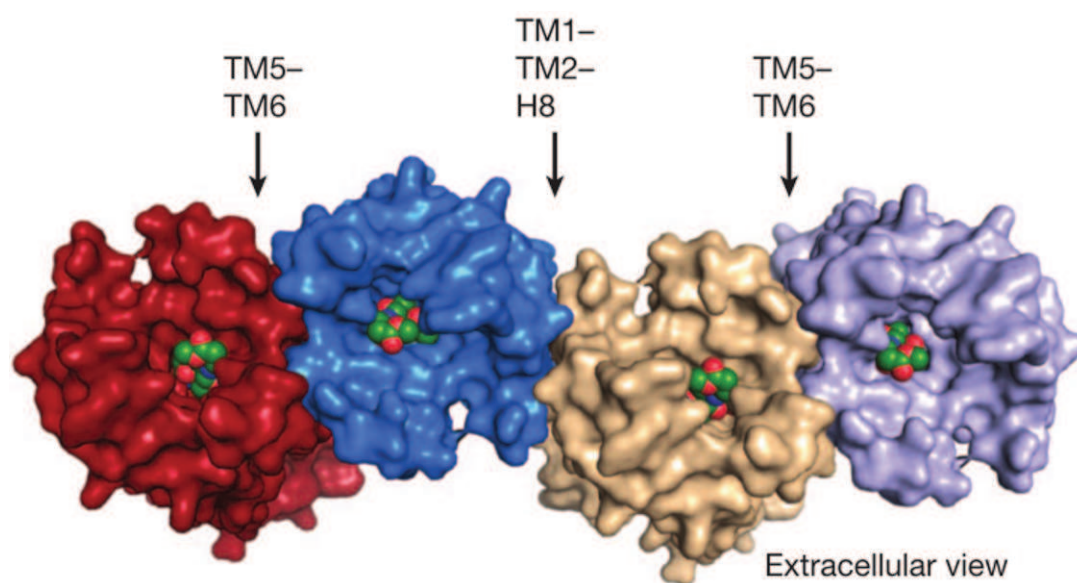


Figure 7. Crystal packing of the MOR as described by Manglik *et al.*⁷ Note the close association between TM5 and TM6 of the monomers, as well as the interaction between TM1, TM2 and helix 8.

Further *in vitro* analysis of this ligand gave interesting results. Yekkirala *et al.* demonstrated that the activity of their bivalent ligands was dependent on the length of the spacer.²⁹ Administration of MDAN-21 to HEK-293 cells expressing both MOR and DOR showed a lack of internalization of this heterodimer. However, MDAN-16, a similar ligand with a shorter spacer, was able to induce internalization. Similarly, when the pharmacophores were administered as separate units with a model spacer, internalization of the heterodimer was also observed. This effect was thought to be due to the optimal spacer length of MDAN-21 preventing internalization by holding the dimer in place. In the case of MDAN-16, the authors suggested that the shorter linker may preclude the ligand from binding both pharmacophores simultaneously, behaving as if the two pharmacophoric units had been administered as separate drugs. Pre-treatment of cells with naltrindole, followed by MDAN-21 rescued heterodimer internalization. These results suggest that it is not enough to target the heterodimer, but control of its internalization behavior may also be critical in determining clinical outcomes.

Similarly, Le Naour *et al.* described a bivalent ligand again based on oxymorphone as the MOR agonist pharmacophore, but utilizing SR-141716 as the CB₁R antagonist pharmacophore

(Figure 8).³¹ It was demonstrated in mice that these bivalent ligands lacked any tolerance liabilities that are typical of the classical monovalent morphinan opioids. Again, it was noted that spacer length played a significant role in the pharmacology of these ligands. This again suggests the possibility of specifically targeting MOR heterodimers as therapeutic targets for the treatment of pain.

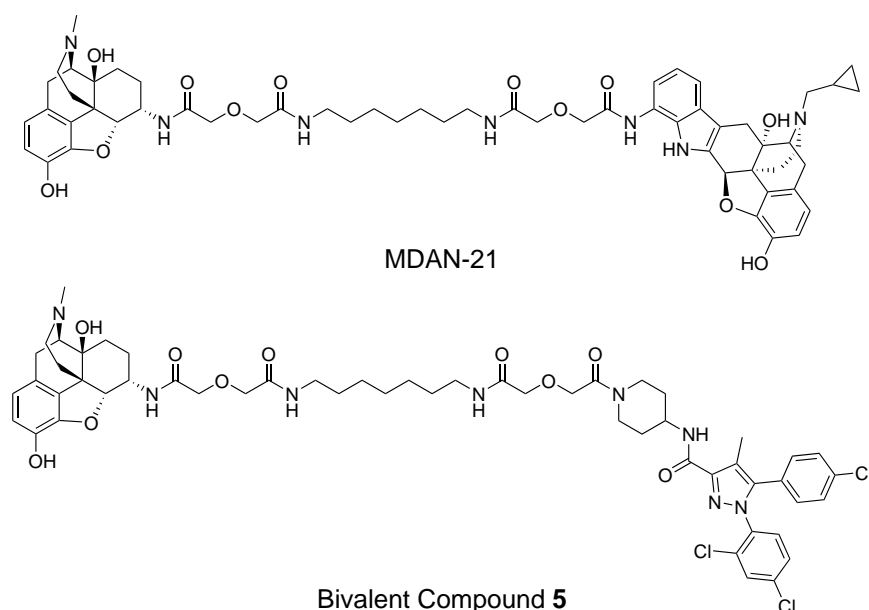


Figure 8. The bivalent ligands MDAN-21 and bivalent compound 5, designed to target the MOR-DOR and MOR-CB₁R heterodimers respectively.^{31,32} Both incorporate oxycodone as the MOR agonist conjugated to the appropriate antagonist pharmacophore for targeting the second GPCR monomer.

1.1.4 Monovalent μ -Opioid Receptor Biased Ligands

Developing specific bivalent ligands is not the only way to target these heterodimers. There are difficulties in that the individual pharmacophores may possess their own signalling biases, and as such when integrated into a bivalent ligand may elicit behaviors specific to that ligand. Substitution of the pharmacophore is not always feasible due to a lack of a reasonable linkage point, so the designs are limited by what ligands can be linked to the secondary pharmacophore. Due to this, a simpler, and more drug-like approach may be to develop monovalent ligands which are biased towards binding to a specific heterodimeric pair. Although designing these

sorts of ligands may be difficult using the current drug development paradigm, examples of these biased ligands are known for the MOR. Although not all these ligands have a desirable side-effect profile, they do demonstrate the possibility of developing heterodimer specific monovalent ligands.

Morphine has been demonstrated to bind selectively to the MOR-DOR heterodimer.³³ Morphine actually demonstrates higher affinity for the MOR when in the presence of DOR, despite having relatively low affinity for the DOR. Disruption of this binding can be achieved by pre-treatment with a DOR-specific antagonist such as naltrindole.³⁴ Furthermore, morphine does not induce robust internalization of the MOR-DOR heterodimer via β -arrestin 2 mediated endocytosis. Morphine only activates a few of the second messenger systems known to be activated by peptide agonists.^{35,36} This suggests that the analgesic effects may be mediated by a distinct set of processes from the development of tolerance and dependence to clinical opioids.

Similarly, DAMGO is also known to bind to the MOR-DOR heterodimer, but is known to have differing pharmacology.²⁷ Unlike morphine, DAMGO exhibits fewer tolerance and dependence liabilities. This may be due to the robust internalization of the heterodimer via β -arrestin 2 recruitment, an effect that can be inhibited by pre-treatment with DOR antagonists. Furthermore, compared to morphine, DAMGO activates a wider variety of second messenger pathways.^{35,36} This suggests that a "rounded" activation of the MOR may result in reduced tolerance and dependence liabilities.

Even more perplexingly, herkinorin, a derivative of the natural product Salvinorin A lacking the usual nitrogenous centre, has also been shown to bind to the MOR.³⁷ Unlike DAMGO, it does not induce internalization of the MOR upon binding, but behaves more like morphine. However, animal models suggest that herkinorin lacks the tolerance and dependence liabilities that plague morphine, suggesting that internalization is not the sole factor in determining opioid tolerance and dependence.²² Furthermore, Lamb *et al.* have also shown that herkinorin is able to induce analgesia in morphine-tolerant mice.²² Why this is the case is unclear, but suggests multiple second messenger pathways leading to analgesia may be involved. Clearly, this is not simply a case of receptor turnover explaining these deleterious effects, as

has previously been suggested.³⁸

From these three examples, it is clear that not only is heterodimer bias involved in determining the pharmacological outcome of various agents, but there is also a secondary bias in the signalling cascade that results from the binding event. Taken together, it is clear that developing opioid agents for the treatment of pain and opioid dependence requires detailed understanding of the second messenger biases that lead to the desired pharmacological outcomes without inducing the undesired side-effects.

More recent work by Manglik *et al.* has resulted in the discovery of PZM21, an opioid agonist that appears to provide analgesia while lacking the classical opioid side effects of respiratory depression and constipation.³⁹ Although its heterodimer binding profile was not characterized, it was found to favor exclusively the G_i pathway, with no secondary signalling via the β -arrestin 2 pathway. Interestingly, it was found to perform well in mice under the hotplate analgesia assay, but not the tail-flick analgesia assay. The authors suggest this is due to the separation of CNS mediated and reflexive pain responses. This is unique to PZM21 and has yet to be understood fully. This again reveals the complexity of the opioid signalling cascade, and how simplistic assays are not sufficient to elucidate pharmacological outcomes.

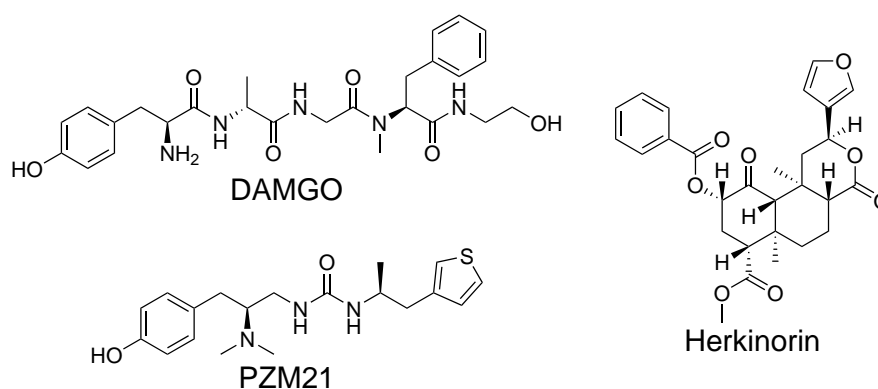


Figure 9. Various biased ligands that all bind to the MOR, but have distinctly different pharmacological outcomes. Each ligand potentially represents a different active conformer of the receptor, giving rise to the various signalling cascades observed.

1.2 Opioid-Fluorophore Conjugates

Studying GPCRs is typically achieved using labelled receptors or labelled ligands. GPCRs may simply be labelled by conjugating fluorescent proteins such as green fluorescent protein (GFP) to the C-terminal of the receptor. Other associated proteins may also be labelled using orthogonal fluorescent moieties in order to study their function in relation to the receptor of interest. More recently, SNAP domain tagged receptors have gained increased use as fluorescent tags for GPCRs, as this technique allows for specific labelling of cell surface receptor populations without labelling internal populations. This allows for determination of what happens to cell surface populations without the background of global labelling.

Although these approaches have allowed for intimate study of various receptor systems, including the opioid receptors, this system is not perfect. Conjugating a large protein such as GFP or any fluorescent moiety to the receptor will inevitably affect its pharmacology, receptor kinetics and ability of accessory proteins to associate with the receptor and elicit their effects. Rather than modifying the receptor, an alternative approach is to modify the ligand. Attaching fluorescent tags such as Cy5, BODIPY or rhodamines allow for imaging of the ligand trafficking, rather than receptor trafficking. Together, these data offer complementary views of receptor pharmacology, where neither data set provides a "complete" picture on its own. Even so, these fluorescently tagged ligands aren't perfect, as modification of their structure may affect pharmacological bias, and therefore the observed results. Given the lack of any "ideal" system, however, these pieces of data form the evidence with which future research is based.

1.2.1 Peptide-Fluorophore Conjugates

Fluorescent probes for the opioid receptors have long been desired. Compared to other receptor systems, such as the adenosinergic system, few fluorescent ligands have been designed, and even fewer have been utilized productively in the literature. For the most part, the most successful class of fluorescently tagged ligands for the opioid receptors has been the peptide-fluorophore conjugates. The earliest of these examples was described by Fournie-Zaluski *et al.*, where en-

kephalins were conjugated to a 1-(5-dimethylaminonaphthalene) sulfonyl (dansyl) group as the fluorescent tag.⁴⁰ At the time of its synthesis in 1978, the distinction between the opioid receptors were unclear, and hence no receptor subtype specific binding was given. However, using homogenized mice striatum, displacement of radio-labelled Leu-enkephalin, binding was measured. Furthermore, functional activity was determined using guinea-pig ileum, measuring the inhibition of electrical contractions upon administration of the peptide-fluorophore conjugate. These showed that conjugation via the C-terminal of the Met-enkephalin gave a fluorescent derivative with only moderately lowered affinity and activity. Despite this, the dansyl group is not amenable to modern imaging techniques, as the high energy 270 nm UV light needed to excite the fluorophore isn't compatible with most modern techniques as well as damaging the cells. These factors in combination have resulted in this probe seeing few uses in literature.

Following this, Mihara *et al.* similarly describe fluorescent enkephalins, this time conjugated to the fluorescent amino acid *L*-1-pyrenylalanine (Pya).⁴¹ Here, binding was measured by displacement of opioid receptor specific radio-labelled peptides. For this purpose, radio-labelled DADLE and DAMGO were used for the DOR and MOR receptors respectively. Again, their results show minimal to no loss in binding. However, no functional assays were conducted. Again, the optical properties of the Pya group aren't amenable to modern imaging techniques, as it absorbs at around 380 nm, still within the UV wavelengths.

Perhaps the most successful peptide-fluorophore conjugates have been described by Arttamangkul *et al.*⁴² Here, subtype selective peptides were conjugated to modern fluorophores, including Alexa Fluor and BODIPY dyes. Again, a moderate loss of binding in a radioligand displacement assay was observed. However, with the attachment of these specific fluorophores, imaging via modern confocal microscopy becomes possible. As a result, these types of peptide-fluorophore conjugates have seen wider use in the literature, with several follow-up studies detailing their use as tools in studying opioid receptor pharmacology.⁴³⁻⁴⁵

1.2.2 Small Molecule-Fluorophore Conjugates

Although peptide-fluorophore conjugates have allowed for the study of opioid receptors using fluorescence techniques, they lack direct clinical relevance, as these peptides are not used as therapeutics. Therefore, there is continued interest in producing fluorescent tools using clinically relevant targeting pharmacophores. One of the earliest attempts was described by Kolb *et al.* in 1983, where various opioid drugs were conjugated directly to the fluorescent tag fluorescein via a minimal thiosemicarbazone linker.⁴⁶ These included the antagonists naltrexone and naloxone, as well as the agonist oxymorphone. As with the peptide-fluorophore conjugates, attachment of the fluorescent tag reduces the binding of the drug to the target. Again, the distinction between the various opioid receptors were unclear during this period of study, and hence no subtype selectivity was described. Although the agonist oxymorphone was used as one of the ligands, no activity other than binding data was given.

Further development of small molecule-fluorophore conjugates were described by Archer *et al.* in 1992, where naltrexamine, a close analogue of naltrexone, was conjugated to the fluorescent tag 7-nitrobenzo-2-oxa-1,3-diazole (NBD) to give the probe compound ASM-5-10.⁴⁷ Here, a short linker was employed to distance the active pharmacophore from the fluorescent tag, one of the first examples of this method being implemented in opioid-fluorophore probes. Again, this conjugate lost activity compared to the native compound. One interesting aspect found was that the introduction of a short linker enabled the probe to be selective for the MOR over the other classical opioid receptors, whilst removal of the linker abolished subtype selectivity. This highlights the importance of a spacer between the active ligand and the fluorophore.

The lack of useful small molecule-fluorophore probes prompted Emmerson *et al.* to continue the development of these conjugates.⁴⁸ Here, nitrocinnamoylaminocodeinone was conjugated to a BODIPY tag to give the probe compound WA-III-62. Here, a short linker was again used, enabling moderate subtype selectivity. The use of the BODIPY probe here was one of the first small molecule-fluorophore probes to utilize a fluorophore compatible with modern

confocal microscopy. The affinity of these probes enabled low concentrations of the conjugate to be used, where previous probes required higher concentrations, potentially obscuring results. However, the probe described was an antagonist, limiting its use.

The most recent attempt was described by Schembri *et al.* in 2015, where opioids based on the orvinol core were conjugated to various fluorescent tags, including Cy5, BODIPY, tetrazine and rhodamine dyes.⁴⁹ Of all these, it was found that the Cy5 conjugated compound was optimal, as it possessed optimal optical properties without binding non-specifically to the cell surface. Although these probes were again determined to be antagonists, they were assessed for their utility as reference compounds in determining affinity constants for a variety of other drugs. Using a fluorescence displacement method, it was found that affinity constants were in good agreement with radioligand based method, suggesting a safer method for determining the screening of new drug candidates.

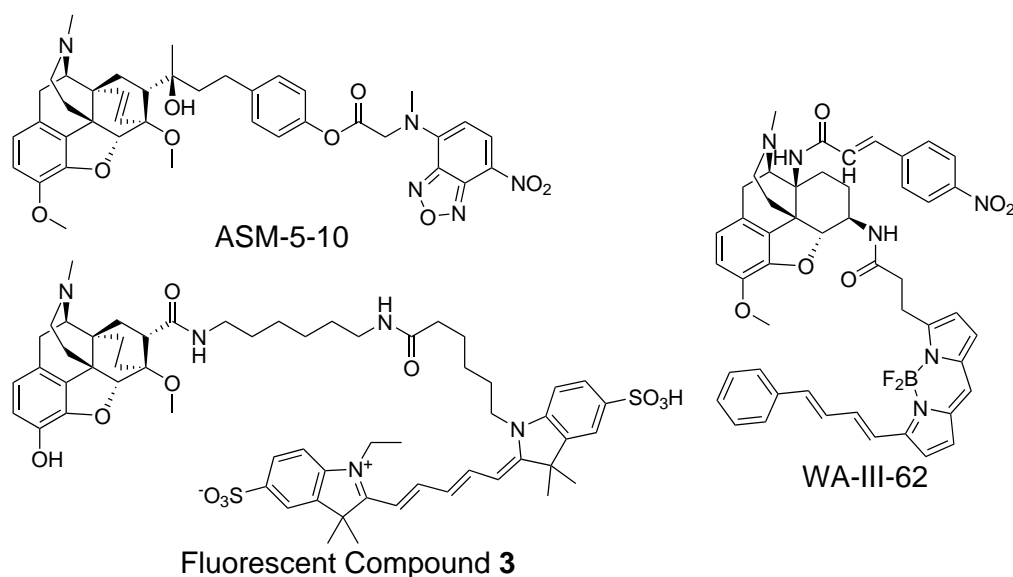


Figure 10. Various small molecule fluorescent probes that have been described in literature. ASM-5-10 utilized naltrexamine as the active pharmacophore with an NBD fluorescent tag.⁴⁷ WA-III-62 utilized nitrocinnamoylaminocodeinone as the active pharmacophore, whilst BODIPY was used as the fluorescent tag.⁴⁸ This was one of the first examples of small molecule probes where a red-emitting fluorophore was used, making it more compatible with modern imaging techniques. Schembri *et al.* described the synthesis of fluorescent compound **3**, utilizing an orvinol targeting pharmacophore with Cy5 as the fluorescent tag.⁴⁹

1.3 Nanoparticles, an Overview

The examples given thus far have all utilized organic fluorophores. However, an increasingly common approach is to utilize nanoparticles as the fluorescent tag. These provide an alternative method of imaging which may provide differing data. Nanoparticles are generally sub-micrometer sized particles, typically ranging anywhere from 5 to 500 nm in diameter. These particles can be made from a variety of materials, ranging from inorganic metals, or from organic polymeric subunits. Nanoparticles can have various properties depending on the materials with which they are made. Some are fluorescent, others may be readily conjugated to as drug-delivery vehicles, and yet others are pH sensitive. The varied properties of nanoparticles have led to the development of various nanoparticle-based systems, both for clinical and experimental use.

1.3.1 Overview of Commonly Used Nanoparticle Probes in Bioimaging

One of the more recent uses for nanoparticles has been for bioimaging. Various fluorescent nanoparticles have been described in the literature, with some finding quite regular use as part of imaging systems. The earliest and most commonly used nanoparticle probes are quantum dots (QDs), with their initial synthesis dating back to 1982 by Russian scientist Alexey Ekimov.⁵⁰ These systems typically consist of a cadmium-based alloy, with a secondary component such as lead or selenium. The most common QDs consist of a cadmium-selenide core. These types of nanoparticles may fluoresce under incident radiation, as electrons are promoted from the ground state to a higher energy level, the difference between the two being termed the band-gap. This band-gap can be tuned simply by tuning the nanoparticle size. Further enhancement in their fluorescent properties can be achieved by coating this cadmium-selenide core with a secondary layer in a core@shell type structure. This shell increases the band-gap of the system, allowing for better control of the fluorescent properties and increasing the Stoke's shift, enabling better imaging of these types of probes.⁵¹ Again, these shells may be made of a variety of materials such as zinc sulfide.

One of the earliest examples of imaging using QDs was described by Rosenthal *et al.* in 2002, where CdSe@ZnS QDs were decorated using serotonin in order to visualize serotonin transporter protein in HeLa cells.⁵² A notable development of this technique was described by Fichter *et al.*, where QDs conjugated to anti 5-HT_{1A} antibodies via a biotin-streptavidin method were used to study the kinetics of 5-HT_{1A} receptor trafficking.⁵³ Their results indicate that there are two pathways through which the receptor is recycled. Trafficking through early endosomes followed by recycling to the cell surface could be differentiated from a longer pathway in which some of the early endosomal populations were first trafficked into recycling endosomes before returning to the cell surface. This detail was enabled by the ability to image single QDs, giving higher resolution data than organic fluorophores. However, Schieber *et al.* suggested that the QD may be responsible for the slower kinetics observed, as their transferrin conjugated QDs exhibited slower uptake via endocytosis compared to transferrin conjugated to small-molecule organic fluorophores.⁵⁴ This suggests that the QDs may alter the kinetics of the biological process due to its bulk. However, it is still unclear if the slower kinetics are inherent in the system, or absolutely due to the QDs themselves.

The disadvantage of these systems is that they tend to be toxic. The use of toxic heavy metals such as cadmium and lead limit their use, as these metals can leach out of the nanoparticle, causing cell death. This specific issue may be overcome using more modern quantum dots that do not involve the use of cadmium, such as the zinc selenide QDs.⁵⁵ However, their relatively poor optical properties must be enhanced by doping with materials such as chromium or cobalt, again reintroducing a toxic substance into the cell. Furthermore, functionalization of quantum dots tends to be relatively difficult. Although various standardized methods have been described, these still tend to be relatively difficult, in part due to the synthesis of QDs resulting in nanoparticles coated in a hydrophobic trioctylphosphine oxide (TOPO) layer.^{52,54,56} For biological use, these must be exchanged for something hydrophilic and biocompatible. Functionalization of QDs is done using 2 general methods. The first is direct displacement of the hydrophobic TOPO coating. One such method is described by Liu *et al.*, where TOPO coated QDs were functionalized with a radical addition-fragmentation chain transfer (RAFT)

polymer consisting of PEG and imidazole units, directly displacing the TOPO coating with a hydrophilic one.⁵⁶ The second approach is to simply wrap the TOPO layer with a more biocompatible polymer. An example of this was described by Schieber *et al.*, where TOPO coated QDs were simply wrapped with a polystyrene-*co*-maleic anhydride polymer.⁵⁴ These could then be treated with amino-PEG chains to ring-open the maleic anhydride moieties to introduce a water-solubilizing group.

Spherical gold nanoparticles (AuNPs) have also been utilized as imaging tools in the past. Their ease of synthesis, their non-toxic nature, and their ease of functionalization are all attractive features. Synthesis of these AuNPs is simply achieved by refluxing aqueous gold salts in a solution of sodium citrate, and was first described by John Turkevich in 1951.⁵⁷ This enables both the reduction of the gold salts, as well as the coating of nanoparticle in a citrate layer. Although optimizations to his original procedure have been described, such as the early size control described by Frens,⁵⁸ or the more recent morphology and dispersity control described by Schulz *et al.*,⁵⁹ the "Turkevich synthesis" has remained much the same. Gold, being an inert element, shows no toxicity in cells, and hence is useful from a biological standpoint. Furthermore, the AuNP-citrate chemistry is well known, enabling easy displacement using a variety of ligands. Finally, gold exhibits a behavior known as surface plasmon resonance (SPR), essentially the oscillation of electrons on the surface of the material.⁶⁰ This enables AuNPs to fluoresce, allowing them to be used as imaging agents. Like QDs, the optical properties of these nanoparticles are size-dependant. Although the physical properties of AuNPs have long been known, it wasn't until 2003 when Sokolov *et al.* described the use of these nanoparticles as imaging agents.⁶¹ Here, AuNPs were conjugated to anti-epidermal growth factor receptor (EGFR) antibodies and used as imaging agents for tissue biopsies. More recent examples have demonstrated the multimodal capabilities of AuNPs, where rather than using their fluorescence properties, their SPR behavior was used for surface enhanced Raman spectroscopy (SERS) whilst simultaneously being used for photothermal therapy in cancer cells.⁶²

Rather than using the intrinsically fluorescent nanoparticles, another method that has been adopted is to add small molecule organic fluorophores to a nanoparticle to give it fluo-

rescent properties. This can be accomplished using a variety of nanoparticle cores, but one example of this has been demonstrated by Mader *et al.*, in which inert silica nanoparticles were modified such that fluorophores could be attached via amide linkage or click chemistries.⁶³ Various organic fluorophores were used, including BODIPY, rhodamine and dansyl based dyes. These have been suggested as an alternative to using single organic fluorophores, allowing for biotin-streptavidin binding of biological molecules to be used as probes for bioassays.

1.3.2 Advantages of Nanoparticle Conjugates in Bioimaging

Although various examples of nanoparticle-targeting moiety conjugates have been described in the past, only a few notable examples have been discussed here. Nanoparticles offer several advantages as imaging agents compared to traditional organic fluorescent tags. They tend to be much brighter, and hence can be more easily detected.⁶⁴ Because of this, it is possible to detect a single nanoparticle, whereas it is difficult to detect a single organic fluorophore using conventional techniques.⁶⁵ Although methods are available for the imaging of single molecules, such as total internal reflection fluorescence microscopy (TIRFM), the penetration of such imaging methods is poor, thus limiting images to the cell membrane.⁶⁶

Although their quantum yields are generally lower compared to organic fluorophores, their large surface area compensates by enabling the absorption of far more photons compared to the relatively small cross-sections of organic fluorophores.⁶⁷ Furthermore, their Stoke's Shifts tend to be larger compared to organic fluorophore.⁵¹ This has several advantages depending on their intended use. In addition to this, the use of multiple organic fluorophores is often not possible, as they can potentially cross-excite, obscuring data and giving misleading results. This is, perhaps, due to modern fluorophores all being designed to excite and fluoresce at lower wavelengths to avoid damaging the cells. Cross-excitation may occur if the emission of one fluorophore overlaps with the excitation wavelengths of another, allowing the energy to be transferred in a process known as FRET. Although this effect is desirable in certain assays, it is undesirable where two separate fluorophores need to be imaged individually. In addition, metal-based nanoparticle fluorophores are completely photostable and can be continually imaged

without photodegradation.⁶⁸

Perhaps one of the biggest advantages of nanoparticles is the ability to functionalize the surface. Their large surface area enables large biomolecules to be conjugated. This has been done in various literature examples using antibodies targeting specific cell surface proteins.^{53,64,69} Furthermore, it enables the development of complex multivalent systems that simply isn't possible using a small molecule approach. The individual components needed to make up the whole nanoparticle system may be individually synthesized, then combined in a concerted approach to give the decorated nanoparticles. With small molecules, this approach is not always feasible.

1.3.3 Gold Nanorods

Gold nanorods (AuNRs) are a more recent addition to the family of fluorescent nanoparticles, with their wet chemical synthesis only dating back to 2001 when it was first described by Catherine Murphy's group.^{70,71} These methods described the use of gold nanoseeds to act as nucleation sites, allowing the gold nanoparticle to grow within a micellar tube of cetyltrimonium bromide (CTAB) as the template. Use of excess silver nitrate was found to assist in the formation of nanorods, as without it spherical particles tended to form. However, these methods would often result in the formation of imperfect nanorods, often giving needle-like and ϕ -shaped particles in addition to spherical impurities. Since then, active development and optimization have led to the refinement in AuNR synthesis. The first real practical synthesis was described by the El-Sayed group, where rather than adjusting the concentration of gold salts and gold nanoseeds used in the synthesis, the amount of silver nitrate added was adjusted, allowing for far better shape control to give true nanorods, as well as a significant reduction in the number of spherical particles formed.⁷² This method has become known as the "Nikoobakht synthesis". Even more recently, aromatic derivatives such as salicylic acid have been shown to improve the monodispersity and morphology control of gold nanorod growth, as well as enabling significant reductions in the concentration of CTAB used in the synthesis.⁷³ These developments have enabled AuNRs to be studied for their potential utility in a variety of applications, in areas as

diverse as bioimaging, drug delivery,⁷⁴ and even in photovoltaic systems.⁷⁵

AuNRs have unique geometric properties. Geometric shape can be described using the Miller Index system, or the Bravais-Miller Index system for more complex, non-Platonic or Archimedean shapes. AuNRs, being anisotropic (or non-dimensionally symmetrical) particles, have two general parts that can be described in this way; the main "cylinder" and the semi-spherical caps. Recent high-resolution transmission electron microscopy (TEM) shows these cylindrical bodies are composed of $\{250\}$ facets elongated along the $\langle 001 \rangle$ vector (Figure 11).⁷⁶ These are terminated by the semi-spherical caps, which have been shown to be semiregular polyhedral prisms with an octahedral cross-section, composed of $\{111\}$ and $\{110\}$ facets. This unique geometry is responsible for the optical properties observed. Unlike AuNPs, which display a single SPR band, AuNRs have two bands.⁷⁷ These two resonance bands, termed the longitudinal surface plasmon resonance (LSPR) and the transverse surface plasmon resonance (TSPR) are mediated by the different types of facets present. The LSPR is mediated by the $\{250\}$ facets, while the TSPR is mediated by the $\{111\}$ and $\{110\}$ facets.

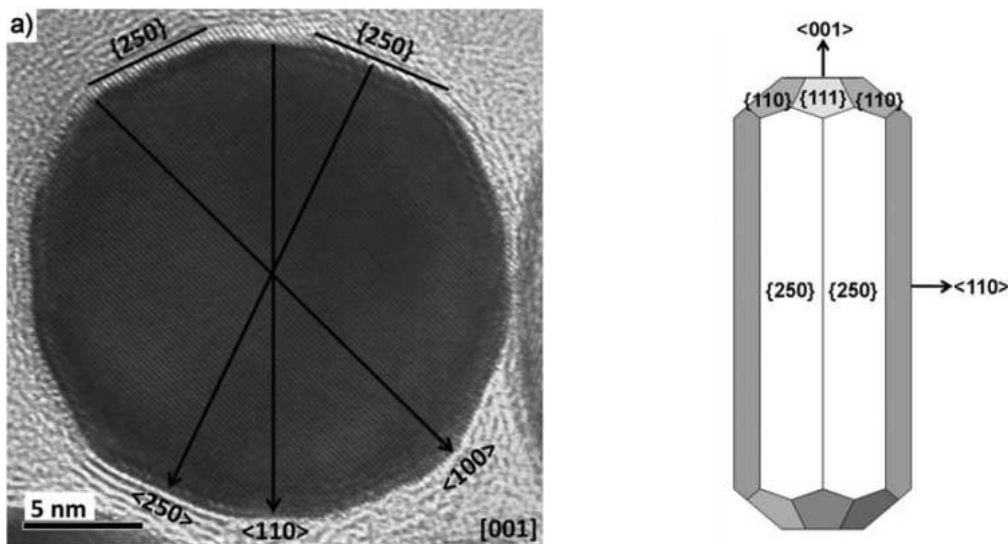


Figure 11. Recent high-resolution TEM image of AuNRs down the axis of the particle have revealed $\{250\}$ facets. This has led to a new proposed model for the structure of AuNRs, forming an octagonal cross-section rather than the previously accepted hexagonal geometry. Figure adapted from Carbó-Argibay et al.⁷⁶

Unlike other nanoparticles, the optical properties of AuNRs don't vary with absolute

size. Rather, aspect ratio (AR) determines their absorbance bands. As discussed, AuNRs have two SPR bands, and each exhibits absorbance bands of their own. The TSPR typically occurs around 510 nm and does not vary significantly. This is primarily due to the synthesis limiting the possible diameter of the nanorod, and hence the size of the terminal facets, as CTAB can only form micelles of a particular size. On the other hand, the LSPR can vary significantly. However, rather than varying with absolute size, the LSPR absorbance varies according to the particle AR. The greater the AR, the more red-shifted the absorbance band. For the Nikoobakht synthesis, a maximum absorbance of around 850 nm is typically observed due to the silver limiting growth to a maximum AR of 4.5.⁷² Examples of AuNR colloids and their absorbance spectra are shown in Figure 12.

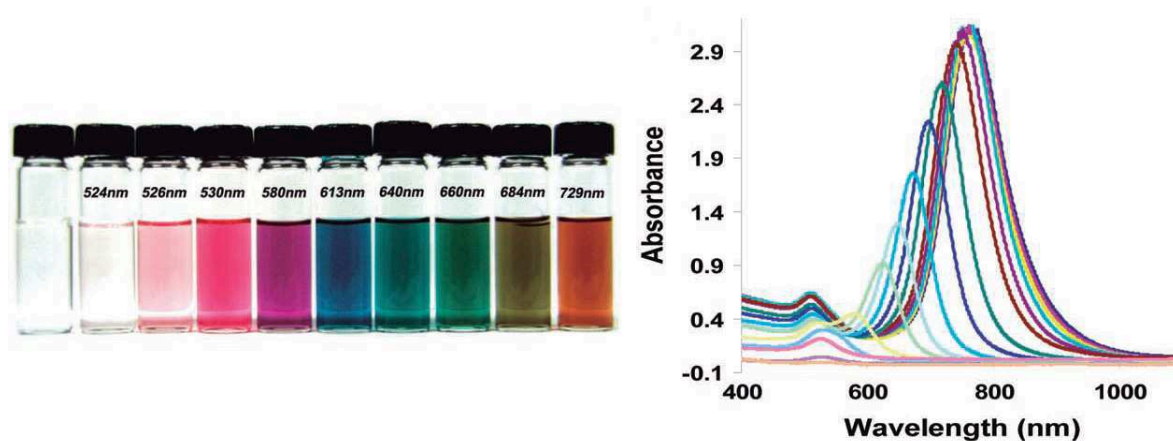


Figure 12. Examples of AuNR colloids and AuNR UV-Vis absorbance spectra. Note the change in color of the colloid as the maximal absorbance increases. The LSPR of the sample increases with increasing AR and varies between 600 - 800 nm depending on the sample, whereas the TSPR (at approximately 510 nm) remains relatively consistent. This is due to the TSPR being correlated with the diameter of the nanoparticle, which does not vary significantly due to the restraints of CTAB template. Also note that the LSPR peak gives a far stronger signal compared to the TSPR, which appears as a minor peak. Figure adapted from Vigderman et al.⁷⁸

AuNRs are interesting in that they can be utilized in different modes of imaging. As with traditional organic fluorophores, they are able to fluoresce when excited by incident radiation. This fluorescence varies with two factors; the wavelength of the incident radiation and the nanorod AR. Varying either will produce differing emission wavelengths which may be

theoretically calculated.⁷⁹ However, in all cases an emission band at approximately 740 nm is always observed. This emission is also observed in all gold-based nanoparticles and nanoclusters. Various suggestions have been put forth as to the origins of this emission, however none have been conclusively proven thus far. Eustis and El-Sayed suggest that since this Raman emission band is observed in all gold nanoparticle types, it may be an inherent property of the material, where electronic recombination causes a band-edge emission which is enhanced by SPR effects.⁷⁹ This effect would therefore be enhanced in AuNRs as their rod-like morphology enhances SPR effects, and the evidence to date support this hypothesis. Although the quantum yield of AuNR fluorescence is relatively low compared to QDs and traditional small molecules, somewhere in the range of 10^{-4} , they are still sufficiently bright to be observed at the single molecule level.⁷⁷

Apart from simple fluorescence, AuNRs are also able to undergo a process known as two-photon luminescence (TPL). More generally, this effect can be termed multi-photon luminescence (MPL), where the precise number of absorbed photons is irrelevant. The efficiency of this process can be measured in Goeppert-Mayer units (GM). Organic fluorophores tend to have quite low efficiencies for this process, with molecules designed specifically for this purpose reaching a maximum of 300 GM.⁶⁹ AuNRs have been measured to have efficiencies around 2000 GM.⁸⁰ Although QDs tend to have higher efficiencies for MPL, varying between 2000 to 47,000 GM, this value is inconsistent and varies according to QD size, material, coating and core@shell structure. For AuNRs, this tends to be more consistent, as it is thought to be an inherent property of the material. Wang *et al.* have further shown that AuNRs may be excited using various wavelengths, with the intensity of the emission dependent on both the incident radiation and the AR.⁸¹ Furthermore, they showed that the emission intensity of AuNRs with lower ARs tended to be brighter compared to those with larger ARs.

1.3.4 Synthesis of Gold Nanorods

The most commonly used synthesis of gold nanorods is known as the "Nikoobahkt synthesis", as described by the El-Sayed group.⁷² This has been depicted in Figure 13. In this method,

gold nanoseeds are first generated from chloroauric acid in the presence of CTAB using sodium borohydride. The solution is rapidly stirred to ensure formation of 4 - 6 nm sized nanoseeds, which occurs over 5 minutes. Ageing of this seed solution allows the excess sodium borohydride to degrade so as to not interfere with the actual nanorod growth. A growth solution of chloroauric acid, silver nitrate and CTAB are then combined and initially reduced using ascorbic acid. This reduces the gold from a +3 oxidation state to a +1 state. This is due to the ascorbic acid not having a high enough reduction potential to fully reduce the gold to the elemental state. Introduction of the gold nanoseeds provides a catalytic surface that reduces the reduction potential required for the reduction of Au(I) to elemental gold. This allows the nanorod to grow within the CTAB micelle, creating new surfaces on which new growth can occur.

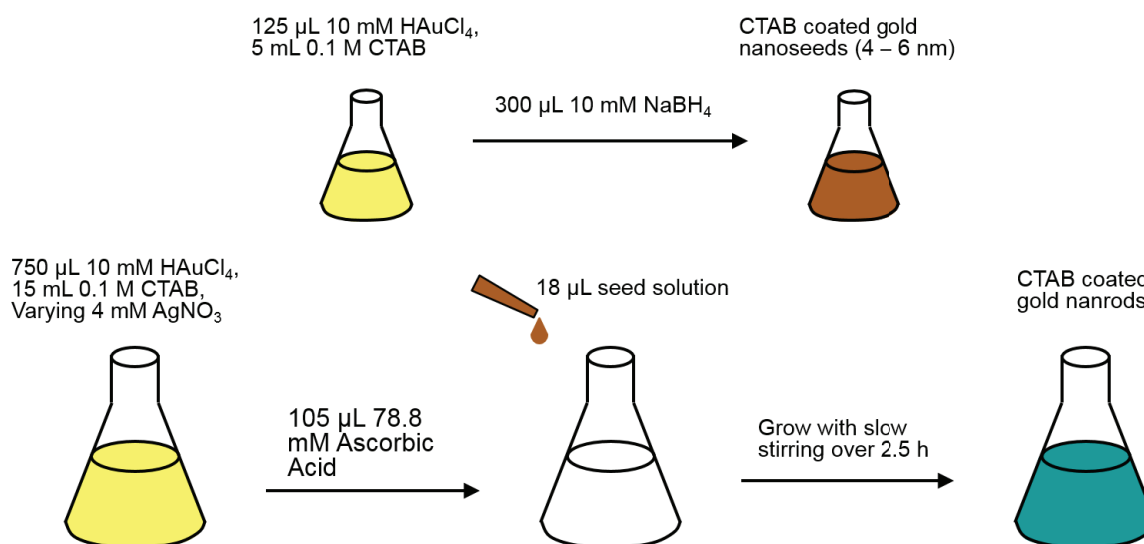


Figure 13. An adaptation of the Nikoobahkt synthesis used during this work. Although the concentrations and volumes of reagents depicted here vary somewhat from the literature procedure, the final concentrations in the "active" solutions remain the same.

With this synthesis, the role of most of the components are known. The chloroauric acid acts as the gold source, CTAB provides the soft micellar template in which the nanorod grows as well as complexing to the particle surface to act as a stabilizing agent, sodium borohydride and ascorbic acid both act as reducing agents, while the nanoseeds act as the catalyst for nanorod growth. The exception here is the precise role of silver nitrate. It is known that addition

of a silver source enables better control of the aspect ratio, however its exact mechanism is unknown. There is evidence to show that silver is present on the surface of the AuNRs, but the reason for this and how it controls nanorod formation is unclear.⁸² It has been suggested that the silver coating allows the nanorod to grow longer. This is generally true for shorter nanorods, as increased titrations of silver nitrate lead to longer nanorods. However, this effect is only true up to an AR of 4.5.⁷² Further addition of silver does not lead to increased rod length, but instead begins to produce shorter nanorods.

Alternative syntheses of AuNRs have been described. One of the more recent methods has been to use a radical reductant that can be induced via UV radiation.⁸³ In this method described by Ahmed and Narain, chloroauric acid, CTAB and silver nitrate are mixed to give the growth solution. Rather than using nanoseeds, the nanorods are grown directly using the photoinitiator known commercially as Irgacure-2959, or I-2959. Addition of this reagent, followed by UV radiation enabled rapid growth of nanorods in 30 min. This method was based on previously published methods, where UV activated acetone was used as the radical reductant. However, I-2959 was far more easily activated by UV radiation, and therefore allowed for easy and rapid reduction. In this synthesis, the role of organic solvents was also explored, and it was found that addition of organic solvents to the bulk aqueous phase enabled better control of nanorod diameter. The effects of acetone and cyclohexane were explored, and were found to reduce nanorod diameter. It was hypothesized that addition of these organic solvents increased the flexibility of the CTAB tubular micelle, hence reducing the nanorod diameter.

More recently, an improvement on the Nikoobahkt synthesis was described, where instead of using ascorbic acid as the reducing agent, dopamine was used.⁸⁴ This enabled synthesis of nanorods with reduced CTAB concentrations, as well as more consistent morphology and size. It was hypothesized that the lower reduction potential of dopamine compared to ascorbic acid prolonged the reaction time. In general, the slower the nanorod growth, the better formed the particles. Furthermore, the use of dopamine gave nanorods of smaller diameter, roughly 9 nm instead of the usual 15 nm as in the normal Nikoobahkt synthesis. It was suggested that this was due to dopamine acting in a similar manner to salicylic acid, increasing the flexibility of

the CTAB micelle and allow for better size control.⁷³

1.3.5 Gold Nanorods in Bioimaging

Despite the promise of AuNRs, few examples of their use as bioimaging agents have been described, owing to their relatively recent development. Perhaps one of the earliest attempts at using AuNRs for the imaging of biological systems was described by Wang *et al.*,⁸⁰ where AuNRs were used to image tissue using their TPL properties. Here, unfunctionalized AuNRs were simply injected into mouse ears and visualized using TPL imaging in order to observe the blood vessels present. Although a relatively simple proof-of-concept experiment, it was early evidence that AuNRs could be used not only in bioimaging, but also in living systems and visualized through tissue. However, it should be noted that in this example the AuNRs used did not conform to a true rod-like morphology. Rather, they were more akin to ϕ -shaped particles (Figure 14).

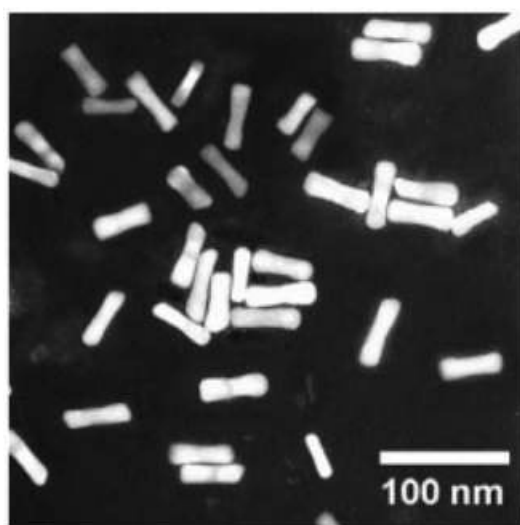


Figure 14. ϕ -shaped AuNRs used by Wang *et al.* Note the slightly wider diameter of the terminal ends of the AuNR, instead of a perfectly cylindrical body. Figure adapted from Wang *et al.*⁸⁰

Following this, Huang *et al.* demonstrated the specificity of anti-EGFR coated AuNRs binding to malignant cells of various types.⁸⁵ Here, the cytotoxic CTAB bilayer was first displaced using poly(sodium 4-styrenesulfonate) (PSS), a negatively charged polymer on which

the anti-EGFR antibodies could be electrostatically anchored. Rather than utilizing their fluorescent or MPL properties, light scattering microscopy was used, highlighting the multiple imaging methods possible using these types of systems. Furthermore, they demonstrated the ability of these systems in killing the malignant cells through photothermal therapy. Although this has previously been shown to be possible using AuNPs, the wavelength of light required is too high for it to be viable, as the incident radiation would not penetrate into deep tissue.⁶⁴ Here, longer wavelengths of light could be used to achieve this effect, which would enable better tissue penetration. This highlights the potential of AuNRs as "theranostics", nanoparticle systems which may act both as a diagnostic tool, as well as a therapeutic treatment. Use of theranostics enables both the diagnosis and treatment phases to be completed in a single step, therefore requiring shorter treatment times and potentially improving patient outcomes.

Durr *et al.* took another step forward, taking the system Huang *et al.* had designed into a bioimaging setting.⁶⁹ In addition to the functionalization steps previously described using a PSS coating followed by attachment of anti-EGFR antibodies, the decorated AuNRs were further mixed with PEG (MW 15 kDa) in order to further enhance their stability. Skin cancer cell line A431 treated with these coated AuNRs could be imaged using TPL microscopy, with no non-specific binding observed. Although background signal could be observed with TPL imaging, the laser power required for this was more than an order of magnitude higher than the laser power required to image the AuNRs. What this suggests is that under the right conditions, AuNRs can be used for bioimaging using TPL microscopy without significant background signal.

TPL microscopy of AuNRs on cells was further refined by Hutter *et al.*, where various cell lines were treated with a variety of gold-based nanomaterials coated with different stabilizing agents.⁸⁶ Of particular note was when mouse hippocampal neurons were treated with unfunctionalized AuNRs. The neurons were stained with MitoTracker green dye, a mitochondrial specific dye, and treated with AuNR@CTAB. Both components could be imaged separately without any interference from the other. Although the point of this experiment was to observe the non-specific binding of the cationic CTAB coated AuNRs on the anionic cell

surface, it still demonstrates the potential of AuNRs as imaging agents. Furthermore, when coated with PEG, the AuNRs failed to "stick" to the cell surface, suggesting that an appropriate biocompatible coating prevents non-specific adhesion to the cell surface. This example is one of the first where AuNRs were imaged with a second fluorescent moiety in the same frame. It demonstrates the potential of being able to image without any background fluorescence.

Apart from the antibody conjugated system described earlier, small molecule conjugated AuNRs have also been described. Yao *et al.* described the functionalization of AuNRs first using cystamine to displace the cytotoxic CTAB, followed by amide coupling of folic acid to the free amine.⁸⁷ This gave AuNRs with a surface decorated by folic acid, which were then used to image HepG2 carcinoma cells. Several important characterizations were carried out in this study. First, that not all cationic coats are cytotoxic, as demonstrated by the difference between AuNR@CTAB and AuNR@cystamine. CTAB reduces the viability of cells in a dose-dependent manner, with up to 80% cell death at 100 $\mu\text{g}/\text{mL}$ AuNR in media. In comparison, cystamine coated AuNRs, which are still cationic, do not cause any significant cell death. This is likely due to the cystamine being strongly bound to the AuNR surface, whereas CTAB is only a weak binder, readily desorbing from the surface and having a cytotoxic effect as a single chemical entity. Imaging of cells coated with AuNRs were conducted using two different excitation wavelengths, and the results recorded at the corresponding emission wavelengths. As discussed, it is known that AuNRs will emit at different wavelengths depending on the incident radiation. This suggests the capability to simply capture the image using different excitation wavelengths if cross-excitation is an issue.

1.3.6 Functionalization of Gold Nanorods for Biocompatibility

For other classes of nanoparticles, the functionalization of the surface has become a relatively standardized, straightforward process. Depending on the desired coat, different protocols may be employed, but most follow the same general principles. However, in the case of AuNRs, this is not the case, as there is currently no standardized method. This is, in part, due to the instability of AuNRs in the absence of CTAB in solution, as this relatively weakly bound

ligand will dissociate from the particle surface if the concentration of free CTAB drops below the critical micelle concentration (CMC) of 1 mM.⁸⁸

Direct functionalization methods enable direct displacement of the CTAB coat from the AuNR surface. Bogliotti *et al.* have shown that it is possible to directly coat AuNRs using various PEG-thiol surfactants.⁸⁹ Simply titrating a solution of the desired PEG-thiol into pre-washed AuNRs and allowing them to simply rest for 48 h resulted in stable PEG coated AuNRs, which can then be further washed to remove excess reagents. Although this method is useful, it is strictly limited to PEG-thiol surfactants, limiting its usefulness if other types of surface coats are desired. An improvement of this method enabled much faster loading of the PEG-thiol onto AuNRs. Zhang *et al.* describe a method in which rather than simply using water, these surfactants are mixed with pre-washed AuNRs in acidic Tris buffer and gently stirred.⁹⁰ This enabled the AuNRs to be coated in 30 min. These could then be resuspended in phosphate buffer following centrifugation to remove excess reagents.

As Huang and Durr have both demonstrated, AuNRs may also be directly coated using PSS, on which targeting moieties may be electrostatically attached.^{69,85} Although these systems are have been shown to be more biocompatible, the exact mechanism of of this was unclear. Whether the PSS simply electrostatically coated the CTAB layer or actually displaced the CTAB altogether was unclear. This was clarified by Leonov *et al.*, where it was shown that PSS was able to displace the CTAB layer by its removal as a PSS-CTAB complex.⁹¹ Simultaneously, PSS forms a weakly bound coating on the AuNR surface, keeping it in a meta-stable state. Huang *et al.* have shown that AuNRs functionalized in such a way are only stable for a few days if stored at 4°C.⁸⁵ Such transient stability is useful if samples need to be freshly prepared, but is unsuitable for long-term storage or use.

An extension of this method was described by Mehtala *et al.*, where rather than simply leaving the AuNRs coated in PSS, this was used as a stepping stone to a more stable system.⁹² After detoxifying CTAB coated AuNRs by washing with several rounds of PSS, they could then be incubated with sodium citrate to replace the PSS coat with a citrate one. This then enables the AuNRs to be stored for longer periods of time. In addition to this, it enables the

use of well-established gold-citrate chemistry developed for the functionalization of citrated coated AuNPs. In both works described by Leonov and Mehtala, it was suggested that various non-ionic surfactants may be used to further increase the stability and biocompatibility.

1.4 Need for Pharmacological Tools

1.4.1 Aims

Although great strides have been made in the study of opioid receptors, significant gaps in knowledge have prevented the development of analgesics devoid of side-effects, as well as better treatments for opioid dependence. With other receptor systems, chemical probes have been a great aid in studying their pharmacology,⁹³⁻⁹⁸ and we envisioned that a similar approach could be used to study the MOR. Further, we envisioned a nanoparticle-based system that could be used to study opioid receptor heterodimers, allowing more detailed study of their trafficking that isn't possible using conventional small-molecule probes.

The aim of this project was to produce fluorescent probes that can be used to study μ OR heterodimers. These probes will be achieved in four stages:

1. Functionalization of the selected targeting ligands to allow for conjugation to the fluorescent tags.
2. Conjugation of functionalized ligands to organic fluorescent tags as tool compounds and as a reference for nanoparticle-based systems.
3. Synthesis and functionalization of the desired nanoparticles for colloidal stability and biocompatibility.
4. Conjugation of the targeting ligand to the nanoparticles.

At each stage, the products will be validated in the appropriate assays in order to ensure each component works as expected. This cycle will be repeated for every targeting ligand used throughout. The final nanoparticle conjugates may then be used to study GPCR heterodimerization.

1.4.2 Hypothesis

These opioid agonist fluorescent probes will assist in the study of the signal transduction and recycling pathways of MOR heterodimers.

1.5 The Monash-Nottingham Joint Doctoral Training Program Rotations

As this PhD was completed as part of the new Monash-Nottingham Joint Doctoral Training Program, "lab rotations" were required to be completed. This involved working in different labs within the faculty for a period of six weeks each. The objective of each rotation was to learn varying skill sets that may be utilized throughout the project. Each of the rotations have been covered in the relevant chapters, as the work done integrates into the primary objectives of the project. For this purpose, the three rotations were as follows:

1. Dr David Chalmer's lab doing computational chemistry, performing some preliminary docking and molecular dynamics simulations.
2. A/Prof. Bim Graham's lab exploring nanoparticle chemistry, beginning the synthesis of gold nanorods and exploring various coats for the particles.
3. Prof. Peter J. Scammells' lab beginning the synthesis of opiate congeners for elaboration into fluorescent probes.

References

- (1) Granier, S., Manglik, A., Kruse, A. C., Kobilka, T. S., Thian, F. S., Weis, W. I., and Kobilka, B. K., (2012). Structure of the δ -opioid receptor bound to naltrindole. *Nature* *485*, 400–404.
- (2) Spetea, M., Asim, M. F., Wolber, G., and Schmidhammer, H., (2013). The opioid receptor and ligands acting at the μ opioid receptor, as therapeutics and potential therapeutics. *Curr. Pharm. Des.* *19*, 7415–7434.
- (3) Matthes, H. W. D., Maldonado, R., Simonin, F., Valverde, O., Slowe, S., Kitchen, I., Befort, K., Dierich, A., Le Meur, M., Dollé, P., Tzavara, E., Hanoune, J., Roques, B. P., and Kieffer, B. L., (1996). Loss of morphine-induced analgesia, reward effect and withdrawal symptoms in mice lacking the μ -opioid-receptor gene. *Nature* *383*, 819–823.
- (4) Mollereau, C., Parmentier, M., Mailleux, P., Butour, J.-L., Moisand, C., Chalon, P., Caput, D., Vassart, G., and Meunier, J.-C., (1994). ORL1, a novel member of the opioid receptor family: Cloning, functional expression and localization. *FEBS Lett.* *341*, 33–38.
- (5) Thompson, A. A., Liu, W., Chun, E., Katritch, V., Wu, H., Vardy, E., Huang, X.-P., Trapella, C., Guerrini, R., Calo, G., Roth, B. L., Cherezov, V., and Stevens, R. C., (2012). Structure of the nociceptin/orphanin FQ receptor in complex with a peptide mimetic. *Nature* *485*, 395–399.
- (6) Bodnar, R. J., (2013). Endogenous opiates and behavior: 2012. *Peptides* *50*, 55–95.
- (7) Manglik, A., Kruse, A. C., Kobilka, T. S., Thian, F. S., Mathiesen, J. M., Sunahara, R. K., Pardo, L., Weis, W. I., Kobilka, B. K., and Granier, S., (2012). Crystal structure of the μ -opioid receptor bound to a morphinan antagonist. *Nature* *485*, 321–326.
- (8) Huang, W., Manglik, A., Venkatakrisnan, A. J., Laeremans, T., Feinberg, E. N., Sanborn, A. L., Kato, H. E., Livingston, K. E., Thorsen, T. S., Kling, R. C., Granier, S., Gmeiner, P., Husbands, S. M., Traynor, J. R., Weis, W. I., Steyaert, J., Dror, R. O.,

-
- and Kobilka, B. K., (2015). Structural insights into μ -opioid receptor activation. *Nature* 524, 315–321.
- (9) Wu, H., Wacker, D., Mileni, M., Katritch, V., Han, G. W., Vardy, E., Liu, W., Thompson, A. A., Huang, X.-P., Carroll, F. I., Mascarella, S. W., Westkaemper, R. B., Mosier, P. D., Roth, B. L., Cherezov, V., and Stevens, R. C., (2012). Structure of the human κ -opioid receptor in complex with JDTic. *Nature* 485, 327–332.
- (10) Blakemore, P. R., and White, J. D., (2002). Morphine, the Proteus of organic molecules. *Chem. Commun.* 1159–1168.
- (11) Bohn, L. M., Gainetdinov, R. R., Lin, F. T., Lefkowitz, R. J., and Caron, M. G., (2000). μ -Opioid receptor desensitization by β -arrestin-2 determines morphine tolerance but not dependence. *Nature* 408, 720–723.
- (12) Bohn, L. M., Dykstra, L. A., Lefkowitz, R. J., Caron, M. G., and Barak, L. S., (2004). Relative opioid efficacy is determined by the complements of the G protein-coupled receptor desensitization machinery. *Mol. Pharmacol.* 66, 106–112.
- (13) United Nations Office on Drugs and Crime, Afghanistan Opium Survey 2014 - Cultivation and Production., 2014, p 67.
- (14) United Nations Office on Drugs and Crime, Afghanistan Opium Survey 2016 - Cultivation and Production., December, 2016, p 65.
- (15) European Monitoring Centre for Drugs and Drug Addiction, European Drug Report 2017: Trends and Developments., Luxembourg, 2017, p 90.
- (16) United Nations Office on Drugs and Crime, World Drug Report 2016., 2016, p 174.
- (17) Rudd, R. A., Aleshire, N., Zibbell, J. E., and Gladden, R. M., (2016). Increases in drug and opioid overdose deaths - United States, 2000-2015. *Cent. Dis. Prev. - Morb. Mortal. Wkly. Rep.* 65, 2010–2015.
- (18) Monheit, B., Pietrzak, D., and Hocking, S., (2016). Prescription drug abuse - a timely update. *Focus (Madison)*. 45, 862–866.

REFERENCES

- (19) Jamieson, A., Finding without inquest into the death of Frank Edward Froom., tech. rep., Melbourne: Coronors Court of Victoria, 2016.
- (20) *Australian Medicines Handbook 2017*; AMH Pty Ltd: Adelaide, 2017.
- (21) Binyaminy, B., Gafni, M., Shapira, M., and Sarne, Y., (2008). Agonist-specific down regulation of mu-opioid receptors: Different cellular pathways are activated by different opioid agonists. *Life Sci.* 82, 831–839.
- (22) Lamb, K., Tidgewell, K., Simpson, D. S., Bohn, L. M., and Prisinzano, T. E., (2012). Antinociceptive effects of herkinorin, a MOP receptor agonist derived from salvinorin A in the formalin test in rats: new concepts in mu opioid receptor pharmacology: from a symposium on new concepts in mu-opioid pharmacology. *Drug Alcohol Depend.* 121, 181–188.
- (23) Connor, M., Osborne, P. B., and Christie, M. J., (2004). μ -Opioid receptor desensitization: is morphine different? *Br. J. Pharmacol.* 143, 685–696.
- (24) Yu, Y., Zhang, L., Yin, X., Sun, H., Uhl, G. R., and Bei, J., (1997). μ Opioid receptor phosphorylation, desensitization, and ligand efficacy. *J. Biol. Chem.* 272, 28869–28874.
- (25) Lee, C., and Ho, I.-K., (2013). Pharmacological profiles of oligomerized μ -opioid receptors. *Cells* 2, 689–714.
- (26) Pfeiffer, M., Kirscht, S., Stumm, R., Koch, T., Wu, D., Laugsch, M., Schröder, H., Höllt, V., and Schulz, S., (2003). Heterodimerization of substance P and μ -opioid receptors regulates receptor trafficking and resensitization. *J. Biol. Chem.* 278, 51630–51637.
- (27) Fujita, W., Gomes, I., and Devi, L. A., (2015). Heteromers of μ - δ opioid receptors: new pharmacology and novel therapeutic possibilities. *Br. J. Pharmacol.* 172, 375–387.
- (28) Daniels, D. J., Lenard, N. R., Etienne, C. L., Law, P.-Y., Roerig, S. C., and Portoghese, P. S., (2005). Opioid-induced tolerance and dependence in mice is modulated by the distance between pharmacophores in a bivalent ligand series. *Proc. Natl. Acad. Sci. U. S. A.* 102, 19208–19213.

-
- (29) Yekkirala, A. S., Kalyuzhny, A. E., and Portoghese, P. S., (2013). An immunocytochemical-derived correlate for evaluating the bridging of heteromeric mu-delta opioid protomers by bivalent ligands. *ACS Chem. Biol.* *8*, 1412–1416.
- (30) Aceto, M. D., Harris, L. S., Negus, S. S., Banks, M. L., Hughes, L. D., Akgün, E., and Portoghese, P. S., (2012). MDAN-21: A bivalent opioid ligand containing mu-agonist and delta-antagonist pharmacophores and its effects in rhesus monkeys. *Int. J. Med. Chem.* *2012*, 1–6.
- (31) Le Naour, M., Akgün, E., Yekkirala, A., Lunzer, M. M., Powers, M. D., Kalyuzhny, A. E., and Portoghese, P. S., (2013). Bivalent ligands that target μ opioid (MOP) and cannabinoid1 (CB1) receptors are potent analgesics devoid of tolerance. *J. Med. Chem.* *56*, 5505–5513.
- (32) Portoghese, P. S., Nelson, W. L., and Takemoris, A. E., (1992). δ Opioid antagonist activity and binding studies of regioisomeric isothiocyanate derivatives of naltrindole: evidence for δ receptor subtypes. *J. Med. Chem.* *35*, 4086–4091.
- (33) Golebiewska, U., Johnston, J. M., Devi, L., Filizola, M., and Scarlata, S., (2011). Differential response to morphine of the oligomeric state of μ -opioid in the presence of δ -opioid receptors. *Biochemistry* *50*, 2829–2837.
- (34) Yekkirala, A. S., Banks, M. L., Lunzer, M. M., Negus, S. S., Rice, K. C., and Portoghese, P. S., (2012). Clinically employed opioid analgesics produce antinociception via μ - δ opioid receptor heteromers in Rhesus monkeys. *ACS Chem. Neurosci.* *3*, 720–727.
- (35) Thompson, G. L., Lane, J. R., Coudrat, T., Sexton, P. M., Christopoulos, A., and Canals, M., (2015). Biased agonism of endogenous opioid peptides at the μ -opioid receptor. *Mol. Pharmacol.* *88*, 335–346.
- (36) Thompson, G. L., Lane, J. R., Coudrat, T., Sexton, P. M., Christopoulos, A., and Canals, M., (2016). Systematic analysis of factors influencing observations of biased agonism at the mu-opioid receptor. *Biochem. Pharmacol.* *113*, 70–87.

- (37) Tidgewell, K., Groer, C. K., Harding, W. W., Lozama, A., Schmidt, M., Marquam, A., Hiemstra, J., Partilla, J. S., Dersch, C. M., Rothman, R. B., Bonn, L. M., and Prisinzano, T. E., (2008). Herkinorin analogues with differential β -arrestin-2 interactions. *J. Med. Chem.* *51*, 2421–2431.
- (38) Kim, J. A., Bartlett, S., He, L., Nielsen, C. K., Chang, A. M., Waldhoer, M., Ou, C. J., Taylor, S., Ferwerda, M., and Whistler, J. L., (2008). Morphine-induced endocytosis of the mu opioid receptor in a novel knock in mouse enhances analgesia and reduces tolerance and dependence. *Curr. Biol.* *18*, 129–135.
- (39) Manglik, A., Lin, H., Aryal, D. K., McCorvy, J. D., Dengler, D., Corder, G., Levit, A., Kling, R. C., Bernat, V., Hübner, H., Huang, X.-P., Sassano, M. F., Giguère, P. M., Löber, S., Duan, D., Scherrer, G., Kobilka, B. K., Gmeiner, P., Roth, B. L., and Shoichet, B. K., (2016). Structure-based discovery of opioid analgesics with reduced side effects. *Nature* *537*, 185–190.
- (40) Fournie-Zaluski, M. C., Gacel, G., Roques, B. P., Senault, B., Lecomte, J. M., Malfroy, B., Swerts, J. P., and Schwartz, J. C., (1978). Fluorescent enkephalin derivatives with biological activity. *Biochem. Biophys. Res. Commun.* *83*, 300–305.
- (41) Mihara, H., Lee, S., Shimohigashi, Y., Aoyagi, H., Kato, T., Izumiya, N., and Costa, T., (1985). δ And μ opiate receptor probes: fluorescent enkephalins with high receptor affinity and specificity. *FEBS Lett.* *193*, 35–38.
- (42) Arttamangkul, S., Alvarez-Maubecin, V., Thomas, G., Williams, J. T., and Grandy, D. K., (2000). Binding and internalization of fluorescent opioid peptide conjugates in living cells. *Mol. Pharmacol.* *58*, 1570–1580.
- (43) Arttamangkul, S., Torrecilla, M., Kobayashi, K., Okano, H., and Williams, J. T., (2006). Separation of μ -opioid receptor desensitization and internalization: endogenous receptors in primary neuronal cultures. *J. Neurosci.* *26*, 4118–4125.

- (44) Macey, T. A., Ingram, S. L., Bobeck, E. N., Hegarty, D. M., Aicher, S. A., Arttamangkul, S., and Morgan, M. M., (2010). Opioid receptor internalization contributes to dermorphin-mediated antinociception. *Neuroscience* 168, 543–550.
- (45) Macey, T. A., Bobeck, E. N., Suchland, K. L., Morgan, M. M., and Ingram, S. L., (2015). Change in functional selectivity of morphine with the development of antinociceptive tolerance. *Br. J. Pharmacol.* 172, 549–561.
- (46) Kolb, V. M., Koman, A., and Terenius, L., (1983). Fluorescent probes for opioid receptors. *Life Sci.* 33, 423–426.
- (47) Archer, S., Medzihradsky, F., Seyed-Mozaffari, A., and Emmerson, P. J., (1992). Synthesis and characterization of 7-nitrobenzo-2-oxa-1,3-diazole (NBD)-labeled fluorescent opioids. *Biochem. Pharmacol.* 43, 301–306.
- (48) Emmerson, P. J., Archer, S., El-Hamouly, W., Mansour, A., Akil, H., and Medzihradsky, F., (1997). Synthesis and characterization of 4,4-difluoro-4-bora-3a,4a-diaza-s-indacene (BODIPY)-labeled fluorescent ligands for the mu opioid receptor. *Biochem. Pharmacol.* 54, 1315–1322.
- (49) Schembri, L. S., Stoddart, L. A., Briddon, S. J., Kellam, B., Canals, M., Graham, B., and Scammells, P. J., (2015). Synthesis, biological evaluation, and utility of fluorescent ligands targeting the μ -opioid receptor. *J. Med. Chem.* 58, 9754–9767.
- (50) Ekimov, A., and Onushchenko, A., (1982). Quantum size effect in the optical-spectra of semiconductor micro-crystals. *Sov. Phys. Semicond.* 16, 775–778.
- (51) Deerinck, T. J., (2008). The application of fluorescent quantum dots to confocal, multiphoton, and electron microscopic imaging. *Toxicol. Pathol.* 36, 112–116.
- (52) Rosenthal, S. J., Tomlinson, I., Adkins, E. M., Schroeter, S., Adams, S., Swafford, L., McBride, J., Wang, Y., DeFelice, L. J., and Blakely, R. D., (2002). Targeting cell surface receptors with ligand-conjugated nanocrystals. *J. Am. Chem. Soc.* 124, 4586–4594.

- (53) Fichter, K. M., Flajolet, M., Greengard, P., and Vu, T. Q., (2010). Kinetics of G-protein-coupled receptor endosomal trafficking pathways revealed by single quantum dots. *Proc. Natl. Acad. Sci. U. S. A.* *107*, 18658–18663.
- (54) Schieber, C., Bestetti, A., Lim, J. P., Ryan, A. D., Nguyen, T. L., Eldridge, R., White, A. R., Gleeson, P. A., Donnelly, P. S., Williams, S. J., and Mulvaney, P., (2012). Conjugation of transferrin to azide-modified CdSe/ZnS core-shell quantum dots using cyclooctyne click chemistry. *Angew. Chemie - Int. Ed.* *51*, 10523–10527.
- (55) Huy, B. T., Seo, M.-H., Kumar, A. P., Jeong, H., and Lee, Y.-I., (2014). Synthesis and photoluminescence of Cr-, Ni-, Co-, and Ti-doped ZnSe nanoparticles. *J. Alloys Compd.* *588*, 127–132.
- (56) Liu, W., Greytak, A. B., Lee, J., Wong, C. R., Park, J., Marshall, L. F., Jiang, W., Curtin, P. N., Ting, A. Y., Nocera, D. G., Fukumura, D., Jain, R. K., and Bawendi, M. G., (2010). Compact biocompatible quantum dots via RAFT-mediated synthesis of imidazole-based random copolymer ligand. *J. Am. Chem. Soc.* *132*, 472–483.
- (57) Turkevich, J., Stevenson, P. C., and Hillier, J., (1951). A study of the nucleation and growth processes in the synthesis of colloidal gold. *Discuss. Faraday Soc.* *11*, 55–75.
- (58) Frens, G., (1973). Controlled nucleation for the regulation of the particle size in monodisperse gold suspensions. *Nat. Phys. Sci.* *241*, 20–22.
- (59) Schulz, F., Homolka, T., Bastús, N. G., Puentes, V. F., Weller, H., and Vossmeier, T., (2014). Little adjustments significantly improve the turkevich synthesis of gold nanoparticles. *Langmuir* *30*, 10779–10784.
- (60) Amendola, V., Pilot, R., Frasconi, M., Maragò, O. M., and Iatì, M. A., (2017). Surface plasmon resonance in gold nanoparticles: a review. *J. Phys. Condens. Matter* *29*, 203002–203050.
- (61) Sokolov, K., Follen, M., Aaron, J., Pavlova, I., Malpica, A., Lotan, R., and Richards-kortum, R., (2003). Real-time vital optical imaging of precancer using anti-epidermal

-
- growth factor receptor antibodies conjugated to gold nanoparticles. *Cancer Res.* *63*, 1999–2004.
- (62) Aioub, M. S., and El-Sayed, M. A., (2016). A real-time surface enhanced Raman spectroscopy study of plasmonic photothermal cell death using targeted gold nanoparticles. *J. Am. Chem. Soc.* *138*, 1258–1264.
- (63) Mader, H., Li, X., Saleh, S., Link, M., Kele, P., and Wolfbeis, O. S., (2008). Fluorescent silica nanoparticles. *Ann. N. Y. Acad. Sci.* *1130*, 218–223.
- (64) El-Sayed, I. H., Huang, X., and El-Sayed, M. A., (2006). Selective laser photo-thermal therapy of epithelial carcinoma using anti-EGFR antibody conjugated gold nanoparticles. *Cancer Lett.* *239*, 129–135.
- (65) Chang, J. C., and Rosenthal, S. J., (2012). Visualization of lipid raft membrane compartmentalization in living RN46A neuronal cells using single quantum dot tracking. *ACS Chem. Neurosci.* *3*, 737–743.
- (66) Hutter, E., and Maysinger, D., (2011). Gold nanoparticles and quantum dots for bioimaging. *Microsc. Res. Tech.* *74*, 592–604.
- (67) Yorulmaz, M., Khatua, S., Zijlstra, P., Gaiduk, A., and Orrit, M., (2012). Luminescence quantum yield of single gold nanorods. *Nano Lett.* *12*, 4385–4391.
- (68) Dreaden, E. C., Alkilany, A. M., Huang, X., Murphy, C. J., and El-Sayed, M. A., (2012). The golden age: gold nanoparticles for biomedicine. *Chem. Soc. Rev.* *41*, 2740–2779.
- (69) Durr, N. J., Larson, T., Smith, D. K., Korgel, B. A., Sokolov, K., and Ben-Yakar, A., (2007). Two-photon luminescence imaging of cancer cells using molecularly targeted gold nanorods. *Nano Lett.* *7*, 941–945.
- (70) Jana, N. R., Gearheart, L., and Murphy, C. J., (2001). Wet chemical synthesis of high aspect ratio cylindrical gold nanorods. *J. Phys. Chem. B* *105*, 4065–4067.

- (71) Jana, N. R., Gearheart, L., and Murphy, C. J., (2001). Seed-mediated growth approach for shape-controlled synthesis of spheroidal and rod-like gold nanoparticles using a surfactant template. *Adv. Mater.* *13*, 1389–1393.
- (72) Nikoobakht, B., and El-Sayed, M. A., (2003). Preparation and growth mechanism of gold nanorods (NRs) using seed-mediated growth method. *Chem. Mater.* *15*, 1957–1962.
- (73) Ye, X., Jin, L., Caglayan, H., Chen, J., Xing, G., Zheng, C., Doan-Nguyen, V., Kang, Y., Engheta, N., Kagan, C. R., and Murray, C. B., (2012). Improved size-tunable synthesis of monodisperse gold nanorods through the use of aromatic additives. *ACS Nano* *6*, 2804–2817.
- (74) Zhong, Y., Wang, C., Cheng, L., Meng, F., Zhong, Z., and Liu, Z., (2013). Gold nanorod-cored biodegradable micelles as a robust and remotely controllable doxorubicin release system for potent inhibition of drug-sensitive and resistant cancer cells. *Biomacromolecules* *14*, 2411–2419.
- (75) Mubeen, S., Lee, J., Lee, W.-R., Singh, N., Stucky, G. D., and Moskovits, M., (2014). On the plasmonic photovoltaic. *ACS Nano* *8*, 6066–6073.
- (76) Carbó-Argibay, E., Rodríguez-González, B., Gómez-Graña, S., Guerrero-Martínez, A., Pastoriza-Santos, I., Pérez-Juste, J., and Liz-Marzán, L. M., (2010). The crystalline structure of gold nanorods revisited: evidence for higher-index lateral facets. *Angew. Chem. Int. Ed. Engl.* *49*, 9397–9400.
- (77) Mohamed, M. B., Volkov, V., Link, S., and El-Sayed, M. A., (2000). The ‘lightning’ gold nanorods: fluorescence enhancement of over a million compared to the gold metal. *Chem. Phys. Lett.* *317*, 517–523.
- (78) Vigderman, L., Khanal, B. P., and Zubarev, E. R., (2012). Functional gold nanorods: synthesis, self-assembly, and sensing applications. *Adv. Mater.* *24*, 4811–4841.

- (79) Eustis, S., and El-Sayed, M., (2005). Aspect ratio dependence of the enhanced fluorescence intensity of gold nanorods: experimental and simulation study. *J. Phys. Chem. B* *109*, 16350–16356.
- (80) Wang, H., Huff, T. B., Zweifel, D. A., He, W., Low, P. S., Wei, A., and Cheng, J.-X., (2005). In vitro and in vivo two-photon luminescence imaging of single gold nanorods. *Proc. Natl. Acad. Sci. U. S. A.* *102*, 15752–15756.
- (81) Wang, T., Halaney, D., Ho, D., Feldman, M. D., and Milner, T. E., (2013). Two-photon luminescence properties of gold nanorods. *Biomed. Opt. Express* *4*, 584–595.
- (82) Jackson, S. R., McBride, J. R., Rosenthal, S. J., and Wright, D. W., (2014). Where’s the silver? Imaging trace silver coverage on the surface of gold nanorods. *J. Am. Chem. Soc.* *136*, 5261–5263.
- (83) Ahmed, M., and Narain, R., (2010). Rapid synthesis of gold nanorods using a one-step photochemical strategy. *Langmuir* *26*, 18392–18399.
- (84) Su, G., Yang, C., and Zhu, J.-J., (2015). Fabrication of gold nanorods with tunable longitudinal surface plasmon resonance peaks by reductive dopamine. *Langmuir* *31*, 817–823.
- (85) Huang, X., El-Sayed, I. H., Qian, W., and El-Sayed, M. A., (2006). Cancer cell imaging and photothermal therapy in the near-infrared region by using gold nanorods. *J. Am. Chem. Soc.* *128*, 2115–2120.
- (86) Hutter, E., Boridy, S., Labrecque, S., Lalancette-Hébert, M., Kriz, J., Winnik, F. M., and Maysinger, D., (2010). Microglial response to gold nanoparticles. *ACS Nano* *4*, 2595–2606.
- (87) Yao, S., Cai, H.-H., Liu, M., and Yang, P.-H., (2014). Fluorescent labeling of cellular targets and multicolor imaging with gold nanorods. *Dye. Pigment.* *101*, 286–294.

REFERENCES

- (88) Burrows, N. D., Lin, W., Hinman, J. G., Dennison, J. M., Vartanian, A. M., Abadeer, N. S., Grzincic, E. M., Jacob, L. M., Li, J., and Murphy, C. J., (2016). The surface chemistry of gold nanorods. *Langmuir* 32, 9905–9921.
- (89) Bogliotti, N., Oberleitner, B., Di-Cicco, A., Schmidt, F., Florent, J.-C., and Semetey, V., (2011). Optimizing the formation of biocompatible gold nanorods for cancer research: functionalization, stabilization and purification. *J. Colloid Interface Sci.* 357, 75–81.
- (90) Zhang, Z., and Lin, M., (2014). Fast loading of PEG-SH on CTAB-protected gold nanorods. *RSC Adv.* 4, 17760–17767.
- (91) Leonov, A. P., Zheng, J., Clogston, J. D., Stern, S. T., Patri, A. K., and Wei, A., (2008). Detoxification of gold nanorods by treatment with polystyrenesulfonate. *ACS Nano*, 2481–2488.
- (92) Mehtala, J. G., Zemlyanov, D. Y., Max, J. P., Kadasala, N., Zhao, S., and Wei, A., (2014). Citrate-stabilized gold nanorods. *Langmuir* 30, 13727–13730.
- (93) Stoddart, L. A., Vernall, A. J., Briddon, S. J., Kellam, B., and Hill, S. J., (2015). Direct visualisation of internalization of the adenosine A₃ receptor and localization with arrestin3 using a fluorescent agonist. *Neuropharmacol.* 98, 68–77.
- (94) Vernall, A. J., Stoddart, L. A., Briddon, S. J., Ng, H. W., Laughton, C. A., Doughty, S. W., Hill, S. J., and Kellam, B., (2013). Conversion of a non-selective adenosine receptor antagonist into A₃-selective high affinity fluorescent probes using peptide-based linkers. *Org. Biomol. Chem.* 11, 5673–5682.
- (95) Middleton, R. J., Briddon, S. J., Cordeaux, Y., Yates, A. S., Dale, L., George, M. W., Baker, J. G., Hill, S. J., and Kellam, B., (2007). New fluorescent adenosine A₁-receptor agonists that allow quantification of ligand - receptor interactions in microdomains of single living cells. *J. Med. Chem.* 50, 782–793.

REFERENCES

- (96) Baker, J. G., Hall, I. P., and Hill, S. J., (2003). Pharmacology and direct visualisation of BODIPY-TMR-CGP: a long-acting fluorescent β_2 -adrenoceptor agonist. *Br. J. Pharmacol.* *139*, 232–242.
- (97) Baker, J. G., Middleton, R., Adams, L., May, L. T., Briddon, S. J., Kellam, B., and Hill, S. J., (2010). Influence of fluorophore and linker composition on the pharmacology of fluorescent adenosine A_1 receptor ligands: themed section: imaging in pharmacology research paper. *Br. J. Pharmacol.* *159*, 772–786.
- (98) Vernall, A. J., Stoddart, L. A., Briddon, S. J., Hill, S. J., and Kellam, B., (2012). Highly potent and selective fluorescent antagonists of the human adenosine A_3 receptor based on the 1,2,4-triazolo[4,3-a]quinoxalin-1-one scaffold. *J. Med. Chem.* *55*, 1771–1782.

2 Molecular Modelling of the Opioid Receptors

2.1 Receptor Subtype Selectivity based on Docking Methods

Molecular modelling was first conducted in an attempt to develop a computational model to enable the design of MOR selective congeners using the molecular modelling package Maestro from Schrödinger. Due to the availability of the crystal structures of the MOR, DOR and KOR, receptor subtype selectivity was explored via a docking method.¹⁻³ Briefly, the antagonist-bound crystal structures of all three classical opioid receptors were prepared for docking by removal of the crystal structure ligand, as well as any lipids, salts and accessory water molecules present. Those water molecules thought to play an important role in hydrogen-bonding networks were left in the structure. These three molecules were selected based on the discussion from Manglik *et al.* and were thought to participate in a critical water mediated hydrogen-bonding network¹. A boundary box of 10 Å around the crystal structure ligand was set to limit poses outside the binding pocket. Using these prepared structures, a library of literature ligands (both agonists and antagonists, see Appendix 8.1.1) with known K_D values at all classical opioid receptors were docked into each receptor using Glide. The results were then manually inspected for reasonably docked poses and the Glide scores were ranked against the K_D ranking (Figure 15). The MOR showed good Spearman rank correlation with a score of 0.77, indicating good agreement between the Glide score and the literature K_D value (Figure 15). However, this was not true of the DOR and KOR, where no correlation was observed.

Many factors may have affected the outcomes observed. The receptors themselves are a static snapshot of a dynamic system. In addition to this, they are all posed as antagonist-bound structures, potentially biasing them towards selecting antagonists over agonists. Furthermore, the type of ligand bound may have affected the specific antagonist structure. In the case of MOR, β -FNA was used, which is an irreversible antagonist, removing it from the clinically used reversible ligands.¹ Secondly, the ligand selection may not have been ideal. Generally for these types of studies, a variety of ligands spanning a wide range of potencies are used, with K_D ranging between the nanomolar and micromolar ranges. However, quite often this type of data is not available, as poorly binding novel ligands are not published, which is especially true of

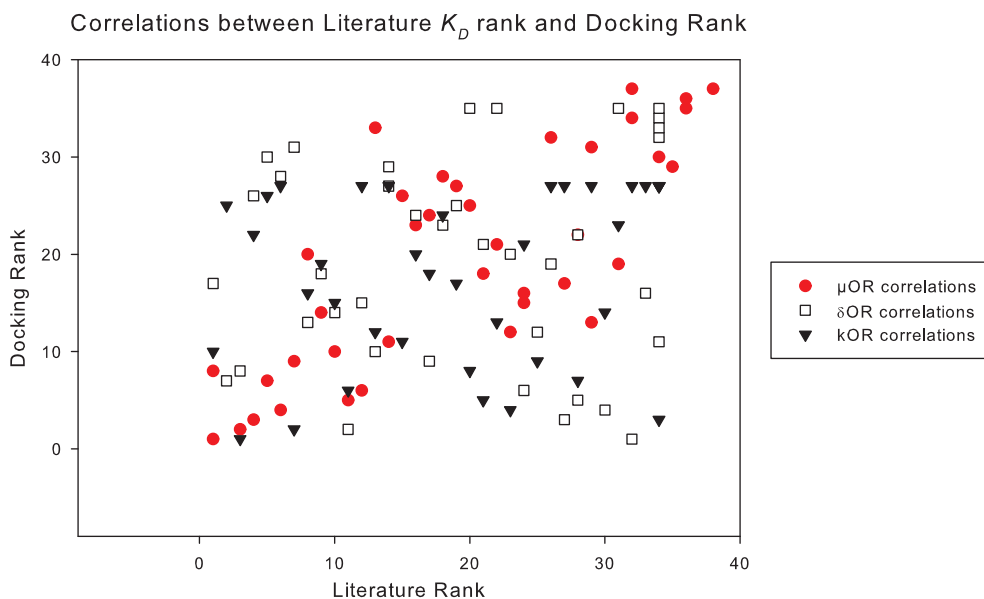


Figure 15. A comparison of the docking Glide score rank against the literature K_D rank. Note the lack of any correlation for both the DOR and KOR. A Spearman rank correlation of 0.77 was calculated for the MOR. Together, these data suggest that subtype selectivity cannot be determined using these crystal structure models.

the opioid receptors due to the vast body of work already done on this class of ligands. Further compounding the issue in this particular case is the requirement of having ligands where K_D 's are known for all the classical opioid receptor subtypes. Again, this data is usually only assessed if the compounds prove to be promising. This lack of data limits the array of compounds that can be used for this sort of study. Due to these limitations, compounds of relatively similar K_D 's were used, potentially limiting the scope of the study.

Various attempts were conducted to optimize this. Varying the boundary box, altering the presence of the "essential" water molecules, and changing force field conditions all failed to give better results. Furthermore, when a flexible docking method was attempted, an overall decrease in Spearman rank correlation was observed. It was thought that a flexible docking method would allow the amino acid sidechains to move in order to accommodate varying ligands. Instead, this method allowed the ligands to be packed into the binding pocket in a variety of poses, rather than adopting more reasonable ones.

2.2 Molecular Dynamics Simulations Attempting to Generate An Agonist Homology Structure

At the time of this work, the crystal structure of an agonist-bound MOR had yet to be described. In an attempt to optimize these models to be more agonist specific, molecular dynamics (MD) simulations were run in an attempt to generate agonist structure homology models. To begin, the structure of the receptor had to be completed, as the crystal structure utilized a fusion protein in order to attain protein crystallization.¹ This T4 lysozyme fusion protein was removed and the IL3 loop rebuilt with the correct sequence (UniProtKB P42866) and minimized. The prototypical opiate morphine was then docked into the MOR using Glide as per the previously described methodology (Chapter 2.1). This structure was then embedded in a membrane and solvated using the molecular dynamics (MD) simulation software DESMOND (D. E. Shaw Research group) (Figure 16). This system was then relaxed using a 1 ns simulation where the protein and ligand were held stationary, allowing the water and lipids to relax. This was followed by another 1 ns simulation where only the ligand and protein backbone were held rigid, allowing the amino acid sidechains to relax. The resulting system was then allowed to simulate for 70 ns.

Following this simulation, snapshots from every 5 ns were taken. The ligand, lipids and water were all removed, leaving only those "essential" water molecules participating in the hydrogen-bonding network. These were then prepared for docking using three different methods; simple preprocessing using standard precision docking, standard protein preparation with standard precision docking, or standard protein preparation with extra precision docking. For the purposes of assessing these snapshots, a training set of compounds was assembled (see Appendix 8.1.2). Specifically, all ligands selected were known agonists or partial agonists of the MOR, with known K_D values across all classical opioid receptors. This is obviously a much stricter set of compounds compared to those used for the initial docking study. However, as we wished to assess whether we could select an agonist pose, it was important to eliminate any known antagonists, or where the pharmacological activity was unclear.

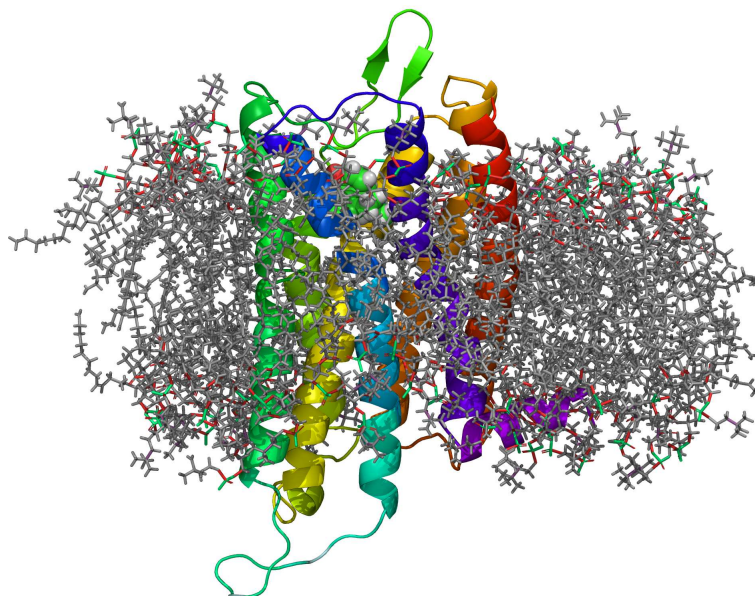


Figure 16. The reconstructed MOR embedded in a membrane ready for an MD simulation. Here, the water and salt molecules have been removed for clarity.

Table 1: Datasets from MD snapshot frame docking. Three different docking methods were utilized; simply preprocessing the receptor as per standard method then docking using standard precision, running the receptor structure through the standard preparation wizard then docking using standard precision, and finally running the structure preparation wizard followed by docking using extra precision. These results were then analyzed using Spearman rank correlation. These results show that docking with the 30 ns snapshot using the extra precision method gave the best Spearman rank correlation using the training set of compounds.

	4DKL	5 ns	10 ns	15 ns	20 ns	25 ns	30 ns	35 ns
Preprocessed	0.50	0.35	0.48	0.36	0.39	0.37	0.48	0.11
Prepwizard	0.60	0.21	0.55	0.34	0.45	0.41	0.67	0.39
Prepwizard XP	0.47	0.46	0.50	0.39	0.30	0.37	0.69	0.43

	40 ns	45 ns	50 ns	55 ns	60 ns	65 ns	70 ns
Preprocessed	0.21	0.29	0.29	0.42	0.31	0.49	0.38
Prepwizard	0.49	0.39	0.15	0.50	0.06	0.55	0.29
Prepwizard XP	0.39	0.20	0.17	0.23	0.36	0.50	0.48

The training compounds were then docked into each receptor using three different preparation methods, after which reasonable poses for each ligand were selected and Spearman rank correlations calculated for each snapshot. These were all compared to the prepared crystal structure. The results are summarized in Table 1. As can be seen, the Spearman rank correlations for the native protein were lower compared to the previous docking study where a mix of antagonists and agonists were used. This may be due to the native antagonist bound structure docking antagonists better than agonists, hence giving a better rank correlation compared to here where only agonists have been used. Overall, using the extra precision docking on the 30 ns model gave the best results, with a Spearman rank correlation of 0.69 (Figure 17). However, using a test set (see Appendix 8.1.3), these results could not be replicated, giving a Spearman rank correlation of -0.50 (Figure 18).

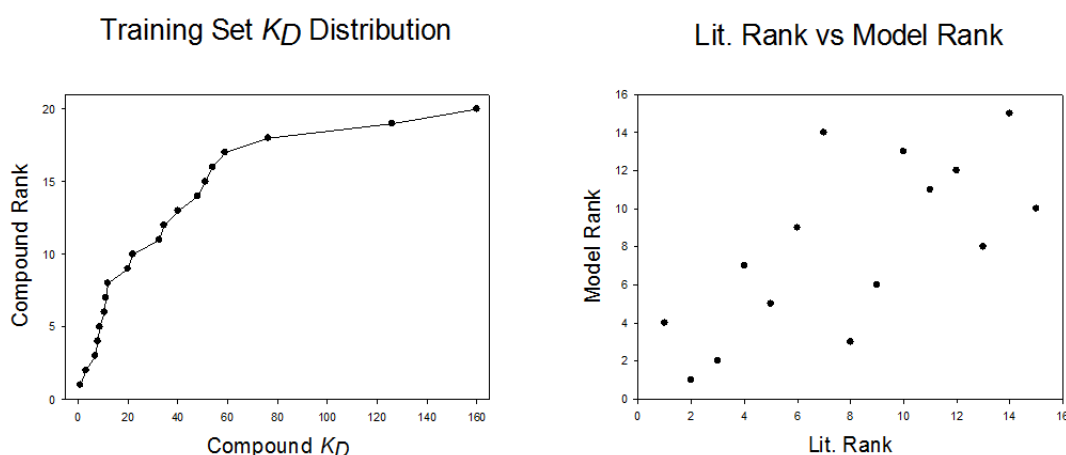


Figure 17. Graphs showing the K_D distribution of the training set compounds (left, K_D 's given in nM), as well a plot comparing the docking vs literature ranking for the 30 ns model (right). Docking of this training set into the model gave a Spearman rank correlation of 0.69.

Although this is a negative result, it is not unexpected. As discussed in Chapter 1.1.1, multiple signalling biases are known for the MOR, giving rise to a variety of pharmacological outcomes. Different ligands may induce varying conformational changes in the receptor, giving rise to these biases. Although ligand biases are known for the more well known clinically used opiates such as morphine,^{4,5} for more novel opioids these are not extensively studied and are therefore unknown. Ideal training and test sets in this case would be composed of compounds

2.2 Molecular Dynamics Simulations Attempting to Generate An Agonist Homology Structure

with known K_D values for all opioid receptors across a range of values, and where the signalling biases are consistent across all compounds. This type of data is unavailable for a variety of reasons. As previously discussed, compounds where the binding data is not promising are generally not further evaluated for binding at other receptor subtypes or for their signalling biases. For these reason the ideal training and test sets could not be assembled, potentially resulting in the negative result observed.

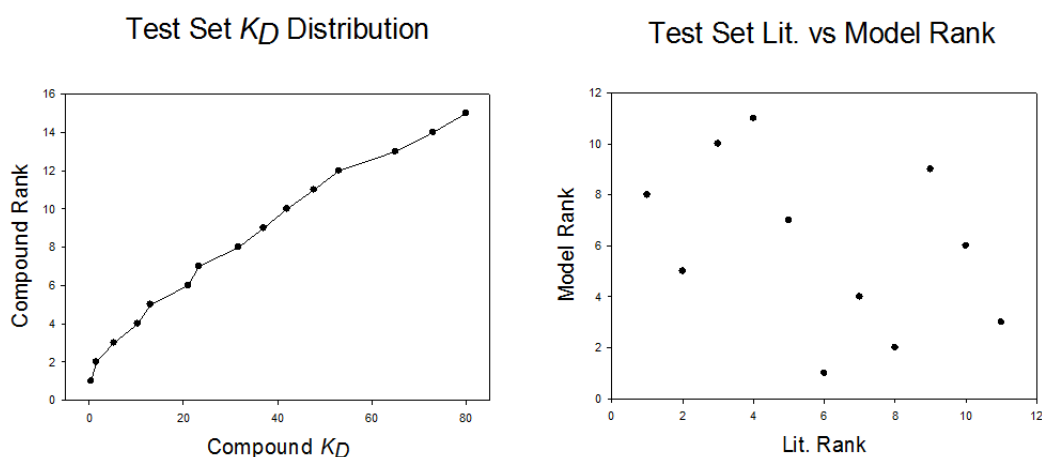


Figure 18. Graphs showing the K_D distribution of the test set compounds (left, K_D 's given in nM), as well a plot comparing the docking vs literature ranking for the 30 ns model (right). Docking of this test set into the model gave a Spearman rank correlation of -0.50. These data suggest that the binding of these ligands to the structures may be highly specific, different ligands may cause a variety of conformational changes, all of which may be active conformers.

Several limitations were inherent with this study. First, the limited simulation time may not have given the system sufficient time to adopt an "agonist" pose. The 70 ns simulation time was chosen as a compromise between giving the system sufficient time to move and a reasonable computer time (roughly 10 days). Furthermore, snapshots were selected at regular intervals. Ideally, smaller intervals could be used, or a statistical method could be used to identify the most diverse range of snapshots that would potentially give the most promising results. The use of an automated script would also increase the likelihood of finding a homology, as this would enable searching of a far larger number of structures throughout the duration of the simulation. However, given the time restraints for this section of the project, these could

not be done. In addition to this, the agonist pose of a GPCR is typically not as stable as the inactive conformation,⁶ and requires accessory proteins to stabilize this conformation. In whole cells, this is accomplished by the association of the G proteins to the intracellular loops and tail. The lack of the necessary accessory proteins throughout the simulation may have also reduced the probability of attaining an agonist pose through this method.

Despite this, several interesting observations were made during MD studies regarding the interactions between morphine and the MOR. First, it was noted that the 3-OH phenol was critical for binding, as it participates in a water mediated hydrogen-bonding network with HIS297, which is similar to the binding observed in the crystal structure. Indeed, it is known that modification of the 3-OH phenol results in loss of binding affinity, as is observed for codeine compared to morphine.⁷ Contrary to the crystal structure where this network is mediated by 2 water molecules, only a single molecule was observed to mediate this particular interaction. While it is unclear why this was the case, it could be that the irreversible antagonist used in the crystal structure necessitated an additional water to bridge the gap to form the required interactions, or the smaller size of morphine allowed it to bury itself deeper into the binding pocket during the MD simulation compared to the static crystal structure. In either case, this observation suggests that ligand-specific water mediated hydrogen-bonding networks may form. The second water molecule now appears to mediate hydrogen-bonding between the 6-OH alcohol, TYR148, and the 3-OH phenol, which was not observed in the crystal structure. Modification at the C-6 position is known to be tolerated. Indeed, heterocodeine, where the 6-OH is methylated rather than the 3-OH in codeine, actually has a higher affinity for the MOR compared to morphine,⁷ suggesting the 6-OH acts primarily as a hydrogen-bond acceptor rather than as a donor. Why this second water molecule has "moved" from the HIS297 hydrogen-bonding network to form a secondary network with TYR148 is unclear, but may be due to the unrestrained nature of morphine allowing it to bury itself deeper into the binding pocket.

Throughout the MD simulation, it was observed that the first water molecule mediating hydrogen-bonds to HIS297 was retained and remained relatively static throughout the simulation time. The second water molecule mediating hydrogen-bonds to TYR148 was observed to

exchange with the bulk solvent. However, another water molecule would always take the same position and form the same hydrogen-bonds. These data suggest that although water mediated hydrogen-bonding is important, second water molecule is exchangeable and may play a lesser role in holding the ligand in place. The salt bridge between the tertiary amine of morphine and ASP147 appeared to be a critical interaction. The ligand appeared to rotate around this critical interaction with the correct bonding geometry being maintained throughout. Indeed, it is known that modification of this tertiary amine has a significant impact on binding affinity, and almost all opioids contain an ionizable amine specifically for ionic interactions with ASP147.

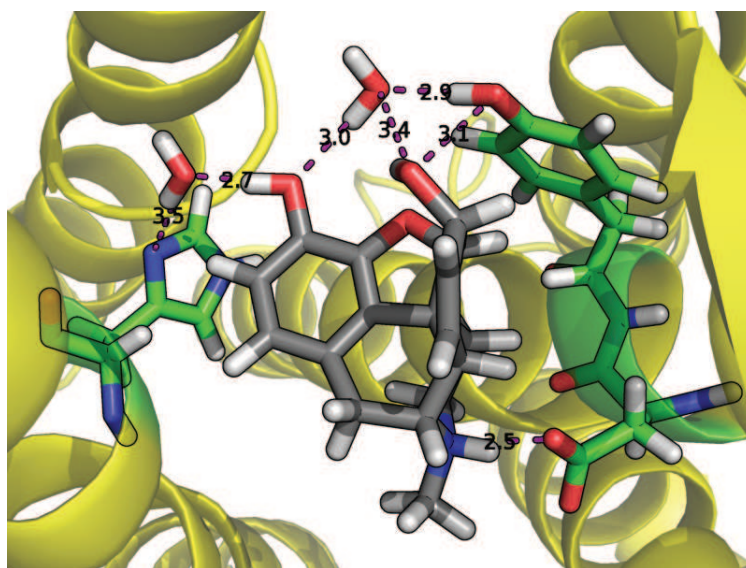


Figure 19. Morphine at the 30 ns snapshot of the MD simulation. Distances are given in Å. Note the two water molecules that are involved in the hydrogen-bonding network. The first water molecule mediating hydrogen-bonding between the 3-OH and HIS297 does not leave the binding pocket throughout the duration of the MD simulation. The second water molecule mediating hydrogen-bonding between the 6-OH and TYR148 is more labile and exchanges with the bulk solvent. Also note the salt bridge formed between the tertiary amine and ASP147, which was observed to be a critical interaction.

2.2.1 Comparison of Generated Agonist Model with Published Structures

Following this work, an agonist-bound crystal structure was published bound to the agonist BU72, an orvinol-based opioid.⁶ This was achieved by stabilizing the agonist conformation using antibody fragments derived from immunization of llamas with purified MOR bound to

the peptide agonist DALDA. Comparison between the antagonist bound structure (4DKL¹), the agonist bound structure (5C1M⁶) and the 30 ns simulation structure could now be done. Again, these are imperfect structures due to the artificial nature of protein crystallization. In the case of the antagonist bound structure 4DKL, a fusion protein had to be used, whilst in the case of the agonist bound structure 5C1M an antibody fragment was used to artificially stabilize a selected agonist pose. However, these structures provide an interesting glimpse into at least one potential active conformation of the receptor.

Overlay of the three structures provides some insight (Figure 20). Many of the comparisons between the antagonist and agonist bound structures have already been extensively discussed by Huang *et al.* in their publication.⁶ The intracellular face of TM6 is displaced about 10 Å into the membrane compared to the antagonist bound structure. Other subtle deviations are also observed, however the actual binding pocket appears to be maintained between all three structures presented. Perhaps the most enlightening observation is that helices of the MD model are still positioned quite similarly to the antagonist bound structure, reinforcing the idea that the 70 ns simulation time was insufficient to generate an agonist homology and that accessory proteins may be required to stabilize the active conformation.

2.3 Conclusion

Throughout this work, it was found that subtype selectivity was difficult to ascertain based solely on the available crystal structures. The docking studies utilizing the antagonist bound crystal structures of the MOR, DOR and KOR failed to correctly rank compounds based on their affinity for each of the receptors. No correlation between the docking rank and literature K_D rank was observed for the DOR and KOR, while a Spearman rank correlation of 0.77 was found for the MOR using a mixed set of agonists and antagonists. Further optimization of the docking method did not improve results.

In addition to this, MD simulations were performed using DESMOND with morphine as the ligand. Although these simulations failed to generate an agonist homology as hoped, it still offered some interesting insights into the binding of morphine to the MOR. The critical water

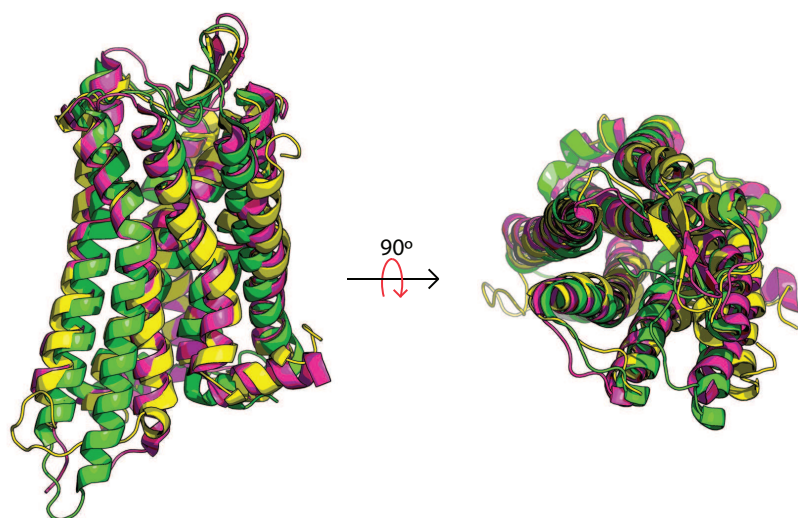


Figure 20. Overlay of the antagonist bound (magenta), agonist bound (green) and 30 ns MD models (yellow). Note the similarity between all three structures in the actual binding pocket. The greatest change in conformation is observed on transmembrane helix 6 (TM6). In the agonist bound structure, the intracellular end of this helix is displaced 10 Å into the membrane compared to the antagonist bound structure. Subtle changes in the overall structures between all three structures are also evident.

mediated hydrogen-bonding network was maintained throughout the simulation. Furthermore, it was found that of the two water molecules, only the one mediating hydrogen-bonding between the 3-OH phenol and HIS297 was critical and remained stationary. The water mediating hydrogen-bonding between the 6-OH alcohol and TYR148 was exchangeable with the bulk solvent.

The data gathered from these modelling studies assisted in the design of our fluorescent morphine conjugates. All the data gathered suggests that the C-6 position is an ideal position for functionalization and attachment of synthetic handles for conjugation to fluorescent tags. Furthermore, the inclusion of a hydrogen-bond accepting group at this position was critical in order to maintain the water-mediated hydrogen-bonding network observed in the simulations. No modifications could be made to the C-3 phenol as it disrupted this network. Maintaining this network was critical, as a probe simulating the behavior of morphine as closely as possible was desired. The introduction of a linking group at the C-6 position could be achieved by derivatization of the native secondary alcohol to groups such as esters, amides or ethers, followed

by an appropriate spacer to distance the active morphine pharmacophore from the fluorescent tag.

2.4 Experimental

Docking Procedure

All ligands used were build using the Schrödinger Maestro package and minimized using the MMFFs forcefield. Reasonable tautomeric and protonated states were generated manually for each ligand where necessary.

The receptor structures (PDB or generated) were prepared by removing any excess lipids, accessory proteins, salts and water molecules that were deemed to be unimportant. Those water molecules deemed to be important for the formation of water-mediated hydrogen-bonding networks were left in the structure. A Glide grid of 10 Å was generated using default settings. The prepared ligands were docked into the grid, allowing for ring conformations. 20k poses were calculated for each ligand tautomeric and protonated state, and the top 40 poses were written. For each ligand, all poses were manually inspected, and the top pose for each ligand selected, with only one tautomeric/protonated state selected. These were then analyzed using the required statistical technique.

Molecular Dynamics Simulation

Morphine was docked into the PDB structure 4DKL using the previously described method.¹ The loops were rebuilt using the UniProtKB literature sequence P42866 and minimized using the MMFFs forcefield. The resulting structure was placed into a lipid membrane using the default settings of the MD software DESMOND (D. E. Shaw Research Group) and solvated using TIP3P water with a physiological pH salt concentrations. The protein and ligand were restrained and a 1 ns MD simulation run to relax the lipid and water molecules. The final state of this simulation was taken, the protein backbone and ligand restrained and again subjected to a 1 ns MD simulation to relax the amino acid sidechains. The final state of this relaxation simultaion was taken and a fully unrestrained simulation was run for the requisite time (70 ns). The structures generated were then used for further analysis.

References

- (1) Manglik, A., Kruse, A. C., Kobilka, T. S., Thian, F. S., Mathiesen, J. M., Sunahara, R. K., Pardo, L., Weis, W. I., Kobilka, B. K., and Granier, S., (2012). Crystal structure of the μ -opioid receptor bound to a morphinan antagonist. *Nature* *485*, 321–326.
- (2) Granier, S., Manglik, A., Kruse, A. C., Kobilka, T. S., Thian, F. S., Weis, W. I., and Kobilka, B. K., (2012). Structure of the δ -opioid receptor bound to naltrindole. *Nature* *485*, 400–404.
- (3) Wu, H., Wacker, D., Mileni, M., Katritch, V., Han, G. W., Vardy, E., Liu, W., Thompson, A. A., Huang, X.-P., Carroll, F. I., Mascarella, S. W., Westkaemper, R. B., Mosier, P. D., Roth, B. L., Cherezov, V., and Stevens, R. C., (2012). Structure of the human κ -opioid receptor in complex with JDTic. *Nature* *485*, 327–332.
- (4) Thompson, G. L., Lane, J. R., Coudrat, T., Sexton, P. M., Christopoulos, A., and Canals, M., (2015). Biased agonism of endogenous opioid peptides at the μ -opioid receptor. *Mol. Pharmacol.* *88*, 335–346.
- (5) Thompson, G. L., Lane, J. R., Coudrat, T., Sexton, P. M., Christopoulos, A., and Canals, M., (2016). Systematic analysis of factors influencing observations of biased agonism at the mu-opioid receptor. *Biochem. Pharmacol.* *113*, 70–87.
- (6) Huang, W., Manglik, A., Venkatakrisnan, A. J., Laeremans, T., Feinberg, E. N., Sanborn, A. L., Kato, H. E., Livingston, K. E., Thorsen, T. S., Kling, R. C., Granier, S., Gmeiner, P., Husbands, S. M., Traynor, J. R., Weis, W. I., Steyaert, J., Dror, R. O., and Kobilka, B. K., (2015). Structural insights into μ -opioid receptor activation. *Nature* *524*, 315–321.
- (7) Cunningham, C. W., Mercer, S. L., Hassan, H. E., Traynor, J. R., Eddington, N. D., and Coop, A., (2008). Opioids and efflux transporters. Part 2: P-Glycoprotein substrate activity of 3- and 6-substituted morphine analogs. *J. Med. Chem.* *51*, 2316–2320.

3 Fluorescent Opioid Partial Agonist Probes for the μ -Opioid Receptor

3.1 Morphine-based Fluorescent Probes, Paper Context

Although our ultimate goal was to produce nanoparticle-based probes for the MOR, we first decided to address the lack of small molecule fluorescent agonist probes for the MOR. Not only would this fill a significant gap in the literature, it would also form the foundation for all further work in trying to produce the desired nanoparticle-based probe. Furthermore, we envisioned that these compounds could act as a "control" system, as small molecule fluorescent probes have been used in the characterization of other receptor systems with success.¹⁻⁵ We anticipated that initial characterization of the MOR could be done using small molecule fluorescent probes, which we could then follow up with our nanoparticle-based system. The results could then be compared to reveal any similarities or differences and the validity of our novel imaging approach.

For our purposes, the partial agonist morphine was selected as our targeting ligand as its pharmacology is of particular interest due to its wide use as a clinical analgesic. Furthermore, this enabled focus on the design of the conjugation method rather than the ligand itself, as the structure-activity relationships of morphine are relatively well understood. Using the modelling data presented in Chapter 2, various conjugation designs based on the proposed ester, amide and ether linkage methods were synthesized and assessed. The following work describes our efforts in the design and synthesis of morphine-based fluorescent agonist probes for the MOR, as well as their initial characterization in MOR-expressing HEK293 cells.

3.2 Fluorescently Labelled Morphine Derivatives for Bioimaging (Paper)

Raymond Lam^{†,§}, Arisbel B. Gondin^{‡,#}, Meritxell Canals[‡], Barrie Kellam[§], Stephen J. Briddon[#], Bim Graham[†], Peter J. Scammells^{*,†}

[†] Medicinal Chemistry and [‡] Drug Discovery Biology, Monash Institute of Pharmaceutical Sciences, Monash University, Parkville, Victoria 3052, Australia.

Email:Peter.Scammells@monash.edu

[§] School of Pharmacy, Centre for Biomolecular Sciences, University of Nottingham, Nottingham NG7 2RD, U.K.

[#] Cell Signalling Research Group, School of Life Sciences, Queen's Medical Centre, University of Nottingham, NG7 2UH, U.K.

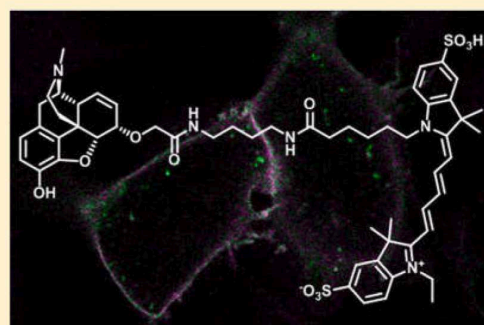
This work was conducted in collaboration with Arisbel B. Gondin and Dr Meritxell Canals of the Monash Institute of Pharmaceutical Sciences, Drug Discovery Biology. Arisbel, who is also part of the Monash-Nottingham Joint Doctoral Training Program, performed the imaging experiments at Queen's Medical Centre at the University of Nottingham. Dr Meritxell Canals performed the CAMYEL BRET assays which were used to assess compound activity.

Fluorescently Labeled Morphine Derivatives for Bioimaging Studies

Raymond Lam,^{†,§} Arisbel B. Gondin,^{‡,#} Meritxell Canals,[‡] Barrie Kellam,[§] Stephen J. Briddon,[#] Bim Graham,[†] and Peter J. Scammells^{*,†,¶}[†]Medicinal Chemistry and [‡]Drug Discovery Biology, Monash Institute of Pharmaceutical Sciences, Monash University, Parkville, Victoria 3052, Australia[§]School of Pharmacy, Centre for Biomolecular Sciences, University of Nottingham, Nottingham NG7 2RD, U.K.[#]Cell Signalling Research Group, School of Life Sciences, Queen's Medical Centre, University of Nottingham, Nottingham NG7 2UH, U.K.

Supporting Information

ABSTRACT: Opioids, like morphine, are the mainstay analgesics for the treatment and control of pain. Despite this, they often exhibit severe side effects that limit dose; patients often become tolerant and dependent on these drugs, which remains a major health concern. The analgesic actions of opioids are primarily mediated via the μ -opioid receptor, a member of the G protein-coupled receptor superfamily. Thus far, development of small molecule fluorescent ligands for this receptor has resulted in antagonists, somewhat limiting the use of these probes. Herein, we describe our work on the development of a small molecule fluorescent probe based on the clinically used opiate morphine and initial characterization of its behavior in cell-based assays.



INTRODUCTION

Opioids represent a useful class of drugs for the control and management of pain. Morphine and codeine, the active ingredients in opium from the plant *Papaver somniferum*, have been used for this purpose since early history.¹ More recently, semi-synthetic opioids such as oxycodone have also become important therapeutic agents. Semi-synthetic opioid antagonists such as naloxone and naltrexone are also important therapeutics used to treat opioid overdose. Despite their clinical effectiveness, opioid agonists suffer from significant drawbacks; dose-limiting side effects such as constipation, sedation, and respiratory depression are common.¹ In addition to this, opioid drugs tend to be addictive and require higher doses as the patient develops a tolerance for them, further compounding the problem. In the United States alone, the CDC reported that opioid related deaths accounted for 61% of drug overdose related deaths between 2010 and 2015.² Furthermore, the number of incidents has increased dramatically, with death rates tripling during this period compared to 1999.

Opioids act via the three opioid receptor subtypes, namely the μ , κ , and δ opioid receptors (MOR, KOR, and DOR respectively). The more recently discovered nociception/orphanin FQ peptide receptor (NOPr) is another member of the opioid receptor family but does not bind these clinically used morphinan opioids.³ Herein, we will only discuss the MOR, as this receptor is the primary target of the most commonly used analgesics⁴ and therefore holds significant clinical interest for the development of future analgesics.

Binding of an agonist to MOR typically activates $G_{i/o}$ proteins, resulting in inhibition of adenylate cyclase and therefore a reduction in cyclic adenosine monophosphate (cAMP) levels.¹ This results in an influx of K^+ via G protein-mediated K^+ channels, causing neuron hyperpolarization and blockade of voltage-gated Ca^{2+} channels.⁵ Hyperpolarization reduces firing potential, and therefore blockade of pain signaling, giving opioids their analgesic effects. Upon prolonged activation, β -arrestin 2 recruitment to the MOR terminates signaling and induces internalization of the receptor.

However, not all opioids recruit arrestin and internalize with the same efficacy and, indeed, β -arrestin biased ligands have been discovered which give different pharmacological outcomes.⁶ The prototypical opiate morphine causes very little β -arrestin 2 recruitment following MOR receptor activation while also inducing significant dependence and tolerance in the patient.⁷ Herkinorin, like morphine, also provides analgesia with little β -arrestin 2 recruitment but shows very low dependence and tolerance liabilities in animal models.⁸ DAMGO, a peptidic agonist, induces β -arrestin 2 recruitment while having reduced dependence and tolerance liabilities.⁷ PZM21, a more recent example, appears to be biased toward G_i signaling, lacking any significant β -arrestin 2 recruitment.⁶ Analgesia in mice has been demonstrated with fewer side effects compared to morphine. Just from these few examples, it can be seen that different agonists have different pharmacological

Received: December 10, 2017

Published: January 1, 2018

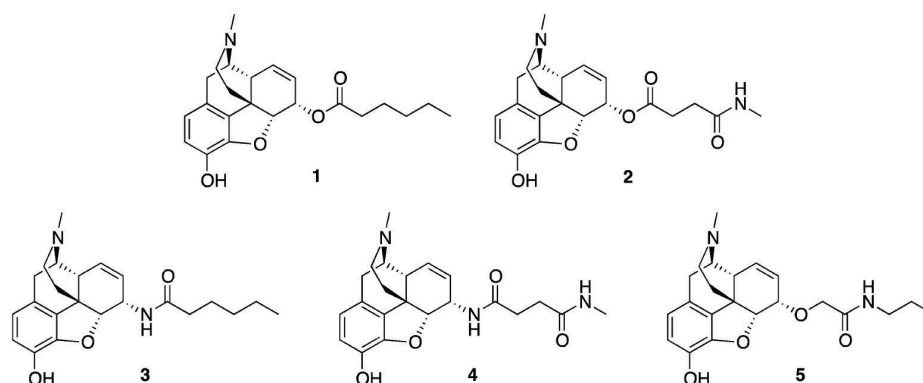
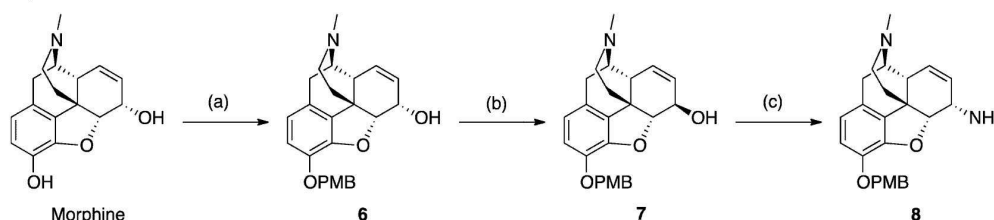


Figure 1. Precongengers synthesized for assessing linker suitability. Note preservation of the C-6 stereocenter.

Scheme 1. Synthesis of C-6 Position Amine^a



^aReagents and conditions: (a) 3 M KOH in MeOH, PMB-Cl, DMF, RT, 4 h, 46%; (b) (i) benzoic acid, PPh₃, DIAD, toluene, 0 °C to RT, 4 h, (ii) 1:1 EtOH/1 M KOH, reflux, 20 min, 78%; (c) (i) phthalimide, PPh₃, DIAD, toluene, 0 °C to RT, 4 h, (ii) EtOH, N₂H₄·H₂O, reflux, 1 h, 34%.

outcomes despite all acting at MOR. Furthermore, Bohn et al. have demonstrated that tolerance and dependence are not necessarily correlated, as β -arrestin 2 knockout mice still develop a dependence toward morphine but lack the expected tolerance.⁹

Understanding the mechanisms behind the different abilities of opioid ligands to promote arrestin recruitment and regulate receptor signaling poses a significant challenge. The development of fluorescent ligands to visualize G protein-coupled receptors (GPCRs) in live cells represents a major advantage that circumvents the use of recombinant cells and allows the study of these receptors in natively expressing systems. One of the earliest examples of a fluorescent opioid is described by Fournie-Zaluski et al., in which enkephalins were conjugated to a fluorescent dansyl sulfonyl group.¹⁰ This particular ligand has seen limited use, perhaps due to the UV excitation maximum and poor quantum yield of the dansyl sulfonyl group not being particularly suitable to modern live cell imaging techniques. The same was true of probes described by Mihara et al., who conjugated enkephalins to the fluorophore L-1-pyrenylalanine.¹¹ In both cases, introduction of the fluorescent moiety resulted in a reduction in binding affinity compared to the native ligand. More recent variants of these peptidic conjugates have been described by Arttamangkul et al. using more modern fluorophores.¹² These new fluorescent ligands have been used to study MOR internalization, desensitization, and recycling.^{13–15}

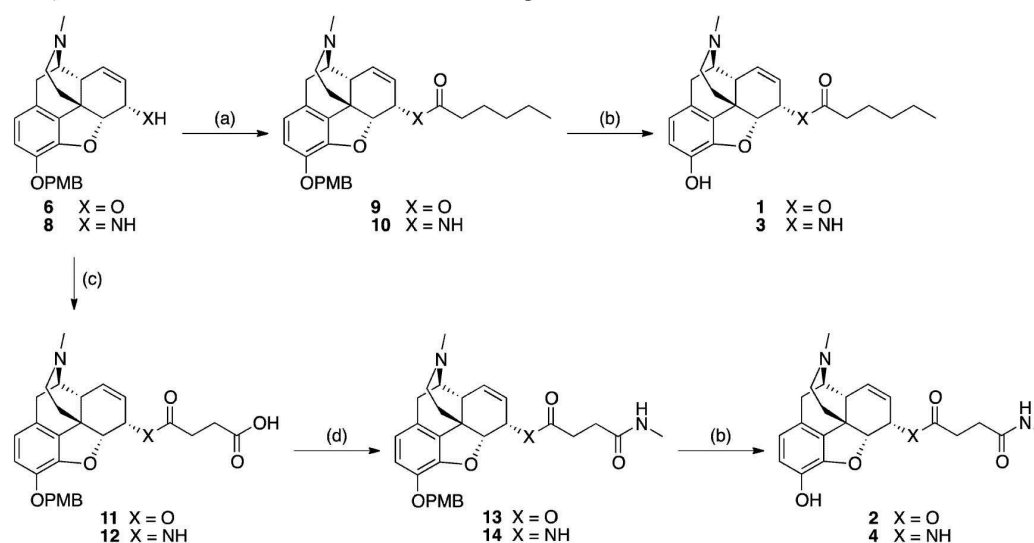
Small molecule fluorescent opioids have also been described. Kolb et al. described the synthesis of several fluorescent antagonists based on naloxone and naltrexone.¹⁶ Another opioid probe bearing a 7-nitrobenzo-2-oxa-1,3-diazole fluorescent label was described by Archer et al.,¹⁷ quickly followed

by another example from Emmerson et al.¹⁸ Most recently, Schembri et al. synthesized a series of orvinols based on the buprenorphine scaffold and conjugated them to a range of fluorophores.¹⁹ However, in all of these cases, the fluorescent probes described were antagonists. Although fluorescent antagonists are still useful to visualize receptors at the plasma membrane and to assess receptor binding, by definition, they do not allow the study of events that follow receptor activation. Herein, we describe our work on the synthesis and evaluation of small molecule fluorescent opioid partial agonists.

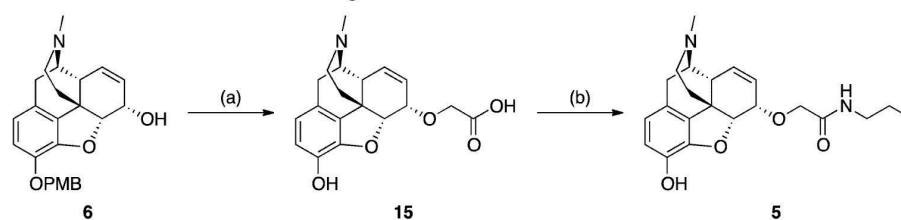
RESULTS

Model Morphine Congeners. Our aim was to develop fluorescent derivatives of morphine, as this clinically used drug is of particular interest. The C-6 position was chosen as our linking point, as the body of prior literature suggests that modifications at this point have minimal effect on ligand activity compared to alternative positions.^{20,21} To assess whether our linking modifications would affect ligand activity, we first assessed the proposed structural modifications. To this end, we designed and synthesized model compounds comprising the targeting ligand with short chain linker modifications. Several linking methods were proposed, and these model compounds are illustrated in Figure 1. Importantly, these compounds and their syntheses were designed such that the C-6 stereocenter would be preserved as the native *S* configuration.

Synthesis of our model compounds employed morphine as the starting material. This approach necessitated initial protection of the C-3 phenol, for which we chose the *para*-methoxybenzyl (PMB) group, and this was installed in modest yield to afford **6** (Scheme 1). This material formed the basis for all further synthetic manipulations.

Scheme 2. Synthesis of C-6 Position Ester and Amide Precongeners^a

^aReagents and conditions: (a) hexanoyl chloride, pyridine, 70 °C, 18 h, 49–80%; (b) triethylsilane, TFA, DCM, RT, 20 min, 16–39%; (c) succinic anhydride, DMAP, TEA, MeCN, 65 °C, 16 h, 28–77%; (d) EDC·HCl, HOBt, TEA, methylamine (2 M in THF), MeCN or DMF, RT, 3 h, 63–84%.

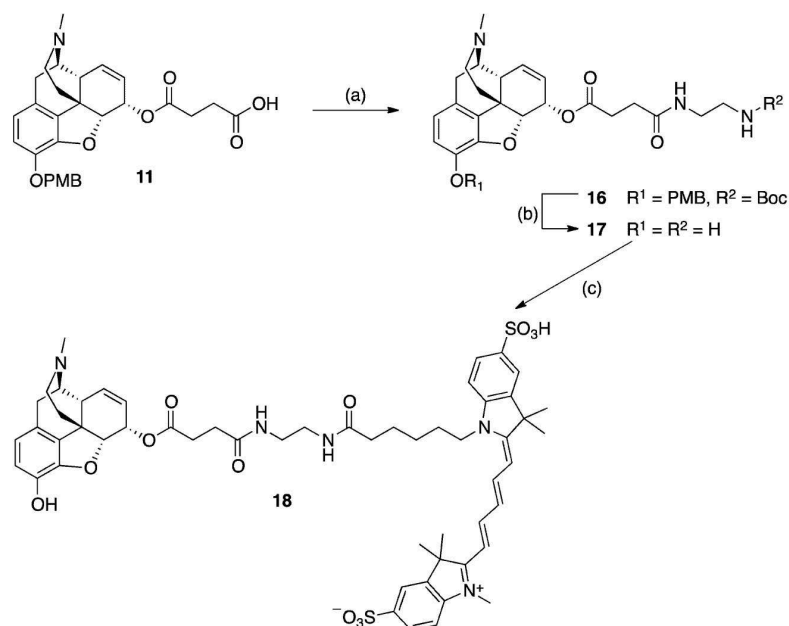
Scheme 3. Synthesis of C-6 Position Ether Precongener^a

^aReagents and conditions: (a) (i) NaH, *tert*-butyl bromoacetate, THF, 0 °C to RT, 1 h, (ii) triethylsilane, TFA, DCM, RT, 1 h, 58%; (b) HCTU, TEA, propylamine, DMF, RT, 19 h, 17%.

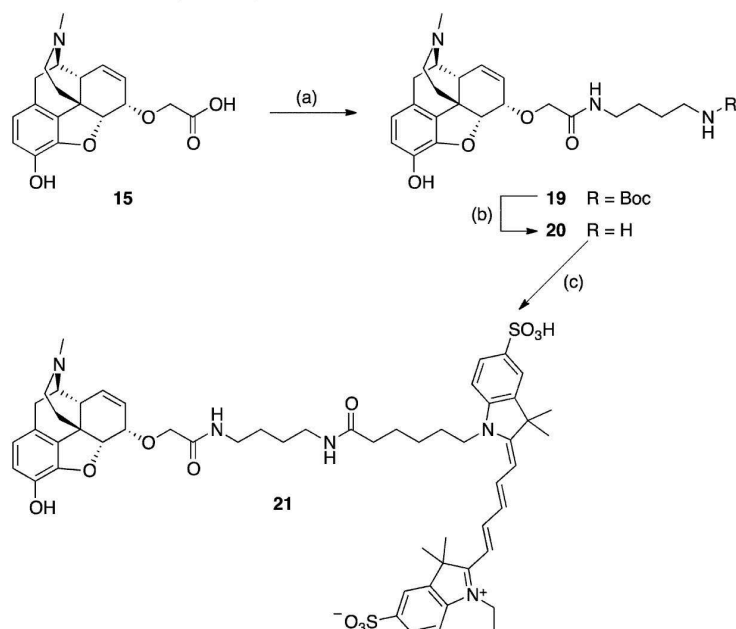
Table 1. pEC_{50} of Model Compounds As Assessed in a cAMP CAMYEL BRET Assay against hMOR

Cpd	6-Substituent	$pEC_{50} \pm SEM^a$	Relative potency ^b	$E_{max} \pm SEM^{a,c}$	Relative efficacy ^d
Morphine	-OH	7.07 ± 0.13	-	35.7 ± 1.7	-
1		6.46 ± 0.11	0.24	37.1 ± 1.9	1.04
2		6.45 ± 0.11	0.24	28.6 ± 1.4	0.80
3		5.98 ± 0.11	0.08	28.9 ± 1.9	0.81
4		5.35 ± 0.71	0.02	23.3 ± 11.7	0.65
5		6.81 ± 0.14	0.55	37.5 ± 2.4	1.05

^aResults presented are the average of 3 independent experiments. ^bRelative to morphine. Relative potency was calculated by dividing $EC_{50}(\text{morphine})$ by $EC_{50}(\text{compound})$. ^c E_{max} is the % inhibition of Forskolin-induced cAMP. ^dRelative to morphine. Relative efficacy was calculated by dividing $E_{max}(\text{compound})$ by $E_{max}(\text{morphine})$.

Scheme 4. Synthesis of Ester Linked Morphine-Cy5 Probe 18^a

^aReagents and conditions: (a) *N*-Boc-diaminoethane, HCTU, TEA, DMF, RT, 19 h, 83%; (b) triethylsilane, TFA, DCM, RT, 1 h, 51%; (c) sulfo-Cy5 NHS ester (Lumiprobe), HCTU, TEA, DMF, RT, 21 h, 33%.

Scheme 5. Synthesis of Ether Linked Morphine-Cy5 Probe 21^a

^aReagents and conditions: (a) *N*-Boc-diaminobutane, EDC-HCl, HOBT, TEA, DMF, RT, 17 h, 36%; (b) TFA, CHCl₃, RT, 1 h, quantitative; (c) sulfo-Cy5, HCTU, TEA, DMF, RT, 18 h, 40%.

An amine moiety was subsequently introduced into the 6-position to provide a point of attachment which retains the capacity to act as a hydrogen bond donor as per the 6-OH of morphine after the linker has been attached. As we also wished to maintain the native stereochemistry of the C-6 position, a

double Mitsunobu approach was employed to install this amine, noting that the Mitsunobu reaction has previously been reported to invert this stereocenter in closely related opiates.^{22–25} Accordingly, 6-OH was first inverted using benzoic acid under Mitsunobu conditions followed by

saponification of the resultant ester to give the 6-isomorphine derivative **7**. A comparison of the NMR spectra of compounds **6** and **7** (Supporting Information, Figure S1) demonstrated stereospecific inversion of this chiral center. Compound **7** was subsequently converted to the desired *S*-stereoisomer via a phthalimide promoted Mitsunobu reaction. Treatment of the phthalimide group with hydrazine hydrate afforded **8**, allowing for linking and elongation to the desired model compounds (Scheme 1).

Two different approaches for ester and amide conjugation were trialed. The first, using an acid chloride, yielded compounds **1** and **3** following phenolic deprotection (Scheme 2). Fluorophore conjugation via acyl chloride chemistry is not a viable synthetic strategy, and we therefore designed a method which would facilitate milder reaction conditions. Ring opening of succinic anhydride via the C-6 amine or alcohol provided a convenient handle for further elongation and subsequent fluorophore conjugation under milder conditions. Methylamine capping of this handle, followed by phenolic deprotection, gave model compounds **2** and **4** (Scheme 2).

As an alternative linking method, an ether linker was also proposed. Using *tert*-butyl bromoacetate to give the C-6 ether, followed by global deprotection, gave **15**, again possessing a convenient handle for further linker elongation. This handle was capped with propylamine to provide the final model amide **5** (Scheme 3).

Model compounds were functionally assessed and compared to morphine using a bioluminescence resonance energy transfer (BRET)-based cAMP sensor using YFP-Epac-RLuc assay (CAMYEL) in HEK293 cells expressing the human MOR (hMOR) and normalized against forskolin (Table 1). All compounds were less potent than morphine, however the ester linked model compounds (**1** and **2**) maintained potencies in the mid nM range, while the amide-linked model compounds (**3** and **4**) showed a significant loss in potency beyond the μ M range. The ether linked model compound **5**, however, maintained the same level of maximum activity and was the most potent model congener.

Morphine-Cy5 Conjugates. We then proceeded to synthesize two fluorescent probes based on linker designs **2** and **5**. Sulfo-Cy5 was chosen as the fluorescent tag, as previous work by Schembri et al. suggested that this particular fluorophore had the least potential for inducing nonspecific binding to the cell membrane.¹⁹ The functional handles on **11** and **15** were elongated with a simple Boc-protected diamine chain, followed by global deprotection and chemoselective conjugation to sulfo-Cy5 to give the final fluorescent morphine probes **18** and **21** (Schemes 4 and 5, respectively). In the case of **18**, the coupling reaction with sulfo-Cy5 NHS ester failed to proceed to completion after 7 h. As it was thought this may have resulted from the hydrolysis of the NHS ester to the corresponding carboxylic acid, HCTU was added to drive the reaction to completion (Scheme 4). In the case of **21**, sulfo-Cy5 free acid was used in place of the NHS ester and was installed under standard HCTU coupling conditions (Scheme 5).

Functional assessment of **18** and **21** was conducted in the same manner as the model conjugates (Table 2). Although both sulfo-Cy5 derivatives were still able to activate MOR with potencies in the nM range, they showed a significant loss of efficacy (E_{max}). This loss in activity is consistent with previous literature compounds, where attachment of a fluorescent tag typically results in decreased activity.^{12,26} A comparison with DAMGO in the same assay revealed that **21** clearly behaves as a

Table 2. pEC_{50} Assessment of Morphine-Cy5 Probes

probe	$pEC_{50} \pm SEM^a$	relative potency ^b	$E_{max} \pm SEM^{a,c}$	relative efficacy ^d
morphine	7.07 ± 0.13		35.7 ± 1.7	
18	7.34 ± 0.37	1.85	10.7 ± 1.2	0.30
21	6.30 ± 0.44	0.17	15.0 ± 3.2	0.42

^aResults presented are the average of 3 independent experiments. ^bRelative to morphine. Relative potency was calculated by dividing $EC_{50}(\text{morphine})$ by $EC_{50}(\text{compound})$. ^c E_{max} is the % inhibition of forskolin-induced cAMP. ^dRelative to morphine. Relative efficacy was calculated by dividing $E_{max}(\text{compound})$ by $E_{max}(\text{morphine})$.

partial agonist, albeit with a lower efficacy compared to the parent compound morphine (Figure 2).

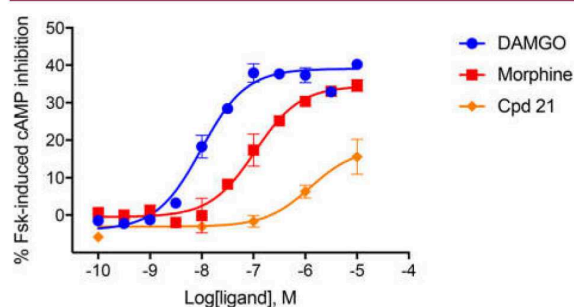


Figure 2. CAMYEL assay comparing DAMGO, morphine and **21**. The probe compound **21** is clearly a partial agonist compared to the full agonist DAMGO. Morphine is known to be a partial agonist but may give differing levels of efficacy depending on the assay used. Results for DAMGO and morphine are consistent with those previously reported.^{27,28} Results presented are an average of 3 independent experiments, with error bars representing SEM.

We then assessed whether compounds **18** and **21** were suitable for receptor visualization using confocal microscopy. Initial experiments were conducted to determine whether **18** and **21** bound specifically to the MOR. HEK293 stably expressing SNAP-tagged hMOR (SNAP-hMOR) were pre-incubated with cell impermeable SNAP-Surface 488 (BG-488, New England BioLabs, Figure 3) to label the cell surface

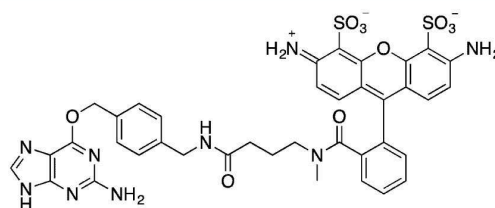


Figure 3. SNAP-Surface 488 (New England BioLabs), a cell impermeable dye targeted to the SNAP domain of SNAP-tagged receptors. This dye enables exclusive labeling of cell surface receptor populations.

SNAP-hMOR, then incubated in the presence or absence of the antagonist naloxone and before exposure to the fluorescent probes. Despite having a higher apparent pEC_{50} value, **18** showed no specific binding to the cell surface receptor population (Figure 4A). On the other hand, **21** was observed to localize at the surface of cells expressing SNAP-hMOR

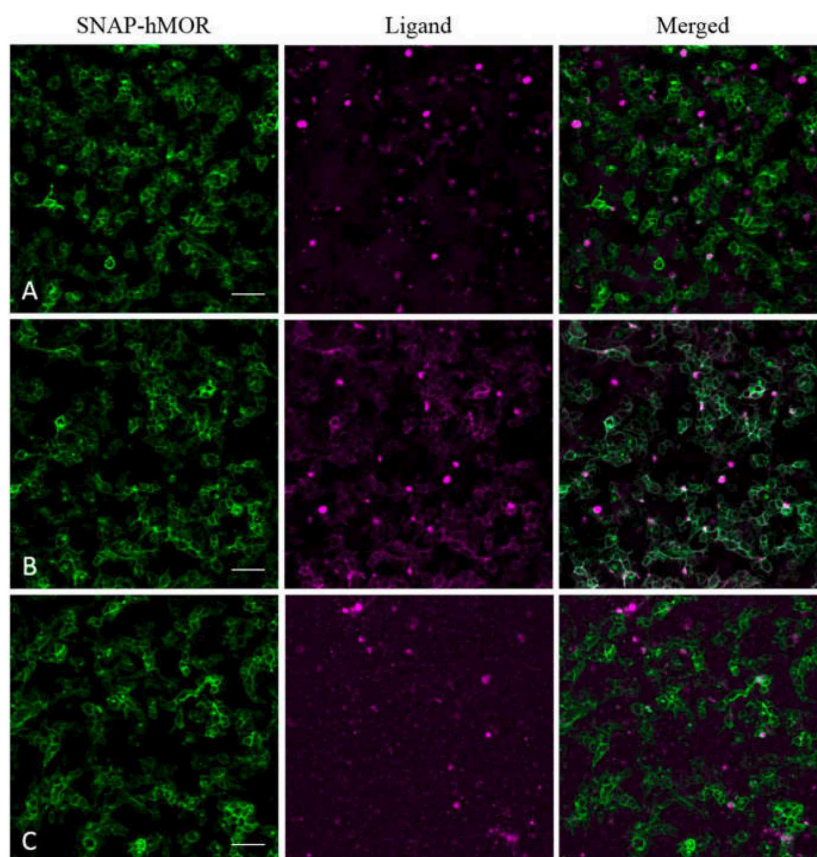


Figure 4. Initial high-content imaging of probes with HEK293 cells expressing SNAP-hMOR. Images are representative of 3 independent experiments. (A) **18** at $3\ \mu\text{M}$, no specific binding of the probe to the cell surface was observed. (B) **21** at $1\ \mu\text{M}$, binding of the probe to the cell surface was observed. (C) **21** at $1\ \mu\text{M}$ preincubated with naloxone ($1\ \mu\text{M}$, 30 min, $37\ ^\circ\text{C}$), complete blockade of probe binding was observed. Scale bars, $50\ \mu\text{m}$.

(Figure 4B). **21** binding was abolished by preincubation with naloxone (Figure 4C).

Having demonstrated that **21** could be used to visualize specific binding to the MOR on HEK293 cell membranes, this probe was selected for subsequent study. In HEK293 cells stably expressing SNAP-hMOR and preincubated with BG-488, it was found that **21** co-localized with SNAP-hMOR predominantly on the cell membrane (Figure 5A,B), which was prevented by preincubation with naloxone, confirming the membrane binding of **21** was to the hMOR (Figure 5C). The bulk of the co-localized fluorescence remained at the cell surface. Although some co-localized signals within the cells were present, the signal from intracellular compartments was very weak compared to that at the plasma membrane. These data are in keeping with literature data, which suggests that morphine only poorly induces internalization of the receptor–ligand complex.⁷ Because incubation with BG-488 only labels cell surface populations of SNAP-hMOR, any internalized receptor population must therefore have previously been on the cell surface. In keeping with prior literature, it was found that a wash step removed bound ligand (Figure 5D).¹⁹ This is consistent with the fast k_{off} rate of nonpeptide opioids and the known fast k_{off} rate of morphine, so this behavior is not unexpected. In any case, a wash step is typically not included in confocal microscopy experiments, particularly where there is no

significant background from extracellular ligand, as in this case.^{19,29–31}

In the previous experiments, the EC_{50} concentration of $500\ \text{nM}$ was used, thus we wanted to assess the behavior of **21** above this concentration. The use of $10\ \mu\text{M}$ of **21** necessitated a wash step to remove background fluorescence from any excess ligand (Figure 6A). As demonstrated, the level of observed co-localization between **21** and SNAP-hMOR in the intracellular compartment is significantly increased, with minimal cell surface co-localization due to the wash step as expected. Furthermore, this signal could be removed by blockade with naloxone, further demonstrating the lack of nonspecific binding of **21** even at this higher concentration (Figure 6B).

To directly compare, experiments were conducted using the parent compound morphine as the ligand (Figure 7). Obviously, the lack of a fluorescent tag prevents direct visualization of the ligand, but observation of the tagged receptor fluorescence is still of value as it enables visual comparisons to be made between the behavior of our fluorescently tagged probe and its parent compound. A baseline level of receptor internalization was first determined in cells with no ligand present (Figure 7A). These data show that a low constitutive level of receptor internalization is present, even without stimulation. Morphine at $500\ \text{nM}$ does not induce any

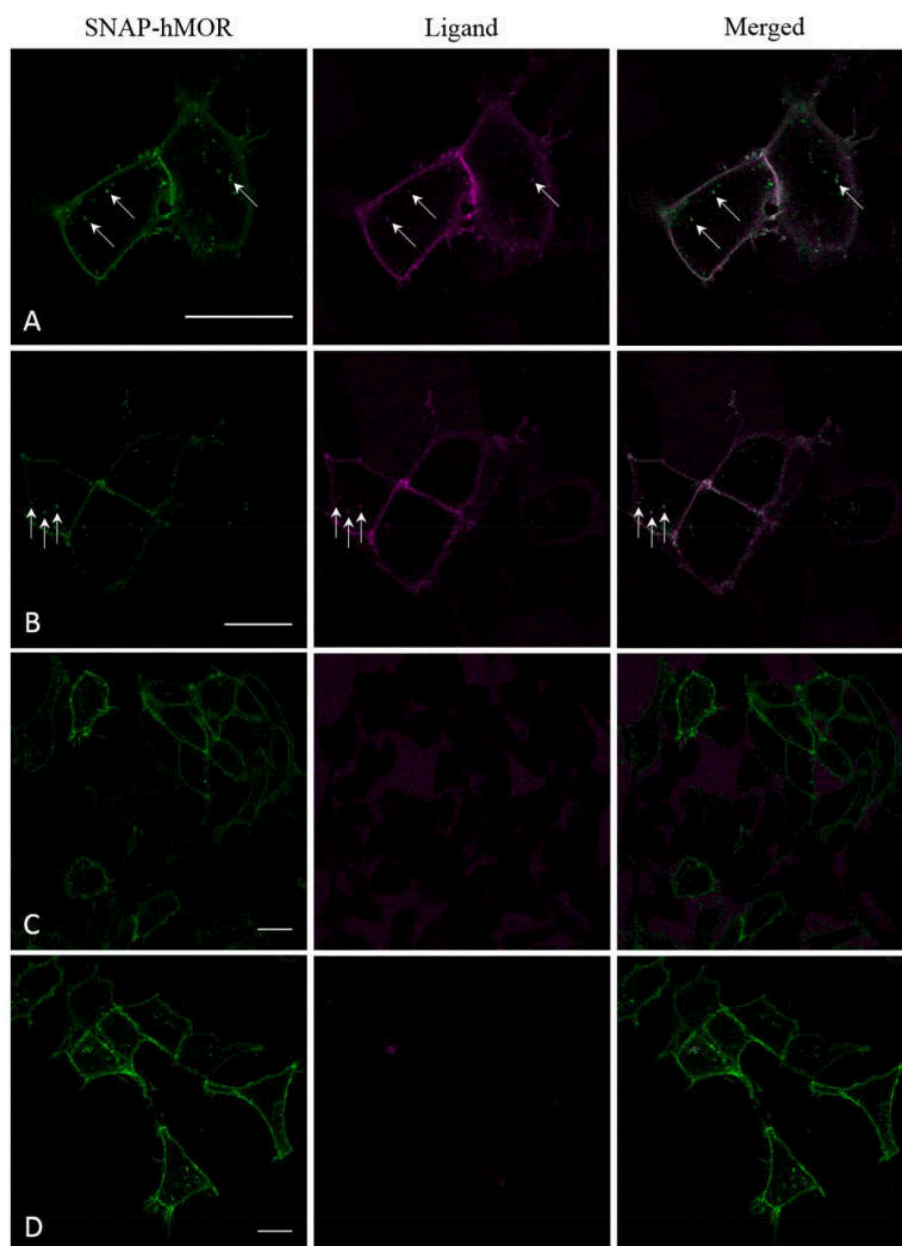


Figure 5. Live cell confocal imaging of **21** in cells expressing SNAP-hMOR. Images are representative of 3 independent experiments. In all cases, **21** was incubated at 500 nM for 30 min at 37 °C following pretreatment (with or without naloxone). (A,B) Typical results obtained from confocal microscopy; the white arrows indicate areas where co-localization of intracellular receptor populations with the fluorescent ligand were observed. (C) **21** following preincubation with naloxone (1 μ M, 30 min, 37 °C), indicating specific binding of the probe to hMOR. (D) Loss of ligand signal following a postincubation wash. This is typical of nonpeptide opioids, which tend to have a fast k_{off} rate. Scale bars, 20 μ m.

significant receptor internalization, with levels similar to that of the baseline level (Figure 7B). Furthermore, these levels of internalization are similar to when 500 nM of **21** was used (Figure 5A,B). This reinforces the idea that morphine is only weakly able to induce internalization of the MOR. Furthermore, at 10 μ M morphine, the level of internalization was comparable to that observed with 10 μ M of **21** (Figure 7C compared to Figure 6A). Taken together, these data suggest

that our probe behaves very similarly to morphine, which may make it a useful tool in the study of morphine pharmacology.

DISCUSSION AND CONCLUSIONS

Herein, we have described the design and synthesis of a fluorescent partial agonist probe for MOR based on the commonly used analgesic morphine. Our studies have shown that probe compound **21** is able to bind to hMOR on cell membranes and behaves in a similar manner to the parent

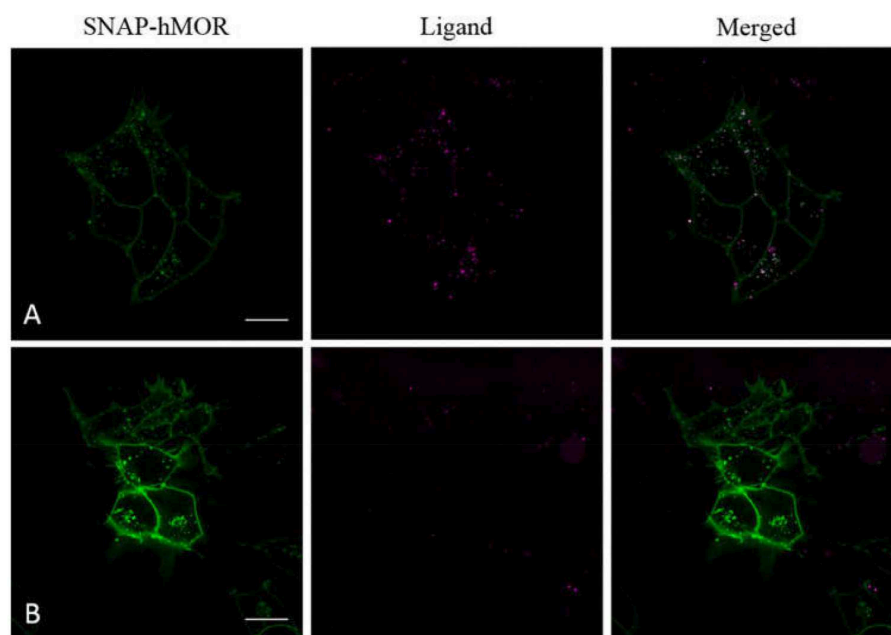


Figure 6. Live cell confocal imaging of **21** at increased concentration in cells expressing SNAP-hMOR. Images are representative of 3 independent experiments. (A) **21** at 10 μM , note the increased level of internalized receptor populations compared to the data presented in Figure 4. (B) **21** at 10 μM following preincubation with naloxone (1 μM , 30 min, 37 $^{\circ}\text{C}$), demonstrating specific displacement of **21** with little background fluorescence. Scale bars, 20 μm .

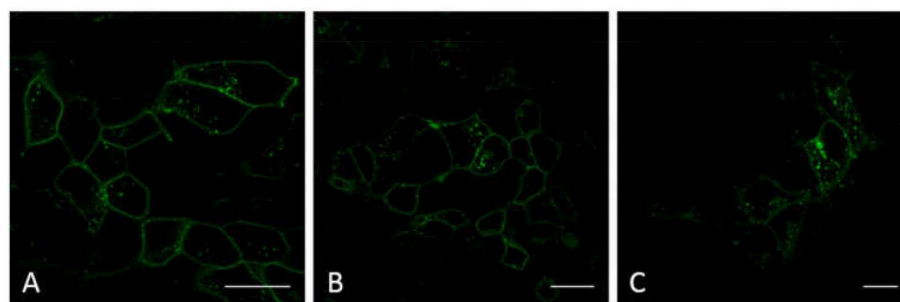


Figure 7. Live cell confocal imaging of SNAP-hMOR in cells exposed to morphine for comparison to **21**. Images are representative of 3 independent experiments. (A) Cells with no stimulation, note the constitutive receptor turnover, even in the absence of any external internalizing stimuli. (B) 500 nM morphine, the level of internalization is similar to that observed when no stimuli is applied, which is in keeping with literature data suggesting morphine's inability to induce internalization. (C) 10 μM morphine, significantly more receptor populations are observed to internalize and therefore can be attributed to the ligand stimulus. Scale bars, 20 μm .

compound morphine. At EC_{50} concentrations, the probe does not induce internalization of the receptor but is present in intracellular compartments at levels consistent with constitutive turnover. At higher concentrations, the probe is able to induce internalization at similar levels to morphine. These data suggest that the probe compound **21** may be used as a tool compound to simulate the behavior of morphine, much in the same way DERM-A594 is used as a tool compound for the study of endogenous opioid peptides.¹⁵ It is clear that morphine has significantly different signaling profile compared to peptides,^{23,24} and therefore small molecule-based fluorescent probes may lead to different outcomes compared to studies where fluorescent peptides have been utilized. This new tool compound could also be used in conjunction with the previously described small-molecule fluorescent opioid antag-

onists to study the differences in ligand–receptor complexes in natively expressing systems rather than in transfected systems.¹⁹

■ EXPERIMENTAL SECTION

Chemistry. Chemicals and solvents were purchased from standard suppliers and used without further purification. Davisil silica gel (40–63 μm) for flash column chromatography was supplied by Grace Davison Discovery Sciences (Victoria, Australia), and deuterated solvents were purchased from Cambridge Isotope Laboratories, Inc. (USA, distributed by Novachem PTY. Ltd., Victoria, Australia). Davisil reverse phase silica gel (C18, 10–14 μm) for reverse phase flash column chromatography was supplied by Grace Davison Discovery Sciences (Victoria, Australia) and run using the following buffers; buffer A, 0.1% TFA in H_2O ; buffer B, 0.1% TFA in MeCN.

Reactions were monitored by thin layer chromatography on commercially available precoated aluminum-backed plates (Merck

Kieselgel 60 F₂₅₄). Visualization was done by examination under UV light (254 and 366 nm). General staining was carried out with KMnO₄ or phosphomolybdic acid. Organic solvents were evaporated in vacuo at ≥40 °C (water bath temperature). Purification using preparative layer chromatography (PLC) was carried out on Analtech preparative TLC plates (200 mm × 200 mm × 2 mm).

¹H NMR and ¹³C NMR spectra were recorded on a Bruker Avance Nanobay III 400 MHz Ultrashield Plus spectrometer at 400.13 and 100.62 MHz, respectively. Chemical shifts (δ) are recorded in parts per million (ppm) with reference to the chemical shift of the deuterated solvent. Coupling constants (J) are recorded in Hz and the significant multiplicities described by singlet (s), doublet (d), triplet (t), quadruplet (q), broad (br), multiplet (m), doublet of doublets (dd), and doublet of triplets (dt).

LC-MS were run to verify reaction outcome and purity using an Agilent 6120 series single quad coupled to an Agilent 1260 series HPLC. The following buffers were used; buffer A, 0.1% formic acid in H₂O; buffer B, 0.1% formic acid in MeCN. The following gradient was used with a Poroshell 120 EC-C18 50 mm × 3.0 mm 2.7 μm column and a flow rate of 0.5 mL/min and total run time of 5 min; 0–1 min 95% buffer A and 5% buffer B, from 1 to 2.5 min up to 0% buffer A and 100% buffer B, held at this composition until 3.8 min, 3.8–4 min 95% buffer A and 5% buffer B, and held until 5 min at this composition. Mass spectra were acquired in positive and negative ion mode with a scan range of 100–1000 *m/z*. UV detection was carried out at 214 and 254 nm.

Preparative HPLC was performed using an Agilent 1260 infinity coupled with a binary preparative pump and Agilent 1260 FC-PS fraction collector, using Agilent OpenLAB CDS software (Rev C.01.04), and an Altima 5 μM C8 22 mm × 250 mm column. The following buffers were used; buffer A, 0.1% TFA in H₂O; buffer B, 0.1% TFA in MeCN, with sample being run at a gradient of 5% buffer B to 100% buffer B over 15 min, at a flow rate of 15 mL/min. All screening compounds were of >95% purity.

High resolution mass spectrometry–time-of-flight (HRMS–TOF) was conducted using an Agilent 6224 TOF LC-MS mass spectrometer coupled to an Agilent 1290 Infinity. Chromatographic separation was performed using an Agilent Zorbax SB-C18 Rapid Resolution HT 2.1 mm × 50 mm, 1.8 μm column using a gradient of 5–100% buffer B in buffer A over 3.5 min at 0.5 mL/min, where buffers are as defined for LC-MS. All mass data was acquired and reference mass corrected via a dual-spray ESI source. Mass spectra were created by averaging scans across each peak and background subtracting against the first 10 s of the total ion count. Acquisition was performed using the Agilent Mass Hunter Data Acquisition software and analysis performed using Mass Hunter Qualitative Analysis software. The mass spectrometer was run using the following conditions: drying gas flow 11 L/min, nebulizer 45 PSI, drying gas temperature 325 °C, capillary voltage 4000 V, fragmentor 160 V, skimmer 65 V, OCT RFV 750 V, scan range acquired 100–150 *m/z*, internal reference ions positive ion mode = *m/z* = 121.050873 and 922.009798.

General Deprotection Procedure A. The protected compound was dissolved in dry DCM (typically 5 mL) under an N₂ atmosphere. Triethylsilane (15 equiv) and TFA (20 equiv) were added to the reaction and the vessel purged with N₂. The reaction was allowed to stir for 30–60 min then reduced in vacuo. The resulting residue could then be purified via chromatography.

6-O-Hexanoylmorphine (1). Compound 9 (67 mg, 0.13 mmol, 1 equiv) was deprotected using general deprotection procedure A. The resulting oil was purified by flash column chromatography (94:5:1 CHCl₃/MeOH/TEA), and the resulting yellow oil was further purified by prep-HPLC to give the product as a solid white TFA salt (12 mg, 17%). ¹H NMR (DMSO-*d*₆) δ 10.04 (s, 1H), 9.17 (s, 1H), 6.58 (d, *J* = 8.1 Hz, 1H), 6.50 (d, *J* = 8.1 Hz, 1H), 5.71–5.59 (m, 1H), 5.52–5.39 (m, *J* = 22.7, 9.8 Hz, 1H), 5.26–5.14 (m, 1H), 5.12–5.00 (m, *J* = 20.5, 6.6 Hz, 1H), 4.13 (s, 1H), 3.31 (d, *J* = 9.0 Hz, 1H), 3.19 (d, *J* = 19.7 Hz, 1H), 3.06 (d, *J* = 4.5 Hz, 1H), 2.98 (s, 1H), 2.92–2.78 (m, *J* = 41.2 Hz, 3H), 2.71 (dd, *J* = 20.0, 6.7 Hz, 1H), 2.44–2.29 (m, 2H), 2.21 (td, *J* = 13.5, 4.6 Hz, 1H), 1.98–1.70 (m, *J* = 46.3, 12.5 Hz, 1H), 1.64–1.51 (m, 2H), 1.34–1.21 (m, 4H), 0.87 (t, *J* = 6.9 Hz, 3H). ESI-

TOF HRMS *m/z* [M + H]⁺ C₂₃H₂₉NO₄⁺ calcd 384.2169, found 384.2174.

6-O-(4-Methylamino-4-oxobutanoyl)morphine (2). Compound 13 (26 mg, 0.050 mmol, 1 equiv) was deprotected using general deprotection procedure A. The resulting oil was purified by prep-HPLC to give the product as a solid white TFA salt (4 mg, 16%). ¹H NMR (DMSO-*d*₆) δ 10.04 (s, 1H), 9.23 (s, 1H), 7.85 (d, *J* = 4.4 Hz, 1H), 6.61–6.56 (m, *J* = 8.0, 3.1 Hz, 1H), 6.54–6.48 (m, *J* = 8.1, 4.7 Hz, 1H), 5.65 (d, *J* = 10.0 Hz, 1H), 5.52–5.39 (m, *J* = 24.1, 10.0 Hz, 1H), 5.24–5.14 (m, 1H), 5.09–4.99 (m, *J* = 22.2, 6.7 Hz, 1H), 4.13 (s, 1H), 3.34–3.25 (m, *J* = 8.5 Hz, 1H), 3.23–3.13 (m, *J* = 19.7 Hz, 1H), 3.06 (d, *J* = 4.8 Hz, 1H), 2.98 (s, 1H), 2.89 (d, *J* = 3.1 Hz, 2H), 2.82–2.67 (m, 2H), 2.62–2.58 (m, *J* = 6.9, 4.1 Hz, 2H), 2.57–2.55 (m, *J* = 4.5 Hz, 3H), 2.40 (t, *J* = 6.9 Hz, 2H), 2.21 (td, *J* = 13.4, 4.4 Hz, 1H), 1.94–1.74 (m, *J* = 46.2, 11.8 Hz, 1H). ESI-TOF HRMS *m/z* [M + H]⁺ C₂₂H₂₇N₂O₅⁺ calcd 399.1914, found 399.1922.

N¹-((4*R*,4*aR*,7*S*,7*aR*,12*bS*)-9-Hydroxy-3-methyl-2,3,4,4*a*,7,7*a*-hexahydro-1*H*-4,12-methanobenzofuro[3,2-*e*]isoquinolin-7-yl)-hexanamide (3). Compound 10 (39 mg, 0.10 mmol, 1 equiv) was deprotected using general deprotection procedure A. The resulting oil was purified by prep-HPLC to give the product as a solid white TFA salt (12 mg, 31%). [α]_D²⁵ –21.4 (c 1.21 mg/mL, MeOH). ¹H NMR (DMSO-*d*₆) δ 10.11–9.88 (m, 1H), 9.28 (s, 1H), 8.20–8.05 (m, *J* = 25.3, 8.5 Hz, 1H), 5.73 (dt, *J* = 10.3, 3.1 Hz, 1H), 5.58 (d, *J* = 10.5 Hz, 1H), 5.16–5.02 (m, *J* = 25.4 Hz, 1H), 3.85 (t, *J* = 8.7 Hz, 1H), 3.74 (s, 1H), 3.27–3.20 (m, *J* = 7.0 Hz, 1H), 3.18 (s, 1H), 3.12–3.02 (m, *J* = 19.8, 6.3 Hz, 1H), 2.98 (s, 1H), 2.89 (s, 3H), 2.77–2.56 (m, *J* = 48.6, 9.6 Hz, 2H), 2.40 (d, *J* = 8.1 Hz, 1H), 2.17–1.97 (m, 3H), 1.87 (d, *J* = 11.8 Hz, 1H), 1.56–1.43 (m, 2H), 1.31–1.14 (m, 4H), 0.85 (t, *J* = 7.0 Hz, 3H). ESI-TOF HRMS *m/z* [M + H]⁺ C₂₃H₃₁N₂O₅⁺ calcd 383.2329, found 383.2324.

N¹-((4*R*,4*aR*,7*S*,7*aR*,12*bS*)-9-Hydroxy-3-methyl-2,3,4,4*a*,7,7*a*-hexahydro-1*H*-4,12-methanobenzofuro[3,2-*e*]isoquinolin-7-yl)-N²-methylsuccinamide (4). Compound 14 (19 mg, 0.037 mmol, 1 equiv) was deprotected using general deprotection procedure A. The resulting oil was purified by prep-HPLC to give the product as a solid white TFA salt (7 mg, 39%). [α]_D²⁵ –21.9 (c 0.78 mg/mL, MeOH). ¹H NMR (DMSO-*d*₆) δ 10.08–9.73 (m, *J* = 44.4 Hz, 1H), 9.25 (s, 1H), 8.28–8.06 (m, *J* = 29.6, 9.0 Hz, 1H), 7.79 (d, *J* = 4.6 Hz, 1H), 5.78–5.68 (m, 1H), 5.65–5.57 (m, 1H), 5.10 (t, *J* = 13.6 Hz, 1H), 3.94 (d, *J* = 4.6 Hz, 1H), 3.86 (t, *J* = 8.5 Hz, 1H), 3.22 (s, 1H), 3.17 (d, *J* = 19.5 Hz, 1H), 3.10–2.96 (m, 2H), 2.89 (d, *J* = 4.6 Hz, 2H), 2.79–2.65 (m, 1H), 2.55 (d, *J* = 4.6 Hz, 3H), 2.43–2.21 (m, 5H), 2.11–1.97 (m, 1H), 1.92–1.67 (m, 1H). ESI-TOF HRMS *m/z* [M + H]⁺ C₂₂H₂₈N₃O₄⁺ calcd 398.2074, found 398.2079.

6-O-(2-Oxo-2-(propylamino)ethyl)morphine (5). Compound 15 (54 mg, 0.12 mmol, 1 equiv), HCTU (59 mg, 0.14 mmol, 1.2 equiv), and TEA (50 μL, 0.36 mmol, 3 equiv) were dissolved in dry DMF (800 μL) under an N₂ atmosphere and allowed to stir at room temperature for 30 min. A solution of propylamine (12 μL, 0.14 mmol, 1.2 equiv) in DMF (200 μL) was then added and the resulting solution allowed to stir at room temperature for 19 h. The solvent was then removed in vacuo and the residue taken up in buffer B and again reduced in vacuo. The residue was purified by flash column chromatography (74:25:1 MeOH/CHCl₃/NH₄OH) and the solvent removed in vacuo and purified again by prep-HPLC to give the product as a solid white TFA salt (10 mg, 17%). [α]_D²⁵ –106.1 (c 1.14 mg/mL, MeOH). ¹H NMR (DMSO-*d*₆) δ 9.81 (s, 1H), 9.18 (s, 1H), 7.74 (t, *J* = 5.7 Hz, 1H), 6.62–6.52 (m, 1H), 6.52–6.43 (m, 1H), 5.82 (d, *J* = 9.7 Hz, 1H), 5.41–5.24 (m, 1H), 5.18–5.02 (m, 1H), 4.16–3.97 (m, 4H), 3.29 (s, 1H), 3.20 (d, *J* = 19.8 Hz, 2H), 3.14–3.04 (m, 3H), 2.97 (s, 1H), 2.90 (d, *J* = 3.9 Hz, 3H), 2.83 (d, *J* = 16.0 Hz, 2H), 2.74 (dd, *J* = 19.8, 6.6 Hz, 1H), 2.18 (td, *J* = 13.8, 4.9 Hz, 1H), 2.03–1.79 (m, 1H), 1.45 (h, *J* = 7.3 Hz, 2H), 0.84 (t, *J* = 7.4 Hz, 3H). ESI-TOF HRMS *m/z* [M + H]⁺ C₂₂H₂₉N₂O₄⁺ calcd 385.2122, found 385.2130.

3-O-(4-Methoxybenzyl)morphine (6). Morphine (394 mg, 1.4 mmol, 1 equiv) was dissolved in DMF (1 mL), and KOH (3 M in MeOH, 552 μL, 1.7 mmol, 1.2 equiv) was added. The resulting mixture was stirred for 10 min, then *para*-methoxybenzyl chloride

(215 μL , 1.6 mmol, 1.15 equiv) was added dropwise. After stirring for 4 h at room temperature, aqueous citric acid (1 M, 10 mL) was added. The resulting solution was washed successively with EtOAc (3×10 mL), and aqueous NH_4OH (28%, 10 mL) was added to the aqueous phase. The resulting turbid solution was extracted with 3:1 $\text{CHCl}_3/\text{iPrOH}$ (5×10 mL). The combined organic layers were backwashed with brine, dried over Na_2SO_4 , and the solvent removed in vacuo. The resulting yellow oil was purified by flash column chromatography (98:1:1 DCM/MeOH/TEA). The resulting clear oil was redissolved in EtOAc and evaporated again to give the product as a white solid (259 mg, 46%). ^1H NMR (CDCl_3) δ 7.33 (d, $J = 8.4$ Hz, 1H), 6.88 (d, $J = 8.4$ Hz, 1H), 6.71 (d, $J = 8.2$ Hz, 1H), 6.53 (d, $J = 8.1$ Hz, 1H), 5.67 (d, $J = 9.7$ Hz, 1H), 5.27 (d, $J = 9.7$ Hz, 1H), 5.04 (dd, $J = 28.7$, 11.4 Hz, 1H), 4.87 (d, $J = 6.3$ Hz, 1H), 4.15 (d, $J = 2.5$ Hz, 1H), 3.80 (s, 2H), 3.36 (d, $J = 2.4$ Hz, 1H), 3.03 (d, $J = 18.7$ Hz, 1H), 2.86 (s, 1H), 2.69 (s, 1H), 2.61 (dd, $J = 11.8$, 3.9 Hz, 1H), 2.44 (s, 1H), 2.39 (dd, $J = 12.2$, 3.1 Hz, 1H), 2.30 (dd, $J = 18.6$, 6.0 Hz, 1H), 2.08 (td, $J = 12.4$, 4.8 Hz, 1H), 1.87 (d, $J = 11.7$ Hz, 1H). ^{13}C NMR (101 MHz, CDCl_3) δ 159.5, 147.1, 141.3, 133.6, 131.3, 129.5, 129.4, 128.2, 127.7, 119.7, 116.0, 114.0, 91.3, 71.7, 66.5, 59.0, 55.4, 46.6, 43.1, 42.9, 40.7, 35.8, 20.6. LC-MS m/z [$\text{M} + \text{H}$] $^+$ $\text{C}_{25}\text{H}_{28}\text{NO}_4$ $^+$ calcd 406.2, found 406.2.

(4*R*,4*aR*,7*R*,7*aR*,12*bS*)-9-((4-Methoxybenzyl)oxy)-3-methyl-2,3,4,4*a*,7,7*a*-hexahydro-1*H*-4,12-methanobenzofuro[3,2-*e*]isoquinolin-7-yl (7). Compound 6 (229 mg, 0.57 mmol, 1 equiv), benzoic acid (104 mg, 0.85 mmol, 1.5 equiv), and triphenylphosphine (223 mg, 0.85 mmol, 1.5 equiv) were dissolved in anhydrous toluene (4 mL) and cooled to 0 °C. DIAD (167 μL , 0.85 mmol, 1.5 equiv) in anhydrous toluene (0.5 mL) were then added dropwise over 2 min. The reaction was then warmed to room temperature and allowed to stir for 4 h, after which the solvent was removed in vacuo. The resulting residue was purified by flash column chromatography (59:40:1 DCM/EtOAc/TEA) to give a white solid and oil mixture. This residue was dissolved in a 1:1 mixture of EtOH and 1 M aqueous KOH (6 mL) and heated to reflux for 20 min. The reaction was then reduced in vacuo, and 1 M citric acid (20 mL) was added to the residue. The aqueous phase was then washed with EtOAc (3×20 mL), then neutralized with aqueous NH_4OH (28%, 20 mL). The resulting solution was extracted with 3:1 $\text{CHCl}_3/\text{iPrOH}$ (3×20 mL). The combined organic layers were backwashed with brine (20 mL), dried over Na_2SO_4 , and the solvent removed in vacuo to give a white solid as the pure product (179 mg, 78%). ^1H NMR (CDCl_3) δ 7.36–7.31 (m, 1H), 6.90–6.85 (m, 1H), 6.70 (d, $J = 8.2$ Hz, 1H), 6.50 (d, $J = 8.2$ Hz, 1H), 6.00–5.93 (m, 1H), 5.60 (dd, $J = 9.8$, 1.9 Hz, 1H), 5.05 (q, $J = 11.4$ Hz, 1H), 4.79 (s, 1H), 4.20 (d, $J = 5.5$ Hz, 1H), 3.79 (s, 1H), 3.40 (dd, $J = 5.6$, 3.2 Hz, 1H), 3.17 (s, 1H), 3.03 (d, $J = 18.7$ Hz, 1H), 2.66 (dd, $J = 12.2$, 3.9 Hz, 1H), 2.48 (s, 1H), 2.45–2.33 (m, 1H), 2.18 (td, $J = 12.5$, 4.9 Hz, 1H), 1.85 (dd, $J = 12.7$, 2.0 Hz, 1H). ^{13}C NMR (CDCl_3) δ 159.5, 146.5, 141.3, 132.8, 131.4, 130.6, 129.6, 129.5, 127.2, 119.0, 116.4, 113.9, 94.2, 71.7, 68.0, 59.3, 55.4, 47.2, 43.9, 42.9, 39.6, 35.5, 20.7. LC-MS m/z [$\text{M} + \text{H}$] $^+$ $\text{C}_{25}\text{H}_{28}\text{NO}_4$ $^+$ calcd 406.2, found 406.3.

(4*R*,4*aR*,7*S*,7*aR*,12*bS*)-9-((4-Methoxybenzyl)oxy)-3-methyl-2,3,4,4*a*,7,7*a*-hexahydro-1*H*-4,12-methanobenzofuro[3,2-*e*]isoquinolin-7-amine (8). Compound 7 (174 mg, 0.43 mmol, 1 equiv), phthalimide (79 mg, 0.64 mmol, 1.5 equiv), and triphenylphosphine (169 mg, 0.64 mmol, 1.5 equiv) were dissolved in anhydrous toluene (4 mL) and cooled to 0 °C. DIAD (127 μL , 0.64 mmol, 1.5 equiv) in anhydrous toluene (0.5 mL) was then added dropwise over 2 min. The reaction was then warmed to room temperature and allowed to stir for 4 h, after which the solvent was removed in vacuo. The resulting residue was purified by flash column chromatography (59:40:1 DCM/EtOAc/TEA) to give a white solid and oil mixture. To this residue, EtOH (10 mL) and $\text{N}_2\text{H}_4 \cdot \text{H}_2\text{O}$ (0.5 mL) were added and the mixture heated to reflux for 1 h. After cooling, the resulting precipitate was filtered and washed with EtOH. The filtrate was evaporated in vacuo, redissolved in CHCl_3 , and the resulting precipitate removed. The filtrate was again evaporated in vacuo and the residue purified by flash column chromatography (89:10:1 $\text{CHCl}_3/\text{MeOH}/\text{TEA}$) to give the product as a yellow oil (59 mg, 34%). ^1H NMR (CDCl_3) δ 7.35–7.30

(m, 1H), 6.89–6.80 (m, 1H), 6.70 (d, $J = 8.2$ Hz, 1H), 6.55 (d, $J = 8.2$ Hz, 1H), 5.79–5.60 (m, 1H), 5.13–4.99 (m, 1H), 4.94 (d, $J = 2.3$ Hz, 1H), 3.78 (s, 2H), 3.59 (d, $J = 4.2$ Hz, 1H), 3.03 (d, $J = 18.7$ Hz, 1H), 2.73 (d, $J = 9.1$ Hz, 1H), 2.55 (dd, $J = 12.1$, 3.6 Hz, 1H), 2.48–2.37 (m, 2H), 2.29 (td, $J = 12.1$, 3.7 Hz, 1H), 2.03 (s, 1H), 1.99–1.93 (m, 1H), 1.83–1.77 (m, 1H). ^{13}C NMR (CDCl_3) δ 159.4, 145.0, 142.2, 139.3, 130.1, 129.6, 129.5, 127.7, 123.9, 118.9, 116.3, 113.9, 87.4, 71.5, 56.2, 55.3, 49.2, 46.9, 46.3, 43.2, 40.9, 35.5, 20.0. LC-MS m/z [$\text{M} + \text{H}$] $^+$ $\text{C}_{25}\text{H}_{29}\text{N}_2\text{O}_3$ $^+$ calcd 405.5, found 405.2.

6-*O*-Hexanoyl-3-*O*-(4-methoxybenzyl)morphine (9). Compound 6 (68 mg, 0.17 mmol, 1 equiv) and hexanoyl chloride (70.4 μL , 0.50 mmol, 3 equiv) were dissolved in pyridine (1 mL) and heated at 70 °C in a sealed vessel for 19 h. Water (2 mL) and MeOH (1 mL) were added and the resulting mixture evaporated. MeCN (5 mL) was added, and the mixture was again evaporated to give a yellow oil. Saturated aqueous NaHCO_3 (10 mL) was added and the resulting solution extracted with 3:1 $\text{CHCl}_3/\text{iPrOH}$ (3×10 mL). The combined organic layers were backwashed with brine, dried over Na_2SO_4 , and the solvent removed in vacuo to give a yellow oil. Ether was added and the resulting precipitate filtered. The filtrate was evaporated and purified by flash column chromatography (94:5:1 EtOAc/MeOH/TEA) to give the product as a yellow oil (67 mg, 80%). ^1H NMR (CDCl_3) δ 7.35–7.31 (m, 1H), 6.89–6.84 (m, 1H), 6.67 (d, $J = 8.2$ Hz, 1H), 6.49 (d, $J = 8.2$ Hz, 1H), 5.67–5.61 (m, 1H), 5.46–5.39 (m, 1H), 5.19 (ddd, $J = 8.1$, 5.1, 2.9 Hz, 1H), 5.12 (dd, $J = 6.7$, 0.8 Hz, 1H), 5.06 (s, 1H), 3.79 (s, 1H), 3.77 (dd, $J = 3.6$, 2.0 Hz, 1H), 3.40 (dd, $J = 5.6$, 3.2 Hz, 1H), 3.02 (d, $J = 18.7$ Hz, 1H), 2.83 (s, 1H), 2.64 (dd, $J = 12.0$, 3.9 Hz, 1H), 2.47 (s, 2H), 2.42–2.28 (m, 2H), 2.10 (td, $J = 12.5$, 4.9 Hz, 1H), 1.88 (dd, $J = 12.7$, 1.8 Hz, 1H), 1.69–1.58 (m, 1H), 1.35–1.20 (m, 3H), 0.92–0.80 (m, 3H). ^{13}C NMR (CDCl_3) δ 173.4, 159.4, 147.6, 141.2, 130.9, 129.7, 129.5, 129.2, 128.9, 119.4, 117.3, 113.8, 88.0, 71.8, 68.0, 59.3, 55.3, 43.0, 42.5, 40.4, 35.2, 34.1, 31.4, 24.6, 22.4, 20.7, 14.02. LC-MS m/z [$\text{M} + \text{H}$] $^+$ $\text{C}_{31}\text{H}_{37}\text{NO}_5$ $^+$ calcd 504.3, found 504.3.

N-((4*R*,4*aR*,7*S*,7*aR*,12*bS*)-9-((4-Methoxybenzyl)oxy)-3-methyl-2,3,4,4*a*,7,7*a*-hexahydro-1*H*-4,12-methanobenzofuro[3,2-*e*]isoquinolin-7-yl)hexanamide (10). Compound 8 (65 mg, 0.16 mmol, 1 equiv) and hexanoyl chloride (67 μL , 0.48 mmol, 3 equiv) were dissolved in pyridine (2 mL) and heated at 70 °C for 18 h. After cooling, the solvent was removed in vacuo, and the resulting residue was purified by flash column chromatography (94:5:1 EtOAc/MeOH/TEA) to give the product as a yellow oil (39 mg, 49%). ^1H NMR (CDCl_3) δ 7.37–7.30 (m, 2H), 6.89–6.84 (m, 2H), 6.72 (d, $J = 8.2$ Hz, 1H), 6.59 (d, $J = 8.2$ Hz, 1H), 5.76 (ddd, $J = 10.3$, 3.5, 2.8 Hz, 1H), 5.60 (dd, $J = 10.3$, 1.1 Hz, 1H), 5.40 (d, $J = 9.6$ Hz, 1H), 5.09–5.00 (m, 2H), 4.94–4.92 (m, 1H), 4.23–4.14 (m, 1H), 3.79 (s, 3H), 3.24 (dd, $J = 5.8$, 2.7 Hz, 1H), 2.99 (d, $J = 18.8$ Hz, 1H), 2.73 (dd, $J = 18.8$, 6.1 Hz, 1H), 2.56–2.49 (m, 1H), 2.39 (s, 3H), 2.27 (td, $J = 11.7$, 4.5 Hz, 1H), 2.18–2.12 (m, 2H), 2.10 (dd, $J = 10.2$, 2.8 Hz, 1H), 1.92–1.79 (m, 2H), 1.64–1.56 (m, 2H), 1.36–1.22 (m, 5H), 0.88 (t, $J = 7.0$ Hz, 3H). ^{13}C NMR (CDCl_3) δ 173.1, 159.4, 144.9, 142.2, 134.7, 129.6, 129.5, 129.1, 128.2, 126.2, 119.5, 116.5, 113.9, 86.6, 71.5, 56.7, 55.4, 47.7, 47.0, 44.3, 43.3, 41.1, 36.9, 35.6, 31.5, 25.5, 22.5, 20.0, 14.1. LC-MS m/z [$\text{M} + \text{H}$] $^+$ $\text{C}_{31}\text{H}_{39}\text{N}_2\text{O}_6$ $^+$ calcd 503.3, found 503.4.

6-*O*-(3-Carboxypropanoyl)-3-*O*-(4-methoxybenzyl)morphine (11). Compound 6 (41 mg, 0.10 mmol, 1 equiv), succinic anhydride (15 mg, 0.15 mmol, 1.5 equiv), DMAP (19 mg, 0.15 mmol, 1.5 equiv), and TEA (29 μL , 0.20 mmol, 2 equiv) were dissolved in dry MeCN (1 mL) under N_2 and heated at 65 °C for 15.5 h. The mixture was then evaporated and the residue purified via flash column chromatography (79:20:1 $\text{CHCl}_3/\text{MeOH}/\text{NH}_4\text{OH}$) to give the product as a white foam (40 mg, 77%). ^1H NMR (CDCl_3) δ 9.98 (brs, 1H), 7.36–7.31 (m, 2H), 6.89–6.84 (m, 2H), 6.68 (d, $J = 8.2$ Hz, 1H), 6.49 (d, $J = 8.2$ Hz, 1H), 5.62 (d, $J = 10.0$ Hz, 1H), 5.34–5.29 (m, 1H), 5.25–5.18 (m, $J = 13.8$, 9.3, 4.7 Hz, 2H), 5.09 (s, 2H), 3.78 (s, 4H), 3.16 (s, 1H), 3.13–3.05 (m, 1H), 2.99 (d, $J = 19.3$ Hz, 1H), 2.75 (ddd, $J = 17.4$, 10.0, 3.8 Hz, 1H), 2.63 (s, 3H), 2.62–2.53 (m, $J = 10.5$, 5.7 Hz, 3H), 2.49–2.38 (m, 2H), 1.89 (d, $J = 11.5$ Hz, 1H). ^{13}C NMR (CDCl_3) δ 177.6, 172.9, 159.5, 147.8, 141.6, 130.3, 129.7, 129.5, 129.5, 127.6, 124.7, 119.6, 118.3, 113.9, 87.9, 72.0, 67.8, 59.1, 55.4, 46.6, 41.5, 41.1,

37.6, 33.1, 30.8, 30.0, 21.3. LC-MS m/z $[M + H]^+$ $C_{29}H_{32}NO_7^+$ calcd 506.2, found 506.2.

4-(((4*R*,4*aR*,7*S*,7*aR*,12*bS*)-9-((4-Methoxybenzyl)oxy)-3-methyl-2,3,4,4*a*,7,7*a*-hexahydro-1*H*-4,12-methanobenzofuro[3,2-*e*]-isoquinolin-7-yl)amino)-4-oxobutanoic Acid (12). Compound **8** (71 mg, 0.18 mmol, 1 equiv), succinic anhydride (26 mg, 0.26 mmol, 1.5 equiv), DMAP (32 mg, 0.26 mmol, 1.5 equiv), and TEA (49 μ L, 0.35 mmol, 2 equiv) were dissolved in MeCN (3 mL) and heated to 70 °C for 18 h. The solvent was then removed in vacuo, and the resulting solid was triturated with EtOAc. The resulting material was suspended in hot EtOH and the resulting precipitate filtered to give the product as a white solid (25 mg, 28%). ¹H NMR (DMSO-*d*₆) δ 7.35–7.29 (m, 2H), 6.95–6.89 (m, 2H), 6.78 (d, J = 8.2 Hz, 1H), 6.61 (d, J = 8.2 Hz, 1H), 5.69–5.63 (m, 1H), 5.56 (dd, J = 10.4, 1.2 Hz, 1H), 5.01–4.96 (m, 3H), 3.74 (s, 3H), 3.16 (s, 1H), 3.13 (dd, J = 5.7, 2.6 Hz, 1H), 2.87 (d, J = 18.7 Hz, 1H), 2.46 (d, J = 7.2 Hz, 1H), 2.44–2.39 (m, 3H), 2.34–2.30 (m, 1H), 2.28 (s, 3H), 2.15 (dd, J = 10.5, 2.7 Hz, 1H), 2.13–2.05 (m, 2H), 1.83 (td, J = 12.3, 4.7 Hz, 1H), 1.60 (d, J = 11.1 Hz, 1H). ¹³C NMR (101 MHz, DMSO-*d*₆) δ 174.1, 171.3, 159.0, 147.4, 144.4, 141.6, 136.0, 129.7, 129.4, 129.2, 128.0, 125.0, 118.9, 115.6, 113.7, 106.8, 86.2, 70.2, 55.3, 55.1, 46.2, 43.4, 42.8, 38.8, 34.9, 30.0, 29.7, 29.2, 19.6. LC-MS m/z $[M + H]^+$ $C_{29}H_{33}N_2O_6^+$ calcd 505.2, found 505.3.

3-O-(4-Methoxybenzyl)-6-O-(4-Methylamino-4-oxobutanoyl)-morphine (13). Compound **11** (40 mg, 0.079 mmol, 1 equiv), EDC·HCl (23 mg, 0.12 mmol, 1.5 equiv), anhydrous HOBT (16 mg, 0.12 mmol, 1.5 equiv), and TEA (22 μ L, 0.16 mmol, 2 equiv) were dissolved in MeCN (2 mL) and stirred at room temperature for 1 h. Methylamine (2 M solution in THF, 79.2 μ L, 0.1584 mmol, 2 equiv) was then added and stirred for an additional 2 h. The reaction mixture was then evaporated and purified by flash column chromatography (0.5–6% MeOH in CHCl₃ with 1% TEA) to give the product as a slightly yellow oil (26 mg, 63%). ¹H NMR (CDCl₃) δ 7.36–7.28 (m, 2H), 6.90–6.84 (m, 2H), 6.71 (d, J = 8.2 Hz, 1H), 6.52 (d, J = 8.2 Hz, 1H), 5.80 (d, J = 4.0 Hz, 1H), 5.63–5.57 (m, 1H), 5.47–5.38 (m, 1H), 5.17 (ddd, J = 8.9, 5.0, 3.0 Hz, 1H), 5.09 (dd, J = 6.9, 0.8 Hz, 1H), 5.04–4.97 (m, 2H), 3.79 (s, 3H), 3.37 (dd, J = 5.7, 3.2 Hz, 1H), 3.05 (dd, J = 8.8, 5.9 Hz, 1H), 3.02–2.98 (m, 1H), 2.78 (s, 1H), 2.73–2.67 (m, 2H), 2.60 (d, J = 4.8 Hz, 3H), 2.45 (s, 3H), 2.43–2.27 (m, 4H), 2.07 (td, J = 12.4, 5.0 Hz, 1H), 1.86 (dd, J = 12.7, 1.6 Hz, 1H), 1.37 (t, J = 7.3 Hz, 1H). ¹³C NMR (CDCl₃) δ 172.1, 172.1, 159.7, 147.2, 141.2, 130.9, 129.7, 129.4, 129.1, 128.5, 127.7, 119.5, 116.0, 114.0, 87.9, 71.7, 68.0, 59.3, 55.4, 46.8, 45.9, 43.1, 42.5, 40.4, 35.3, 31.5, 30.4, 26.4, 20.5, 9.0. LC-MS m/z $[M + H]^+$ $C_{30}H_{35}N_2O_6^+$ calcd 519.3, found 519.2.

N¹-(((4*R*,4*aR*,7*S*,7*aR*,12*bS*)-9-((4-Methoxybenzyl)oxy)-3-methyl-2,3,4,4*a*,7,7*a*-hexahydro-1*H*-4,12-methanobenzofuro[3,2-*e*]-isoquinolin-7-yl)-N¹-methylsuccinamide (14). Compound **12** (24 mg, 0.48 mmol, 1 equiv), EDC·HCl (14 mg, 0.072 mmol, 1.5 equiv), anhydrous HOBT (10 mg, 0.072 mmol, 1.5 equiv), and TEA (13 μ L, 0.096 mmol, 2 equiv) were dissolved in dry DMF (1 mL) and stirred at room temperature for 1 h. Methylamine (2 M in THF, 48 μ L, 0.096 mmol, 2 equiv) was then added and the reaction allowed to stir for 19 h. Additional EDC·HCl (18 mg, 0.094 mmol, 2 equiv) and HOBT (11 mg, 0.084 mmol, 1.7 equiv) were added, and following 30 min of stirring, further methylamine (2 M in THF, 48 μ L, 0.096 mmol, 2 equiv) was added. The reaction was then allowed to stir at room temperature for a further 24 h and the solvent removed in vacuo. The resulting brown oil was purified by PLC (89:10:1 CHCl₃/MeOH/TEA) to give the product as a white solid (21 mg, 84%). ¹H NMR (CDCl₃) δ 7.35–7.30 (m, 2H), 6.89–6.83 (m, 2H), 6.71 (d, J = 8.2 Hz, 1H), 6.58 (d, J = 8.2 Hz, 1H), 6.30 (d, J = 9.5 Hz, 1H), 6.06 (d, J = 4.2 Hz, 1H), 5.75 (ddd, J = 10.3, 3.5, 2.9 Hz, 1H), 5.59 (dd, J = 10.3, 1.1 Hz, 1H), 5.08–5.00 (m, 2H), 4.95–4.91 (m, 1H), 4.16–4.07 (m, 1H), 3.79 (s, 3H), 3.23 (dd, J = 5.9, 2.7 Hz, 1H), 2.97 (d, J = 18.7 Hz, 1H), 2.76 (d, J = 4.8 Hz, 3H), 2.65 (d, J = 6.1 Hz, 1H), 2.55–2.44 (m, 5H), 2.39 (s, 3H), 2.27 (td, J = 12.0, 3.7 Hz, 1H), 2.17 (dd, J = 10.3, 2.8 Hz, 1H), 1.88 (td, J = 12.2, 4.8 Hz, 1H), 1.84–1.76 (m, 1H). ¹³C NMR (101 MHz, CDCl₃) δ 172.7, 172.4, 159.4, 145.0, 142.3, 134.6, 129.6, 129.5, 129.2, 128.1, 126.1, 119.4, 116.5, 113.9, 86.7, 71.6, 56.5,

55.4, 47.0, 47.0, 46.2, 44.6, 43.2, 41.0, 35.5, 32.0, 31.7, 26.5, 20.1, 10.7. LC-MS m/z $[M + H]^+$ $C_{30}H_{36}N_3O_5^+$ calcd 518.3, found 518.4.

6-O-Carboxymethylmorphine (15). Compound **6** (93 mg, 0.23 mmol, 1 equiv) was dissolved in dry THF (3 mL) and cooled to 0 °C under an N₂ atmosphere. To this solution, a suspension of prewashed NaH (60%, 37 mg, 0.92 mmol, 4 equiv) in THF (1 mL) was added dropwise. The solution was then allowed to warm to room temperature and stirred for 15 min. A solution of *tert*-butyl bromoacetate in THF (1 mL) was then added dropwise and allowed to stir at room temperature for 1 h. The reaction was then quenched with saturated NH₄Cl (2 mL), and then MeCN (2 mL) was added. The resulting solution was reduced in vacuo, and saturated NaHCO₃ (20 mL) was added and extracted with CHCl₃ (3 \times 20 mL). The combined organic phases were backwashed with brine (20 mL), dried over Na₂SO₄, and the solvent removed in vacuo to give a brown oil. The crude oil was dissolved in DCM (3 mL) under an N₂ atmosphere. Triethylsilane (1.1 mL, 6.9 mmol, 30 equiv) and TFA (1 mL) were then added and the reaction vessel purged with N₂. The reaction was allowed to stir for 1 h, then reduced in vacuo. The resulting oil was purified by prep-HPLC to give the product as a solid white TFA salt (61 mg, 58%). ¹H NMR (DMSO-*d*₆) δ 10.13 (s, 1H), 9.16 (s, 1H), 6.56 (d, J = 8.1 Hz, 1H), 6.46 (d, J = 8.1 Hz, 1H), 5.76 (d, J = 9.9 Hz, 2H), 5.35 (d, J = 9.7 Hz, 2H), 5.14–5.04 (m, 2H), 4.19 (s, 3H), 4.12 (dd, J = 16.4, 3.9 Hz, 3H), 3.30 (d, J = 12.7 Hz, 2H), 3.20 (d, J = 19.8 Hz, 1H), 3.02 (d, J = 26.9 Hz, 2H), 2.89 (s, 3H), 2.82 (s, 2H), 2.74 (dd, J = 19.1, 7.3 Hz, 1H), 2.19 (td, J = 13.6, 4.1 Hz, 1H), 1.95 (d, J = 12.5 Hz, 1H). ¹³C NMR (DMSO-*d*₆) δ 171.6, 146.2, 139.3, 131.9, 128.8, 125.9, 121.9, 119.3, 117.2, 87.1, 73.4, 65.4, 59.6, 46.5, 41.4, 40.5, 38.2, 32.8, 20.8. LC-MS m/z $[M + H]^+$ $C_{19}H_{22}NO_5^+$ calcd 344.2, found 344.2.

3-O-PMB-(6-O-(4-((2-*tert*-butoxycarbonyl)amino)ethyl)amino-4-oxobutanoyl)morphine (16). Compound **11** (96.5 mg, 0.19 mmol, 1 equiv), HCTU (95 mg, 0.23 mmol, 1.2 equiv), and TEA (54 μ L, 0.38 mmol, 2 equiv) were dissolved in dry DMF (1.5 mL) under an N₂ atmosphere and was allowed to stir at room temperature for 30 min. *tert*-Butyl (4-aminoethyl)carbamate (37 mg, 0.23 mmol, 1.2 equiv) was then added as a solution in dry DMF (0.5 mL) and allowed to stir at room temperature for 19 h. EtOAc (20 mL) was then added, and the resulting solution was washed with half-saturated NaHCO₃ (3 \times 10 mL), saturated NaHCO₃ (20 mL), half-saturated brine (2 \times 10 mL), and brine (20 mL). The organic phase was then dried over Na₂SO₄ and the solvent removed in vacuo. The resulting residue was purified by flash column chromatography (98:1:1 CHCl₃/MeOH/TEA) to give the product as a clear glass (102 mg, 83%). ¹H NMR (CDCl₃) δ 7.30 (d, J = 8.6 Hz, 2H), 6.86 (d, J = 8.6 Hz, 2H), 6.72 (d, J = 8.2 Hz, 1H), 6.54 (d, J = 8.2 Hz, 1H), 6.31 (t, J = 5.5 Hz, 1H), 5.59 (d, J = 10.1 Hz, 1H), 5.47–5.39 (m, 1H), 5.30 (s, 1H), 5.18–5.08 (m, 2H), 4.98 (s, 2H), 3.77 (s, 3H), 3.33 (dd, J = 5.5, 3.3 Hz, 1H), 3.30–3.23 (m, 1H), 3.11–2.97 (m, 3H), 2.96–2.87 (m, 1H), 2.73 (s, 1H), 2.70–2.61 (m, 2H), 2.57 (dd, J = 12.2, 3.8 Hz, 1H), 2.41 (s, 3H), 2.40–2.34 (m, 1H), 2.29 (ddd, J = 18.1, 9.0, 4.5 Hz, 3H), 2.07–1.97 (m, 1H), 1.84 (d, J = 11.1 Hz, 1H), 1.33 (s, 9H). ¹³C NMR (CDCl₃) δ 171.9, 171.8, 159.8, 156.4, 146.5, 141.2, 130.8, 129.9, 129.5, 128.6, 128.4, 127.7, 119.6, 114.8, 114.0, 87.7, 71.3, 67.7, 59.2, 55.4, 46.8, 43.1, 42.4, 40.6, 40.4, 39.9, 35.2, 31.8, 30.5, 28.4, 20.3. LC-MS m/z $[M + H]^+$ $C_{36}H_{46}N_3O_8^+$ calcd 648.3, found 648.4.

6-O-(4-((2-Aminoethyl)amino)-4-oxobutanoyl)morphine (17). Compound **16** (102 mg, 0.16 mmol, 1 equiv) was deprotected using general deprotection procedure A. The resulting residue was purified by prep-HPLC to give the product as a solid white mono-TFA salt (43 mg, 51%). ¹H NMR (DMSO-*d*₆) δ 10.01 (s, 1H), 9.22 (s, 1H), 8.10 (t, J = 5.7 Hz, 1H), 7.75 (s, 3H), 6.59 (d, J = 8.1 Hz, 1H), 6.51 (dd, J = 8.0, 4.2 Hz, 1H), 5.65 (d, J = 10.0 Hz, 1H), 5.52–5.39 (m, 1H), 5.25–5.14 (m, 1H), 5.09–4.98 (m, 1H), 4.13 (s, 1H), 3.27 (dd, J = 12.2, 6.2 Hz, 2H), 3.19 (d, J = 19.8 Hz, 1H), 3.06 (d, J = 4.7 Hz, 1H), 2.97 (s, 1H), 2.89 (s, 2H), 2.84 (dd, J = 12.1, 6.0 Hz, 2H), 2.71 (dd, J = 20.0, 6.7 Hz, 1H), 2.65–2.59 (m, 2H), 2.45 (t, J = 6.8 Hz, 2H), 2.20 (dd, J = 13.4, 9.1 Hz, 1H), 1.84 (dd, J = 46.3, 11.7 Hz, 1H). LC-MS m/z $[M + H]^+$ $C_{23}H_{30}N_3O_5^+$ calcd 428.2, found 428.2.

2-((1*E*,3*E*,5*Z*)-5-(1-(6-((2-(4-(((4*R*,4*aR*,7*S*,7*aR*,12*bS*)-9-Hydroxy-3-methyl-2,3,4,4*a*,7,7*a*-hexahydro-1*H*-4,12-methanobenzofuro[3,2-*e*]isoquinolin-7-yl)oxy)-4-oxobutanamido)ethyl)amino)-6-oxohexyl)-3,3-dimethyl-5-sulfoindolin-2-ylidene)pent-1,3-dien-1-yl)-1,3,3-trimethyl-3*H*-indol-1-ium-5-sulfonate (**18**). Compound **17** (7.1 mg, 0.013 mmol, 2 equiv), sulfo-Cy5 NHS ester (Lumiprobe, 5 mg, 0.0066 mmol, 1 equiv), and TEA (2.8 μ L, 0.020 mmol, 3 equiv) was dissolved in dry DMF (150 μ L) under an N₂ atmosphere and allowed to stir at room temperature for 7 h. HCTU (2.7 mg, 0.0066 mmol, 1 equiv) was then added and the reaction stirred for an additional 16 h. Water (20 mL) and MeCN (1 mL) were then added and the solvent removed by freeze-drying. The resulting residue was purified by reverse phase chromatography (5–30% buffer B in buffer A, 1% jump per column volume). Clean fractions were collected and freeze-dried to give the product as a dark-blue solid TFA salt (2.6 mg, 33%). ¹H NMR (DMSO-*d*₆) δ 9.82 (s, 1H), 9.20 (s, 1H), 8.35 (t, *J* = 13.1 Hz, 1H), 7.91 (s, 1H), 7.81 (s, 2H), 7.77 (s, 1H), 7.64 (dd, *J* = 7.6, 3.9 Hz, 2H), 7.31 (d, *J* = 8.4 Hz, 2H), 6.62–6.44 (m, 5H), 6.28 (dd, *J* = 18.3, 13.9 Hz, 2H), 5.59 (d, *J* = 9.9 Hz, 1H), 5.41 (d, *J* = 9.7 Hz, 1H), 5.12–4.93 (m, 2H), 4.08 (s, 4H), 3.59 (s, 2H), 3.16–3.02 (m, 7H), 2.89 (s, 4H), 2.60–2.54 (m, 3H), 2.39 (t, *J* = 6.6 Hz, 3H), 2.03 (t, *J* = 7.1 Hz, 2H), 1.68 (s, 12H), 1.58–1.48 (m, 2H), 1.29 (ddd, *J* = 17.8, 13.8, 8.6 Hz, 5H), 1.17 (t, *J* = 7.3 Hz, 2H). ES-TOF HRMS *m/z*: [M + H]⁺ C₅₅H₆₆N₅O₁₂S₂⁺ calcd 1052.4144, found 1052.4119; [M + 2H]²⁺ C₅₅H₆₇N₅O₁₂S₂⁺ calcd 526.7108, found 526.7113.

6-*O*-((4-((tert-Butoxycarbonyl)amino)butyl)carbamoyl)morphine (**19**). Compound **15** (130 mg, 0.28 mmol, 1 equiv), anhydrous HOBt (42 mg, 0.31 mmol, 1.1 equiv), EDC-HCl (60 mg, 0.31 mmol, 1.1 equiv), and TEA (119 μ L, 85 mmol, 3 equiv) were dissolved in DMF (2 mL) under an N₂ atmosphere and allowed to stir at room temperature for 1 h. *tert*-Butyl (4-aminobutyl)carbamate (64 mg, 0.34 mmol, 1.2 equiv) was then added as a solution in dry DMF (1 mL) and the reaction stirred at room temperature for 17 h. The solvent was then removed in vacuo and the residue purified by reverse phase chromatography (6–35% buffer B in buffer A, 1% jump per column volume). Clean fractions were collected and freeze-dried to give the product as a light-orange solid TFA salt (65 mg, 36%). ¹H NMR (MeOD) δ 6.65 (dd, *J* = 8.1, 1.4 Hz, 1H), 6.58 (d, *J* = 8.1 Hz, 1H), 5.92–5.83 (m, 1H), 5.42 (d, *J* = 9.9 Hz, 1H), 5.19–5.12 (m, 1H), 4.91 (s, 9H), 4.28–4.10 (m, 4H), 3.39 (dd, *J* = 13.3, 3.7 Hz, 1H), 3.34 (d, *J* = 6.5 Hz, 1H), 3.26 (d, *J* = 7.3 Hz, 1H), 3.20 (d, *J* = 20.2 Hz, 1H), 3.12–2.94 (m, 7H), 2.87 (dd, *J* = 19.8, 6.8 Hz, 1H), 2.34 (td, *J* = 13.6, 5.0 Hz, 1H), 2.12 (d, *J* = 13.9 Hz, 1H), 1.75–1.62 (m, 3H), 1.60–1.47 (m, 2H), 1.42 (s, 3H). ¹³C NMR (MeOD) δ 172.6, 147.4, 132.9, 129.9, 126.6, 121.2, 118.7, 89.0, 75.3, 69.8, 69.7, 62.3, 42.9, 41.7, 40.3, 40.0, 39.7, 39.1, 34.3, 28.8, 28.3, 27.7, 27.4, 25.8, 22.2. LC-MS *m/z* [M + H]⁺ C₂₈H₄₀N₃O₆⁺ calcd 514.3, found 514.3.

6-*O*-((4-Aminobutyl)carbamoyl)morphine (**20**). Compound **19** (65 mg, 0.10 mmol, 1 equiv) was dissolved in CHCl₃ (1 mL) and TFA (0.5 mL) and the resulting solution allowed to stir for 1 h. The solvent was then removed in vacuo and the resulting residue dissolved in buffer A and freeze-dried to give the product as a brown oil TFA salt (60 mg, quantitative). ¹H NMR (MeOD) δ 6.65 (d, *J* = 8.1 Hz, 1H), 6.58 (d, *J* = 8.2 Hz, 1H), 5.86 (d, *J* = 10.0 Hz, 1H), 5.41 (d, *J* = 9.8 Hz, 1H), 5.15 (d, *J* = 5.7 Hz, 1H), 4.28–4.10 (m, 4H), 3.38 (dd, *J* = 13.2, 3.8 Hz, 1H), 3.33 (d, *J* = 6.7 Hz, 1H), 3.27 (d, *J* = 20.0 Hz, 1H), 3.18 (d, *J* = 12.0 Hz, 1H), 3.07 (dd, *J* = 13.3, 3.5 Hz, 1H), 3.04–2.93 (m, 6H), 2.87 (dd, *J* = 19.9, 6.7 Hz, 1H), 2.36 (td, *J* = 13.6, 4.6 Hz, 1H), 2.09 (d, *J* = 12.0 Hz, 1H), 1.77–1.58 (m, 4H). ¹³C NMR (101 MHz, MeOD) δ 172.5, 147.4, 141.0, 132.8, 129.9, 126.7, 123.2, 121.2, 118.7, 89.0, 75.4, 69.7, 62.2, 42.9, 41.7, 40.3, 39.8, 39.1, 34.2, 27.3, 26.8, 25.8, 22.2. LC-MS *m/z* [M + H]⁺ C₂₃H₃₂N₃O₄⁺ calcd 414.2, found 414.3.

1-Ethyl-2-((1*E*,3*E*,5*Z*)-5-(1-(6-((4-((2-(((4*R*,4*aR*,7*S*,7*aR*,12*bS*)-9-hydroxy-3-methyl-2,3,4,4*a*,7,7*a*-hexahydro-1*H*-4,12-methanobenzofuro[3,2-*e*]isoquinolin-7-yl)oxy)acetamido)butyl)amino)-6-oxohexyl)-3,3-dimethyl-5-sulfoindolin-2-ylidene)pent-1,3-dien-1-yl)-3,3-dimethyl-3*H*-indol-1-ium-5-sulfonate (**21**). Sulfo-Cy5 TFA salt (6.0 mg, 7.8 μ mol, 1 equiv), HCTU (3.9 mg, 9.3 μ mol, 1.2 equiv), and TEA (10 μ L) were dissolved in DMF (600 μ L) under an N₂ atmosphere and stirred at room temperature for 1 h. Compound **20** (8.2 mg, 16 μ mol, 2 equiv) was then added as a solution in DMF

(200 μ L) and allowed to stir at room temperature for 18 h. Buffer A was added and the resulting solution freeze-dried. The residue was purified by reverse phase chromatography (5–30% buffer B in buffer A, 1% jump per column volume). Clean fractions were collected and freeze-dried to give the product as a dark-blue solid TFA salt (3.6 mg, 40%). ¹H NMR (DMSO-*d*₆) δ 10.22 (s, 1H), 9.19 (s, 1H), 8.35 (t, *J* = 12.6 Hz, 2H), 7.82 (s, 2H), 7.78–7.71 (m, 2H), 7.68–7.61 (m, 2H), 7.34–7.30 (m, 2H), 7.18 (s, 1H), 7.05 (s, 1H), 6.59–6.55 (m, 2H), 6.46 (d, *J* = 8.1 Hz, 1H), 6.30 (d, *J* = 14.0 Hz, 1H), 5.77 (dd, *J* = 10.2, 2.2 Hz, 1H), 5.28 (d, *J* = 10.0 Hz, 1H), 5.07 (d, *J* = 5.9 Hz, 1H), 4.15–3.93 (m, 10H), 3.19 (d, *J* = 19.3 Hz, 1H), 3.14–3.04 (m, 5H), 3.02–2.96 (m, 3H), 2.89 (s, 3H), 2.82 (s, 1H), 2.75–2.66 (m, 1H), 2.23–2.13 (m, 1H), 2.02 (t, *J* = 6.9 Hz, 2H), 1.95–1.89 (m, 1H), 1.58–1.48 (m, 3H), 1.43–1.29 (m, 8H), 1.25 (t, *J* = 7.3 Hz, 6H), 1.17 (t, *J* = 7.3 Hz, 2H). ES-TOF HRMS *m/z* [M + H]⁺ C₅₆H₇₀N₅O₁₁S₂⁺ calcd 1052.4508, found 1052.4545, [M + Na]⁺ C₅₆H₆₉N₅O₁₁S₂Na⁺ calcd 1074.4327, found 1074.4338.

Pharmacology. *cAMP BRET CAMYEL Assay.* HEK293 cells were transfected with 2 μ g of hMOR pEF5/FRT construct cDNA and 3 μ g of CAMYEL sensor cDNA. The cDNA was mixed with 30 μ g of polyethylenimine and made up to 250 μ L with 0.15 M NaCl, then allowed to incubate for 15–20 min at room temperature. This mixture was then added to the cells dropwise and gently mixed. The cells were then incubated for 24 h in post transfection media (PTM), after which they were resuspended in 15 mL of PTM and replated onto white poly-D-lysine coated plates at 100 μ L per well and maintained for 24 h. The media was then aspirated and the cells washed once with 100 μ L/well HBSS at 37 °C. HBSS (70 μ L/well) was then added back and the cells incubated for 30 min at 37 °C in the absence of CO₂. Coelenterazine H (10 μ L, 5 μ M final) was added and the cells incubated in the dark for 10 min at 37 °C. The drugs (10 μ L) were then added at the desired concentration, followed immediately by forskolin (10 μ L, 30 μ M final), then incubated for 5 min inside a LUMistar Omega plate reader set at 37 °C. Luminescence for RLuc8 (480 nm) and fluorescence for YFP (530 nm) were then measured. Baseline and vehicle control values were subtracted, and the BRET signal was normalized as a percentage of forskolin response.

Confocal Microscopy. HEK293 cells stably expressing N-terminal SNAP-hMOR were cultured in Dulbecco's Modified Eagle's Medium (DMEM) supplemented with 10% (v/v) fetal calf serum (FCS) and 1 mg/mL G418. Cells were grown in poly-D-lysine-coated 8-well Labtek borosilicate chambered-cover glasses (Nalgen Nunc International, Fisher Scientific). On the day of experimentation, SNAP tag labeling was performed by incubating cells in 500 nM BG-488 in fresh cell culture media for 30 min at 37 °C. Cells were washed in prewarmed HEPES-buffered saline solution (HBS) containing 4.5 mM D-glucose and incubated for 30 min at 37 °C in the presence or absence of 1 μ M naloxone prior to addition and incubation with the relevant concentration of **21** for 30 min at 37 °C. Where the concentration of **21** was 10 μ M, the cells were washed with HBS prior to imaging. Confocal images were captured using a Zeiss LSM710 laser scanning microscope using a Plan-Apochromat 63 \times 1.3NA oil-immersion objective lens (1024 \times 1024 pixels, averaging at four frames). The 633 nm HeNe and 488 nm argon lasers were used to excite sulfo-Cy5 and BG-488, respectively. Emission was captured at 638–759 nm and 493–628 nm, respectively. Confocal settings for laser power, offset, and gain were kept constant throughout acquisition. Images were processed in Zeiss Zen 2011, with any linear adjustments made equally across all images within a data set.

■ ASSOCIATED CONTENT

Supporting Information

The Supporting Information is available free of charge on the ACS Publications website at DOI: 10.1021/acs.jmedchem.7b01811.

Comparison of the NMR spectra of compounds **6** and **7** (PDF)

Molecular formula strings (CSV)

AUTHOR INFORMATION

Corresponding Author

*Phone: +61 (0)3 9903 9542. Fax: +61 (0)3 9903 9582. E-mail: peter.scammells@monash.edu.

ORCID

Barrie Kellam: 0000-0003-0030-9908

Peter J. Scammells: 0000-0003-2930-895X

Notes

The authors declare no competing financial interest.

ACKNOWLEDGMENTS

R.L. thanks the Australian Government Research Training Program Scholarship for their financial support. We acknowledge the support of the Monash–Nottingham Joint Doctoral Training Centre program, to which both R.L. and A.B.G. are a part, and has made this work possible. Microscopy work performed at the University of Nottingham was supported by Medical Research Council grant MR/N020081/1. We also acknowledge the assistance and expertise of Dr Luke S. Schembri and Dr Gaik Orbell in opiate chemistry. We acknowledge GSK Australia for providing the morphine used in the synthesis of all our compounds.

ABBREVIATIONS USED

BRET, bioluminescence resonance energy transfer; cAMP, cyclic adenosine monophosphate; DIAD, diisopropyl azodicarboxylate; DMAP, 4-dimethylaminopyridine; DOR, δ opioid receptor; EDC, *N*-(3-(dimethylamino)propyl)-*N*'-ethylcarbodiimide; GPCR, G protein-coupled receptor; HCTU, *O*-(1*H*-6-chlorobenzotriazole-1-yl)-1,1,3,3-tetramethyluronium hexafluorophosphate; KOR, κ opioid receptor; MOR, μ opioid receptor; NOPr, nociception/orphanin FQ peptide receptor; PMB, *para*-methoxybenzyl; NHS, *N*-hydroxysuccinimide; TEA, triethylamine; TFA, trifluoroacetic acid

REFERENCES

- (1) Blakemore, P. R.; White, J. D. Morphine, the Proteus of Organic Molecules. *Chem. Commun.* **2002**, 1159–1168.
- (2) Rudd, R. A.; Aleshire, N.; Zibbell, J. E.; Gladden, R. M. Increases in Drug and Opioid Overdose Deaths — United States, 2000–2014. *Cent. Dis. Prev. - Morb. Mortal. Wkly. Rep.* **2016**, *64*, 1378–1382.
- (3) Thompson, A. A.; Liu, W.; Chun, E.; Katritch, V.; Wu, H.; Vardy, E.; Huang, X.-P.; Trapella, C.; Guerrini, R.; Calo, G.; Roth, B. L.; Cherezov, V.; Stevens, R. C. Structure of the Nociceptin/orphanin FQ Receptor in Complex with a Peptide Mimetic. *Nature* **2012**, *485*, 395–399.
- (4) Matthes, H. W. D.; Maldonado, R.; Simonin, F.; Valverde, O.; Slowe, S.; Kitchen, I.; Befort, K.; Dierich, A.; Le Meur, M.; Dollé, P.; Tzavara, E.; Hanoune, J.; Roques, B. P.; Kieffer, B. L. Loss of Morphine-Induced Analgesia, Reward Effect and Withdrawal Symptoms in Mice Lacking the μ -Opioid-Receptor Gene. *Nature* **1996**, *383*, 819–823.
- (5) Bodnar, R. J. Endogenous Opiates and Behavior: 2012. *Peptides* **2013**, *50*, 55–95.
- (6) Manglik, A.; Lin, H.; Aryal, D. K.; McCorvey, J. D.; Dengler, D.; Corder, G.; Levit, A.; Kling, R. C.; Bernat, V.; Hübner, H.; Huang, X.-P.; Sassano, M. F.; Giguère, P. M.; Löber, S.; Duan, D.; Scherrer, G.; Kobilka, B. K.; Gmeiner, P.; Roth, B. L.; Shoichet, B. K. Structure-Based Discovery of Opioid Analgesics with Reduced Side Effects. *Nature* **2016**, *537*, 185–190.
- (7) Connor, M.; Osborne, P. B.; Christie, M. J. μ -Opioid Receptor Desensitization: Is Morphine Different? *Br. J. Pharmacol.* **2004**, *143*, 685–696.

(8) Lamb, K.; Tidgewell, K.; Simpson, D. S.; Bohn, L. M.; Prisinzano, T. E. Antinociceptive Effects of Herkinorin, a MOP Receptor Agonist Derived from Salvinorin A in the Formalin Test in Rats: New Concepts in μ Opioid Receptor Pharmacology: from a Symposium on New Concepts in μ -opioid Pharmacology. *Drug Alcohol Depend.* **2012**, *121*, 181–188.

(9) Bohn, L. M.; Gainetdinov, R. R.; Lin, F. T.; Lefkowitz, R. J.; Caron, M. G. μ -Opioid Receptor Desensitization by β -Arrestin-2 Determines Morphine Tolerance but not Dependence. *Nature* **2000**, *408*, 720–723.

(10) Fournie-Zaluski, M. C.; Gacel, G.; Roques, B. P.; Senault, B.; Lecomte, J. M.; Malfroy, B.; Swerts, J. P.; Schwartz, J. C. Fluorescent Enkephalin Derivatives with Biological Activity. *Biochem. Biophys. Res. Commun.* **1978**, *83*, 300–305.

(11) Mihara, H.; Lee, S.; Shimohigashi, Y.; Aoyagi, H.; Kato, T.; Izumiya, N.; Costa, T. δ and μ Opiate Receptor Probes: Fluorescent Enkephalins with High Receptor Affinity and Specificity. *FEBS Lett.* **1985**, *193*, 35–38.

(12) Arttamangkul, S.; Alvarez-Maubecin, V.; Thomas, G.; Williams, J. T.; Grandy, D. K. Binding and Internalization of Fluorescent Opioid Peptide Conjugates in Living Cells. *Mol. Pharmacol.* **2000**, *58*, 1570–1580.

(13) Arttamangkul, S.; Torrecilla, M.; Kobayashi, K.; Okano, H.; Williams, J. T. Separation of μ -Opioid Receptor Desensitization and Internalization: Endogenous Receptors in Primary Neuronal Cultures. *J. Neurosci.* **2006**, *26*, 4118–4125.

(14) Macey, T. A.; Ingram, S. L.; Bobeck, E. N.; Hegarty, D. M.; Aicher, S. A.; Arttamangkul, S.; Morgan, M. M. Opioid Receptor Internalization Contributes to Dermorphin-mediated Antinociception. *Neuroscience* **2010**, *168*, 543–550.

(15) Macey, T. A.; Bobeck, E. N.; Suchland, K. L.; Morgan, M. M.; Ingram, S. L. Change in Functional Selectivity of Morphine with the Development of Antinociceptive Tolerance. *Br. J. Pharmacol.* **2015**, *172*, 549–561.

(16) Kolb, V. M.; Koman, A.; Terenius, L. Fluorescent Probes for Opioid Receptors. *Life Sci.* **1983**, *33*, 423–426.

(17) Archer, S.; Medzihradsky, F.; Seyed-Mozaffari, A.; Emmerson, P. J. Synthesis and Characterization of 7-Nitrobenzo-2-oxa-1,3-diazole (NBD)-labeled Fluorescent Opioids. *Biochem. Pharmacol.* **1992**, *43*, 301–306.

(18) Emmerson, P. J.; Archer, S.; El-Hamouly, W.; Mansour, A.; Akil, H.; Medzihradsky, F. Synthesis and Characterization of 4,4-Difluoro-4-Bora-3a,4a-Diaza-s-Indacene (BODIPY)-Labeled Fluorescent Ligands for the μ Opioid Receptor. *Biochem. Pharmacol.* **1997**, *54*, 1315–1322.

(19) Schembri, L. S.; Stoddart, L. A.; Bridson, S. J.; Kellam, B.; Canals, M.; Graham, B.; Scammells, P. J. Synthesis, Biological Evaluation, and Utility of Fluorescent Ligands Targeting the μ -Opioid Receptor. *J. Med. Chem.* **2015**, *58*, 9754–9767.

(20) Cunningham, C. W.; Mercer, S. L.; Hassan, H. E.; Traynor, J. R.; Eddington, N. D.; Coop, A. Opioids and Efflux Transporters. Part 2: P-Glycoprotein Substrate Activity of 3- and 6-Substituted Morphine Analogs. *J. Med. Chem.* **2008**, *51*, 2316–2320.

(21) Beale, J. M. J.; Block, J. H. *Wilson and Gisvold's Textbook of Organic Medicinal and Pharmaceutical Chemistry*, 12th ed.; Lippincott Williams & Wilkins: Baltimore, MD, 2011.

(22) Simon, C.; Makleit, S.; Hosztafi, S. Application of the Mitsunobu Reaction for the Preparation of Isomorphine and Isocodeine Derivatives. *Synth. Commun.* **1991**, *21* (3), 407–412.

(23) Simon, C.; Hosztafi, S.; Makleit, U. Stereoselective Synthesis of β -Naltrexol, β -Naloxol, β -Naloxamine, β -Naltrexamine and Related Compounds by the Application of the Mitsunobu Reaction. *Tetrahedron* **1994**, *50* (32), 9757–9768.

(24) Várad, A.; Hosztafi, S.; Le Rouzic, V.; Tóth, G.; Urai, Á.; Noszál, B.; Pasternak, G. W.; Grinnell, S. G.; Majumdar, S. Novel 6 β -Acylaminomorphinans with Analgesic Activity. *Eur. J. Med. Chem.* **2013**, *69*, 786–789.

(25) Urai, A.; Varadi, A.; Szocs, L.; Komjati, B.; Le Rouzic, V.; Hunkele, A.; Pasternak, G. W.; Majumdar, S.; Hosztafi, S. Synthesis

and Pharmacological Evaluation of Novel Selective MOR Agonist 6 β -Pyridinyl Amidomorphines Exhibiting Long-Lasting Antinociception. *MedChemComm* **2017**, *8* (1), 152–157.

(26) Middleton, R. J.; Briddon, S. J.; Cordeaux, Y.; Yates, A. S.; Dale, L.; George, M. W.; Baker, J. G.; Hill, S. J.; Kellam, B. New Fluorescent Adenosine A₁-Receptor Agonists that Allow Quantification of Ligand – Receptor Interactions in Microdomains of Single Living Cells. *J. Med. Chem.* **2007**, *50*, 782–793.

(27) Thompson, G. L.; Lane, J. R.; Coudrat, T.; Sexton, P. M.; Christopoulos, A.; Canals, M. Biased Agonism of Endogenous Opioid Peptides at the μ -Opioid Receptor. *Mol. Pharmacol.* **2015**, *88* (2), 335–346.

(28) Thompson, G. L.; Lane, J. R.; Coudrat, T.; Sexton, P. M.; Christopoulos, A.; Canals, M. Systematic Analysis of Factors Influencing Observations of Biased Agonism at the Mu-Opioid Receptor. *Biochem. Pharmacol.* **2016**, *113*, 70–87.

(29) Stoddart, L. A.; Vernall, A. J.; Briddon, S. J.; Kellam, B.; Hill, S. J. Direct Visualisation of Internalization of the Adenosine A₃ Receptor and Localization with Arrestin Using a Fluorescent Agonist. *Neuropharmacology* **2015**, *98*, 68–77.

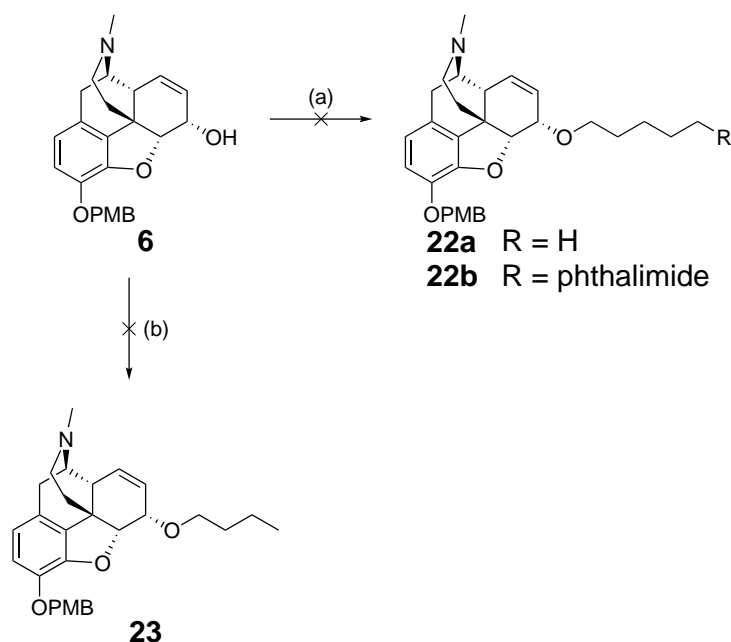
(30) Vernall, A. J.; Stoddart, L. A.; Briddon, S. J.; Hill, S. J.; Kellam, B. Highly Potent and Selective Fluorescent Antagonists of the Human Adenosine A₃ Receptor Based on the 1,2,4-triazolo[4,3-*a*]quinoxalin-1-one Scaffold. *J. Med. Chem.* **2012**, *55* (4), 1771–1782.

(31) Baker, J. G.; Middleton, R.; Adams, L.; May, L. T.; Briddon, S. J.; Kellam, B.; Hill, S. J. Influence of Fluorophore and Linker Composition on the Pharmacology of Fluorescent Adenosine A₁ Receptor Ligands. *Br. J. Pharmacol.* **2010**, *159* (4), 772–786.

3.2.1 Additional Notes

Compound references here will refer directly to the numbering scheme in the paper, and should be viewed independently from the rest of this dissertation.

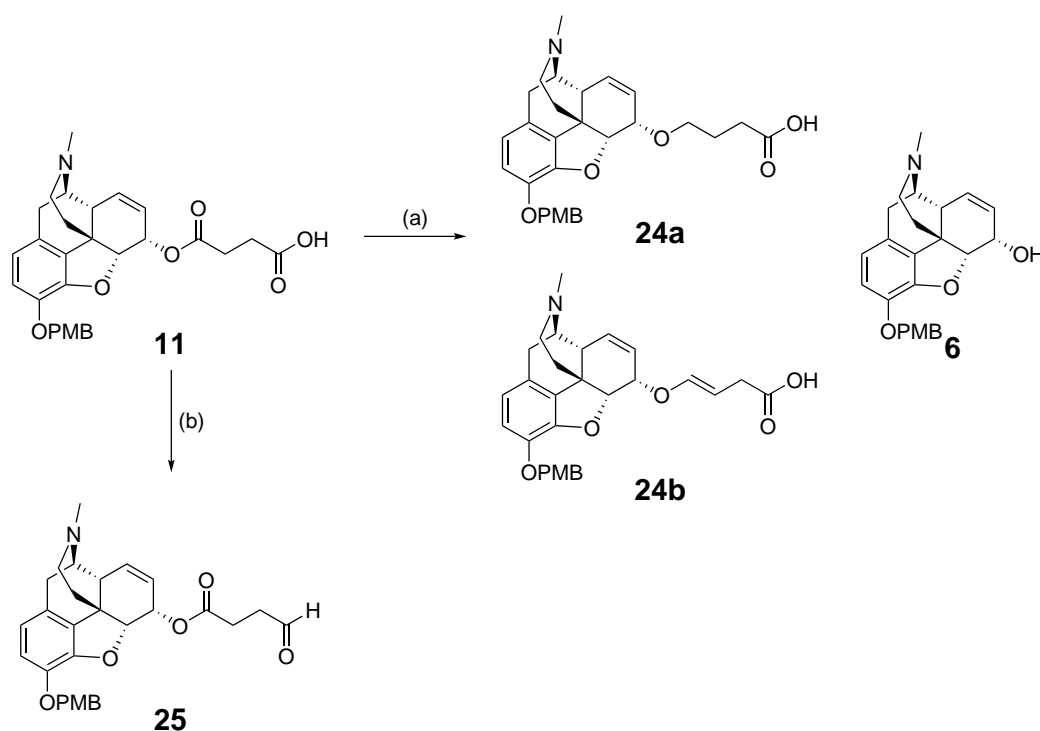
In addition to the described methods of producing an ether-linked model congener, several other synthetic attempts were made to give ether-linked model congeners. Direct alkylation of compound **6** at the C-6 position using 2-(6-bromohexyl)isoindoline-1,3-dione using sodium hydride in THF failed to give any product. Simplification of this reaction to using 1-bromohexane as a model again failed to give any appreciable product, returning mostly the starting material by LC-MS and NMR. Using toluene or dioxane as solvents, or using LiHMDS as the base gave similar results by LC-MS. Using 1-iodobutane under similar conditions gave partial conversion to the C-6 alkylated product, but tended not to go to completion and gave a variety of by-products such as the *N*-alkyl by product.



Scheme 1. Attempted alkylation of the C-6 secondary alcohol. Reagents and Conditions: (a) alkyl bromide, base (NaH or LiHMDS), solvent (THF, toluene, dioxane), rt or -78°C to rt, 18 h; (b) 1-iodobutane, NaH, THF, rt, 18 h.

Das *et al.* demonstrated that esters could be reduced using the reagent triiron dode-

carbonyl ($\text{Fe}_3(\text{CO})_{12}$), an organo carbonyl complex.⁶ In conjunction with a silane such as 1,1,3,3-tetramethyldisiloxane (TMDS) in toluene, they showed that the ester may be reduced in the presence of other functional groups such as halogens, methoxy groups and alkenes. A test reaction was carried out using ethyl 4-bromobenzoate showed this reaction did indeed proceed with few by-products observed. With these results in mind, compound **11** was subjected to these conditions in an attempt to selectively reduce the ester to an ether. Although some product was observed via LC-MS analysis (compound **24a**), the reaction did not proceed to completion in addition to giving various reduced side-products. Two of these were identified to be the cleaved ester returning compound **6** and a reduction of the ester to an enol ether (compound **24b**). Heating in a microwave reactor rather than by thermal heating resulted in fewer side-products, but also reduced the free acid to the corresponding aldehyde.



Scheme 2. Attempts at using $\text{Fe}_3(\text{CO})_{12}$ for the selective reduction of esters to ethers. Reagents and conditions: (a) $\text{Fe}_3(\text{CO})_{12}$, TMDS, toluene, 100 °C, 20 h; (b) $\text{Fe}_3(\text{CO})_{12}$, TMDS, toluene, μW reactor 100 °C, 2 h.

Although this reaction has been shown to work in literature, and the test reaction sugge-

sted this may have been a valid method, the structural complexity of compound **11** in addition to the various heteroatoms may have interfered with it. Perhaps protecting the heteroatoms by capping or introducing protecting groups would have enabled the reaction to proceed to the desired product. In particular, Das *et al.* did not show that this reaction was orthogonal to free acids, so perhaps first capping it as the amide would have resulted in a more positive outcome. Nevertheless, $\text{Fe}_3(\text{CO})_{12}$ was found to be useful as a catalyst for another reaction involving alkaloids, which will be discussed in Chapter 5.

References

- (1) Middleton, R. J., Briddon, S. J., Cordeaux, Y., Yates, A. S., Dale, L., George, M. W., Baker, J. G., Hill, S. J., and Kellam, B., (2007). New fluorescent adenosine A₁-receptor agonists that allow quantification of ligand - receptor interactions in microdomains of single living cells. *J. Med. Chem.* 50, 782–793.
- (2) Stoddart, L. A., Vernall, A. J., Briddon, S. J., Kellam, B., and Hill, S. J., (2015). Direct visualisation of internalization of the adenosine A₃ receptor and localization with arrestin3 using a fluorescent agonist. *Neuropharmacol.* 98, 68–77.
- (3) Baker, J. G., Middleton, R., Adams, L., May, L. T., Briddon, S. J., Kellam, B., and Hill, S. J., (2010). Influence of fluorophore and linker composition on the pharmacology of fluorescent adenosine A₁ receptor ligands: themed section: imaging in pharmacology research paper. *Br. J. Pharmacol.* 159, 772–786.
- (4) Baker, J. G., Adams, L., Salchow, K., Mistry, S., Middleton, R. J., Hill, S. J., and Kellam, B., (2011). Synthesis and characterization of high-affinity 4,4-difluoro-4-bora-3a,4a-diaza-s-indacene-labeled fluorescent ligands for human β -adrenoceptors. *J. Med. Chem.* 54, 6874–6887.
- (5) Baker, J. G., Hall, I. P., and Hill, S. J., (2003). Pharmacology and direct visualisation of BODIPY-TMR-CGP: a long-acting fluorescent β_2 -adrenoceptor agonist. *Br. J. Pharmacol.* 139, 232–242.
- (6) Das, S., Li, Y., Junge, K., and Beller, M., (2012). Synthesis of ethers from esters via Fe-catalyzed hydrosilylation. *Chem. Commun.* 48, 10742–10744.

4 Development of Gold Nanorod-based Imaging Systems

Following the development of the morphine-based fluorescent partial agonist probes for the MOR, the focus was shifted to designing our AuNR-based imaging system. Here, the goal was to explore nanoparticle fluorophores as alternatives to traditional organic fluorophores such as Cy5, as well as to create a platform from which multiple ligands may be attached in order to visualize opioid receptor heterodimers. Using prior knowledge from the design of our fluorescent morphine probes (Chapter 3), similar approaches were used in order to maintain known active conjugation methods. Note that for all discussions involving nanoparticles, "core@shell" notation will be used, where the chemical species preceding the "@" is being "wrapped" by the chemical entity proceeding the "@". Where the core is coated in multiple chemical species, the second species will be shown as a percentage of the total coating in the format core@shell(species x%).

4.1 Synthesis of Gold Nanorods

AuNRs were synthesized via the Nikoobakht method (see Chapter 1.3.4, Figure 13 for a visual summary).¹ This method involves a two-step seed-mediated growth procedure. First, gold nanoseeds were generated by reducing a solution of chloroauric acid with an ice-cold solution of sodium borohydride in the presence of the surfactant CTAB, producing seeds of approximately 4 - 6 nm. Next, a growth solution was produced by adding chloroauric acid, ascorbic acid, and varying amounts of silver nitrate to a solution of CTAB. The ascorbic acid acts as a reductant, reducing Au(III) to Au(I). Subsequent addition of the seed solution catalyses the reduction of Au(I) to Au(0), elongating the seeds into nanorods with the CTAB micelles acting as a template for the growth to give AuNR@CTAB. The titration of silver nitrate controls the AuNR aspect ratio. These AuNRs may then be purified by centrifugation and washing with water. It is known that at low concentrations of CTAB below the critical micellar concentration of 1 mM, AuNR@CTAB become colloiddally unstable and aggregate, hence careful control of the CTAB concentration is vital. Further purification of AuNR@CTAB was achieved by washing with a CTAB solution.

Variations of this synthesis were attempted in order to achieve AuNRs. Alternations in

reagent concentrations, reaction volume, temperature, and ageing time were trialled. However, the most successful method was still essentially a scaled up synthesis of the Nikoobakht method. Slight changes in conditions have been demonstrated to have significant effects on AuNR growth. Changes in these conditions can result in formation of undesired products, such as spherical AuNPs. These have been demonstrated by the Murphy group in their initial attempts at trying to achieve AuNRs in high purity with carefully controlled aspect ratios.^{2,3} Therefore, close adherence to the Nikoobakht method was maintained, as it was determined these conditions were optimal for our purposes.

Organic additives were also trialled, as it was thought these might enable improved control over AuNR growth. Two additives were tested; acetone and ethylenediaminetetraacetic acid (EDTA). Acetone has been suggested to increase the flexibility of the CTAB membrane, giving AuNRs of smaller diameter.⁴ It was suggested that this effect could be controlled by varying the concentration of acetone in the growth solution, giving CTAB templates of varying diameter. EDTA was used in the synthesis of spherical AuNPs to give more consistent and monodisperse nanoparticles.⁵ While the exact mechanism of this improvement is unknown, one of the hypotheses was that this could be due to the EDTA assisting in the removal of trace impurity metals that may affect the growth of AuNPs.

Using the standard Nikoobakht method, acetone was added as a small percentage of the solution (36:1 water/acetone). Upon addition of the nanoseeds to the growth solution, a blue solution was formed, which is in contrast to previous batches of AuNRs where they typically vary between green and red. UV-vis absorbance spectra showed two distinct peaks similar to those of well-formed AuNRs. However, upon imaging via TEM large quantities of spherical particles were observed, as well as non-uniform ones. These resembled ϕ -shaped particles, but were malformed and not uniform (Figure 21). Addition of EDTA at a final concentration of 0.02 M in both the seed and growth solutions gave interesting results. The seed solution gave a red solution, rather than the usual brown nanoseed solution. Addition of the EDTA nanoseeds to the corresponding growth solution resulted in a purple solution forming. UV-Vis spectroscopy suggested these were not rod-like in geometry, but had a malformed morphology

(Figure 22). Although two different absorbance bands were observed, the relative intensity of the peak at 675 nm is unusually low. It would be expected that a real LSPR band would absorb light far more effectively than the TSPR band, and hence would have a much greater intensity. Furthermore the peak shape of the band at 530 nm is inconsistent with known AuNR absorbance behavior. Here, the peak observed was relatively sharp, whereas in known AuNR samples this peak tends to be broader and less intense relative to the LSPR band. These observations suggest AuNRs did not form as desired, giving malformed particles instead. With these results in mind, addition of auxiliary organic additives was not carried forward.

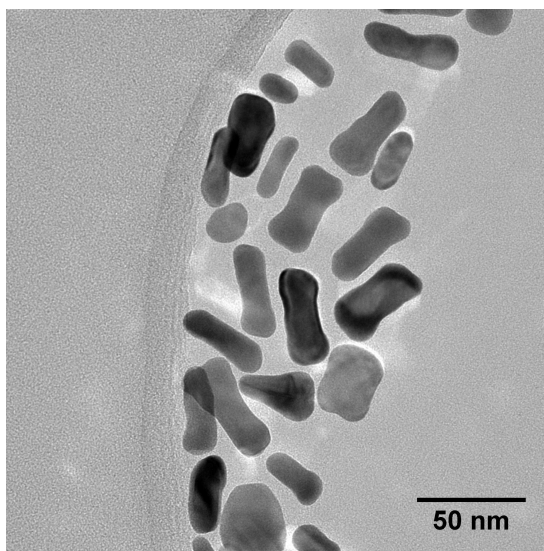


Figure 21. Malformed AuNRs due to the addition of acetone to the growth solution. Although this sample still gave a reasonable UV-Vis spectra (data not shown), the particles themselves are not rod-shaped. This highlights the importance of using TEM to characterize AuNRs, as the absorbance spectra is not enough to make a full characterization where new methods are being trialled.

4.1.1 Characterization of Gold Nanorods

AuNRs were characterized via UV-Vis spectroscopy and TEM. While TEM is the ideal method for characterizing nanoparticles, the lack of ready access limited its utility, though it was still an important tool for determining particle shape and uniformity. UV-Vis spectroscopy was used as an initial tool to determine whether or not AuNRs had successfully been formed. Successful

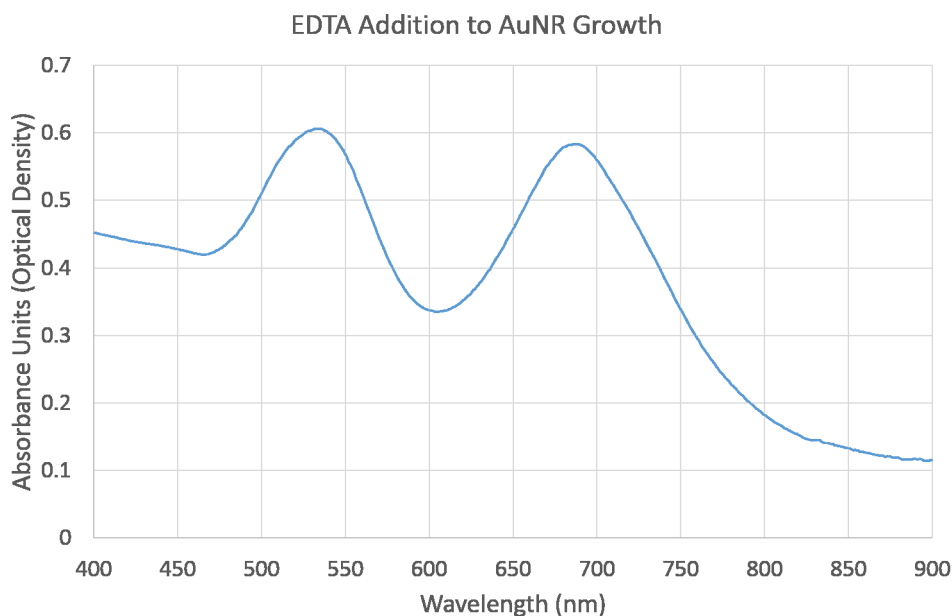


Figure 22. UV-Vis absorbance spectra of AuNRs synthesized in the presence of EDTA. The peak shapes here are inconsistent with known AuNR absorbance behavior, suggesting the formation of malformed particles.

formation of AuNRs was indicated by the presence of two absorbance bands, the TSPR and LSPR bands. These absorbance bands could be used to estimate AuNR aspect ratio. Where AuNR growth was suggested to be successful, TEM images were acquired to ensure correct particle shape and to determine the level of impurity. These two analytical techniques were used in conjunction to perfect the synthesis technique.

A typical UV-Vis absorbance spectra is shown in Figure 23. As can be seen, two major peaks are visible. The TSPR peak at ≈ 510 nm is typical for all AuNRs, as this is mediated by the $\{110\}$ and $\{111\}$ facets on the ends of the rods. The more significant LSPR peak shifts according to the aspect ratio: the greater the aspect ratio, the greater the LSPR wavelength. These typically vary between 600 - 800 nm using the Nikoobakht method, as the added silver nitrate restricts the aspect ratio to a maximum of about 4.5. In this particular example, the LSPR was found to be 738 nm. TEM images shown in Figure 24 are representative of good quality AuNRs. As can be seen in these images, the nanorods are well formed, with cylindrical bodies along the $\langle 250 \rangle$ vector, terminated by $\{110\}$ and $\{111\}$ facets.

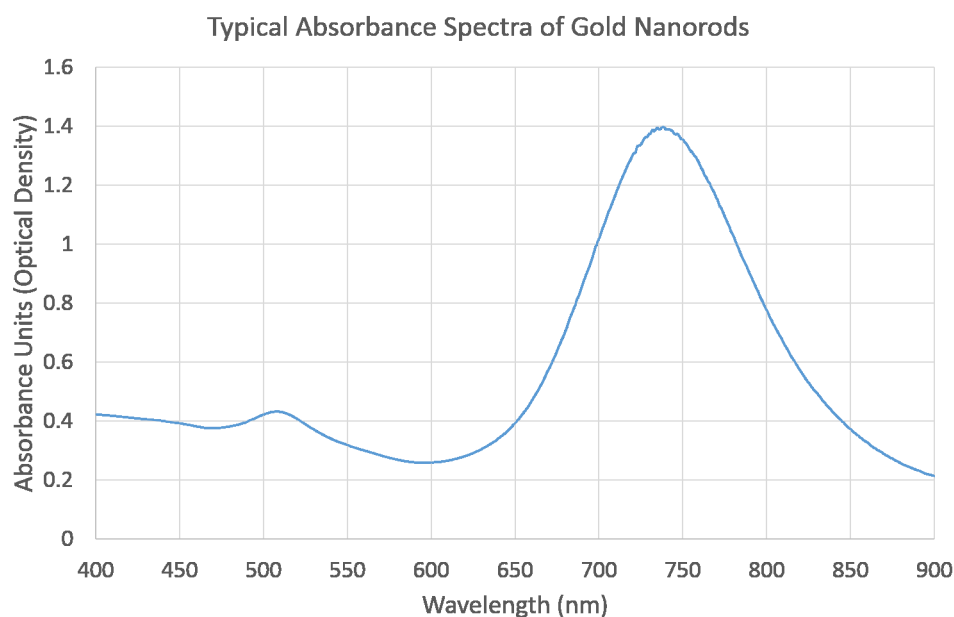


Figure 23. A typical UV-vis absorbance spectra of AuNRs. In this particular sample, the LSPR was determined to be 738 nm, while the TSPR was 510 nm. Note the LSPR absorbance peak is significantly stronger than the TSPR, which is again typical of AuNRs.

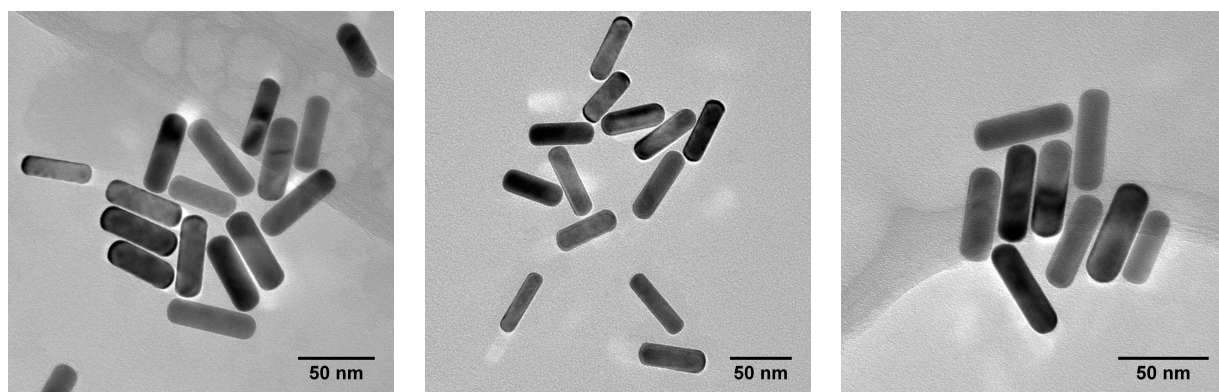


Figure 24. Representative examples of well formed AuNRs. Note the well formed rod shape, with uniform cylindrical body along the $\langle 250 \rangle$ vector, which are terminated by $\{110\}$ and $\{111\}$ facets. This sample had an LSPR of 726 nm.

Figure 25 demonstrates the monodispersity of the AuNR batch. As can be seen visually, the particles in this batch are quite similar in size in both dimensions. Statistical analysis shows this batch of AuNRs had an average size of 16.7 ± 2.0 nm in the transverse direction and 52.8 ± 4.7 nm in the longitudinal direction, corresponding to an aspect ratio of 3.2 ± 0.5 . In addition to this, few impurities are present, again suggesting good control over AuNR formation.

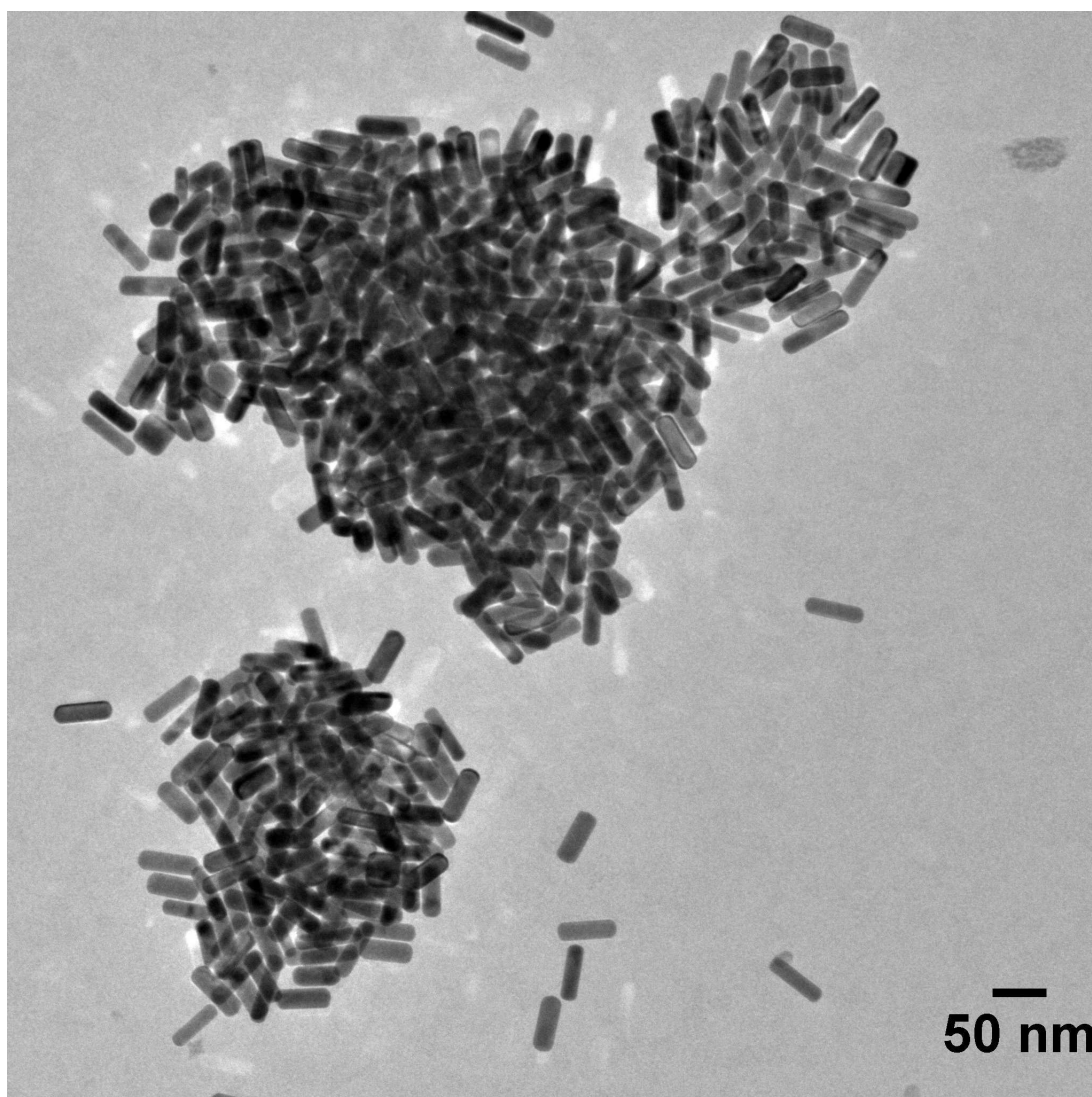


Figure 25. TEM images showing a large number of AuNRs clustered together. Note the monodispersity of the particles, as well as the low number of undesired impurities. AuNRs shown here have an aspect ratio of 3.2 ± 0.5 . The sample shown here is the same batch as depicted in Figure 24.

4.1.2 Attempted Alternative Synthesis via Radical Reduction Method

Recently, Ahmed and Narain published a method for synthesizing AuNRs in a single step, wet chemical method using a radical reductant.⁴ Previously published radical methods had used ketyl radicals generated from acetone via UV irradiation at 254 or 300 nm.⁶ However, these methods require long radiation times, as the generation of ketyl radicals is relatively slow, with optimal irradiation time being several hours. The improvement made was by introducing a source of ketyl radicals using the photoinitiator 4-(2-hydroxyethoxy)phenyl-(2-hydroxy-2-propyl)ketone, known industrially as Irgacure-2959 or I-2959. Upon irradiation at 350 nm, this generates ketyl radicals with short half lives, rapidly reducing Au(III) to Au(0).

Following the method described by Ahmed and Narain, the alternative synthesis was attempted using I-2959 in the presence of CTAB, acetone, and silver nitrate. As previously discussed, the silver nitrate is used to control the aspect ratio of the AuNRs. Acetone is used to improve the flexibility of the CTAB template, allowing AuNRs of smaller diameters to be produced. A Rayonet RPR-200 photoreactor at 254 nm wavelength radiation was used as the radiation source, removing some of the lamps in an attempt to reduce the intensity to match the literature intensity. Several observations were made in this experiment. First, when the chloroauric acid was added to the aqueous CTAB/acetone solution, complexation of Au(III) to CTAB was observed and resulted in visible precipitation of the complex. This was thought to be due to the addition of acetone reducing the solubility of the CTAB-Au(III) complex. Lowering the concentration of gold added by half did not improve this and still resulted in precipitation of the gold complex. After addition of I-2959 as a solution in methanol, irradiation for a prolonged period of time with stirring did not produce any sign of nanorod formation, with the CTAB-Au(III) complex remaining as a precipitate and no color change observed. Furthermore, it appeared that the addition of methanol to the growth solution further reduced the solubility of the gold complex. In addition to this, the irradiation wavelength could not be matched due to a lack of the required equipment. Due to the lack of success, this single-step radical reduction method was abandoned.

4.1.3 Optimization of Cleaning Protocol

While AuNRs have been successfully synthesized using the Nikoobakht method, literature descriptions for the purification of these nanorods is lacking, as it is rarely described. The Nikoobakht method, for example, fails to mention any purification process, simply stating at the conclusion of the growth phase AuNR@CTAB were obtained.¹ It was known that AuNR@CTAB could not simply be stored as synthesized, as the high concentration of CTAB requires elevated temperatures to remain in solution. Lowering the temperature from 30 °C to ambient temperature resulted in crystallization and precipitation of the surfactant, which in turn caused aggregation of AuNRs as they became trapped within the CTAB crystals. It was found that once the crystallization of CTAB occurred, rescue of the AuNRs was often difficult, or not possible. Therefore, centrifugation of the sample following growth and resuspension in an appropriate buffer was the preferred method.

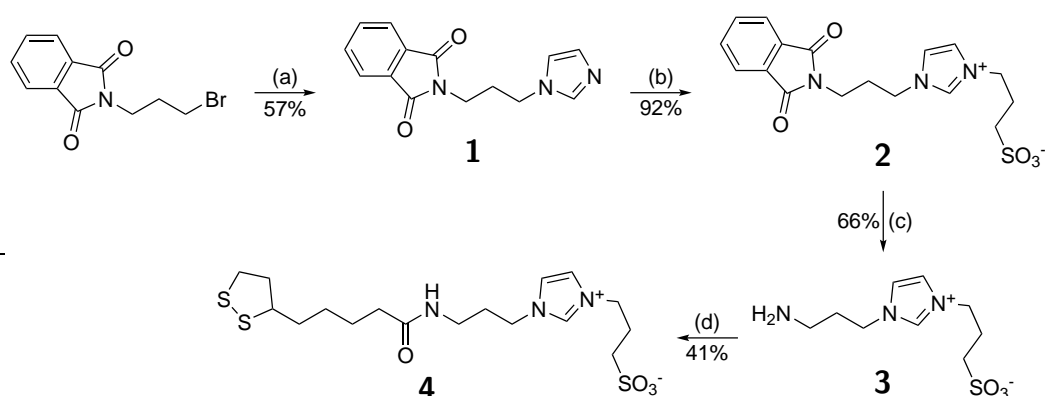
Initially, samples were centrifuged, 90% of the supernatant removed and the colloid was made back to volume using Milli-Q water to lower the CTAB concentration to 10 mM. This could then be repeated to further reduce the surfactant concentration to 1 mM. However, due to the coating procedure developed (Chapter 4.4), a CTAB concentration of 10 mM needed to be maintained. Therefore, only one centrifugation/resuspension cycle was carried out. It was later found that samples that had only been washed once aged over time due to the remaining 10% of the growth reagents, which was determined via UV-Vis spectroscopy. The change in absorbance spectra corresponded to an increase in particle size, although the vector of the change could not be determined. A change in particle size over time was undesirable, as such further purification was required. Following the first centrifugation/resuspension cycle into Milli-Q water, the sample could be washed twice using a 10 mM solution of CTAB. This maintained the required CTAB concentration, while also enabling the removal of excess growth reagents to < 0.1%. This halted any observable change in AuNR absorbance spectra over time, and could therefore be stored long term without any change to their physical and optical qualities.

4.2 Synthesis of a Biocompatible Zwitterionic Surface Coat

Due to the cytotoxic nature of the CTAB coating on as-synthesized AuNR@CTAB, a biocompatible surface coat was required in order for these to be used in biological systems. To this end, a zwitterionic surface coat was designed based on an imidazolium/sulfonate system. Zwitterionic surface coats have been shown to be highly hydrophilic, imparting a "stealth" behavior to the nanoparticle.⁷ Compared to the commonly used PEG coating, these types of coats have several advantages; they are better able to prevent the formation of a protein corona that can inhibit the intended activity of the nanoparticle, they are far lower in molecular weight so tend to have a smaller hydrodynamic diameter, and are less likely to be captured by macrophages. Furthermore, as these species are overall electrically neutral, they are unlikely to form electrostatic interactions with the environment. Previous work in this area has shown that the imidazolium/sulfonate system is better able to resist the formation of the protein corona, as well as having minimal non-specific uptake and does not induce cellular stress compared to anionic, cationic and a zwitterionic quaternary ammonium/sulfonate coats (see Appendix 8.4).⁸

The synthesis is described in Scheme 3. Briefly, imidazole was alkylated using *N*-(3-bromopropyl)phthalimide to give **1**. This was then further alkylated using 1,3-propanesultone to give **2**, installing the cationic imidazolium as well as the anionic sulfonate moieties. The phthalimide was then deprotected to reveal the free amine **3**, which could then be coupled to lipoic acid to give **4**, with the dithiolane acting as an anchoring group to enable attachment to the AuNR surface.

The synthesis of this zwitterionic surface coat has been optimized from an unpublished procedure from within the group. Previously, the conversion of **1** to **2** was effected by simply stirring the reactants together in chloroform at room temperature for several days (typically 5 days). This reaction time was significantly reduced by using MeCN as the solvent as well as heating at 80 °C in a sealed vessel, allowing for the reaction to be completed within 30 min. However, when scaled up, simply refluxing the reaction was adequate, although it took 3 h when not pressurized. Conversion of **3** to the final compound **4** was originally reported to not



Scheme 3. Synthesis of a biocompatible zwitterionic surface coat. Note the imidazolium and sulfonate moieties in the final product **4** acting as the zwitterionic coat. The dithiolane enables attachment of **4** to the AuNR surface. Reagents and Conditions: (a) imidazole, K_2CO_3 , MeCN, reflux, 16 h, 57%; (b) 1,3-propanesultone, MeCN, 80 °C, 30 min, 92%; (c) $N_2H_4 \cdot H_2O$, MeOH, reflux, 1.5 h, 66%; (d) lipoic acid, EDC·HCl, HOBt, DIPEA, RT, 18 h, 41%.

proceed using the amide coupling reagent EDC·HCl, and instead conversion of lipoic acid to the corresponding acid chloride, followed by nucleophilic substitution with **3** was performed in order to effect the coupling. However, it was found that using EDC·HCl in conjunction with HOBt allowed the reaction to proceed. In addition to this, heating the reaction at 60 °C increased the solubility of the reagents and allowed the reaction to proceed faster.

4.2.1 Attempts at Further Optimizing Synthesis of Surface Coat

Several attempts were made in order to further optimize the synthesis of **4** in order to both expedite the process and to increase yield. The initial alkylation of imidazole was one of the steps that had previously not been optimized. In order to improve the yield, increasing the reagent equivalence was tried. The equivalence of imidazole and K_2CO_3 were increased from 3 and 1 to 5 and 2, respectively. However, upon workup no product formation was observed by LCMS or TLC. An alternative method described by Harjani *et al.* was also trialed. Initially, imidazole was deprotonated using NaH, followed by the addition of the alkylating agent.⁹ This was then allowed to stir for an hour at room temperature before heating to reflux. Following workup, a white solid was obtained. However, NMR analysis suggested that this was the

di-alkylated by-product, with no mono-alkylated product observed. Hence, the previously established synthesis for **1** was found to be the most efficient method.

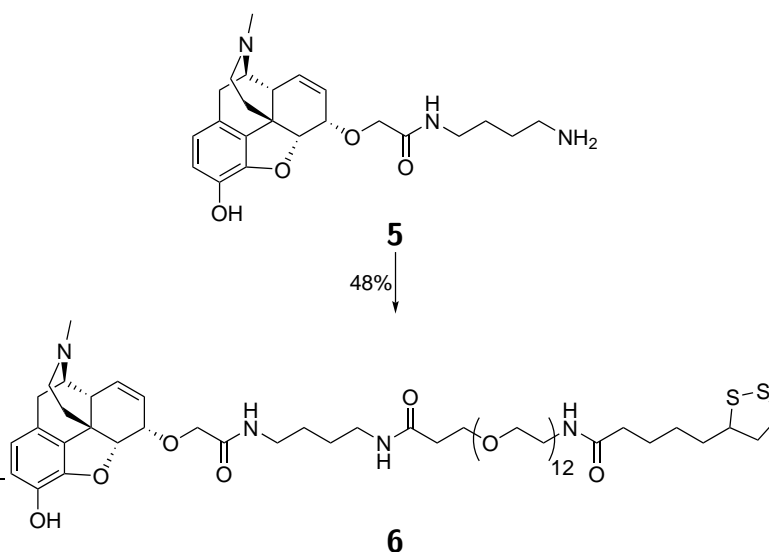
Coupling of **3** to lipoic acid was the second inefficient step in this synthesis. Previously, this was achieved using a combination of EDC·HCl and HOBt. However, the recovered yield was relatively low (41%). Instead, HCTU was used as an alternative to the EDC·HCl HOBt system. However, it was found that the resulting benzotriazole by-product could not be separated from the product under all reverse-phase chromatography conditions tested. Using EDC·HCl without HOBt in an attempt to simplify purification, product formation was observed. However, this was not efficient with minimal product formation and significant by-product formation. While the product could be isolated in low yields (< 10%), the poor conversion did not justify collecting the product.

Next, lipoic acid was converted to an acid chloride, which was then reacted with **3** in dry DMF. Upon quenching, a white precipitate formed, which was determined to be the starting material **3**. No product was observed in the filtrate by LC-MS analysis. Schotten-Baumann conditions were trialled in another attempt to utilize the lipoyl chloride to effect the coupling. Again, lipoic acid was first converted to the corresponding acid chloride using SOCl₂ in DCM. This was then evaporated, redissolved in dry acetonitrile, then gradually added to an aqueous solution of **3** in saturated aqueous (NH₄)₂CO₃/(NH₄)HCO₃, whereupon a yellow precipitate formed. While LC-MS analysis showed relatively little starting material present in the soluble aqueous phase, the precipitate could not be analyzed as it could not be dissolved in any solvent across a variety of pH levels without degradation. While the behaviour of the solid was similar to that of previously synthesized samples, the inability to dissolve the solid meant it could not be confirmed to be the desired product.

Finally, exchange of the phthalimide protecting group for a Boc group proved successful, enabling simple deprotection using TFA to return **3** without a purification step. However, this method was not used on the majority of the samples synthesized.

4.3 Synthesis of a Opiate Congener for Conjugation to Gold Nanorods

Using our previous data from the synthesis of our fluorescent morphine conjugates, a morphine-based congener was designed to enable easy conjugation of the active ligand to the AuNR surface. Synthesis was started using **5** (see Chapter 3, referred to as "compound **20**"), which was designed as part of the work on our morphine-Cy5 conjugates. Compound **5** was coupled to Lipoamido-dPEG[®]₁₂-acid (Quanta BioDesign, Ltd.) using HCTU to give **6** (Scheme 4). Again, a dithiolane moiety was used to anchor the compound to the AuNR surface. dPEG[®] was chosen as the spacer as this particular PEG reagent was synthesized in a step-wise fashion, whereas conventional PEG chains are produced via polymerization to give PEG chains of varying sizes. This gives a precise number of ethylene glycol units, and therefore the exact chemical species is known. Control of the spacer is important as it allows precise characterization of the chemical species being coated onto the AuNR surface, in addition eliminating batch to batch variations. This congener acted as our MOR agonist pharmacophore.



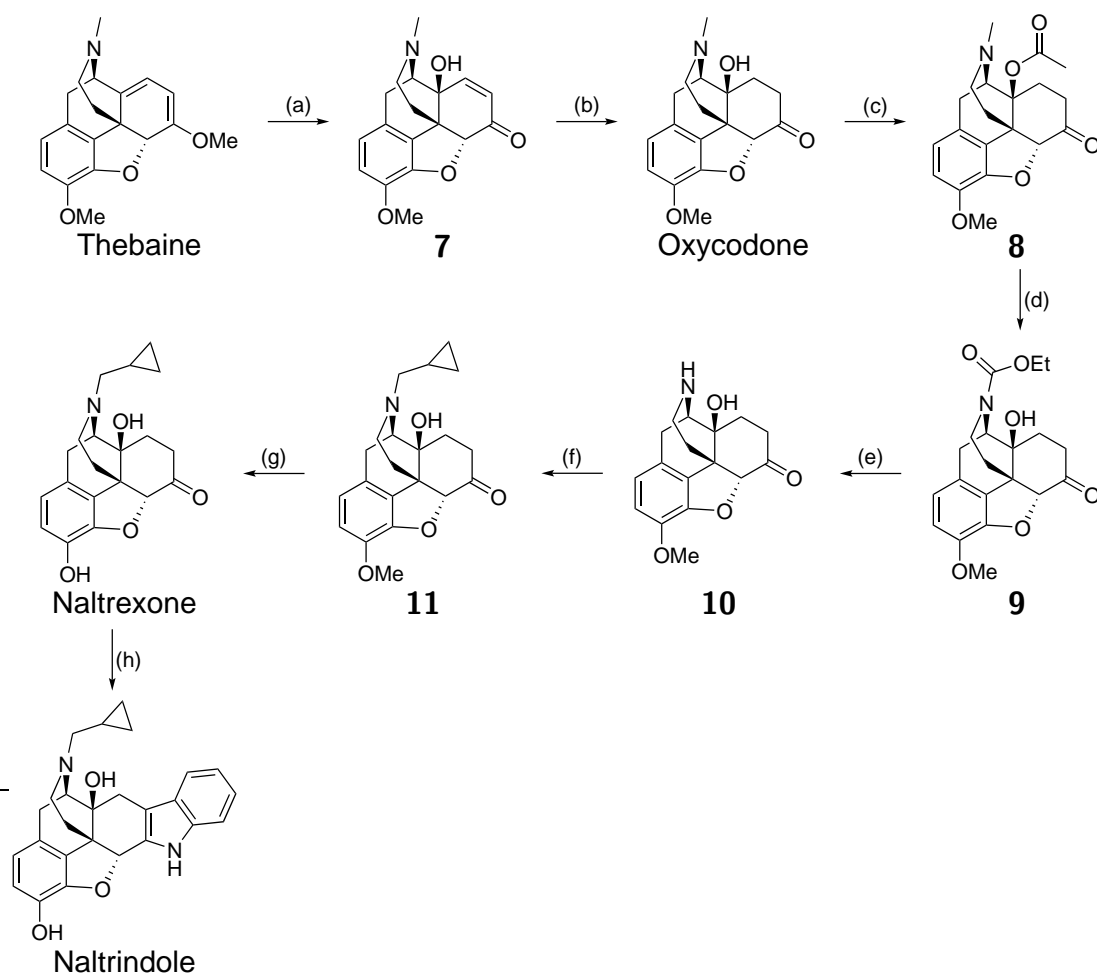
Scheme 4. Synthesis of a morphine-based congener for conjugation to AuNRs. The dithiolane moiety is utilized to anchor the congener to the AuNR surface. Reagents and conditions: Lipoamido-dPEG[®]₁₂-acid, HCTU, TEA, DMF, RT, 18 h, 48%.

As we wanted to image the MOR-DOR heterodimer composed of an active MOR and inactive DOR subunits, a DOR antagonist pharmacophore was required. Naltrindole is a well

known DOR specific antagonist and has been used in the past in the design of bivalent ligand MDAN-21.¹⁰⁻¹³ Structure-activity relationship (SAR) around this compound has found that modifications around the 7'-position were tolerated, and enabled installation of a linking moiety for elongation to a congener.^{11,13,14} In particular, installation of an amine for conjugation via a simple amide coupling maintained antagonist activity.

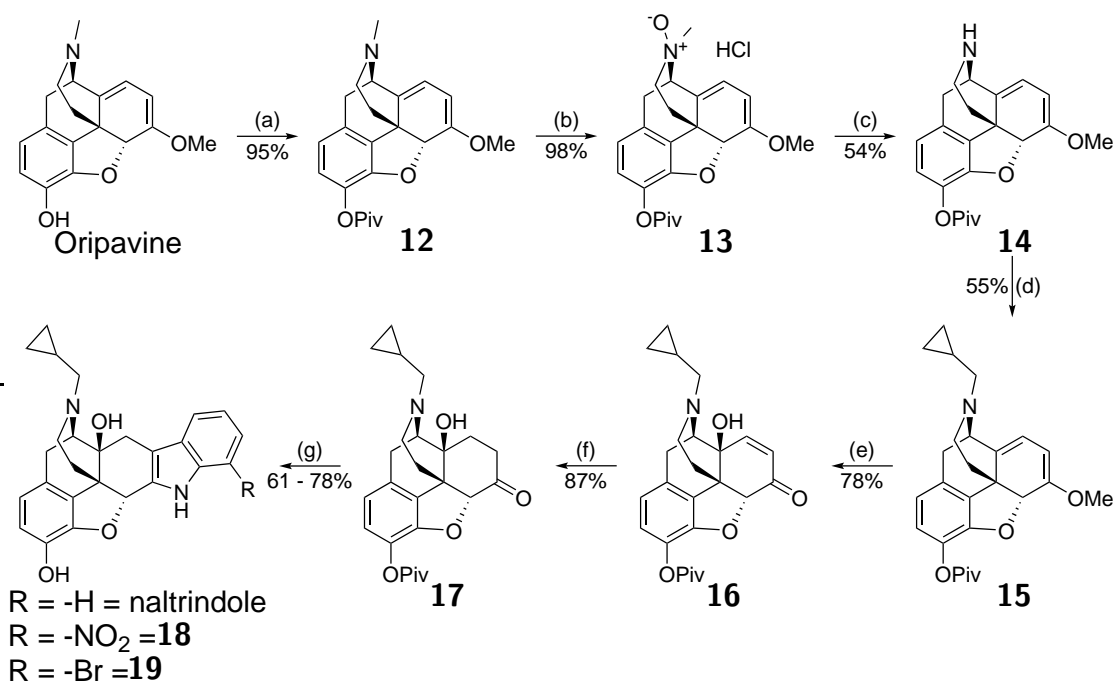
The synthetic pathway used was based on several literature procedures (Scheme 5), altering them in order to accommodate for the different starting substrate, as well as to use an alternative *N*-demethylation method.^{11,14,15} Literature synthesis commenced with thebaine as the starting material, on which 14-oxidation was performed using hydrogen peroxide and formic acid to give **7**.¹⁵ The resulting olefin could be reduced using Pd/C in an H₂ atmosphere to give oxycodone. The 14-hydroxy group could then be acetylated to give **8**, then treated with ethyl chloroformate to give the *N*-demethylated carbamate **9**. The carbamate was then cleaved to return the *N*-nor alkaloid using concentrated sulfuric acid to give **10**, then alkylated with cyclopropylmethyl chloride to install the requisite *N*-alkyl group to give **11**. The 3-O methoxy group can then be cleaved using pyridine and hydrochloric acid to reveal the phenol, giving the MOR antagonist naltrexone as the product. Fisher-indole condensation to give naltrindole may then be performed with phenylhydrazine in conjunction with either acetic acid, hydrochloric acid, or methane sulfonic acid depending on the procedure.^{11,14} Ethanol may also be used as a solvent.¹⁴

For our synthesis of a naltrindole congener, oripavine was used as the starting material due to its ready availability. Furthermore, this enabled the synthesis to be performed without the need to make the Schedule 8 intermediates oxycodone and naltrexone, both of which would be legally problematic due to their restricted nature. Starting with this material, 3-O protection using pivaloyl chloride afforded **12**. *N*-oxidation to **13**, followed by treatment with Fe₃(CO)₁₂ returned the *N*-demethylated product **14**. This particular reaction will be discussed in greater detail in Chapter 5. Alkylation using cyclopropylmethyl bromide gave **15** with the requisite *N*-alkyl group. 14-oxidation with peracetic acid gave **16**, after which the remaining olefin could then be reduced to give **17**.



Scheme 5. A literature synthesis of naltrindole based on two separate procedures described by Tavakol et al. for the synthesis of naltrexone and Portoghese et al. for the conversion of naltrexone to naltrindole.^{11,15} Reagents and conditions: (a) H_2O_2 , formic acid; (b) Pd/C, H_2 ; (c) acetic anhydride; (d) ethyl chloroformate; (e) H_2SO_4 ; (f) cyclopropylmethyl chloride, base; (g) pyridine, HCl; (h) phenylhydrazine, HCl, acetic acid.

Fischer-indole condensation was then performed using the corresponding phenylhydrazine to give naltrindole, the 7'-nitro analogue **18** or the 7'-bromo analogue **19**. Initially, refluxing **17** with the corresponding phenylhydrazine in a mixture of ethanol and acetic acid procedure gave poor yields (< 25%). Further analysis revealed that under these conditions, the hydrazine was preferentially acetylated over participating in the Fischer-indole condensation. The use of hydrochloric acid (10 M) instead of acetic acid gave improved yields in addition to cleaving the pivaloyl protecting group in a single step. Due to changes in regulations restricting access to starting material, naltrexone hydrochloride was purchased from a commercial source instead of synthesizing **17** from oripavine as described. Fischer-indole condensation could be carried out using the same method to afford the corresponding indoles as before. The bulk of indole synthesized for this project was done using the commercially supplied naltrexone hydrochloride.



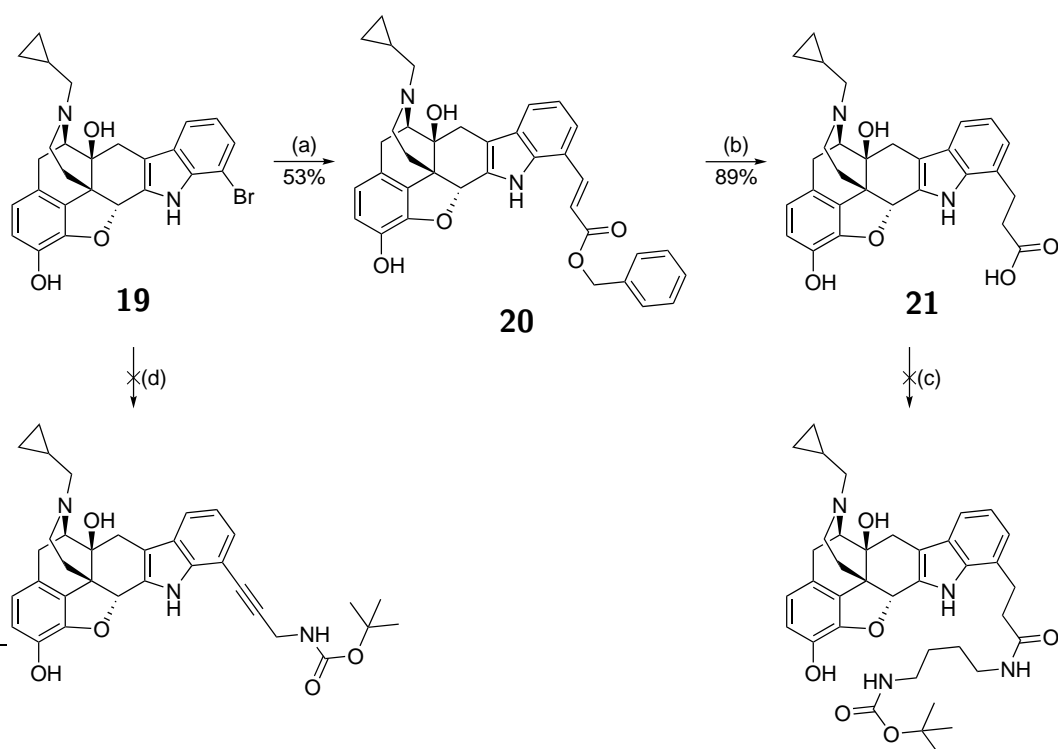
Scheme 6. Synthesis of naltrindole analogues as potential targeting ligands. Reagents and conditions: (a) pivaloyl chloride, TEA, DCM, RT, 3 h, 95%; (b) mCPBA, CHCl₃, 0 °C, 30 min, 98%; (c) Fe₃(CO)₁₂, CHCl₃, RT, 1 h, 54%; (d) cyclopropylmethyl bromide, K₂CO₃, MeCN, RT, 24 h, 55%; (e) oxalic acid, peracetic acid, formic acid, MeCN, water, RT, 1 h, 78%; (f) Pd/C 10%, H₂ (1 atm), MeOH, RT, 18 h, 87%; (g) appropriate phenylhydrazine, EtOH, 10 M HCl, reflux, 17 h, 61 - 78%.

The original intention for the synthesis of **18** was to reduce the nitro moiety to return

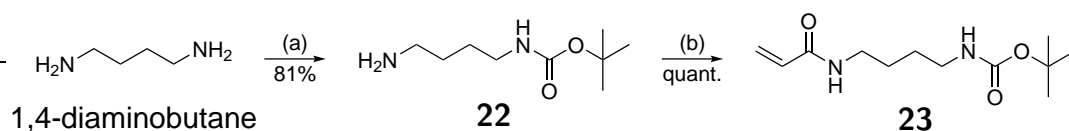
the amine, therefore replicating the same linking method used by Portoghese's group for their work with MDAN-21, which was already known to maintain binding to the DOR.^{12,13} However, difficulties in synthetic manipulation precluded further work. These difficulties will be discussed later in Chapter 4.3.1. Therefore, work proceeded only carrying forward using the bromo analogue **19**. Metal-catalyzed coupling between **19** and a suitable linker was trialled under a variety of conditions. Using *N*-Boc-propargylamine under Sonogashira conditions failed to give any conversion to the desired product.

Modifying approaches, Heck couplings were attempted using a variety of alkenes with varying degrees of success. Benzylacrylate gave good conversion to the desired trans olefin **20** (Scheme 7). Hydrogenation was then performed using Pd/C in an H₂ atmosphere (60 PSI) to simultaneously reduce the olefin and cleave the benzyl protecting group to give **21**. Here, it was found that the reaction would only proceed to partial completion with the initial catalyst loading, giving a variety of products including partial reduction of the olefin, partial cleavage of the benzyl group, and the fully reduced product. Removal of the spent catalyst by filtration and charging the solution with fresh catalyst was done to drive the reaction to completion. However, coupling to *N*-Boc-1,4-diaminobutane proved unsuccessful using either HCTU or EDC·HCl/HOBt as the coupling reagents, returning primarily the starting material **21**.

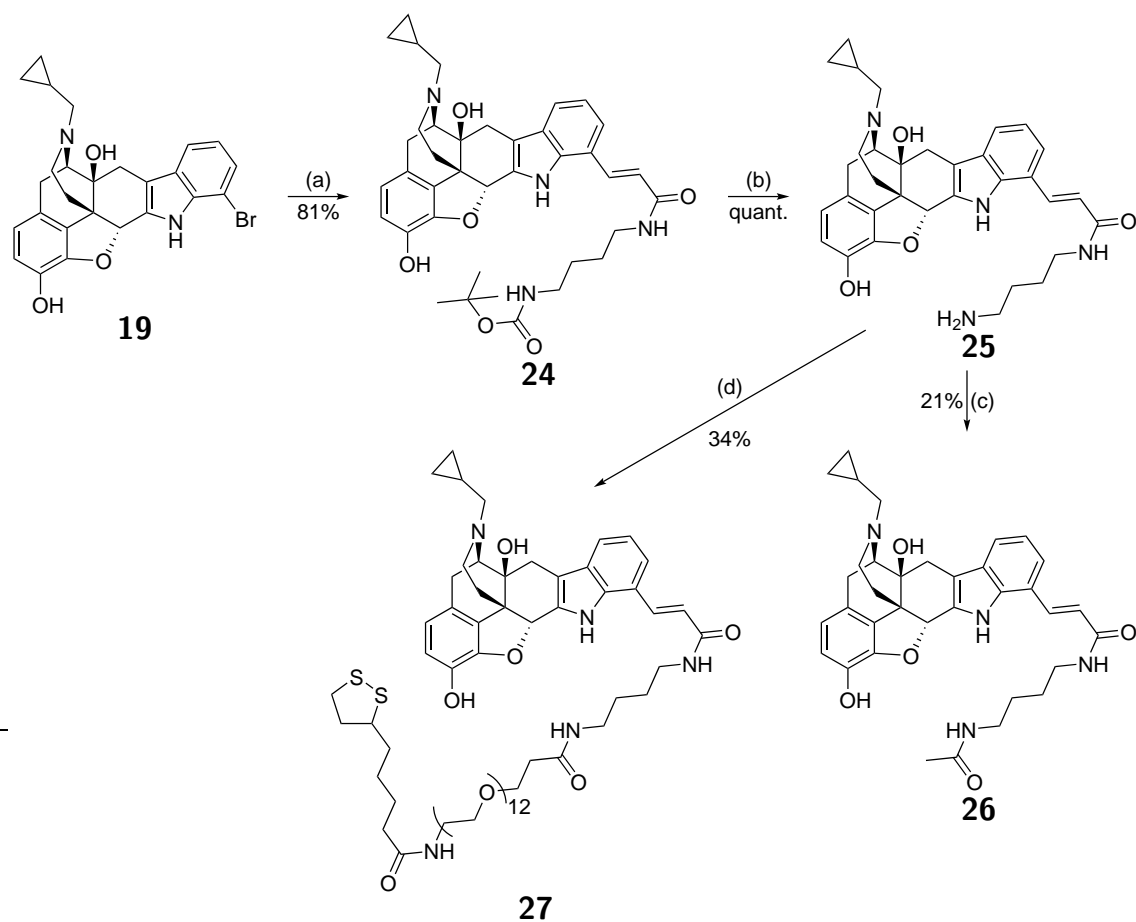
Rather than building the linker whilst conjugated to the opioid, a convergent approach was utilized. Although various substrates were trialled, the most successful methods utilized analogues of acrylic acid. Mono-Boc protection of 1,4-diaminobutane to give **22**, followed by acrylation with acryloyl chloride afforded the requisite linker **23**. Heck coupling as per previous conditions gave **24** in good yield. TFA deprotection to reveal the terminal amine gave **25** with a convenient handle for further conjugation. Amide coupling using HCTU gave an acetyl-capped model compound **26**, while the use of PyBOP was required for coupling to Lipoamido-dPEG®₁₂-acid, enabling conjugation of **27** to AuNRs.



Scheme 7. Initial attempts at linker elongation using **19** using Sonogashira and Heck coupling approaches. Reagents and Conditions: (a) benzylacrylate, TEA, $\text{PdCl}_2(\text{PPh})_2$, DMF, 90 °C, 17 h, 53%; (b) Pd/C 10%, H_2 (60 PSI), RT, MeOH, 48 h, 89%; (c) N-Boc-1,4-diaminobutane, HCTU or EDC·HCl/HOBt, TEA, DMF, 24 h; (d) N-Boc-propargylamine, PPh_3 , $\text{PdCl}_2(\text{PPh})_2$, CuI, TEA, DMF, 60 °C, 15 h.



Scheme 8. Synthesis of the linker for a convergent synthetic approach. Reagents and Conditions: (a) Boc-anhydride, CHCl_3 , RT, 19 h, 81%; (b) acryloyl chloride, TEA, CHCl_3 , 0 °C - RT, 24 h, quantitative.



Scheme 9. Synthesis of the naltrindole-based congener and model compound. Reagents and Conditions: (a) **23**, $\text{PdCl}_2(\text{PPh}_3)_2$, TEA, DMF, 90°C , 24 h, 81%; (b) TFA, CHCl_3 , 2 h, quantitative; (c) HCTU, acetic acid, TEA, DMF, RT, 23 h, 21%; (d) Lipoamido-dPEG $^{\text{R}}$ ₁₂, PyBOP, TEA, DMF, RT, 24 h, 34%.

4.3.1 Problematic 7'-Nitro Naltrindole Reduction

Although reduction of **18** has previously been described by the Portuguese group,¹¹ it was found to be a problematic reaction. Due to safety concerns, the original literature procedure of using Raney Nickel was not immediately employed. Instead, a variety of other reduction conditions were tested in an attempt to achieve the desired amine. The most obvious candidate was the use of Pd/C under an H₂ atmosphere. However, it was found that at atmospheric pressure, this reaction did not proceed. This was not observed for all attempts, and was thought to be due to the specific batch of Pd/C used. Changing batches of Pd/C and increases in H₂ pressure (40 - 60 PSI) showed no conversion to product, tending to give partial reduction to the nitroso. Although nitroso compounds are typically unstable, it was found that in this case the nitroso could not be further reduced upon addition of fresh catalyst under a new H₂ atmosphere at 60 PSI, with no change to the sample observed by LC-MS. Isolation of the nitroso compound was attempted, but was found to co-elute with the parent nitro compound. Crude NMR of the nitroso sample gave a spectra with broad peaks with no fine splitting patterns discernible (see Appendix 8.2).

Although nitroso compounds are typically not formed during Pd/C catalysed hydrogenation, Meng *et al.* have shown that it is possible to purposefully generate it from the parent nitro compound using a nickel/aluminium oxide catalyst.¹⁶ Furthermore, there have also been limited reports of the nitroso being formed under catalytic hydrogenation using Pd/C in an H₂ atmosphere.^{17,18} In addition to this, nitroso compounds can be stabilized and isolated when an amine or aniline is present *ortho* to the nitroso.^{19,20} In this particular case, the indole nitrogen of **18** may be behaving as such, stabilizing the nitroso intermediate upon catalytic reduction, while this would not have been possible where the nitro was in either the 5' or 6' positions.

Alternative reductive conditions were also trialled and analyzed via LC-MS and NMR. Exchanging the Pd/C for Zn, reduction to the nitroso was again observed under a 60 PSI H₂ atmosphere. Switching hydrogen sources from H₂ to N₂H₄ · H₂O gave similar results using both Zn and Pd/C as the catalyst. Chemical reduction using sodium dithionite (Na₂S₂O₄)

and ammonia under reflux again gave the nitroso, while LiAlH_4 gave no observable conversion, as did $\text{Fe}(0)$ with acetic acid. An attempt at using a Raney Nickel cartridge on an H-cube hydrogenator also resulted in conversion to the nitroso. However, due to instrument faults the pressure could not be elevated to more than 5 atm.

With these failed attempts, it was decided that a trial with Raney Nickel would be attempted. As pre-activated commercial Raney Nickel was unavailable, the active catalyst was produced by digestive activation of the inactive aluminium-nickel alloy. Although various literature procedures are available for this, a variation of a procedure from Adkins and Billica was used.²¹ Briefly, the aluminium-nickel alloy is digested in a 50 °C solution of 5 M NaOH for 1 h, after which it is washed to remove excess base, then washed and stored in ethanol to give W-5 Raney Nickel. In the procedure described by Adkins and Billica, use of an H_2 pressurized system gave a very active catalyst, as this enabled adsorption of H_2 to the catalytic surface directly after leaching, giving W-6 Raney Nickel. However, this was not done due to safety concerns. The authors noted that not introducing H_2 during the washing steps would produce a somewhat less active catalyst.

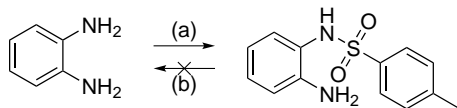
Using Raney Nickel with $\text{N}_2\text{H}_4 \cdot \text{H}_2\text{O}$ in ethanol as described by Portoghese *et al.*,¹¹ partial reduction to the nitroso was observed after a considerably longer reaction duration compared to the literature procedure. Addition of increased equivalents of $\text{N}_2\text{H}_4 \cdot \text{H}_2\text{O}$ resulted in the reaction proceeding somewhat quicker and further, but complete reduction to the amine was not observed. It was found that addition of dilute HCl increased the reaction rate, but again did not result in further reduction to the desired amine.

Although it was known that reduction of the 7'-nitro moiety would be relatively difficult, the work done here has demonstrated the difficulty in full reduction at this position. In Portoghese's work, the 5' and 6' nitro analogues could be reduced simply using Pd/C under an H_2 atmosphere at ambient pressure.¹¹ Their use of Raney Nickel suggests that this particular regioisomer is more difficult to reduce, requiring stronger conditions compared to the typically used Pd/C. Perhaps the use of commercial Raney Nickel would be more successful than that made in-house, as these are typically more active due to H_2 gas being introduced during the

manufacture of the catalyst which was not done here. Furthermore, multiple types of Raney Nickel are available, and are classified based on the manufacture parameters such as NaOH to alloy ratio, time, temperature and washing method.²² As it was never explicitly stated in the original publication which type of Raney Nickel was used, it is likely the type of catalyst used in this work was not reflective of the literature catalyst.¹¹ However, due to the difficulties experienced with this synthetic pathway, an alternative approach utilizing **19** was carried forward as previously described (Chapter 4.3).

4.3.2 Attempted Alternate Pathways to 7'-aminonaltrindole

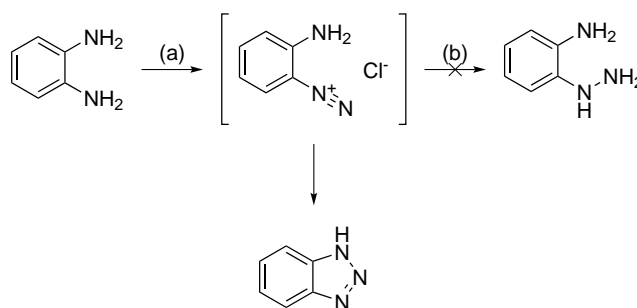
Rather than proceeding to the amine via reduction of a nitro moiety, synthesis of alternative hydrazines was attempted to enable pre-installation of the amine upon Fischer-indole condensation. These attempts were commenced using 1,2-phenylenediamine. Initially, mono-tosyl protection was used as a robust protecting group for a single amine to enable extension of the second amine to a hydrazine. However, due to the difficulty in removing the tosyl protecting group, a test reaction was run to determine if mild deprotection conditions would enable tosyl deprotection. For this purpose, a solution of samarium iodide in THF was used in conjunction with water and pyrrolidine (Scheme 10). No deprotection was observed via LC-MS, but residual starting material was not observed, suggesting that an undesired side-reaction had occurred. This may have been due to the substrate itself, or the bottle of samarium iodide used being an older bottle that may have degraded. Furthermore, stirring in concentrated sulfuric acid gave no observable deprotection, hence this method of deprotection was discarded.



Scheme 10. Attempted tosyl protection and deprotection of 1,2-phenylenediamine. Reagents and Conditions: (a) tosyl chloride, TEA, THF, RT, 24 h; (b) SmI (0.1 M in THF), pyrrolidine, water, RT, 27 h, quantitative.

Rather than starting with a protected substrate, an attempt was made at synthesizing

2-aminophenylhydrazine directly from 1,2-phenylenediamine. Using sodium nitrite with concentrated HCl and MeOH to give the azide, followed by addition of tin (II) chloride to reduce the azide to the corresponding hydrazine did not give the desired product. Instead, cyclization was observed to give benzotriazole (Scheme 11). This was reasoned to be due to an intramolecular nucleophilic attack of the terminal azide by the amine, followed by electron transfer and loss of a proton. This returns aromatization to the system, and therefore gives the thermodynamic product benzotriazole, rather than returning the desired hydrazine. Indeed, the use of NaNO_2 and HCl for the synthesis of benzotriazoles has been documented.^{20,23,24}



Scheme 11. Attempted synthesis of 2-aminophenylhydrazine. Rather than forming the desired hydrazine, cyclization to give the benzotriazole was observed. Reagents and Conditions: (a) NaNO_2 , 10 M HCl, 0 °C, 30 min; (b) $\text{SnCl}_2 \cdot 2\text{H}_2\text{O}$, 10 M HCl.

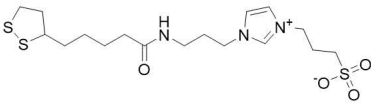
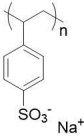
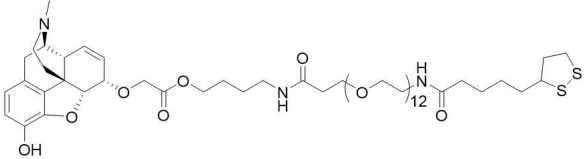
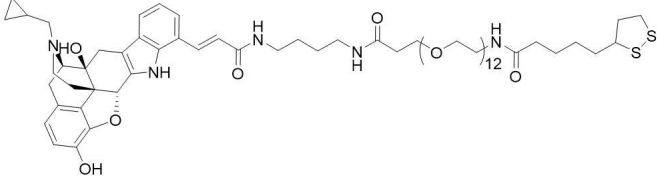
Moving on, an attempt at pre-reducing 2-nitrophenylhydrazine was attempted. For this, Boc-protection of the hydrazine moiety was required. Protection of the hydrazine using Boc-anhydride was successful, returning **28**. This material was then reduced using Pd/C under an H_2 atmosphere. Although a significant change in NMR spectra of the reduced material was observed compared to the starting material, it was not immediately evident that product was obtained. Deprotection using TFA in CHCl_3 showed degradation of the sample by NMR and LC-MS (see Appendix 8.3). Analysis of the LC-MS data suggests some of the by-products formed were 1,2-phenylenediamine and benzotriazole, suggesting that the desired product was unstable and could not be synthesized. Indeed, 2-aminophenylhydrazine is not a readily available commercial reagent.

4.4 Development of Coating Procedures

4.4.1 Initial Attempts and Development of the "2 Step Method"

For the purposes of the core@shell notation, the chemical entities used will be abbreviated for clarity as shown in Table 2. Otherwise, compound numbers will be used as standard.

Table 2: Abbreviations of the chemical entities used to coat AuNRs for clarity.

Abbreviation	Compound	Structure
ZW	4	
PSS	Poly(sodium 4-styrenesulfonate)	
MorPEG	6	
NaltPEG	27	

As a procedure for coating AuNRs with a monomeric zwitterionic surface coat was not available, a method had to be developed specifically for this particular agent. Various trial experiments were conducted, and from these various key points were noted. First, AuNR@CTAB had to be stored in 10 mM CTAB, as coating processes require a centrifugation and resuspension in various solutions in order to introduce a new coat. Since the critical micelle concentration of CTAB is 1 mM, removing 90% of the supernatant from a 10 mM CTAB solution and making the solution back up to volume with Milli-Q water would reach this minimum concentration, and therefore would maintain them in a stable state while the coating was being applied. It was found that lower concentrations of CTAB would result in aggregation of the sample. Second,

4 was found to be insoluble in water at room temperature in its as-purified TFA salt form at 10 mM. Elevated temperatures (30 °C) or basic pH's (8 - 9) were required for full dissolution. Third, **4** could not be directly introduced to CTAB-coated AuNRs, as this would result in aggregation of the sample. Aggregation was simply noted visually, as the colored AuNR colloid would become colorless and a visible black precipitate would form.

With this in mind, the CTAB coat had to be initially displaced using a polymer surfactant to detoxify the AuNRs. Inspiration was taken from a method described by Mehtala *et al.*,²⁵ where PSS (average MW \approx 70 kDa) was used to initially to detoxify the AuNR surface, and was then further displaced by a sodium citrate coat. This was developed to enable citrate coating displacement methods already known for spherical AuNPs to be used for AuNRs. It was reasoned that if citrate, a very weakly binding ligand, could displace PSS, then a more strongly binding ligand such as those containing a dithiolane moiety could also be used.

With these in mind, a coating method was developed to enable the coating of **4** onto AuNRs. First, AuNR@CTAB stored in 10 mM CTAB were centrifuged at 10 kRPM for 10 min. Following this, 90% of the supernatant was then removed and the solution made back up to volume with PSS (0.15% w/w). The resulting mixture was gently mixed for 30 min, then allowed to sit for 30 min. This was then repeated a further two times to give AuNR@PSS. These were then centrifuged as before, and resuspended in a solution of **4** (10 mM, pH 8). This was again allowed to mix gently for 30 min, then allowed to sit overnight (minimum 16 h). This could then be centrifuged and resuspended into Milli-Q water twice to remove excess reagents to give the desired AuNR@ZW (Figure 26).

Further experimentation showed any further centrifugation and resuspension in Milli-Q water would result in complete aggregation of the sample. It was hypothesized this might be due to either a mechanical effect, where the centrifugation was stripping the surface coat from the particle surface, or may have been due to the dilution causing the surface coat to diffuse away from the particle surface. To test this hypothesis, a sample was coated as previously described, but was repeatedly centrifuged and resuspended without removing the supernatant. This sample could be centrifuged without aggregation past the previously established point

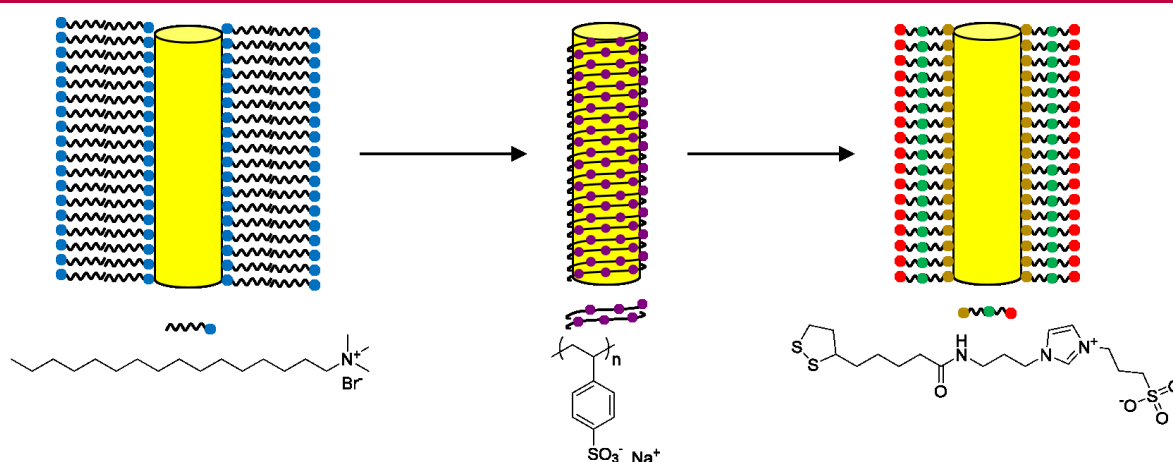


Figure 26. A flowchart illustration the "2 step method" of coating AuNRs. First, the CTAB surfactant is displaced using the polymer PSS, which can then be displaced with the desired biocompatible coat of **4**.

(> 5 rounds of centrifugation), suggesting that the surface coat was diffusing away from the particle surface as the solution was being diluted.

Reducing the dithiolane present in **4** using aqueous NaBH_4 to give the corresponding dithiolate just prior to coating allowed the sample to be centrifuged and resuspended in Milli-Q water three times following coating instead of twice as prior. However, while it did result in a stronger binding of the ligand to the particle surface, this was not continued, as it did not provide significant improvements to colloidal stability.

Further optimization of this procedure was performed in order to determine if a more dilute solution of **4** could be used. It was found that this coating method was successful where using a 1 mM solution of **4** instead of the 10 mM solution previously described. However, this could only be centrifuged once due to the dilution. Further purification could be achieved by dialysing against Milli-Q water (molecular weight cut-off 100 kDa). Further to this, titrations of DMSO were tested to determine if this affected the coating process. To this end, a 10% v/v solution of DMSO in Milli-Q water was titrated into the coating procedure as an increasing percentage of the coating mix (10 - 30%). This served two purposes; first, to see if the small percentage of DMSO would negatively affect the coating process, and second, to determine if the dilutions resulting from titrating in the targeting ligand would result in less stable nano-

particles. These experiments showed no difference in colloidal stability upon addition of the DMSO solution.

4.4.2 Addition of Targeting Ligand to Gold Nanorod Surface

With the successful coating of AuNRs using **4** to give AuNR@ZW, targeting ligands could be introduced into this process to give targeted AuNR conjugates. For initial experiments, **6** was used as the test ligand in order to develop the coating method.

Compound **6** was found to be insoluble in water at the required concentrations (1 or 5 mM) at pH 8 - 9, nor was it soluble when MeOH, MeCN, or EtOH were added as cosolvents at 5% v/v. However, this congener was fully soluble when DMSO was used as 10% v/v of the solvent in Milli-Q water at 1 mM. This solution could then be used as a percentage of the coating solution as previously described (Chapter 4.4.1). As an initial test, several samples were generated where the 1 mM solution of **6** was introduced as 10, 20 or 30% of the coating solution using the established 2 step method. AuNR@ZW(MorPEG 10%) was found to be the most stable active ligand sample. For samples AuNR@ZW(MorPEG 20%) and AuNR@ZW(MorPEG 30%), partial aggregation of the sample was observed visually from the formation of a black precipitate.

Although samples coated in **4** were stable and showed no signs of aggregation if cleaned correctly, the introduction of **6** at higher percentage loadings appears to destabilize the colloid. Typically, PEG chains with an average molecular weight of 5 kDa or greater are used to stabilize colloidal nanoparticles.²⁶⁻²⁹ In this case, the dPEG₁₂ chain had a molecular weight of about 740 Da, so was unlikely to have contributed to stabilizing the nanoparticle. Therefore, this loss in the stabilizing coat may have resulted in the observed aggregation. So although a known quantity of **6** was titrated into the AuNR coating mixture, for those samples where aggregation was observed it is unknown how much of the surface was coated in the ligand. Particles with higher loadings would be more likely to aggregate, while those with a lower loading would remain colloidally stable. Hence the nanoparticles that remain in the colloidal state are likely to be coated to a lesser percentage than the titrated amount.

4.5 Validation of Coating Success

Following coating of the AuNRs, success needed to be verified using analytical techniques. Although nanoparticle analysis is not a new field, limitations in instrumentation, as well as the nature of the nanoparticles themselves resulted in relatively difficult characterization. Furthermore, we did not simply want to "take it on faith" that the nanoparticles had been coated as desired, as many literature procedures seem to do.

4.5.1 Changes in UV-Vis Absorbance Spectra

Prior literature has suggested that upon coating with a stabilizing coat, a shift on the UV-Vis absorbance spectra tends to happen with AuNRs.^{25,28,30} Specifically, an increase in colloidal stability is characterized by a blue-shift in LSPR absorbance maxima, whilst a decrease in colloidal stability is observed via a red-shift in the maxima. Following coating, differences in absorbance spectra between AuNR@ZW and AuNR@CTAB were compared. It was found that a blue-shift of 10 nm was observed, indicating successful stabilization of the AuNR (Figure 27). Upon coating, a slight loss in optical density was observed. This is likely due to minor amounts of aggregation during the coating process as well as removal of some AuNRs in the supernatant that were still suspended.

4.5.2 pERK1/2 Assay to Determine Biological Activity of Coated Gold Nanorods

In addition to showing AuNRs could be coated, we needed to show that the active ligands on the particle surface were still able to activate cell surface receptors. A number of methods for doing this were postulated, but it was determined that a functional cell-based assay was the best way forward. For this purpose, a phospho-extracellular signal-regulated kinase 1/2 (pERK1/2) assay was used, giving a proxy reading to the level of MOR activation. In addition to showing binding of the active ligand to the desired receptor, the pERK1/2 assay could also give any indication of cell stress or non-specific binding, as any activation of pERK1/2 would be measured. Testing AuNR@ZW and AuNR@PSS in addition to the active AuNR conjugates

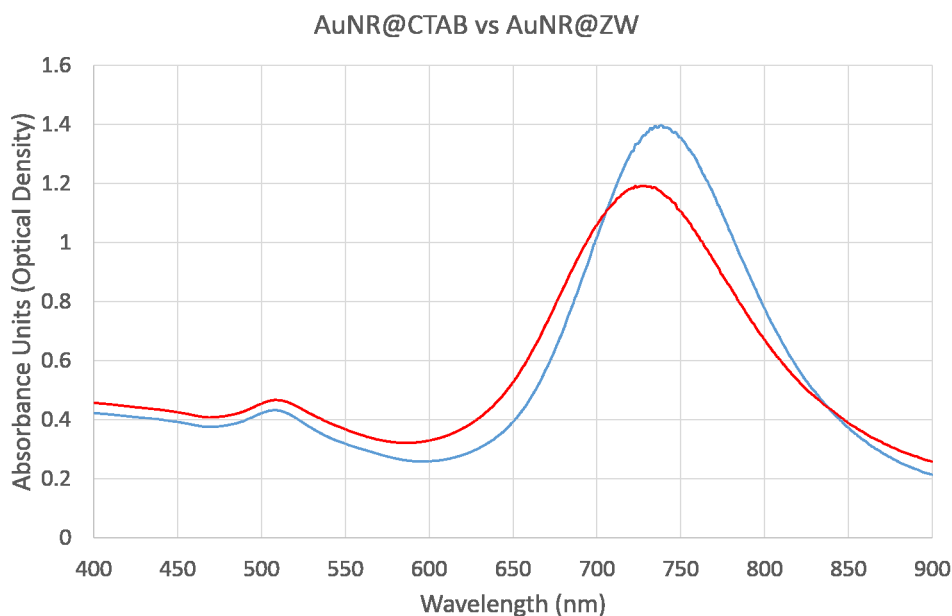


Figure 27. Comparison between AuNR@CTAB and AuNR@ZW. Note the slight shift in LSPR from 738 nm (AuNR@CTAB, blue curve) to 728 nm (AuNR@ZW, red curve). This blue-shift in LSPR suggests AuNR@ZW are more stable than AuNR@CTAB.

would allow for assessment of cell stress upon exposure to the AuNR conjugates. Other MOR specific assays such as a MOR-coupled BRET assay may not give an indication of cell stress.

The pERK1/2 assay was performed using an AlphaScreen kit purchased from PerkinElmer. Briefly, Chinese hamster ovary (CHO) cells stably expressing MOR were serum starved overnight prior to the assay. The cells were then exposed to the coated AuNR samples for 5 min, then digested for 10 min using a lysis solution. Donor and acceptor beads were then added, incubated for 1 h in the dark, and the resulting activity measured using an ELISA plate reader.

These results show that AuNR@PSS nanoparticles activate pERK1/2 activity, suggesting that PSS activates pERK1/2. Indeed, it is known that PSS itself has some biological activity, and has been shown to act as an antimicrobial agent, although the precise mechanism is unknown.³¹ Whether the activity seen here is non-specific or activating pERK1/2 via another pathway is unclear. In contrast, AuNR@ZW show no activity compared to buffer control, suggesting that this coating prevents non-specific binding and activation of surface proteins.

This is also a good indication that the coating method developed successfully removed the intermediate PSS coat prior to being coated with the desired surface ligands. Furthermore, upon titration of **6** to give AuNR@ZW(MorPEG 10%), activity was observed, suggesting the active ligand is still able to bind to and activate the receptor despite being conjugated to the AuNR. Increases in **6** titration gave varied results. As discussed in Chapter 4.4.2, the higher the titration of **6**, the less stable the nanoparticles and hence more aggregation was observed. The errors observed for AuNR@ZW(MorPEG 20%) and AuNR@ZW(MorPEG 30%) are likely due to a combination of sample aggregation and non-uniform coating of the surface with the active ligand.

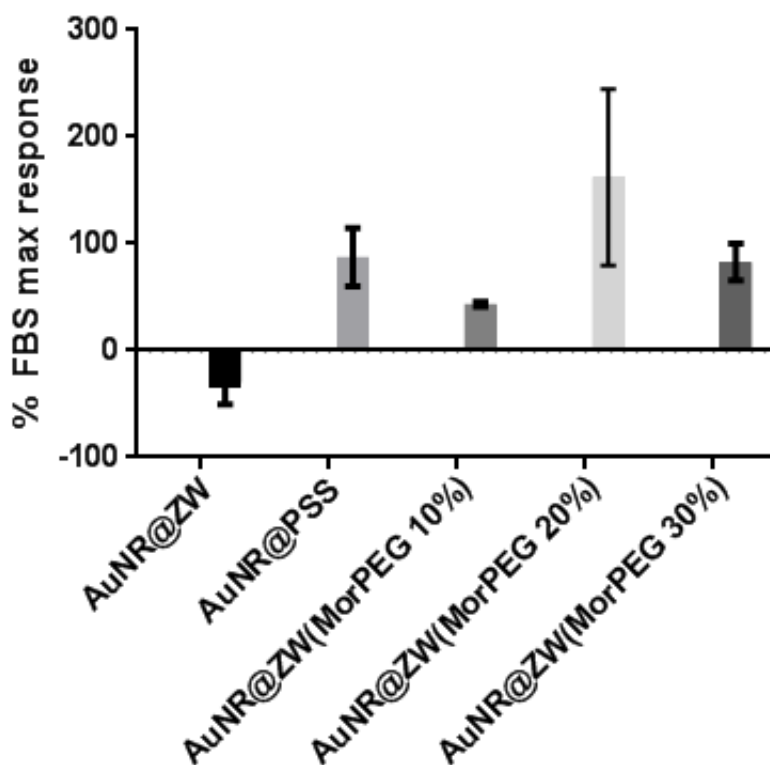


Figure 28. *pERK1/2* data showing the active ligand is still able to activate the MOR in living cells. AuNR@ZW show minimal activity compared to baseline, whilst AuNR@PSS shows significant response. This suggests that coating the AuNRs in **4** has made them biocompatible with no non-specific activation of the cell. Increasing titrations of **6** to give the varying AuNR@ZW(MorPEG) showed that the active ligand is still able to bind to and activate the receptor. The large errors observed for the 20 and 30% coated samples are likely due to sample aggregation. $n = 3$.

4.5.3 Other Attempts at Validating Coating Methods

Due to the extremely low concentration of AuNRs in the colloid, analyzing the surface chemistry was difficult. Conventionally, surface analysis is done using techniques such as inductively coupled plasma - mass spectrometry (ICP-MS), X-ray photoelectron spectroscopy (XPS), or SERS where possible. Typically, nanoparticle concentrations in the micromolar range are used. However, rough calculations suggest that the AuNR concentration to be approximately 0.25 nM. Despite this, SERS analysis was attempted on some of these samples, namely the AuNR@CTAB and AuNR@ZW samples. Raman spectroscopy is an infrared (IR) type experiment, measuring the vibration of covalent bonds upon irradiation by an IR or near IR source. The addition of an active metal surface, such as gold or silver, enhances this signal as well as enabling the evolution of signals that aren't detected by conventional Raman spectroscopy to be measured. It was thought that since gold and silver are inherently SERS active surfaces, the close association between the nanoparticle surface and the surface coat would enable some signals to be detected.

Although several attempts were made at trying to record a SERS spectra at various irradiation wavelengths, power levels and on different instruments, no conclusive SERS spectra could be recorded. This was concluded to be due to the extremely low concentration of the nanoparticles in solution. This may have had two impacts on the outcome; first, the low nanoparticle concentration resulted in there being a low surface area for the surface enhanced Raman effect to take place, and second, the low nanoparticle concentration means a relatively low surface coat concentration, so fewer organic molecules to produce the requisite vibrations, giving a very low signal-to-noise ratio. Although prior literature has shown that AuNRs may be used as SERS substrates to increase signal detection, the conditions required tend to be quite specific.³² Perhaps due to the lack of the specific instrumentation and conditions required, a SERS spectra could not be recorded.

4.6 Coating of Multiple Ligands onto AuNRs

Following validation of the coating method that enabled functionalization of AuNRs with the designed dithiolane-anchored ligands, work progressed to coating these nanoparticles with multiple ligands. Compound **6** bearing the MOR partial agonist pharmacophore morphine and **27** bearing the DOR antagonist pharmacophore naltrindole were used, as this combination could be used to study the MOR-DOR heterodimer. A schematic representation of the desired outcome is shown in Figure 29. As prior, coating solutions of these ligands at 1 mM in 10% v/v DMSO in water were made as stock solutions. The zwitterionic coat **4** was also used as previously described.

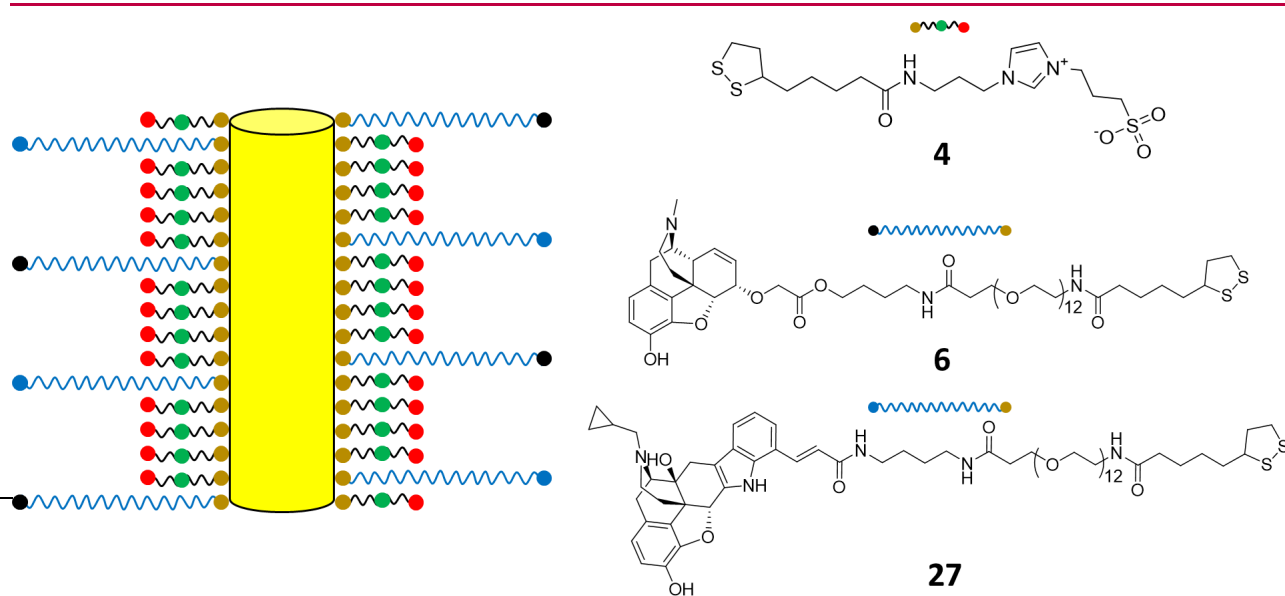


Figure 29. A schematic representation of the desired multifunctional AuNRs. These utilize **4** as the zwitterionic stabilizing coat, with **6** as the MOR partial agonist pharmacophore and **27** as the DOR antagonist pharmacophore.

Using the 2 step method, samples were generated with 5% each of the **6** and **27** solutions, with the remaining 90% of the coat being composed of **4**. This gave AuNR@ZW(MorPEG 5%, NaltPEG 5%) as the desired multifunctional nanoparticle system. For control purposes, AuNR@ZW(MorPEG 5%), AuNR@ZW(NaltPEG 5%), AuNR@ZW(NaltPEG 10%) were also produced, as well as the previously generated AuNR@ZW(MorPEG 10%) sample.

Using a cell-based system expressing both the MOR and DOR receptors, these coated AuNRs could be used to study the differences when targeting either receptor individually, or when both receptors are targeted simultaneously. The changes in pharmacology would offer interesting data as to the *in vitro* behavior of these receptors. Should these be successful at the cellular level, there is potential for these systems to be used in tissue samples, as the AuNR may be imaged using an MPL method through living tissue. This would give data more relevant to an *in vivo* setting. These systems are currently awaiting further evaluation as potential tools for the study of the MOR-DOR heterodimer.

4.7 Synthesis of a Control System for Comparison

As these AuNR-based imaging systems are still quite new, a control system was designed in order to assess whether these would behave in a similar manner to conventional organic fluorophores, or if they would reveal novel pharmacologies due to their size and multi-dentate structure. For this purpose, the adenosinergic receptor system was used, as fluorescent ligands have previously been used to characterize this system in great detail by the Kellam and Hill groups.³³⁻³⁸ Two previously used ligands were selected for use in this model system; xanthine amine congener (XAC) and 5'-(*N*-ethylcarboxamido)adenosine (NECA) (Figure 30).

XAC is a non-selective adenosine A₁ and A₃ receptor (A₁AR and A₃AR) antagonist. Fluorescent derivatives of this has previously been used to study these receptor systems in living cells.³⁹ Furthermore, these tool compounds have been developed into standard compounds to be used for high content screening.⁴⁰ In addition, inclusion of peptide fragments into the linker have been shown to increase subtype selectivity, making it a more useful compound for studying receptor subtype pharmacology.³⁴ NECA, a non-selective A₁AR, A_{2A}AR and A₃AR agonist, has also been modified to incorporate a fluorescent probe, enabling study of this receptor via FCS.³⁵ Again, modification of the linker and fluorophore altered its pharmacological properties, indicating the importance of linker design and fluorophore selection.³⁷ The use of these two literature ligands in coating AuNRs would provide a good point of comparison to study the differences between using a nanoparticle tag instead of an organic one.

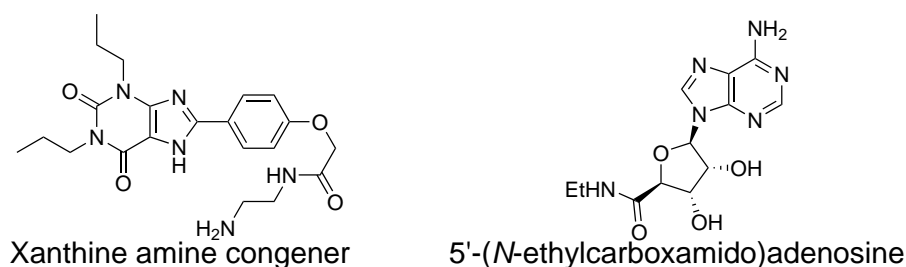


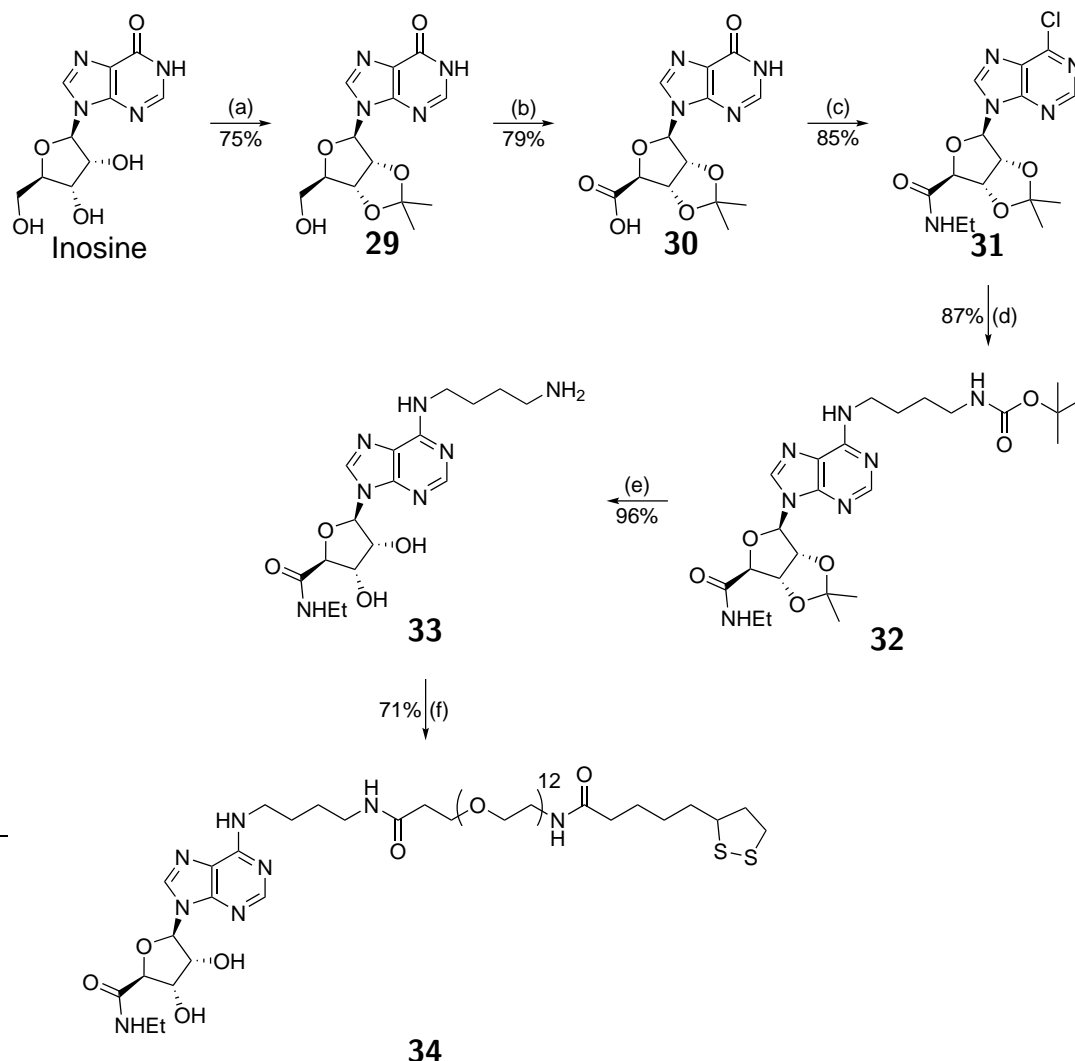
Figure 30. Xanthine amine congener (XAC) and 5'-(N-ethylcarboxamido)adenosine (NECA), two previously used ligands used as the targeting pharmacophore for the fluorescence imaging of adenosinergic receptors.

Initially, conjugation of XAC with Lipoamido-dPEG[®]₁₂-acid using EDC · HCl and HOAt gave the required XAC congener for conjugation to AuNRs. However, due to its extremely poor water solubility in the previously established 10% v/v DMSO pH 8 solution, a coating solution could not be made, and therefore coating onto AuNRs was not possible.

Moving on from this, NECA is known to be relatively water soluble, and therefore was a more suitable candidate for coating onto AuNRs. Synthesis was commenced using inosine (Scheme 12). Here, the synthesis was based on the procedure described by Middleton *et al.* with a few modifications.³⁵ Protection of the ribose unit using 2,2-dimethoxypropane gave **29**, which could be oxidized using TEMPO and BAIB to convert the terminal alcohol into the carboxylic acid **30**. A one-pot conversion to the corresponding amide and installation of a chloro moiety at the 6-position was effected using thionyl chloride, followed by treatment with ethylamine to give **31**. Rather than performing nucleophilic aromatic substitution of the 6-position chloro using *N*-benzyl-1,4-diaminobutane as per the literature procedure, *N*-Boc-1,4-diaminobutane was used instead to give **32**. This enabled global deprotection with TFA to give **33**, rather than deprotecting the acetal and the benzyl group separately as with the literature procedure.³⁵ Amide conjugation to Lipoamido-dPEG[®]₁₂-acid using EDC · HCl and HOAt gave the final congener **34**.

Compound **34** could then be used to coat AuNRs as previously described (Chapter 4.4). Titrating this congener in at 5% or 10% again with **4** as the stabilizing agent gave AuNR@ZW(NECA-

PEG 5%) and AuNR@ZW(NECA-PEG 10%).



Scheme 12. Synthesis of the NECA congener for attachment to AuNRs. Reagents and conditions: (a) tosic acid monohydrate, 2,2-dimethoxypropane, acetone, RT, 1.5 h, 75%; (b) TEMPO, BAIB, water/MeCN (1:1), RT, 4 h, 79%; (c) SOCl_2 , DMF, CHCl_3 , reflux, 5 h; then THF, EtNH_2 (2 M in THF), 5 °C, 15 min, 85%; (d) N-Boc-1,4-diaminobutane, TEA, EtOH, reflux, 18 h, 87%; (e) TFA, MeOH, RT, 1 h, 96%; (f) Lipoamido-dPEG[®]₁₂-acid, EDC·HCl, HOAt, TEA, DMF, RT, 1 h, 71%.

As this AuNR-based imaging system is still quite new, preliminary experiments are currently ongoing in order to determine the best approach to enable imaging of both the nanoparticle fluorophore in conjunction with any organic tags that may be used to visualize the receptor. This work is being conducted in collaboration with Dr Steve Briddon of the Queen's Medical Centre, University of Nottingham, U.K. As an initial foray into the potential

of these AuNR systems as imaging agents, we first wanted to demonstrate that these could be visualized using the available techniques. Briefly, AuNR@ZW colloid was simply spotted onto a glass plate, allowed to dry and imaged using fluorescence correlation spectroscopy (FCS). This early data suggests that AuNR@ZW can be visualized using a multi-photon excitation method.

4.8 Conclusions

The work conducted here has led to the successful development of coated AuNRs that are comprised of one or more active ligands with a zwitterionic stabilizing coat. This modular approach means a known ligand conjugated to a standard spacer can be coated onto the AuNR with a standard stabilizing ligand. This approach means a generic protocol can be used, rather than designing new procedures for each ligand.

Our preliminary assessment of this model system suggests that the active ligand maintained the ability to bind to cell surface receptors. AuNR@ZW(MorPEG 10%) show activity in a pERK1/2 assay when compared to buffer and AuNR@ZW controls, suggesting the active ligand is still able to activate the MOR despite being attached to the AuNR. Although the titration of the active ligand is limited by the overall stability of the particle, these types of systems are promising as alternative imaging agents. Traditional small molecule fluorophores have been useful in the characterization of various receptor systems, but increasingly it is becoming clear that receptors do not act as isolated single units. Therefore, tools that address this are needed. These AuNR-based imaging systems have the potential to be used as agents to visualize GPCR heterodimers.

Current early preliminary experiments suggest these AuNRs may be imaged using a multi-photon method via FCS. However, method development is ongoing in order to determine the best approach to visualize both the AuNR samples and the conventionally used organic fluorescent tags for receptor trafficking studies.

4.9 Experimental

General Information

Chemicals and solvents were purchased from standard suppliers and used without further purification unless otherwise stated. Davisil silica gel (40 - 63 μm) for standard phase flash column chromatography and reverse phase silica gen (C18, 10 -14 μm) for reverse phase flash column chromatography was supplied by Grace Davison Discovery Sciences. Reverse phase flash column chromatography was run using the following buffers; buffer A, 0.1% TFA in H_2O ; bffer B, 0.1% TFA in MeCN. Deuterated solvents were purchased from Cambridge Isotope Laboratories, Inc.

Reactions were monitored via thin layer chromatography on commercially purchased precoated aluminum-backed plates (Merck Kieselgel 60 F₂₅₄ and visualized under UV light (254 and 366 nm) or using KMnO_4 or phosphomolybdic acid stains. Organic solvents were evaporated in vacuo at ≥ 40 °C (water bath temperature).

^1H and ^{13}C NMR spectra were recorded on a Bruker Avance Nanobay III 400 MHz Ultrashield Plus spectrometer at 400.13 and 100.62 MHz, respectively. Chemical shifts (δ) are recorded in parts per million (ppm) with reference to the chemical shift of the deuterated solvent as described by Gottlieb *et al.*⁴¹ Coupling constants (J) are recorded in Hz and the significant multiplicities described by singles (s), doublet (d), triplet (t), quadruplet (q), broad (br), multiplet (m), doublet of doublets (dd), and doublet of triplets (dt).

LC-MS were run to monitor reactions, verify reaction outcomes and purity using an Agilet 6120 series single quad coupled to an Agilent 1260 series HPLC. The following buffers were used; buffer A, 0.1% formic acid in H_2O ; buffer B, 0.1% formic acid in MeCN. The following gradient was used with a Poroshell 120 EC-C18 50 mm \times 3.0 mm 2.7 μm column and a flow rate of 0.6 mL/min and a total run time of 5 min; 0 - 1 min 95% buffer A and 5% buffer B, from 1 to 2.5 min up to 0% buffer A and 100% buffer B, held at this composition until 3.8 min, 3.8 - 4 min 95% buffer A and 5% buffer B, and held until 5 min at this composition. Mass spectra were acquired in positive and negative ion mode with a scan range of 100 - 1000 m/z .

UV detection was carried out at 214 and 254 nm.

Preparative HPLC was performed using an Agilent 1260 Infinity HPLC system using Agilent OpenLAB CDS software (Rev C.01.04), and an Altima 5 μM C8 22 mm \times 250 mm column. The following buffers were used; buffer A, 0.1% TFA in H_2O ; buffer B, 0.1% TFA in MeCN, with the sample being run at a gradient of 5% buffer B to 100% buffer B over 15 min, at a flow rate of 15 mL/min.

High resolution mass spectrometry-time-of-flight (HRMS-TOF) was conducted using an Agilent 6224 TOF LC-MS mass spectrometer coupled to an Agilent 1290 Infinity. Chromatographic separation was performed using an Agilent Zorbax SB-C18 Rapid Resolution HT 2.1 mm \times 50 mm, 1.8 μm column using a gradient of 5 - 100% buffer B in buffer A over 3.5 min at 0.5 mL/min, where buffers were as defined for LC-MS. All mass data was acquired and reference mass corrected via a dual-spray ESI source. Mass spectra were created by averaging scans across each peak and background subtracting against the first 10 s of the total ion count. Acquisition was performed using the Agilent Mass Hunter Data Acquisition software and analysis performed using Mass Hunter Qualitative Analysis software. The mass spectrometer was run using the following conditions; drying gas flow 11 L/min, nebulizer 45 PSI, drying gas temperature 325 $^\circ\text{C}$, capillary voltage 400 V, fragmentor 160 V, skimmer 65 V, OCT RFV 750 V, scan range acquired 100-1500 m/z , internal reference ions positive ion mode = m/z 121.050873 and 922.009798.

Synthesis of Gold Nanorods

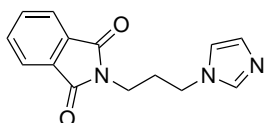
AuNRs were synthesized using a modified version of Nikoobakht and El-Sayed's procedure.¹ All solutions were prepared using Milli-Q grade water. All glassware was cleaned using aqua regia (3:1 conc. HCl/conc. HNO_3), rinsed with Milli-Q grade water, dried in an oven overnight and cooled to room temperature before use. All reactions were conducted in a 30 $^\circ\text{C}$ water bath.

Chloroauric acid (10 mM, 125 μL) was added to CTAB (100 mM, 5 mL). The resulting mixture was stirred rapidly (1 kRPM) and freshly prepared ice-cold aqueous NaBH_4 (10 mM,

300 μL) was injected into the solution. The resulting brown solution was stirred for an additional 5 min, to give the nanoseed solution, which was allowed to age for 1 h before further use.

To prepare the growth solution, chloroauric acid (100 mM, 750 μL) and varying volumes of AgNO_3 (4 mM) were added to CTAB (100 mM, 15 mL). Ascorbic acid (78.8 mM, 105 μL) was then added and the solution stirred rapidly (1 kRPM) for 1 min until the gold-colored solution turned clear. The stirring speed was reduced (100 RPM) and the nanoseed solution (18 μL) was added. The solution was allowed to stir slowly for 2 h to give AuNR@CTAB. These could then be cleaned by centrifuging, removing 90% of the supernatant and adding Milli-Q water to the original volume, followed by two rounds of centrifugation and resuspension in a 10 mM solution of CTAB.

2-[3-(1*H*-Imidazol-1-yl)propyl]-1*H*-isoindole-1,3(2*H*)-dione (1)

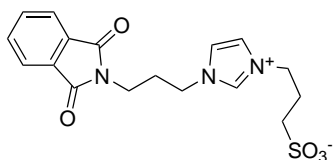


Imidazole (2.59 g, 39 mmol, 3 eq.), *N*-(3-bromopropyl)phthalimide (3.50 g, 13.1 mmol, 1 eq.) and K_2CO_3 (1.80 g, 13.1 mmol, 1 eq.) were added to MeCN (25 mL) and heated to reflux for 17 hours. The reaction was then cooled to room temperature and filtered. The filtrate was then evaporated

and the resulting residue purified by flash chromatography (9:1 MeOH/ CHCl_3 on silica) to give a yellow oil that was scratched to give an off-white solid (1.89 g, 57%).

^1H NMR (400 MHz, CHCl_3) δ_{H} 7.85 - 7.78 (m, 2H), 7.75 - 7.66 (m, 2H), 7.58 (s, 1H), 7.02 (s, 1H), 6.98 (t, $J = 1.2$ Hz, 1H), 4.00 (t, $J = 7.0$ Hz, 2H), 3.71 (t, $J = 6.6$ Hz, 2H), 2.17 (quint, $J = 6.8$ Hz, 2H); ^{13}C NMR (101 MHz, CHCl_3) δ_{C} 168.41, 137.24, 134.31, 131.93, 129.42, 123.47, 118.90, 50.54, 44.65, 35.19, 30.23; LC-MS m/z $[\text{M}+\text{H}]^+$ $\text{C}_{14}\text{H}_{14}\text{N}_3\text{O}_2^+$ calc. 256.1, found 256.2.

3-[1-[3-(1,3-Dioxo-1,3-dihydro-2*H*-isoindol-2-yl)propyl]-1*H*-imidazol-3-ium-3-yl]propane-1-sulfonate (2)

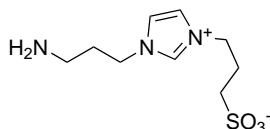


Compound **1** (1.80 g, 7.0 mmol, 1 eq.) and 1,3-propanesultone (0.94 g, 7.7 mmol, 1.1 eq.) were added to dry MeCN in a microwave vial. The vessel was then sealed and purged with N₂ and heated at 80 °C for 30 min, whereupon a white precipitate appears. The reaction was cooled to room temperature and CHCl₃ (20 mL) was added.

The white precipitate was filtered. The filtrate was evaporated and refiltered from CHCl₃. This was repeated and the three crops combined to give the final product (2.18 g, 92%).

¹H NMR (400 MHz, DMSO-*d*₆) δ_H 9.19 - 9.11 (m, 1H), 7.93 - 7.81 (m, 4H), 7.79 (dd, *J* = 3.3, 1.6 Hz, 2H), 4.29 (t, *J* = 6.9 Hz, 2H), 4.22 (t, *J* = 7.3 Hz, 2H), 3.61 (t, *J* = 6.3 Hz, 2H), 2.42 (t, *J* = 7.1 Hz, 2H), 2.17 (dt, *J* = 13.5, 6.8 Hz, 2H), 2.13 - 2.04 (m, 2H); ¹³C NMR (101 MHz, DMSO-*d*₆) δ_C 168.06, 136.44, 134.42, 131.76, 123.09, 122.51, 122.34, 47.89, 47.31, 46.60, 34.36, 28.55, 26.17; LC-MS *m/z* [M+H]⁺ C₁₇H₂₀N₃O₅S calc. 378.1, found 378.2.

3-[1-(3-Aminopropyl)-1*H*-imidazol-3-ium-3-yl]propane-1-sulfonate (3)

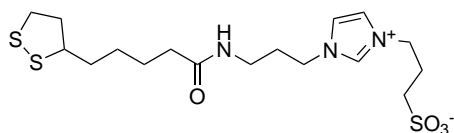


Compound **2** (2.12 g, 5.6 mmol, 1 eq.) was suspended in MeOH (50 mL). N₂H₄ · H₂O (2.7 mL, 10 eq.) was added, whereupon the solid dissolved. The mixture was then heated to reflux for 1 h, after which a large volume of fluffy white precipitate was observed. The reaction was cooled to room

temperature and filtered. The filtrate was evaporated and the resulting residue was purified by reverse phase chromatography (buffer A). The clean fractions were combined and freeze-dried to give the TFA salt as a hard oil (1.30 g, 66%).

¹H NMR (400 MHz, DMSO-*d*₆) δ_H 9.20 (s, 1H), 7.81 (dt, *J* = 20.1, 1.7 Hz, 2H), 4.29 (dt, *J* = 16.8, 6.9 Hz, 4H), 2.85 - 2.76 (m, 2H), 2.46 (t, *J* = 7.2 Hz, 2H), 2.17 - 2.03 (m, 4H); ¹³C NMR (101 MHz, DMSO-*d*₆) δ_C 136.53, 122.76, 122.41, 47.95, 47.38, 46.05, 35.87, 27.72, 26.04; LC-MS *m/z* [M+H]⁺ C₉H₁₈N₃O₃S⁺ calc. 248.1, found 248.2.

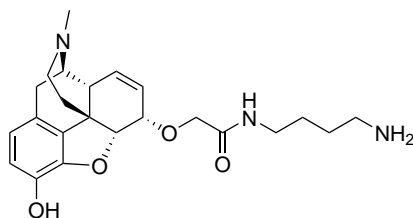
3-(1-(3-(5-(1,2-Dithiolan-3-yl)pentanamido)propyl)-1*H*-imidazol-3-ium-3-yl)propane-1-sulfonate (4)



Lipoic acid (428 mg, 2.3 mmol, 1.1 eq.), EDC · HCl (477 mg, 2.5 mmol, 1.2 eq.), anhydrous HOBt (336 mg, 2.5 mmol, 1.2 eq.) and DIPEA (1.1 mL, 6.2 mmol, 3 eq.) were dissolved in DMF (4 mL) and stirred for 1 h. Compound **3** (749 g, 2.1 mmol, 1 eq.) was then added as a solution in DMF (5 mL), whereupon a precipitate formed. The reaction was stirred at room temperature for 1 h, then heated at 60 °C for another 1 h. The reaction was then evaporated to give a yellow/orange oil, which was purified by reverse phase chromatography twice (20% buffer B in buffer A). The clean fractions were freeze-dried to give the TFA salt as a light yellow gum (476 mg, 41%).

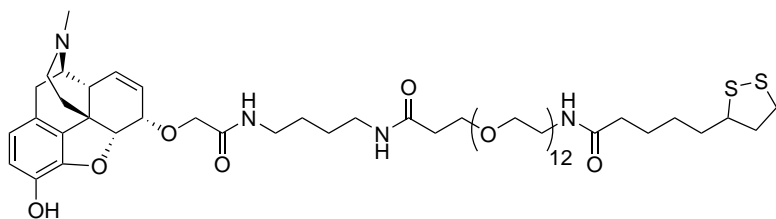
¹H NMR (400 MHz, DMSO-*d*₆) δ_H 9.16 (s, 1H), 7.90 (t, *J* = 5.6 Hz, 1H), 7.80 (t, *J* = 1.7 Hz, 1H), 7.78 (t, *J* = 1.8 Hz, 1H), 4.30 (t, *J* = 7.0 Hz, 2H), 4.15 (t, *J* = 7.0 Hz, 2H), 3.65 - 3.58 (m, 3H), 3.23 - 3.08 (m, 2H), 3.04 (q, *J* = 6.5 Hz, 2H), 2.46 - 2.36 (m, 3H), 2.15 - 2.05 (m, 4H), 1.97 - 1.81 (m, 3H), 1.67 (dtd, *J* = 13.5, 7.5, 5.6 Hz, 1H), 1.60 - 1.46 (m, 3H), 1.35 (dd, *J* = 15.5, 7.7 Hz, 2H); ¹³C NMR (101 MHz, DMSO-*d*₆) δ_C 172.26, 122.53, 122.43, 56.15, 47.91, 47.33, 46.74, 38.11, 35.23, 35.17, 34.12, 29.66, 28.36, 26.11, 24.98; LC-MS *m/z* [M+H]⁺ C₁₇H₃₀N₃O₄S₃⁺ calc. 436.1, found 436.2.

***N*-(4-Aminobutyl)-2-(((4*R*,4*aR*,7*S*,7*aR*,12*bS*)-9-hydroxy-3-methyl-2,3,4,4*a*,7,7*a*-hexahydro-1*H*-4,12-methanobenzofuro[3,2-*e*]isoquinolin-7-yl)oxy)acetamide (5)**



See Chapter 3 for synthesis and characterization. Referred to as "compound **20**".

1-(5-(1,2-Dithiolan-3-yl)pentanamido)-*N*-(4-(2-(((4*R*,4*aR*,7*S*,7*aR*,12*bS*)-9-hydroxy-3-methyl-2,3,4,4*a*,7,7*a*-hexahydro-1*H*-4,12-methanobenzofuro[3,2-*e*]isoquinolin-7-yl)oxy)acetamido)butyl)-3,6,9,12,15,18,21,24,27,30,33,36-dodecaoxanonatriacontan-39-amide (6)



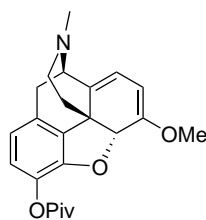
Lipoamido-dPEG[®]₁₂-acid (5.0 mg, 6.2 μ mol, 1 eq.), HCTU (3.1 mg, 6.2 μ mmol, 1.2 eq.) and TEA (10 μ L) were dissolved in DMF (600 μ L) under an N₂ atmosphere and stirred at

room temperature for 1 h. Compound **5** TFA salt (6.5 mg, 12 μ mol, 2 eq.) was then added as a solution in DMF (200 μ L) and allowed to stir at room temperature for 18 h. Buffer A was added and the resulting solution freeze dried. The residue was purified by prep-HPLC to give the product as a yellow gum TFA salt (3.9 mg, 48%).

¹H NMR (400 MHz, DMSO-*d*₆) δ_H 10.35 - 9.91 (m, 1H), 9.19 (s, 1H), 7.88 - 7.70 (m, 2H), 6.58 (dd, *J* = 8.0, 2.9 Hz, 1H), 6.51 - 6.47 (m, 1H), 5.83 (d, *J* = 8.9 Hz, 1H), 5.36 (d, *J* = 9.7 Hz, 1H), 5.15 - 5.06 (m, 1H), 4.16 - 3.99 (m, 2H), 3.70 - 3.45 (m, 53H), 3.39 (td, *J* = 5.5, 2.8 Hz, 2H), 3.32 (d, *J* = 10.9 Hz, 1H), 3.25 - 3.09 (m, 6H), 3.07 - 2.98 (m, 3H), 2.91 (s, 2H), 2.83 (s, 1H), 2.75 (dd, *J* = 19.7, 5.5 Hz, 1H), 2.29 (dd, *J* = 6.1, 3.5 Hz, 2H), 2.23 - 2.15 (m, 1H), 2.07 (dd, *J* = 7.2, 4.5 Hz, 1H), 1.97 (d, *J* = 13.6 Hz, 1H), 1.92 - 1.82 (m, 1H), 1.71 - 1.20 (m, 9H); ESI-TOF HRMS *m/z* [M+Na]⁺ C₅₈H₉₆N₄O₁₈S₂Na⁺ calc. 1223.6053, found 1223.6084, [M+2H]⁺² C₅₈H₉₈N₄O₁₈S₂⁺² calc. 601.3153, found 601.3177.

3-O-Pivaloyl oripavine (12)

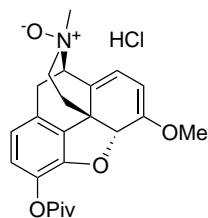
Oripavine (1.8 g, 6.1 mmol, 1 eq.) was dissolved in DCM (35 mL) and cooled to 0 °C. TEA (3.4 mL, 24 mmol, 4 eq.) and pivaloyl chloride (1.5 mL, 12 mmol, 2 eq.) were sequentially added and allowed to stir at room temperature for 3 h. DCM (50 mL) was then added and washed with saturated NaHCO₃ (6



× 30 mL) and brine (40 mL). The organic phase was dried over Na₂SO₄ and the solvent removed *in vacuo*. The resulting residue was redissolved in CHCl₃ (60 mL) and washed sequentially with 1:1 brine/1 M NaOH (3 × 40 mL) and brine (40 mL). The organic phase was dried over Na₂SO₄ and the solvent removed *in vacuo*. The residue was purified by flash chromatography (94:5:1 CHCl₃/MeOH/NH₄OH) to give a light brown foam (2.2 g, 95%).

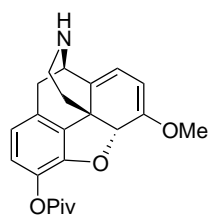
¹H NMR (400 MHz, CDCl₃) δ_H 6.72 (d, *J* = 8.1 Hz, 1H), 6.61 (d, *J* = 8.2 Hz, 1H), 5.54 (d, *J* = 6.4 Hz, 1H), 5.28 (s, 1H), 5.02 (d, *J* = 6.4 Hz, 1H), 3.60 (d, *J* = 6.9 Hz, 1H), 3.58 (s, 3H), 3.31 (d, *J* = 18.2 Hz, 1H), 2.80 (td, *J* = 12.7, 3.6 Hz, 1H), 2.70 - 2.59 (m, 2H), 2.45 (s, 3H), 2.18 (td, *J* = 12.6, 5.1 Hz, 1H), 1.77 (dd, *J* = 12.6, 2.1 Hz, 1H), 1.35 (s, 9H); ¹³C NMR (101 MHz, CDCl₃) δ_C 176.52, 152.59, 148.05, 134.41, 132.98, 132.75, 132.29, 121.76, 119.24, 111.77, 96.35, 89.73, 60.77, 55.09, 46.06, 42.54, 36.95, 29.92, 27.32; LC-MS *m/z* [M+H]⁺ C₂₃H₂₈NO₄⁺ calc. 382.2, found 382.2.

3-O-Pivaloyl oripavine-*N*-oxide hydrochloride (**13**)



Compound **12** (2.2 g, 5.8 mmol, 1 eq.) was dissolved in CHCl₃ (45 mL) and cooled to 0 °C. *m*CPBA (77% purity, 1.6 g, 7.0 mmol, 1.2 eq.) was added in one portion and stirred at 0 °C for 30 min. *i*PrOH (15 mL) and 3:1 CHCl₃/*i*PrOH (45 mL) were then added and the resulting organic phase washed with saturated NaHCO₃ (10 × 15 mL), then 4:1 brine/2 M HCl (5 × 15 mL), dried over Na₂SO₄ and the solvent removed *in vacuo* to give the product as a yellow foam, which was used without further purification or characterization (98%, 2.5 g).

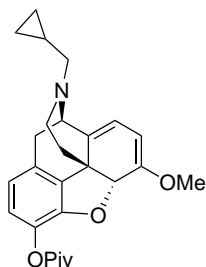
3-O-Pivaloyl nororipavine (**14**)



Compound **13** (2.5 g, 5.7 mmol, 1 eq.) was dissolved in CHCl₃ (125 mL). Fe₃(CO)₁₂ (144 mg, 0.29 mmol, 0.05 eq.) was then added and the resulting solution stirred at room temperature for 1 h. The solvent was then removed *in vacuo* and the residue purified by flash chromatography (94:5:1 CHCl₃/MeOH/NH₄OH) to give the product as a brown foam (1.1 g, 54%).

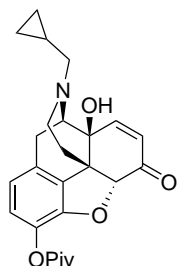
^1H NMR (400 MHz, CDCl_3) δ_H 6.73 (d, $J = 8.1$ Hz, 1H), 6.61 (d, $J = 8.2$ Hz, 1H), 5.45 (d, $J = 6.4$ Hz, 1H), 5.23 (s, 1H), 4.99 (d, $J = 6.4$ Hz, 1H), 3.87 (dd, $J = 5.1, 2.6$ Hz, 1H), 3.57 (s, 3H), 3.21 - 3.09 (m, 3H), 2.89 (dd, $J = 13.9, 4.2$ Hz, 1H), 2.02 (td, $J = 12.5, 5.0$ Hz, 2H), 1.84 (dd, $J = 12.5, 2.7$ Hz, 1H), 1.34 (s, 9H); ^{13}C NMR (101 MHz, CDCl_3) δ_C 176.46, 152.50, 148.09, 134.49, 134.10, 133.19, 132.73, 121.77, 119.20, 110.20, 96.28, 89.79, 55.03, 53.84, 46.77, 40.66, 39.16, 38.51, 38.28, 27.27; LC-MS m/z $[\text{M}+\text{H}]^+$ $\text{C}_{22}\text{H}_{26}\text{NO}_4^+$ calc. 368.2, found 368.2.

(4*R*,7*aR*,12*bS*)-3-(Cyclopropylmethyl)-7-methoxy-2,3,4,7*a*-tetrahydro-1*H*-4,12-methanobenzofuro[3,2-*e*]isoquinolin-9-yl pivalate (15)



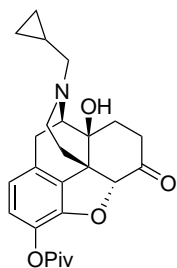
Compound **14** (790 mg, 2.2 mmol, 1 eq.) was dissolved in MeCN (30 mL). K_2CO_3 (594 mg, 4.3 mmol, 2 eq.) and cyclopropylmethyl bromide (250 μL , 2.6 mmol, 1.2 eq.) were then added and the reaction vessel purged with N_2 gas 3 times and the reaction was then allowed to stir at room temperature for 24 h. The reaction was then filtered, the filtrate evaporated and the resulting residue was purified by flash chromatography (96.5:3:0.5 $\text{CHCl}_3/\text{MeOH}/\text{NH}_4\text{OH}$) to give a brown oil (501 mg, 55%).

^1H NMR (400 MHz, CDCl_3) δ_H 6.71 (d, $J = 8.1$ Hz, 1H), 6.58 (d, $J = 8.2$ Hz, 1H), 5.52 (d, $J = 6.4$ Hz, 1H), 5.25 (s, 1H), 5.00 (d, $J = 6.4$ Hz, 1H), 3.90 (d, $J = 6.9$ Hz, 1H), 3.56 (s, 3H), 3.24 (d, $J = 18.2$ Hz, 1H), 2.97 - 2.64 (m, 5H), 2.46 (d, $J = 6.4$ Hz, 2H), 2.17 (td, $J = 12.5, 5.3$ Hz, 1H), 1.73 (dd, $J = 12.6, 1.8$ Hz, 1H), 1.34 (s, 9H), 0.94 - 0.85 (m, 1H), 0.57 - 0.50 (m, 2H), 0.14 (dt, $J = 9.6, 4.6$ Hz, 2H); ^{13}C NMR (101 MHz, CDCl_3) δ_C 176.44, 152.52, 147.94, 134.65, 133.01, 132.67, 132.38, 121.67, 119.16, 112.02, 96.36, 89.78, 59.07, 58.49, 55.03, 46.59, 44.17, 39.14, 36.56, 31.11, 27.26, 9.53, 4.00, 3.85; LC-MS m/z $[\text{M}+\text{H}]^+$ $\text{C}_{26}\text{H}_{32}\text{NO}_4^+$ calc. 422.2, found 422.2.

3-O-Pivaloyl dehydronaltrexone (16)

Compound **15** (501 mg, 1.2 mmol, 1 eq.) was suspended in a mixture of MeCN (200 μ L), water (2 mL) and oxalic acid (54 mg, 0.59 mmol, 0.5 eq.). Formic acid (63 μ L, 1.7 mmol, 1.4 eq.) and peracetic acid (32% in acetic acid, 325 μ L, 1.5 mmol, 1.3 eq.) were then added successively, after which the solid dissolved. The reaction was then allowed to stir at room temperature for 1 h. Water (30 mL) was then added and the mixture was freeze dried. The resulting solid was purified by flash chromatography (99:1 CHCl₃/TEA) to give the product as a white solid (392 mg, 78%)

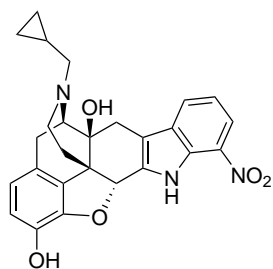
¹H NMR (400 MHz, CDCl₃) δ_H 6.77 (d, J = 8.2 Hz, 1H), 6.65 - 6.60 (m, 2H), 6.18 (d, J = 10.1 Hz, 1H), 4.73 (s, 1H), 3.37 (d, J = 6.0 Hz, 1H), 3.16 (d, J = 18.8 Hz, 1H), 2.74 (dd, J = 12.0, 4.6 Hz, 1H), 2.58 (dd, J = 18.9, 6.1 Hz, 1H), 2.50 - 2.37 (m, 3H), 2.25 (td, J = 12.2, 3.6 Hz, 1H), 1.74 (dd, J = 12.9, 2.4 Hz, 1H), 1.33 (s, 9H), 0.93 - 0.83 (m, 1H), 0.60 - 0.55 (m, 2H), 0.19 - 0.13 (m, 2H); ¹³C NMR (101 MHz, CDCl₃) δ_C 193.39, 176.12, 147.70, 134.95, 132.79, 131.32, 130.22, 122.92, 119.49, 87.70, 67.61, 61.64, 59.17, 47.39, 43.46, 39.16, 29.76, 27.24, 23.50, 9.43, 4.19, 3.91; LC-MS m/z [M+H]⁺ C₂₅H₃₀NO₅⁺ calc. 424.2, found 424.2.

3-O-Pivaloyl naltrexone (17)

Compound **16** (392 mg, 0.93 mmol, 1 eq.) was dissolved in MeOH (40 mL) in a 3-neck flask. The reaction vessel was purged with N₂ 3 times and Pd/C (10% Pd on activated carbon, 98 mg, 25% w/w of substrate) was added. The reaction vessel was again purged with N₂ 3 times, then flushed with H₂ 3 times. The reaction was then allowed to stir under an H₂ atmosphere at 1 atm for 18 h. The reaction mixture was then filtered through a pad of celite. The pad was washed with MeOH (200 mL) and the combined filtrates were evaporated. The resulting pink solid was redissolved in MeOH (15 mL), formic acid added (100 μ L), and the solvent removed *in vacuo* to give the product as a white foam formate salt (409 mg, 87%).

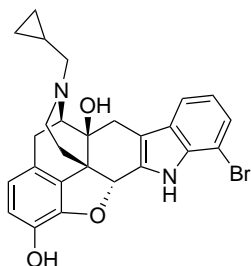
^1H NMR (400 MHz, CDCl_3) δ_H 8.80 (s, 2H), 8.36 (s, 1H), 6.82 (d, $J = 8.2$ Hz, 1H), 6.69 (d, $J = 8.2$ Hz, 1H), 4.77 (s, 1H), 4.00 (d, $J = 4.1$ Hz, 1H), 3.22 (d, $J = 9.0$ Hz, 1H), 3.14 (d, $J = 19.4$ Hz, 1H), 3.10 - 2.89 (m, 3H), 2.81 (dd, $J = 12.0, 5.0$ Hz, 2H), 2.39 (dd, $J = 12.3, 9.2$ Hz, 1H), 2.24 (d, $J = 14.7$ Hz, 1H), 2.14 (d, $J = 12.4$ Hz, 1H), 1.66 - 1.52 (m, 2H), 1.32 (s, 9H), 1.15 (d, $J = 7.8$ Hz, 1H), 0.71 - 0.65 (m, 2H), 0.48 - 0.41 (m, 1H), 0.36 - 0.27 (m, 1H); ^{13}C NMR (101 MHz, CDCl_3) δ_C 176.06, 167.01, 148.28, 133.72, 129.04, 127.39, 123.72, 119.53, 89.94, 70.16, 61.62, 58.75, 49.43, 45.52, 39.13, 35.41, 31.16, 28.45, 27.14, 23.95, 6.87, 5.08, 3.95; LC-MS m/z $[\text{M}+\text{H}]^+$ $\text{C}_{25}\text{H}_{32}\text{NO}_5^+$ calc. 426.2, found 426.2.

7'-Nitronaltrindole (18)



Naltrexone HCl (or equivalent **35**) (100 mg, 0.30 mmol, 1 eq.) and 2-nitrophenylhydrazine (63.5 mg, 0.44 mmol, 1.4 eq.) were suspended in a mixture of EtOH (5 mL) and 10 M HCl (1 mL) and the resulting mixture refluxed for 17 h. The resulting mixture was cooled, then diluted with MeCN and the solvent removed *in vacuo*. The resulting orange solid was purified by flash chromatography (97:2.5:0.5 $\text{CHCl}_3/\text{MeOH}/\text{NH}_4\text{OH}$) to give a yellow solid (107 mg, 79%).

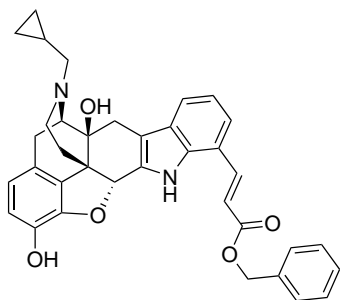
^1H NMR (401 MHz, $\text{DMSO}-d_6$) δ_H 9.00 (s, 1H), 7.85 (dt, $J = 8.8, 0.7$ Hz, 1H), 7.76 (dt, $J = 8.6, 0.9$ Hz, 1H), 7.54 (ddd, $J = 8.8, 6.7, 1.0$ Hz, 1H), 7.43 (ddd, $J = 8.6, 6.7, 0.8$ Hz, 1H), 6.93 (dd, $J = 5.7, 2.6$ Hz, 1H), 6.59 - 6.53 (m, 2H), 5.79 (s, 1H), 4.92 (s, 1H), 4.10 (q, $J = 5.3$ Hz, 2H), 3.04 (d, $J = 18.6$ Hz, 1H), 2.71 (d, $J = 6.0$ Hz, 1H), 2.67 (t, $J = 5.9$ Hz, 1H), 2.43 - 2.25 (m, 5H), 2.11 (td, $J = 12.0, 3.3$ Hz, 1H), 1.51 (d, $J = 10.7$ Hz, 1H), 0.94 - 0.83 (m, 1H), 0.56 - 0.44 (m, 2H), 0.18 - 0.10 (m, 2H); ^{13}C NMR (101 MHz, $\text{DMSO}-d_6$) δ_C 142.60, 140.08, 131.10, 130.80, 130.43, 129.35, 126.59, 125.43, 124.09, 119.13, 119.00, 117.24, 113.53, 83.21, 69.53, 58.66, 46.49, 43.21, 32.38, 30.71, 22.38, 9.17, 3.80, 3.52; LC-MS m/z $[\text{M}+\text{H}]^+$ $\text{C}_{26}\text{H}_{26}\text{N}_3\text{O}_5^+$ calc. 460.2, found 460.2.

7'-Bromonaltrindole (19)

Naltrexone HCl (or equivalent **35**) (100 mg, 0.30 mmol, 1 eq.) and 2-bromophenylhydrazine (92.6 mg, 0.44 mmol, 1.4 eq.) were suspended in a mixture of EtOH (5 mL) and 10 M HCl (1 mL) and the resulting mixture refluxed for 18 h. The resulting mixture was cooled, the solvent removed *in vacuo* and the resulting residue purified using flash chromatography (96:3.5:0.5 CHCl₃/MeOH/NH₄OH) to give a light brown solid (88.2 mg, 61%).

¹H NMR (401 MHz, CDCl₃) δ_H 8.69 (s, 1H), 7.30 (d, $J = 7.8$ Hz, 1H), 7.22 - 7.18 (m, 1H), 6.84 (t, $J = 7.8$ Hz, 1H), 6.59 (d, $J = 8.1$ Hz, 1H), 6.51 (d, $J = 8.1$ Hz, 1H), 5.66 (s, 1H), 3.36 (d, $J = 6.3$ Hz, 1H), 3.11 (d, $J = 18.6$ Hz, 1H), 2.87 (d, $J = 15.7$ Hz, 1H), 2.79 (dd, $J = 18.7, 6.6$ Hz, 1H), 2.72 (dd, $J = 11.4, 4.3$ Hz, 1H), 2.64 (d, $J = 15.5$ Hz, 1H), 2.47 - 2.34 (m, 3H), 2.26 (td, $J = 11.9, 3.2$ Hz, 1H), 1.73 (d, $J = 11.0$ Hz, 1H), 0.94 - 0.80 (m, 1H), 0.62 - 0.50 (m, 2H), 0.21 - 0.10 (m, 2H); ¹³C NMR (101 MHz, CDCl₃) δ_C 142.59, 138.90, 135.88, 130.56, 129.50, 127.93, 125.36, 125.16, 120.52, 119.45, 118.35, 117.37, 113.05, 104.76, 85.51, 72.90, 62.24, 59.54, 48.19, 43.71, 31.52, 29.04, 23.21, 9.45, 4.20, 3.90; LC-MS m/z [M+H]⁺ C₂₆H₂₆BrN₂O₃⁺ calc. 495.1, 496.1, found 494.8, 495.7.

Benzyl (E)-3-((4bS,8R,8aS,14bR)-7-(cyclopropylmethyl)-1,8a-dihydroxy-5,6,7,8,8a,9,14,14b-octahydro-4,8-methanobenzofuro[2,3-a]pyrido[4,3-b]carbazol-13-yl)acrylate (20)

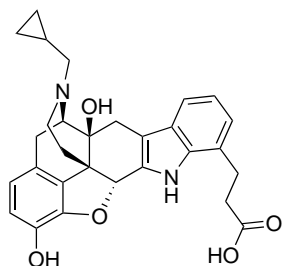


Compound **19** (50 mg, 0.10 mmol, 1 eq.), benzylacrylate (23.3 μ L, 0.15 mmol, 1.5 eq.), TEA (28.3 μ L, 0.20 mmol, 2 eq.) and PdCl₂(PPh)₃ (7 mg, 0.010 mmol, 0.1 eq.) were dissolved in dry DMF (1.5 mL) in a sealed vessel and the solution degassed under an N₂ atmosphere. The resulting mixture was heated at 90 °C for 17 h, after which the solvent was removed *in vacuo*.

The resulting residue was purified by flash chromatography (94:5:1 CHCl₃/MeOH/NH₄OH) to give the product as a yellow glass (31 mg, 53%).

¹H NMR (401 MHz, CDCl₃) δ_H 9.21 (s, 1H), 8.09 (d, $J = 16.1$ Hz, 1H), 7.46 - 7.29 (m, 7H), 7.01 (t, $J = 7.6$ Hz, 1H), 6.66 (d, $J = 8.1$ Hz, 1H), 6.54 (d, $J = 16.1$ Hz, 1H), 6.50 (d, $J = 8.1$ Hz, 1H), 5.69 (s, 1H), 5.27 (s, 2H), 3.35 (d, $J = 6.4$ Hz, 1H), 3.12 (d, $J = 18.6$ Hz, 1H), 2.87 (d, $J = 15.6$ Hz, 1H), 2.78 (dd, $J = 18.8, 6.8$ Hz, 1H), 2.73 (dd, $J = 11.4, 4.3$ Hz, 1H), 2.62 (d, $J = 15.7$ Hz, 1H), 2.48 - 2.35 (m, 3H), 2.29 (td, $J = 11.8, 3.1$ Hz, 1H), 1.81 - 1.76 (m, 1H), 0.88 (dq, $J = 6.5, 5.0$ Hz, 1H), 0.60 - 0.52 (m, 2H), 0.19 - 0.12 (m, 2H); ¹³C NMR (101 MHz, CDCl₃) δ_C 167.6, 143.0, 139.2, 136.2, 136.0, 130.7, 130.1, 128.7, 128.4, 128.4, 128.0, 125.3, 123.1, 121.9, 119.6, 119.2, 118.3, 117.3, 117.2, 112.4, 85.3, 72.8, 66.6, 62.4, 59.6, 48.3, 43.8, 28.9, 23.3, 9.6, 4.2, 3.9; LC-MS m/z [M+H]⁺ C₃₆H₃₅N₂O₅⁺ calc. 575.3, found 574.8.

3-((4bS,8R,8aS,14bR)-7-(cyclopropylmethyl)-1,8a-dihydroxy-5,6,7,8,8a,9,14,14b-octahydro-4,8-methanobenzofuro[2,3-a]pyrido[4,3-b]carbazol-13-yl)propanoic acid (21)



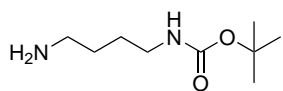
Compound **20** (52 mg, 0.090 mmol, 1 eq.) was dissolved in MeOH (10 mL) and Pd/C (10% Pd on activated carbon, 10 mg) added. The reaction vessel was then purged with N₂ 3 times, then flushed with H₂ 3 times. The reaction was then allowed to stir under an H₂ atmosphere at 60 PSI for 19 h, after which the catalyst was removed by filtration and the catalyst washed with 0.1% TFA in MeOH (20 mL). Pd/C (10% Pd

on activated carbon, 20 mg) was then added to the filtrate and the mixture again subjected to an H₂ atmosphere as before at 60 PSI for 13 h. The catalyst was again removed by filtration, and the solvent removed *in vacuo* to give the product TFA salt as a brown oil (48 mg, 89%).

¹H NMR (401 MHz, DMSO-*d*₆) δ_H 12.15 (s, 1H), 11.38 (s, 1H), 9.28 (s, 1H), 8.96 (s, 1H), 7.18 (s, 1H), 6.96 - 6.86 (m, 2H), 6.68 - 6.55 (m, 1H), 6.52 - 6.39 (m, 1H), 5.66 (s, 1H), 4.10 (s, 1H), 3.59 (s, 2H), 3.13 - 2.57 (m, 8H), 1.93 - 1.75 (m, 1H), 1.69 (s, 1H), 1.26 - 1.05 (m, 2H), 0.94 - 0.82 (m, 1H), 0.75 - 0.57 (m, 2H), 0.53 - 0.37 (m, 2H); LC-MS m/z [M+H]⁺

$C_{29}H_{30}N_2O_5^+$ calc. 486.2, found 486.8.

***N*-Boc-1,4-Diaminobutane (22)**

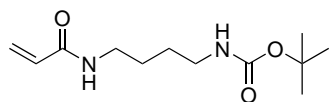


1,4-Diaminobutane (1.0 g, 11.5 mmol, 5 eq.) was dissolved in $CHCl_3$ (20 mL) and cooled to 0 °C. A solution of Boc-anhydride (500 mg, 2.3 mmol, 1 eq.) in $CHCl_3$ (5 mL) was then added dropwise over 5 min.

The resulting mixture was allowed to warm to room temperature and stir for 19 h. The solvent was removed *in vacuo* and the residue redissolved in EtOAc (50 mL), which was washed with half-saturated brine (5×20 mL), dried over Na_2SO_4 and the solvent removed *in vacuo* to give the product as a waxy white solid (349 mg, 81%).

1H NMR (400 MHz, $CDCl_3$) δ_H 4.70 (s, 1H), 3.14 - 3.07 (m, 2H), 2.69 (t, $J = 6.7$ Hz, 2H), 1.54 - 1.43 (m, 4H), 1.42 (s, 9H), 1.29 (s, 2H); ^{13}C NMR (101 MHz, $CDCl_3$) δ_C 156.1, 41.9, 40.5, 31.0, 28.5, 27.6.

***tert*-Butyl (4-acrylamidobutyl)carbamate (23)**

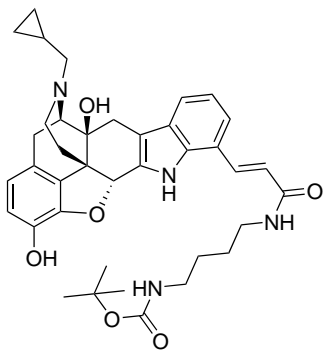


Compound **22** (144 mg, 0.76 mmol, 1 eq.) and TEA (128 μ L, 0.92 mmol, 1.2 eq.) were dissolved in $CHCl_3$ and cooled to 0 °C. A solution of acryloyl chloride (74 μ L, 0.92 mmol, 1.2 eq.) in $CHCl_3$ (2 mL) was added dropwise and the resulting solution allowed to

warm to room temperature and stir for 24 h. $CHCl_3$ (5 mL) was added and the resulting solution washed successively with saturated $NaHCO_3$ (3×10 mL), half-saturated brine (10 mL) and brine (15 mL), then dried over Na_2SO_4 . The solvent was removed *in vacuo* to give a white solid (207 mg, quantitative).

1H NMR (401 MHz, $CDCl_3$) δ_H 6.26 (dd, $J = 17.0, 1.4$ Hz, 1H), 6.10 (dd, $J = 17.0, 10.2$ Hz, 2H), 5.61 (dd, $J = 10.2, 1.3$ Hz, 1H), 4.67 (s, 1H), 3.34 (q, $J = 6.4$ Hz, 2H), 3.13 (dd, $J = 11.8, 5.7$ Hz, 2H), 1.86 (s, 1H), 1.60 - 1.47 (m, 5H), 1.43 (s, 9H); ^{13}C NMR (101 MHz, $CDCl_3$) δ_C 165.8, 131.1, 126.3, 40.2, 39.3, 28.5, 27.9, 26.6.

***tert*-Butyl (4-((*E*)-3-((4*bS*,8*R*,8*aS*,14*bR*)-7-(cyclopropylmethyl)-1,8*a*-dihydroxy-5,6,7,8,8*a*,9,14,14*b*-octahydro-4,8-methanobenzofuro[2,3-*a*]pyrido[4,3-*b*]carbazol-13-yl)acrylamido)butyl)carbamate (24)**

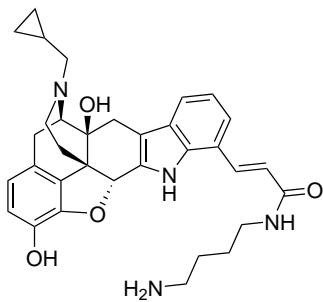


Compound **19** (89 mg, 0.18 mmol, 1 eq.), **23** (87 mg, 0.36 mmol, 2 eq.), TEA (75 μ L, 0.54 mmol, 3 eq.) and PdCl₂(PPh₃)₂ (32 mg, 0.045 mmol, 0.25 eq.) were dissolved in dry DMF (1 mL), purged with N₂ and heated at 90 °C for 24 h. CHCl₃ (20 mL) was then added and the resulting mixture washed successively with 2 M LiCl (3 \times 20 mL), half-saturated brine (20 mL) and brine (20 mL), then dried over Na₂SO₄ and the solvent removed *in vacuo* to give a brown residue.

This was purified by flash chromatography (94:5:1 CHCl₃/MeOH/NH₄OH) to give the product as a light brown solid (96 mg, 81%).

¹H NMR (401 MHz, CDCl₃) δ_H 9.61 (s, 1H), 7.93 (d, *J* = 15.6 Hz, 1H), 7.06 (d, *J* = 6.3 Hz, 1H), 6.94 (d, *J* = 6.6 Hz, 1H), 6.72 (d, *J* = 7.9 Hz, 1H), 6.55 (d, *J* = 8.1 Hz, 1H), 6.44 (d, *J* = 15.7 Hz, 1H), 6.27 - 6.01 (m, 1H), 5.84 (s, 1H), 4.98 (s, 1H), 3.37 (d, *J* = 5.5 Hz, 1H), 3.24 - 3.10 (m, 1H), 3.01 (dd, *J* = 11.6, 5.8 Hz, 1H), 2.89 - 2.53 (m, 7H), 2.48 - 2.20 (m, 4H), 1.83 (d, *J* = 9.1 Hz, 1H), 1.40 (s, 9H), 0.96 - 0.78 (m, 4H), 0.59 - 0.47 (m, 2H), 0.21 - 0.08 (m, 2H); ¹³C NMR (101 MHz, CDCl₃) δ_C 167.9, 156.3, 143.6, 140.1, 137.3, 136.0, 131.0, 129.9, 127.2, 126.3, 124.5, 120.9, 120.2, 119.0, 118.8, 117.1, 111.8, 85.2, 78.9, 73.0, 62.4, 59.6, 48.0, 43.9, 40.1, 39.4, 39.3, 31.8, 28.9, 28.6, 27.1, 26.5, 23.3, 9.5, 4.2, 3.8; LC-MS *m/z* [M+H]⁺ C₃₈H₄₇N₄O₆⁺ calc. 655.3, found 654.8.

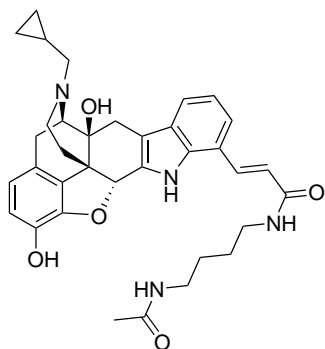
(E)-N-(4-Aminobutyl)-3-((4bS,8R,8aS,14bR)-7-(cyclopropylmethyl)-1,8a-dihydroxy-5,6,7,8,8a,9,14,14b-octahydro-4,8-methanobenzofuro[2,3-a]pyrido[4,3-b]carbazol-13-yl)acrylamide (25)



Compound **24** (96 mg, 0.15 mmol, 1 eq.) was dissolved in CHCl_3 (2 mL) and TFA (1 mL) was added slowly, and the resulting solution allowed to stir at room temperature for 2 h. The solvent was then removed *in vacuo*, water (2 mL) added to the residue and the resulting mixture freeze-dried to give the product a tan solid TFA salt (107 mg, quantitative).

^1H NMR (401 MHz, $\text{DMSO-}d_6$) δ_H 11.82 (s, 1H), 9.30 (s, 1H), 8.98 (s, 1H), 8.20 (t, $J = 5.7$ Hz, 1H), 8.01 (d, $J = 15.6$ Hz, 1H), 7.43 - 7.37 (m, 2H), 7.04 (t, $J = 7.6$ Hz, 1H), 6.75 (d, $J = 15.7$ Hz, 1H), 6.62 (dd, $J = 21.5, 8.1$ Hz, 2H), 6.42 (s, 1H), 5.67 (s, 1H), 4.10 (d, $J = 5.9$ Hz, 1H), 3.48 - 3.34 (m, 2H), 3.30 - 3.22 (m, 3H), 3.18 - 3.10 (m, 2H), 2.99 - 2.92 (m, 2H), 2.86 - 2.80 (m, 2H), 2.75 - 2.71 (m, 1H), 2.62 (dd, $J = 13.2, 4.1$ Hz, 1H), 1.83 (d, $J = 11.1$ Hz, 1H), 1.63 - 1.43 (m, 5H), 1.13 - 1.04 (m, 1H), 0.77 - 0.59 (m, 2H), 0.53 - 0.41 (m, 2H); ^{13}C NMR (101 MHz, $\text{DMSO-}d_6$) δ_C 165.3, 143.2, 140.6, 138.4, 135.6, 134.2, 130.5, 129.1, 127.3, 122.1, 121.5, 119.8, 119.1, 117.8, 108.8, 82.9, 72.1, 56.8, 45.7, 38.6, 38.1, 28.1, 26.2, 24.6; LC-MS m/z $[\text{M}+\text{H}]^+$ $\text{C}_{33}\text{H}_{39}\text{N}_4\text{O}_4^+$ calc. 555.3, found 554.8.

(E)-N-(4-Acetamidobutyl)-3-((4b*S*,8*R*,8a*S*,14b*R*)-7-(cyclopropylmethyl)-1,8a-dihydroxy-5,6,7,8,8a,9,14,14b-octahydro-4,8-methanobenzofuro[2,3-*a*]pyrido[4,3-*b*]carbazol-13-yl)acrylamide (26)

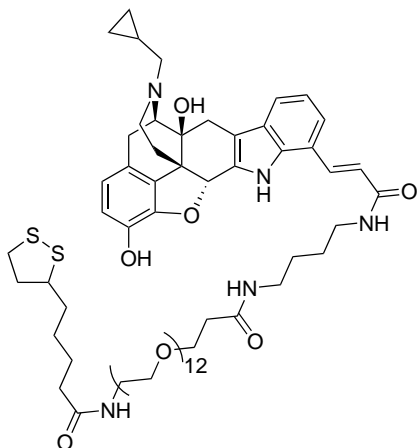


Compound **25** (20 mg, 0.030 mmol, 1 eq.), HCTU (19 mg, 0.045 mmol, 1.5 eq.), acetic acid (2.1 μ L, 0.036 mmol, 1.2 eq.) and TEA (17 μ L, 0.12 mmol, 4 eq.) were dissolved in DMF (300 μ L), purged with N_2 and allowed to stir at room temperature for 23 h. Water (10 mL) was then added and the resulting mixture freeze-dried. The resulting residue was purified by HPLC to give both the product as an off-white solid TFA di-salt (5.2 mg, 21%)

The 3-O acetylated by-product was collected separately, freeze-dried and the remaining residue dissolved in MeOH (1 mL) and 2 M HCl (1 mL) added. The solution was allowed to stir at room temperature for 20 h. Water (10 mL) was then added and the sample freeze-dried to return the product as the hydrochloride salt (9.2 mg, 49%) (total yield 70%).

1H NMR (401 MHz, DMSO- d_6) δ_H 11.82 (s, 1H), 8.97 (s, 1H), 8.17 - 8.13 (m, 1H), 7.99 (dd, $J = 15.6, 4.0$ Hz, 1H), 7.90 - 7.87 (m, 1H), 7.39 (t, $J = 7.9$ Hz, 2H), 7.04 (t, $J = 7.6$ Hz, 1H), 6.76 (dd, $J = 15.6, 4.1$ Hz, 1H), 6.67 - 6.56 (m, 2H), 5.67 (s, 1H), 4.11 (d, $J = 5.3$ Hz, 1H), 3.47 - 3.33 (m, 2H), 3.30 - 3.18 (m, 3H), 3.13 - 2.88 (m, 6H), 2.75 - 2.54 (m, 3H), 1.86 - 1.76 (m, 4H), 1.45 (s, 3H), 1.11 (s, 1H), 0.75 - 0.60 (m, 2H), 0.53 - 0.41 (m, 2H); ESI-TOF HRMS m/z $[M+H]^+$ $C_{35}H_{41}N_4O_5^+$ calc. 597.3071, found 597.3078.

1-(5-(1,2-Dithiolan-3-yl)pentanamido)-N-(4-((E)-3-((4bS,8R,8aS,14bR)-7-(cyclopropylmethyl)-1,8a-dihydroxy-5,6,7,8,8a,9,14,14b-octahydro-4,8-methanobenzofuro[2,3-a]pyrido[4,3-b]carbazol-13-yl)acrylamido)butyl)-3,6,9,12,15,18,21,24,27,30,33,36-dodecaoxanonatriacontan-39-amide (27)



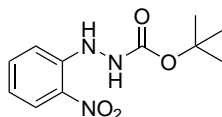
Lipoamido-dPEG®₁₂-acid (22 mg, 0.028 mmol, 1.2 eq.), PyBOP (18 mg, 0.034 mmol, 1.5 eq.), and TEA (13 μ L, 0.090 mmol, 4 eq.) were dissolved in dry DMF (300 μ L) and purged with N₂. The resulting solution was allowed to stir at room temperature for 30 min, before **25** TFA salt (15 mg, 0.022 mmol, 1 eq.) in dry DMF (200 μ L) was added and stirred for 21 h. Water was added and the resulting solution freeze dried. The residue was purified by HPLC, then by reverse phase chromatography (5 - 30% buffer B in A, then flushed

with 50% buffer B in A) to give the product as a solid brown TFA salt (11 mg, 34%).

¹H NMR (401 MHz, DMSO-*d*₆) δ_H 11.83 (s, 1H), 9.22 (s, 1H), 8.94 (s, 1H), 8.08 - 8.06 (m, 1H), 8.00 (d, *J* = 15.8 Hz, 1H), 7.84 (s, 2H), 7.39 (t, *J* = 7.8 Hz, 2H), 7.23 (s, 1H), 7.10 (s, 1H), 7.04 (t, *J* = 7.3 Hz, 1H), 6.98 (s, 1H), 6.73 (d, *J* = 15.8 Hz, 1H), 6.61 (dd, *J* = 18.6, 8.0 Hz, 2H), 6.38 (s, 1H), 5.67 (s, 1H), 4.08 (d, *J* = 5.5 Hz, 1H), 3.51 - 3.48 (m, 53H), 3.41 - 3.36 (m, 1H), 3.28 - 3.05 (m, 4H), 2.99 - 2.88 (m, 2H), 2.33 - 2.28 (m, 3H), 2.06 (t, *J* = 7.3 Hz, 3H), 1.89 - 1.81 (m, 2H), 1.75 (s, 1H), 1.64 (dd, *J* = 12.7, 7.0 Hz, 1H), 1.58 - 1.44 (m, 5H), 1.37 - 1.28 (m, 3H), 1.24 (s, 1H), 1.11 - 1.05 (m, 1H), 0.75 - 0.59 (m, 2H), 0.52 - 0.41 (m, 2H); ESI-TOF HRMS *m/z* [M+Na]⁺ C₆₈H₁₀₃N₅O₁₈S₂Na⁺ calc. 1364.6632, found 1364.6601, [M+2H]²⁺ C₆₈H₁₀₅N₅O₁₈S₂²⁺ calc. 671.8443, found 671.8466.

tert-Butyl 2-(2-nitrophenyl)hydrazine-1-carboxylate (28)

2-Nitrophenylhydrazine (200 mg, 1.3 mmol, 1 eq.) was dissolved in CHCl₃

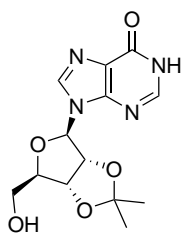


(8 mL) and cooled to 0 °C. Boc-anhydride (342 mg, 1.6 mmol, 1.2 eq.) was

then added dropwise as a solution in CHCl_3 (2 mL). The reaction was then allowed to stir at room temperature for 17 h, after which CHCl_3 was added to the mixture and washed successively with saturated NaHCO_3 (3×10 mL) and half-saturated brine (10 mL). The organic phase was dried over Na_2SO_4 and the solvent removed *in vacuo*. The residue was redissolved in CHCl_3 (20 mL) and washed successively with 0.5 M HCl (3×10 mL) and half-saturated brine (10 mL), then dried over Na_2SO_4 . The solvent was then removed *in vacuo* to give the product as a brown oil (336 mg, quantitative).

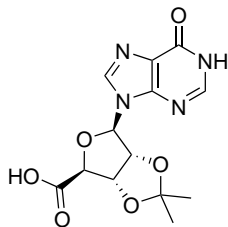
^1H NMR (401 MHz, CDCl_3) δ_{H} 8.92 (s, 1H), 8.17 (dd, $J = 8.5, 1.5$ Hz, 1H), 7.54 - 7.47 (m, 1H), 7.20 (dd, $J = 8.6, 1.0$ Hz, 1H), 6.86 (ddd, $J = 8.4, 7.1, 1.3$ Hz, 1H), 6.43 (s, 1H), 1.52 (s, 9H); ^{13}C NMR (101 MHz, CDCl_3) δ_{C} 155.24, 136.27, 126.54, 118.80, 114.36, 85.33, 82.23, 27.56.

9-((3a*R*,4*R*,6*R*,6a*R*)-6-(Hydroxymethyl)-2,2-dimethyltetrahydrofuro[3,4-*d*][1,3]dioxol-4-yl)-1,9-dihydro-6*H*-purin-6-one (29)



Inosine (1 g, 3.73 mmol, 1 eq.), tosic acid monohydrate (709 mg, 3.73 mmol, 1 eq.) and 2,2-dimethoxypropane (9.3 mL) were suspended in acetone (37.3 mL). The resulting mixture was stirred at room temperature for 1.5 h, after which a fluffy white precipitate formed. NaHCO_3 (313 mg, 3.73 mmol, 1 eq.) in water (7.5 mL) were added to give a clear solution. Following 15 min of stirring, another white precipitate formed. The solvent was then removed *in vacuo*, and the residue recrystallized using the remaining minimal water and dried to give the product as a white, crystalline solid (860 mg, 75%).

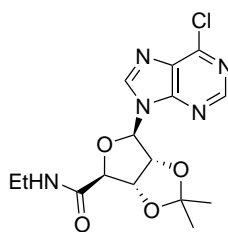
^1H NMR (400 MHz, $\text{DMSO-}d_6$) δ_{H} 12.42 (s, 1H), 8.30 (s, 1H), 8.09 (s, 1H), 6.10 (d, $J = 2.8$ Hz, 1H), 5.26 (dd, $J = 6.1, 2.9$ Hz, 1H), 5.11 (s, 1H), 4.93 (dd, $J = 6.1, 2.5$ Hz, 1H), 4.22 (dd, $J = 7.3, 4.7$ Hz, 1H), 3.54 (d, $J = 4.3$ Hz, 2H), 1.53 (s, 3H), 1.32 (s, 3H); ^{13}C NMR (101 MHz, $\text{DMSO-}d_6$) δ_{C} 156.51, 147.77, 146.03, 138.73, 124.45, 113.08, 89.58, 86.64, 83.80, 81.25, 61.44, 27.01, 25.15; LC-MS m/z $[\text{M}+\text{H}]^+$ $\text{C}_{13}\text{H}_{17}\text{N}_4\text{O}_5^+$ calc. 309, found 309.

(3a*S*,4*S*,6*R*,6a*R*)-2,2-Dimethyl-6-(6-oxo-1,6-dihydro-9*H*-purin-9-yl)tetrahydrofuro[3,4-*d*][1,3]dioxole-4-carboxylic acid (30)

Compound **29** (1.13 g, 3.65 mmol, 1 eq.), BAIB (2.67 g, 8.04 mmol, 2.2 eq.) and TEMPO (114 mg, 0.731 mmol, 0.2 eq.) were dissolved in a 1:1 mixture of water/MeCN (20 mL). The resulting solution was allowed to stir at room temperature in the dark for 4 h. The solvent was then removed *in vacuo* and the resulting solid triturated with acetone (70 mL total), followed by Et₂O (50 mL total). The remaining solid was allowed to dry to give the

product as a white solid (930 mg, 79%).

¹H NMR (400 MHz, DMSO-*d*₆) δ_H 12.91 (s, 1H), 12.37 (s, 1H), 8.20 (s, 1H), 8.01 (s, 1H), 6.32 (s, 1H), 5.47 (dd, *J* = 6.0, 1.6 Hz, 1H), 5.42 (d, *J* = 6.0 Hz, 1H), 4.71 (d, *J* = 1.6 Hz, 1H), 1.51 (s, 3H), 1.34 (s, 3H); ¹³C NMR (101 MHz, DMSO-*d*₆) δ_C 170.68, 156.50, 147.97, 139.72, 124.27, 112.70, 89.67, 85.36, 83.67, 83.53, 26.41, 24.85; LC-MS *m/z* [M+H]⁺ C₁₃H₁₅N₄O₆⁺ calc. 323, found 323.

(3a*S*,4*S*,6*R*,6a*R*)-6-(6-Chloro-9*H*-purin-9-yl)-*N,N*-diethyl-2,2-dimethyltetrahydrofuro[3,4-*d*][1,3]dioxole-4-carboxamide (31)

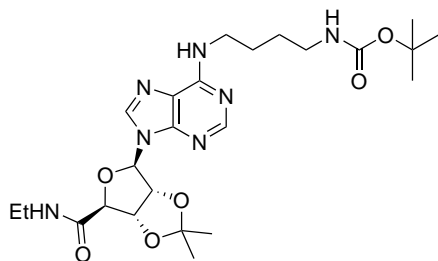
Compound **30** (756 mg, 2.35 mmol, 1 eq.), SOCl₂ (851 μ L, 11.7 mmol, 5 eq.) and anhydrous DMF (452 μ L, 5.86 mmol, 2.5 eq.) were dissolved in CHCl₃ under N₂ and refluxed for 5 h, after which the solvent was removed *in vacuo* to give a grown solid. The resulting residue was redissolved in anhydrous THF (20 mL) at 5 °C under N₂ and EtNH₂ (2 M solution in THF, 2.93 mL, 5.86 mmol, 2.5 eq.) was added dropwise and allowed to stir

for 15 min. The solvent was then removed *in vacuo* and the residue redissolved in DCM (25 mL) and washed successively with half-saturated brine (3 \times 20 mL) followed by brine (25 mL). The organic phase was dried over Na₂SO₄ and the solvent removed *in vacuo*. The resulting brown residue was purified by flash chromatography (97:3 DCM/MeOH) to give the product

as a white foam (730 mg, 85%).

^1H NMR (400 MHz, CDCl_3) δ_{H} 8.74 (s, 1H), 8.24 (s, 1H), 6.21 (d, $J = 2.3$ Hz, 2H), 5.52 - 5.50 (m, 1H), 5.43 (dd, $J = 6.2, 2.2$ Hz, 1H), 4.72 (d, $J = 1.8$ Hz, 1H), 3.08 - 2.97 (m, 2H), 1.62 (s, 3H), 1.39 (s, 3H), 0.76 (t, $J = 7.3$ Hz, 3H); ^{13}C NMR (101 MHz, CDCl_3) δ_{C} 168.19, 152.32, 152.10, 151.01, 132.42, 114.77, 92.13, 86.83, 83.54, 83.07, 34.01, 27.04, 25.19, 14.32.

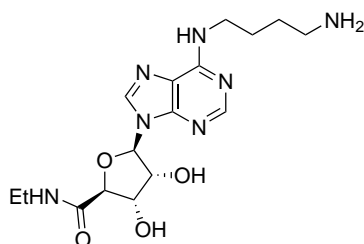
***tert*-Butyl (4-((9-((3*aR*,4*R*,6*S*,6*aS*)-6-(diethylcarbamoyl)-2,2-dimethyltetrahydrofuro[3,4-*d*][1,3]dioxol-4-yl)-9*H*-purin-6-yl)amino)butyl)carbamate (32)**



Compound **31** (300 mg, 0.816 mmol, 1 eq.), **22** (461 mg, 2.45 mmol, 3 eq.) and TEA (171 μL , 1.22 mmol, 1.5 eq.) were dissolved in EtOH and refluxed for 18 h. The solvent was then removed *in vacuo* and the residue dissolved in hot EtOAc and allowed to cool back to room temperature. The resulting precipitate was filtered and the filtrate purified by flash chromatography (99:1 EtOAc/TEA). The resulting residue was redissolved in CHCl_3 and the solvent removed *in vacuo* to give the product as a clear foam (367 mg, 87%).

^1H NMR (400 MHz, CDCl_3) δ_{H} 8.31 (s, 1H), 7.81 (s, 1H), 7.09 (s, 1H), 6.04 (s, 1H), 5.98 (s, 1H), 5.37 - 5.32 (m, 2H), 4.76 (s, 1H), 4.69 (s, 1H), 3.13 (ddd, $J = 17.8, 14.7, 6.7$ Hz, 4H), 1.77 - 1.69 (m, 2H), 1.64 - 1.55 (m, 5H), 1.43 (s, 9H), 1.37 (s, 3H), 0.90 (t, $J = 7.3$ Hz, 3H); ^{13}C NMR (101 MHz, CDCl_3) δ_{C} 168.68, 156.17, 114.72, 92.11, 85.92, 83.72, 82.69, 79.32, 77.36, 34.07, 28.57, 27.25, 25.29, 14.46; LC-MS m/z $[\text{M}+\text{H}]^+$ $\text{C}_{24}\text{H}_{38}\text{N}_7\text{O}_6^+$ calc. 520, found 520.

(2*S*,3*S*,4*R*,5*R*)-5-(6-((4-Aminobutyl)amino)-9*H*-purin-9-yl)-*N,N*-diethyl-3,4-dihydroxytetrahydrofuran-2-carboxamide (33)

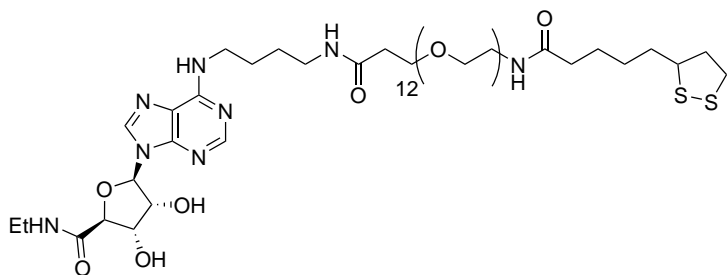


Compound **36** was dissolved in MeOH (3 mL) and cooled to 0 $^{\circ}\text{C}$. TFA (1 mL) was then added dropwise and allowed to warm to room temperature and stirred for 4.5 h. Additional TFA (2 mL) was added and the reaction allowed to stir for 17 h. MeOH (1 mL)

and TFA (2 mL) were added back to the solution and continued to stir for 4 h. The solvent was then removed *in vacuo* and the resulting residue dissolved in a 1:9 MeOH/TFA mixture (5 mL). The resulting mixture was allowed to stir for 1 h, after which the solvent was again removed *in vacuo*, water was added and the mixture freeze-dried to give the tri-TFA salt as a brown oil/foam (473 mg, 96%).

^1H NMR (400 MHz, DMSO- d_6) δ_H 8.77 (s, 1H), 8.66 (s, 1H), 8.52 (s, 1H), 8.49 (s, 1H), 8.35 (s, 1H), 7.72 (s, 3H), 6.00 (d, $J = 7.0$ Hz, 1H), 4.60 (dd, $J = 7.1, 4.6$ Hz, 1H), 4.34 (s, 1H), 4.16 (d, $J = 3.0$ Hz, 1H), 3.53 (s, 2H), 3.26 - 3.15 (m, 2H), 2.82 (dd, $J = 12.6, 6.4$ Hz, 2H), 1.73 - 1.55 (m, 4H), 1.07 (t, $J = 7.2$ Hz, 3H); ^{13}C NMR (101 MHz, DMSO- d_6) δ_C 169.17, 158.93, 158.57, 158.21, 157.84, 140.80, 120.02, 117.12, 114.22, 87.84, 84.56, 73.14, 33.35, 25.80, 24.44, 14.68; LC-MS m/z $[\text{M}+\text{H}]^+$ $\text{C}_{16}\text{H}_{26}\text{N}_7\text{O}_4^+$ calc. 380, found 380.

(2S,3S,4R,5R)-5-(6-((50-(1,2-Dithiolan-3-yl)-6,46-dioxo-9,12,15,18,21,24,27,30,33,36,39,42-dodecaoxa-5,45-diazapentacontyl)amino)-9H-purin-9-yl)-N-ethyl-3,4-dihydroxytetrahydrofuran-2-carboxamide (34)



Lipoamido-dPEG $^{\text{®}}$ ₁₂-acid (100 mg/mL solution in DMF, 272 μL , 0.0338 mmol, 1 eq.), EDC $\cdot\text{HCl}$ (9.7 mg, 0.0507 mmol, 1.5 eq.), HOAt (6.9 mg, 0.0507 mmol, 1.5 eq.) and TEA (30 μL) were dissolved in DMF (0.5 mL) under N_2

and allowed to stir at room temperature for 1 h. Compound **37** (29.2 mg, 0.0405 mmol, 1.2 eq.) was then added as a solution in DMF (0.5 mL) and the resulting mixture was allowed to stir at room temperature for 20 h. The solvent was then removed *in vacuo* and purified by reverse phase chromatography (6 - 30% buffer B in buffer A, 2% increase per column volume, then flushed with 1:1 buffer B in buffer A). The relevant fractions were freeze dried to give the product as a clear oil (31 mg, 71%).

^1H NMR (400 MHz, DMSO- d_6) δ_H 8.80 (s, 1H), 8.49 (s, 1H), 8.33 (s, 1H), 7.82 (dd, $J = 10.3, 5.2$ Hz, 2H), 5.98 (d, $J = 7.4$ Hz, 1H), 4.60 (dd, $J = 7.2, 4.7$ Hz, 2H), 4.33 (d, $J = 1.3$ Hz, 1H), 4.15 (dd, $J = 4.3, 1.3$ Hz, 1H), 3.67 (s, 1H), 3.63 - 3.55 (m, 4H), 3.50 (s, 37H), 3.48 (s, 5H), 3.46 (s, 4H), 3.39 (t, $J = 5.9$ Hz, 2H), 3.32 (s, 1H), 3.25 - 3.03 (m, 7H), 2.68 - 2.66 (m, 1H), 2.45 - 2.36 (m, 1H), 2.34 - 2.32 (m, 1H), 2.28 (t, $J = 6.4$ Hz, 2H), 2.06 (t, $J = 7.3$ Hz, 2H), 1.85 (dq, $J = 13.5, 6.7$ Hz, 1H), 1.71 - 1.40 (m, 8H), 1.33 (dt, $J = 14.1, 7.2$ Hz, 2H), 1.08 (t, $J = 7.2$ Hz, 2H); ESI-TOF HRMS m/z $[\text{M}+\text{H}]^+$ $\text{C}_{51}\text{H}_{91}\text{N}_8\text{O}_{18}\text{S}_2^+$ calc. 1167.5887, found 1167.5894, $[\text{M}+\text{Na}]^+$ $\text{C}_{51}\text{H}_{90}\text{N}_8\text{O}_{18}\text{S}_2\text{Na}^+$ calc. 1189.5707, found 1189.5689.

4.9.1 2 Step Method for Coating Gold Nanorods

1 mL aliquots of AuNR@CTAB stored in a 10 mM CTAB solution were dispensed into 1.5 mL microcentrifuge tubes (multiple samples can be prepared simultaneously in this manner). The aliquots are placed in a microcentrifuge and spun at 10 kRPM for 10 min. 900 μL of the supernatant was then removed and replaced with 900 μL of a PSS solution (0.15% w/v in water). The pellet was then briefly resuspended using a vortex mixer, then allowed to slowly mix by attaching it to a slowly rotating motor for 30 min. The aliquots were then allowed to sit still for 30 min at room temperature. The aliquots were spun down as before and washed twice more with the PSS solution using the same procedure. The aliquots were then spun down as before, 900 μL of the supernatant removed and 900 μL of the coating solution applied to the pellet. This solution is composed of one or more of the following elements:

1. 1 mM aqueous solution of **4** (ZW) at pH 8-9.
2. 1 mM solution of **6** (MorPEG) in 10% v/v DMSO in water.
3. 1 mM solution of **27** (NaltPEG) in 10% v/v DMSO in water.
4. 1 mM solution of **34** (NECA-PEG) in 10% v/v DMSO in water.

The coating solution must consist of a minimum of 90% of the ZW solution for stability, otherwise aggregation of the sample is observed. The various other components may be titrated

in as a single targeting ligand or as a mixture of ligands. Following addition of the solution(s), the pellet is briefly resuspended using a vortex mixer, then allowed to slowly mix by attaching to a slowly rotating motor as before for 30 min. The mixture is then allowed to sit at room temperature for a minimum of 16 h, after which the aliquots are again spun down and the supernatant removed as before. 900 μL of Milli-Q water is then added back and the pellet resuspended using a vortex mixer. The resulting colloid is then further purified by dialysis using a dialysis membrane (MWCO 100 kDA) over 2 days, changing out the dialysate several times (if samples being prepared are the same, they may be combined at this point). The final samples can then be recovered from the dialysis bag and stored at 4 °C.

Using this method, the following AuNR conjugates were produced:

- AuNR@ZW
- AuNR@ZW(MorPEG 5%)
- AuNR@ZW(MorPEG 10%)
- AuNR@ZW(MorPEG 20%)
- AuNR@ZW(MorPEG 30%)
- AuNR@ZW(NaltPEG 5%)
- AuNR@ZW(NaltPEG 10%)
- AuNR@ZW(MorPEG 5%, NaltPEG 5%)
- AuNR@ZW(NEGA-PEG 5%)
- AuNR@ZW(NEGA-PEG 10%)

References

- (1) Nikoobakht, B., and El-Sayed, M. A., (2003). Preparation and growth mechanism of gold nanorods (NRs) using seed-mediated growth method. *Chem. Mater.* *15*, 1957–1962.
- (2) Jana, N. R., Gearheart, L., and Murphy, C. J., (2001). Seed-mediated growth approach for shape-controlled synthesis of spheroidal and rod-like gold nanoparticles using a surfactant template. *Adv. Mater.* *13*, 1389–1393.
- (3) Jana, N. R., Gearheart, L., and Murphy, C. J., (2001). Wet chemical synthesis of high aspect ratio cylindrical gold nanorods. *J. Phys. Chem. B* *105*, 4065–4067.
- (4) Ahmed, M., and Narain, R., (2010). Rapid synthesis of gold nanorods using a one-step photochemical strategy. *Langmuir* *26*, 18392–18399.
- (5) Schulz, F., Homolka, T., Bastús, N. G., Puentes, V. F., Weller, H., and Vossmeier, T., (2014). Little adjustments significantly improve the turkevich synthesis of gold nanoparticles. *Langmuir* *30*, 10779–10784.
- (6) Miranda, O. R., and Ahmadi, T. S., (2005). Effects of intensity and energy of CW UV light on the growth of gold nanorods. *J. Phys. Chem. B* *109*, 15724–15734.
- (7) García, K. P., Zarschler, K., Barbaro, L., Barreto, J. A., O'Malley, W., Spiccia, L., Stephan, H., and Graham, B., (2014). Zwitterionic-coated "stealth" nanoparticles for biomedical applications: recent advances in countering biomolecular corona formation and uptake by the mononuclear phagocyte system. *Small* *10*, 2516–29.
- (8) Pombo-García, K., Rühl, C. L., Lam, R., Barreto, J. A., Ang, C. S., Scammells, P. J., Comba, P., Spiccia, L., Graham, B., Joshi, T., and Stephan, H., (2017). Zwitterionic modification of ultrasmall iron oxide nanoparticles for reduced protein corona formation. *Chempluschem* *82*, 638–646.
- (9) Harjani, J. R., Frišćić, T., MacGillivray, L. R., and Singer, R. D., (2008). Removal of metal ions from aqueous solutions using chelating task-specific ionic liquids. *Dalt. Trans.* 4595–4601.

- (10) Daniels, D. J., Lenard, N. R., Etienne, C. L., Law, P.-Y., Roerig, S. C., and Portoghese, P. S., (2005). Opioid-induced tolerance and dependence in mice is modulated by the distance between pharmacophores in a bivalent ligand series. *Proc. Natl. Acad. Sci. U. S. A.* *102*, 19208–19213.
- (11) Portoghese, P. S., Nelson, W. L., and Takemoris, A. E., (1992). δ Opioid antagonist activity and binding studies of regioisomeric isothiocyanate derivatives of naltrindole: evidence for δ receptor subtypes. *J. Med. Chem.* *35*, 4086–4091.
- (12) Yekkirala, A. S., Banks, M. L., Lunzer, M. M., Negus, S. S., Rice, K. C., and Portoghese, P. S., (2012). Clinically employed opioid analgesics produce antinociception via μ - δ opioid receptor heteromers in Rhesus monkeys. *ACS Chem. Neurosci.* *3*, 720–727.
- (13) Aceto, M. D., Harris, L. S., Negus, S. S., Banks, M. L., Hughes, L. D., Akgün, E., and Portoghese, P. S., (2012). MDAN-21: A bivalent opioid ligand containing mu-agonist and delta-antagonist pharmacophores and its effects in rhesus monkeys. *Int. J. Med. Chem.* *2012*, 1–6.
- (14) Sakami, S., Maeda, M., Kawai, K., Aoki, T., Kawamura, K., Fujii, H., Hasebe, K., Nakajima, M., Endo, T., Ueno, S., Ito, T., Kamei, J., and Nagase, H., (2008). Structure - antitussive activity relationships of naltrindole derivatives. Identification of novel and potent antitussive agents. *J. Med. Chem.* *51*, 4404–4411.
- (15) Tavakol, H., Esfandyari, M., Taheri, S., and Heydari, A., (2011). Investigation of structure, vibrational and NMR spectra of oxycodone and naltrexone: a combined experimental and theoretical study. *Spectrochim. Acta - Part A Mol. Biomol. Spectrosc.* *79*, 574–582.
- (16) Meng, X. C., Cheng, H. Y., Fujita, S., Yu, Y. C., Zhao, F. Y., and Arai, M., (2011). An effective medium of H₂O and low-pressure CO₂ for the selective hydrogenation of aromatic nitro compounds to anilines. *Green Chem.* *13*, 570–572.

-
- (17) Carolan, C. G., Dillon, G. P., Khan, D., Ryder, S. A., Gaynor, J. M., Reidy, S., Marquez, J. F., Jones, M., Holland, V., and Gilmer, J. F., (2010). Isosorbide-2-benzyl carbamate-5-salicylate, a peripheral anionic site binding subnanomolar selective butyrylcholinesterase inhibitor. *J. Med. Chem.* *53*, 1190–1199.
- (18) Cheng, H., Meng, X., Yu, Y., and Zhao, F., (2013). The effect of water on the hydrogenation of o-chloronitrobenzene in ethanol, n-heptane and compressed carbon dioxide. *Appl. Catal. A Gen.* *455*, 8–15.
- (19) Trawczyński, A., Telega, M., and Wróbel, Z., (2015). Expedient Synthesis of 6-Acylindolo[1,2-a]quinoxalines. *Synlett* *26*, 1352–1356.
- (20) Łukasik, E., and Wróbel, Z., (2014). 2-(Arylamino)aryliminophosphoranes as easily available and convenient starting materials in the synthesis of 1,2,3-benzotriazoles. *Synlett* *25*, 1987–1990.
- (21) Adkins, H., and Billica, H. R., (1948). The preparation of Raney Nickel catalysts and their use under conditions comparable with those for platinum and palladium catalysts. *J. Am. Chem. Soc.* *70*, 695–698.
- (22) Calderazzo, F., Carmona, D., Catellani, M., Brintzinger, H., Clerici, M. G., Dwyer, C., Fink, G., Fraile, J., Haynes, A., Howard, P., Morris, G., Oro, L. A., Ricci, M., Strukul, G., and Sunley, G., *Metal-catalysis in industrial organic processes*; Chiusoli, G. P., and Maitlis, P. M., Eds.; The Royal Society of Chemistry: 2006, pp 001–290.
- (23) Tulchinsky, Y., Iron, M. A., Botoshansky, M., and Gandelman, M., (2011). Nitrenium ions as ligands for transition metals. *Nat. Chem.* *3*, 525–531.
- (24) Tulchinsky, Y., Kozuch, S., Saha, P., Mauda, A., Nisnevich, G., Botoshansky, M., Shimon, L. J., and Gandelman, M., (2015). Coordination chemistry of N-heterocyclic nitrenium-based ligands. *Chem. - A Eur. J.* *21*, 7099–7110.
- (25) Mehtala, J. G., Zemlyanov, D. Y., Max, J. P., Kadasala, N., Zhao, S., and Wei, A., (2014). Citrate-stabilized gold nanorods. *Langmuir* *30*, 13727–13730.

- (26) Tatini, F., Landini, I., Scaletti, F., Massai, L., Centi, S., Ratto, F., Nobili, S., Romano, G., Fusi, F., Messori, L., Mini, E., and Pini, R., (2014). Size dependent biological profiles of PEGylated gold nanorods. *J. Mater. Chem. B* 2, 6072–6080.
- (27) Kinnear, C., Dietsch, H., Clift, M. J. D., Endes, C., Rothen-Rutishauser, B., and Petri-Fink, A., (2013). Gold nanorods: controlling their surface chemistry and complete detoxification by a two-step place exchange. *Angew. Chem. Int. Ed. Engl.* 52, 1934–1938.
- (28) Thierry, B., Ng, J., Krieg, T., and Griesser, H. J., (2009). A robust procedure for the functionalization of gold nanorods and noble metal nanoparticles. *Chem. Commun.* 1, 1724–1726.
- (29) Bogliotti, N., Oberleitner, B., Di-Cicco, A., Schmidt, F., Florent, J.-C., and Semetey, V., (2011). Optimizing the formation of biocompatible gold nanorods for cancer research: functionalization, stabilization and purification. *J. Colloid Interface Sci.* 357, 75–81.
- (30) Leonov, A. P., Zheng, J., Clogston, J. D., Stern, S. T., Patri, A. K., and Wei, A., (2008). Detoxification of gold nanorods by treatment with polystyrenesulfonate. *ACS Nano*, 2481–2488.
- (31) Herold, B. C., Bourne, N., Marcellino, D., Kirkpatrick, R., Strauss, D. M., Zaneveld, L. J. D., Waller, D. P., Anderson, R. A., Chany, C. J., Barham, B. J., Stanberry, L. R., and Cooper, M. D., (2000). Poly (sodium 4-styrene sulfonate): an effective candidate topical antimicrobial for the prevention of sexually transmitted diseases. *J. Infect. Dis.* 181, 770–773.
- (32) Matthews, J. R., Payne, C. M., and Hafner, J. H., (2015). Analysis of phospholipid bilayers on gold nanorods by plasmon resonance sensing and surface-enhanced Raman scattering. *Langmuir* 31, 9893–9900.
- (33) Stoddart, L. A., Vernall, A. J., Briddon, S. J., Kellam, B., and Hill, S. J., (2015). Direct visualisation of internalization of the adenosine A₃ receptor and localization with arrestin3 using a fluorescent agonist. *Neuropharmacol.* 98, 68–77.

-
- (34) Vernall, A. J., Stoddart, L. A., Briddon, S. J., Ng, H. W., Laughton, C. A., Doughty, S. W., Hill, S. J., and Kellam, B., (2013). Conversion of a non-selective adenosine receptor antagonist into A3-selective high affinity fluorescent probes using peptide-based linkers. *Org. Biomol. Chem.* *11*, 5673–5682.
- (35) Middleton, R. J., Briddon, S. J., Cordeaux, Y., Yates, A. S., Dale, L., George, M. W., Baker, J. G., Hill, S. J., and Kellam, B., (2007). New fluorescent adenosine A₁-receptor agonists that allow quantification of ligand - receptor interactions in microdomains of single living cells. *J. Med. Chem.* *50*, 782–793.
- (36) Baker, J. G., Hall, I. P., and Hill, S. J., (2003). Pharmacology and direct visualisation of BODIPY-TMR-CGP: a long-acting fluorescent β_2 -adrenoceptor agonist. *Br. J. Pharmacol.* *139*, 232–242.
- (37) Baker, J. G., Middleton, R., Adams, L., May, L. T., Briddon, S. J., Kellam, B., and Hill, S. J., (2010). Influence of fluorophore and linker composition on the pharmacology of fluorescent adenosine A₁ receptor ligands: themed section: imaging in pharmacology research paper. *Br. J. Pharmacol.* *159*, 772–786.
- (38) Vernall, A. J., Stoddart, L. A., Briddon, S. J., Hill, S. J., and Kellam, B., (2012). Highly potent and selective fluorescent antagonists of the human adenosine A3 receptor based on the 1,2,4-triazolo[4,3-a]quinoxalin-1-one scaffold. *J. Med. Chem.* *55*, 1771–1782.
- (39) Briddon, S. J., Middleton, R. J., Cordeaux, Y., Flavin, F. M., Weinstein, J. A., George, M. W., Kellam, B., and Hill, S. J., (2004). Quantitative analysis of the formation and diffusion of A1-adenosine receptor-antagonist complexes in single living cells. *Proc. Natl. Acad. Sci. U. S. A.* *101*, 4673–8.
- (40) Stoddart, L. A., Vernall, A. J., Denman, J. L., Briddon, S. J., Kellam, B., and Hill, S. J., (2012). Fragment screening at adenosine-A3 receptors in living cells using a fluorescence-based binding assay. *Chem. Biol.* *19*, 1105–1115.
- (41) Gottlieb, H. E., Kotlyar, V., and Nudelman, A., (1997). NMR chemical shifts of common laboratory solvents as trace impurities. *J. Org. Chem.* *62*, 7512–7515.
-

5 Alternative Catalysts for Non-Classical Polonovski

***N*-Demethylation of Alkaloids**

5.1 *N*-Demethylation of Alkaloids, a History

N-Demethylation of alkaloids has been a historically important reaction. Many clinically used drugs have been derived from naturally occurring alkaloids, and even today, drug discovery projects continue to be based on this class of compounds. In nature, we find that many alkaloids contain an *N*-methyl moiety, such as in atropine, morphine, nicotine and physostigmine to name a few. Replacement of this group has typically been done to alter the pharmacological properties of the naturally occurring compound to suit the needs of the disease state of interest.

Due to this, various reactions have been developed to enable removal of the *N*-methyl group in order to install alternative alkyl groups. The von Braun reaction enables removal of the *N*-methyl group by first reacting the alkaloid with cyanogen bromide. This displaces the methyl group and installs an amino-nitrile group, which can be cleaved under acidic conditions with varying degrees of success. This reaction is problematic due to the use of cyanogen bromide, an extremely toxic substance that necessitates the use of large amounts of personal protective equipment for handling. Therefore, use on an industrial scale is unfavorable.

The use of chloroformates for the *N*-demethylation of opioids was described by Portoghesi's group in the 70's.¹ Briefly, the opiate alkaloids morphine and codeine were reacted with various chloroformates to give the corresponding carbamate, displacing the *N*-methyl group. This carbamate could then be removed via addition of strong base to return the *N*-nor product. As noted by the authors, fairly harsh conditions were required for cleaving the carbamate, utilizing a 50% w/v solution of potassium hydroxide and refluxing under an inert atmosphere for prolonged periods to return the *N*-nor product. Although other chloroformate reagents have been found that require relatively milder cleavage conditions, these tend to be more expensive, and therefore may be cost-prohibitive in an industrial setting where large quantities of reagent are required. Furthermore, these harsh conditions tend not to be orthogonal to commonly used functional groups in medicinal chemistry, such as esters and amides, potentially limiting its use.

The Polonovski reaction operates via a slightly different mechanism, requiring the use of

the *N*-oxide rather than the simple tertiary amine.² Oxidation to the *N*-oxide can be achieved via various methods, such as using hydrogen peroxide or via the use of organic oxidants such as *m*CPBA.³ This can then be treated with an activating agent such as an acid anhydride to give the corresponding amide, again displacing the *N*-methyl moiety. This amide can then be cleaved under basic conditions similar to other amide cleaves. Again, this reaction suffers from the difficulty in removal of the amide.

More recently, a variation of the Polonovski was described in which ferrous sulfate was used as the activating agent in place of an acid anhydride. This "non-classical" Polonovski reaction enables direct conversion of the alkaloid *N*-oxide directly to the corresponding *N*-nor compound. This was first described by Mary *et al.* using galantamine,⁴ and has since been further explored using other alkaloids and iron species.⁵⁻¹⁵ Generally, iron(0) species tend to work well and can be improved by addition of ferric chloride as a co-catalyst. Additionally, chloroform generally works best as the solvent, with other solvents resulting in sub-optimal yields and increased reaction times.¹¹ Furthermore, use of the *N*-oxide HCl salt is important, as counterion substitution reduces yield.⁶

The non-classical Polonovski is thought to work via a radical oxidative mechanism.¹⁶ Briefly, radical oxidation of the amine via the iron species gives an *N*-centered radical cation, upon which the radical is transferred to the methyl group, losing a proton to give a neutral species. Reduction of the radical gives the methyleneiminium species, which returns the *N*-nor product upon addition of water to cleave methylene group. This mechanism has been proposed for the iron(II) species, which can oxidize to iron(III) and be reduced back to the active catalyst through the catalytic cycle. A competing reaction returns the *N*-methyl compound due to radical oxidation of iron(II) to iron(III) via the *N*-centered radical cation. Therefore, reaction conditions need to favor the radical transfer process over the competing radical oxidation process in order to be efficient. Although shown to be successful as a catalyst for this reaction, the exact mechanism of iron(0) catalysed *N*-demethylation remains to be elucidated. Formation of iron(I) generally only occurs under specific conditions, usually as part of an organo-metallic complex and thus acquiring a formal charge, but is not known to exist as a lone species. Hence,

the catalytic redox cycle between iron(0) and iron(I) is unlikely. Whatever the mechanism, the *N*-demethylation is still achieved using elemental iron.

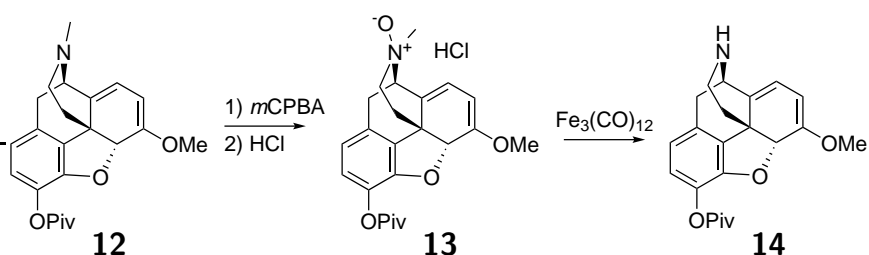
5.2 Green Chemistry, Starting with Solvents

Green chemistry has become an increasingly important area of research. Environmental concerns, the depleting levels of oil reserves and increasing health concerns have all become larger issues, prompting investigation into more sustainable and environmentally friendly methods of performing chemistry. This is particularly true in the pharmaceutical industry, where a significant number of reactions are required to produce an active pharmaceutical ingredient and therefore involves a variety of starting materials and solvents to facilitate these reactions. Typically, solvent use constitutes 80 - 90% of the non-aqueous mass used in the manufacture of active pharmaceuticals, and around 75 - 80% of the environmental impacts of the process.¹⁷ Hence, reducing or finding alternatives to solvents remains an important method of reducing toxic waste.

GSK has recently discussed this topic in detail, and have published a solvent selection guide in order to assist in the decision making process of synthesis.¹⁷ One of the key factors was the use of greener solvent alternatives during the discovery process in order to facilitate easier optimization of synthesis on the industrial scale, as solvent substitution tends to be a difficult step. Furthermore, green solvents are more easily recovered, therefore reducing waste solvent in the overall process. Therefore, initial reaction development should ideally be done using greener solvents to reduce the scale-up optimization time-frame. In addition to exploring new catalysts for the *N*-demethylation of alkaloids, we were interested in exploring their suitability in greener solvents in order to demonstrate the utility of this reaction under greener conditions. For this purpose, ester and alcohol solvents such as ethyl acetate and isopropanol were chosen, as they are considerably less toxic and more easily recovered compared to the previously used chloroform.

5.3 $\text{Fe}_3(\text{CO})_{12}$ as a Solution-Phase Catalyst for *N*-Demethylations, Paper Context

This side project originated during the synthesis of naltrindole. It was found that **13** could not be *N*-demethylated in high yield using the previously established methods.¹¹ The Fe(0) powder used was magnetic and tended to stick to the stir bar used, rather than suspend homogeneously throughout the sample. This was hypothesized to have limited exposure of the catalyst to the bulk solvent and hence the dissolved substrate. In addition, the pivaloyl group used as a protecting group for the C-3 phenol may have also hindered the interaction between the substrate and catalyst. As a result, it was hypothesized that a solution-phase Fe(0) species might be able to better catalyze the reaction, allowing it to proceed.



Scheme 13. Initial discovery of *N*-demethylation of opioid alkaloids using $\text{Fe}_3(\text{CO})_{12}$. The procedure follows the non-classical Polonovski reaction, where first the N-oxide is generated, after which the activating iron species is added, returning the N-nor compound with a repeatable yield of 54% over 2 steps.

As previously mentioned, the iron carbonyl complex triiron dodecacarbonyl had been purchased in an attempt to selectively reduce an ester to an ether, as part of the synthesis of the model morphine congeners (Chapter 3.2.1). Using just 5 mol% of this organo carbonyl complex, it was found that the reaction proceeded to completion within 30 min with decent, repeatable yields (Scheme 13). This prompted the investigation of triiron dodecacarbonyl as a potentially viable catalyst for the *N*-demethylation of alkaloids. The following work was conducted to both investigate its catalytic potential, as well as to explore alternative non-halogenated solvents for this reaction.

5.4 Utility of Iron Nanoparticles and a Solution-Phase Iron Species for the *N*-Demethylation of Alkaloids (Paper)

Jon Kyle Awalt ‡^a, Raymond Lam ‡^{b,c}, Barrie Kellam ^c, Bim Graham ^b, Peter J. Scammells ^{*b} and Robert D. Singer ^{*a}

‡ These authors contributed equally to this work.

^a Atlantic Centre for Green Chemistry, Department of Chemistry, Saint Mary's University, Halifax, Canada B3H 3C3. Email: Robert.Singer@smu.ca

^b Medicinal Chemistry, Monash Institute of Pharmaceutical Sciences, Monash University, Parkville, Victoria 3052, Australia. Email:Peter.Scammells@monash.edu

^c School of Pharmacy, Centre for Biomolecular Sciences, University of Nottingham, Nottingham NG7 2RD, U.K.

This work was conducted in collaboration with Jon Kyle Awalt of Saint Mary's University, Department of Chemistry. Kyle performed all the experiments with the nanoscale zero-valent iron, as well as the LC-MS based reaction rate studies.



Green Chemistry

PAPER

View Article Online
View Journal

Cite this: DOI: 10.1039/c7gc00436b

Utility of iron nanoparticles and a solution-phase iron species for the *N*-demethylation of alkaloids†Jon Kyle Awalt,‡^a Raymond Lam, ‡^{b,c} Barrie Kellam,^c Bim Graham,^b Peter J. Scammells *^b and Robert D. Singer *^aReceived 8th February 2017,
Accepted 5th May 2017

DOI: 10.1039/c7gc00436b

rsc.li/greenchem

The *N*-demethylation of selected *N*-methylalkaloids using a modified Polonovski reaction can be accomplished using a novel green methodology employing nanoscale zero-valent iron, nZVI, in isopropanol. Use of nZVI promotes a much faster conversion to *N*-demethylated products due to much higher surface area on the metal surface as shown by SEM analysis. Rates of conversion can be further enhanced using catalytic quantities of the solubilised iron(0) species triiron dodecacarbonyl, Fe₃(CO)₁₂.

Introduction

The opiate alkaloids morphine and codeine, which are extracted from the opium poppy, *Papaver somniferum*, are common analgesics that have been used for thousands of years for the treatment and control of pain.¹ In addition to being used clinically as therapeutic agents in their own right, they can be used as starting materials in the production of semi-synthetic opioid pharmaceuticals, such as naltrexone, naloxone and buprenorphine.² These particular opioids are useful as therapeutic agents for the treatment of opiate or alcohol dependence, opiate overdose and in pain management. Specifically, naloxone hydrochloride is used to reverse the acute symptoms of opioid overdose and studies have found it to be a cost-effective strategy.³ The rate of drug overdose deaths increased by 140% between the years 2000 and 2014, an increase driven by opioid overdose and, since 2013, in large part due to synthetic opioids including fentanyl.⁴ A key feature in the synthesis of semi-synthetic opioid pharmaceuticals is the loss of the *N*-methyl group, which is replaced by a variety of alkyl groups, such as a cyclopropylmethyl group in naltrexone and buprenorphine, or an allyl group in naloxone (Fig. 1). Inclusion of a non-methyl *N*-alkyl group is rationalized by the “message-address” concept, where varying this

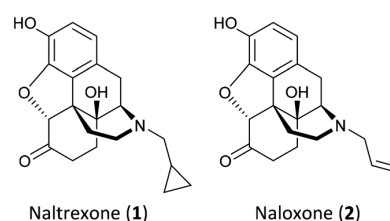


Fig. 1 Semi-synthetic opioid pharmaceuticals used for treatment of opioid overdose.

“message” group typically allows control of agonist or antagonist activity.⁵

Despite the medical utility of these semi-synthetic opioids, *N*-demethylation has traditionally been a difficult step on the industrial scale. The most commonly used methods for the *N*-demethylation of tertiary *N*-methylamines involved the use of cyanogen bromide (von Braun reaction)⁶ and chloroformate reagents.⁷ Both of these methods have significant drawbacks; cyanogen bromide is a highly toxic reagent,⁸ whilst the more effective chloroformate reagents, such as vinyl chloroformate, are quite expensive. In both cases, the resulting product must be further processed in order to return the *N*-nor product; in the case of the von Braun reaction to hydrolyse the resulting cyanamide group, and with the Polonovski reaction to cleave the resulting carbamate.

The *N*-demethylation of a range of alkaloids has also been achieved using the non-classical Polonovski reaction. Galanthamine was *N*-demethylated in good yield by first oxidising this alkaloid with *m*CPBA and subsequently treating the resultant *N*-methylamine oxide with ferrous sulfate.⁹ Iron catalysts have also been successfully investigated and developed into efficient catalysts for the *N*-demethylation of opiate alkaloids utilizing what has been proposed as a non-classical

^aAtlantic Centre for Green Chemistry, Department of Chemistry, Saint Mary's University, Halifax, Canada B3H 3C3. E-mail: Robert.Singer@smu.ca

^bMedicinal Chemistry, Monash Institute of Pharmaceutical Sciences, Monash University, Parkville, Victoria 3052, Australia

^cSchool of Pharmacy, Centre for Biomolecular Sciences, University of Nottingham, Nottingham NG7 2RD, U.K

† Electronic supplementary information (ESI) available: Synthetic procedures. See DOI: 10.1039/c7gc00436b

‡ These authors contributed equally to this work.

Polonovski-type mechanism.¹⁰ Further development of this work showed that the use of solid iron powder as the catalyst allowed its easy removal from the reaction mixture *via* filtration.¹¹

In addition to this, the reaction returns the free *N*-nor compound without the need for further reaction, therefore avoiding additional steps. This system has been subsequently adapted by Nakano *et al.* in a flow process using iron/sand columns, again demonstrating the utility of using these catalysts.¹²

The optimised process requires the formation of the alkaloid *N*-oxide, which can be readily accomplished using a variety of oxidants, such as hydrogen peroxide or *m*CPBA on a laboratory scale.¹⁰ This is then converted to the hydrochloride salt, which was previously found to be an important factor, as the additional proton is essential in the proposed mechanism.¹⁰ Furthermore, the anion used in the salt formation is also important, as departure from the chloride anion results in a reduction in yield.¹³ While the reaction will still proceed using the free *N*-oxide, the yields obtained are suboptimal.¹⁴ Solvent also plays an important role, with chloroform (CHCl₃) giving the highest yield of the solvents tested.¹⁵

The precise nature of the catalytic system is also important. The optimised loading is described as 13 mol% Fe(0) powder with an additional 2 mol% Fe³⁺ in the form of FeCl₃.¹¹ It was demonstrated that while increasing the loading of Fe(0) has little impact on the yield, increasing the loading of Fe³⁺, or even switching to an Fe²⁺ species, results in suboptimal yields. Finally, allowing the reaction to proceed in open air increases the reaction rate, while under an inert nitrogen atmosphere the reaction rate is adversely affected.¹¹ All these factors may be implemented in an industrial setting for cost-effective, relatively safe, and efficient *N*-demethylation of opiates for conversion to other clinically useful drugs (Scheme 1).

While previously described advances have been extremely useful, we have a continued interest in the development of iron catalysts in *N*-demethylations, either for industrial or

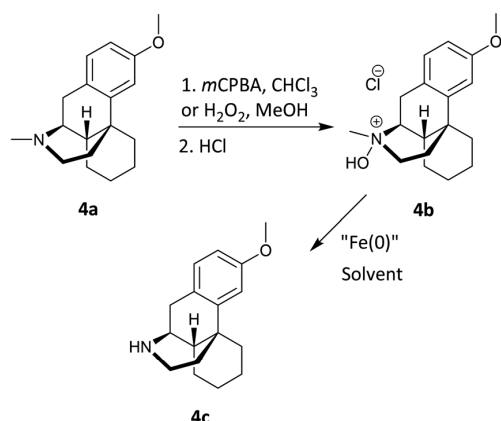
synthetic purposes. While the Fe(0)/Fe(III) system we described earlier is efficient, both in terms of yield and cost, the use of CHCl₃ is undesirable as it is toxic and a potential carcinogen.¹⁶ Furthermore, it is potentially fatal if absorbed or ingested in larger quantities.

Therefore, its use on an industrial scale is highly undesirable. Seeking a solvent replacement is not always a simple task. Reaction kinetics, thermodynamics and yield may be affected by the balance of solvent polarity and protic nature. More specifically in the case of *N*-demethylations, molecular oxygen dissolved in the solvent can also impact on reaction rate and yield.¹¹ The work previously conducted by our group has extensively explored various iron powders, iron salts, as well as steel alloy powders under a variety of conditions.^{10,11,14,15,17,18} In the present study, we present the use of two new iron species as alternatives for the *N*-demethylation of alkaloids whilst also exploring the use of "greener" solvents for this reaction.

Nanoscale zero-valent iron (nZVI) has been prepared using a variety of methods and employed in several different types of reactions.^{19–21} The majority of literature reports involving nZVI describe the remediation of ground water and the removal of contaminants such as arsenic(III),²² chromium(VI),²³ and *E. coli* bacteria.²⁴ There are a number of reports where nZVI has been used in catalytic applications.^{21,25,26} The efficacy of these methods is due in part to the extremely high surface area-to-volume ratio of nZVI. This property, along with our experiences using iron(0) as a catalyst in the modified Polonovski reaction, prompted us to investigate its use for *N*-demethylation reactions. A number of "green" advantages are also presented through the use of nZVI in these systems. The high surface area of nZVI was anticipated to lead to faster reaction rates for *N*-demethylation of the *N*-oxides used in these reactions. Furthermore, the preparation of nZVI can be accomplished in water using minimally toxic sodium borohydride (NaBH₄) and subsequent catalytic demethylations can be conducted in alcoholic solvents such as isopropanol (i-PrOH).

A number of procedures have been reported for the preparation of nZVI. The most common technique involves reduction of an iron(II) or iron(III) salt, such as iron(II) sulfate or iron(III) chloride, to iron(0) using NaBH₄ in aqueous media. This procedure is relatively non-toxic, inexpensive, uncomplicated and can yield nanoscale iron(0) particles in the size range of 10–50 nm.²⁷ The effects of iron and NaBH₄ concentration, atmospheric *versus* inert conditions, the rate of agitation during reaction, the rate of NaBH₄ addition, and how the iron is dried and stored have been extensively studied and optimised.

Triiron dodecacarbonyl (Fe₃(CO)₁₂) is an unusual iron species, typically used as a source of reactive Fe(0) for the synthesis of various iron complexes, or as a reagent. Its utility as a catalyst has, to our knowledge, not been previously described. Previously investigated catalysts tend to be heterogeneous due to the insolubility of iron and iron salts in the tested solvents. In contrast to these, Fe₃(CO)₁₂ is soluble in non-polar organic solvents, with limited solubility in more polar solvents.



Scheme 1 *N*-Demethylation of DXM, 4a, *via* *N*-oxide hydrochloride, 4b.

Furthermore, the carbonyl ligands are easily displaced by Lewis bases, potentially allowing for better interaction with the substrate and hence higher rates of reaction.

Synthesis of iron nanoparticles can also be achieved using $\text{Fe}_3(\text{CO})_{12}$. Previous examples demonstrate that under relatively harsh conditions, $\text{Fe}_3(\text{CO})_{12}$ may undergo controlled decomposition to form either nZVI or magnetite nanoparticles.^{28,29} A solution of $\text{Fe}_3(\text{CO})_{12}$ and PPh_3 in hexane may form graphite coated iron nanoparticles under strong UV irradiation over an extended period of time.²⁸ $\text{Fe}_3(\text{CO})_{12}$ may form magnetite nanoparticles upon prolonged reflux in diethylene glycol, diethyl ether, and oleic acid.²⁹ Both of these methods result in nanoparticles that have an organic coating. As we are interested in “bare” nZVI, these methods were not utilised.

Industrial adoption of any new method for the *N*-demethylation of alkaloids depends on appropriate selection of a green solvent. The environmental impact and waste involved in the synthesis of active pharmaceutical ingredients (API's) is of considerable concern to the pharmaceutical industry.³⁰ With solvents contributing 80–90% of the non-aqueous waste generated, reduction in toxic waste solvent is critical to reducing health and environmental damage. Solvents, nonetheless, are still required for the production of API's, and therefore need to be replaced with greener options. To that end, GSK have assembled a toolkit to assist in the selection of solvents suitable for large-scale industrial applications.³⁰ It has also been suggested that initial reaction development could be guided by this solvent selection process, as this would save both time and money further down the line when optimising such reactions for industrial purposes. With this in mind, we have chosen to approach the problem primarily using greener options.

Herein, we report the use of nZVI and $\text{Fe}_3(\text{CO})_{12}$ as Fe(0) sources for the modified Polonovski reaction in which the *N*-demethylation of various alkaloids in green solvents is demonstrated. The reaction systems have been optimised for the use of *i*-PrOH, a green solvent that is directly compared to the use of the “non-green” solvent CHCl_3 as well as other solvent combinations. The use of nZVI represents an improved green approach to this reaction in that the rate of reaction is significantly enhanced *versus* iron dust while maintaining ease of isolation of products and the use of a green iron(0) catalyst. $\text{Fe}_3(\text{CO})_{12}$, although less green than using nZVI, has favourable solubility properties, allowing for catalytic amounts to be employed in conjunction with the use of *i*-PrOH. The extension of the methodology to a selected array of *N*-methylalkaloids is also reported.

Results and discussion

nZVI was prepared using a previously reported procedure in which ferric sulfate heptahydrate was reduced in aqueous medium using NaBH_4 with mechanical stirring, washed with 50% aqueous methanol *via* repetitive centrifugation, decantation and replacement of solvent.²⁷ The isolated nZVI was then

suspended in the reaction solvent to be used for the modified Polonovski reactions. nZVI prepared using this method could be carefully isolated under inert atmosphere to prevent oxidation, as far as possible, followed by characterisation using scanning electron microscopy (SEM) (Fig. 2). The SEM image shows spherical, monodisperse particles of approximately 75 nm in diameter, forming chain-like secondary structures. Comparison with the SEM of iron dust used in previous studies shows distinctly smaller particle size (*i.e.* 75 nm *vs.* 40 μm) and therefore significantly higher surface area of the iron(0) surface upon which reaction can occur.

The pseudo-opioid dextromethorphan (DXM), **4a**, was chosen as an ideal substrate for preliminary reactions investigating optimisation of reaction conditions. DXM, contained in many common cough medications due to its anti-tussive properties, is structurally similar to naturally occurring opiates possessing an *N*-methyl group, and is a member of the morphinan family of compounds. Unlike naturally occurring opiates, it is not a highly controlled substance and is hence readily available as its hydrobromide salt from commercial sources. DXM hydrobromide is an atmospherically stable solid at room temperature making it easy to manipulate in a laboratory setting. DXM is easily transformed into its *N*-oxide and *N*-oxide hydrochloride derivative, **4b**, in high yields. *N*-Oxidation of **4a** and isolation of the hydrochloride salt **4b** was achieved by treatment of **4a** with either *m*CPBA or H_2O_2 , followed by addition of aqueous HCl using a variation of a literature procedure.¹⁴ In general, *m*CPBA in CHCl_3 was employed as the oxidant as it afforded the desired *N*-oxide after a short reaction time (~1 h). However, H_2O_2 in MeOH has previously been used as a greener alternative for this transformation.^{10,13,18} Despite this, literature procedures tend to vary significantly in equivalents added and the reaction time required. Initial screening using titrated H_2O_2 showed that 10 eq. was sufficient to afford conversion of **4a** to **4b** overnight. Excess H_2O_2 was then degraded to water using minimal MnO_2 . After filtration and removal of the organic solvent *in vacuo*, the HCl salt was subsequently generated by adding dilute acid and removing the excess water using a freeze-dryer. Increasing the molar ratio of H_2O_2 to 20 eq. and 30 eq. offered no significant advantage in terms of reaction time. Overall, this procedure gave comparable yields of the *N*-oxide and eliminated the need

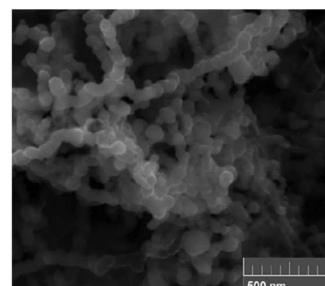


Fig. 2 SEM image of synthesised nZVI.

for chlorinated solvents, replacing them with MeOH and water.

The *N*-oxide **4b** was subsequently converted to the corresponding *N*-nor derivative **4c**. Typically, **4b** was dissolved or suspended in the selected solvent system and nZVI or Fe₃(CO)₁₂ was then added as a solution/suspension in the appropriate solvent and the reaction was stirred at room temperature for the prescribed period of time. The results of these experiments are summarised in Tables 1 and 2. Reaction of **4b** in *i*-PrOH gave a good yield of the *N*-demethylated product, **4c**, using a stoichiometric amount of nZVI (Table 1, entry 1). Use of this

green solvent afforded slightly lower yields than when CHCl₃ was used (Table 1, entry 2), likely due to differences in solubility of the substrate molecules. Switching the solvent to methanol resulted in a noticeable decrease in yield of **4c** (Table 1, entry 3). It has previously been postulated that iron acts as a catalyst in the modified Polonovski reaction.¹⁰ When a catalytic amount of nZVI (*i.e.* 10 mol%) was employed, there was a pronounced decrease in the yield of the *N*-demethylated product, **4c** (Table 1, entries 4–6), regardless of the solvent used. We believe this is due to catalyst poisoning/deactivation as the *N*-demethylated product builds up in the reaction. The coordination of the Lewis basic product, **4c**, to iron prevents further substrate molecules from interacting with the iron catalyst. Conversion of **4b** to **4c** was unsuccessful when nZVI was employed using water as a solvent.

Fe₃(CO)₁₂ proved to be an efficient catalyst for the *N*-demethylation of **4b**. In CHCl₃, good yields were achievable with low catalyst loadings and drastically reduced reaction times. As seen in Table 2, the optimal yield was obtained using 5 mol% Fe₃(CO)₁₂ (Table 2, entry 1), with increases in catalyst loading resulting in slightly reduced yield. When less than 5 mol% of Fe₃(CO)₁₂ is used, the reaction never goes to completion, even if left for extended periods of time. We again rationalise this to be due to poisoning of the catalyst. We suspect that **4c** may be forming stronger coordination bonds to iron than the native carbonyl ligand at the conclusion of the catalytic cycle.

Following optimisation of the reaction in CHCl₃, we proceeded to assess various greener solvents in order to ascertain the ability of Fe₃(CO)₁₂ to perform under alternative conditions. To this end, various ester solvents were tested, with the addition of MeOH to increase the solubility of the sub-

Table 1 *N*-Demethylation of various alkaloid *N*-oxide hydrochlorides using nZVI

Entry	nZVI (mol %)	Substrate (<i>N</i> -oxide)	Solvent/conditions ^a	Time (h)	% Yield ^b (<i>N</i> -nor)
1	100	DXM (4b)	<i>i</i> -PrOH	0.75	4c , 84
2	100	DXM (4b)	CHCl ₃	1	4c , 92
3	100	DXM (4b)	MeOH	3	4c , 59
4	10	DXM (4b)	<i>i</i> -PrOH	21	4c , 78
5	10	DXM (4b)	CHCl ₃	1	4c , 67
6	10	DXM (4b)	MeOH	3	4c , 34
7	100	Noscapine (5b)	<i>i</i> -PrOH	24	— ^c
8	100	Atropine (6b)	<i>i</i> -PrOH	3	6c , 85
9	100	Tropine (7b)	<i>i</i> -PrOH	24	— ^c
10	100	Pivaloyltropine (8b)	<i>i</i> -PrOH	14	8c , 59
11	100	Benzoyltropine (9b)	<i>i</i> -PrOH	14	9c , 58

^a 10 mL of solvent per 100 mg substrate at ambient temperature (measured to be 21 °C on average) under an atmosphere of argon. Reactions were stirred using a 12 mm magnetic bead at 900 RPM. ^b Isolated yield following column chromatography. ^c NMR of crude product mixture showed no evidence of any conversion of *N*-oxide starting material to *N*-nor product.

Table 2 *N*-Demethylation of various alkaloid *N*-oxide hydrochlorides using Fe₃(CO)₁₂

Entry	Fe ₃ (CO) ₁₂ (mol%)	Substrate (<i>N</i> -oxide)	Solvent/conditions ^a	Time (h)	% Yield ^b (<i>N</i> -nor)
1	5	DXM (4b)	CHCl ₃	0.1	4c , 86
2	10	DXM (4b)	CHCl ₃	0.1	4c , 73
3	5	DXM (4b)	<i>i</i> -PrOH	0.7	4c , 92
4	5	DXM (4b)	MeOAc/MeOH (9 : 1)	0.1	4c , 76
5	5	DXM (4b)	DMC/MeOH (9 : 1)	0.1	4c , 15
6	5	DXM (4b)	<i>t</i> BuOAc/MeOH (9 : 1)	0.1	4c , 83
7	5	DXM (4b)	EtOAc/MeOH (9 : 1)	0.1	4c , 74
8	5	DXM (4b)	EtOAc/ <i>i</i> -PrOH (9 : 1)	0.1	4c , 81
9	5	Noscapine (5b)	CHCl ₃	24	5c , 28
10	5	Noscapine (5b)	EtOAc/MeOH (9 : 1)	17	5c , 26
11	5	Noscapine (5b)	EtOAc/ <i>i</i> -PrOH (9 : 1)	2	5c , 30
12	5	Noscapine (5b)	<i>i</i> -PrOH	120	— ^c
13	5	Atropine (6b)	EtOAc/MeOH (9 : 1)	22	6c , 66
14	5	Atropine (6b)	EtOAc/ <i>i</i> -PrOH (9 : 1)	19	6c , 79
15	5	Tropine (7b)	<i>i</i> -PrOH	2.5	— ^c
16	5	Pivaloyltropine (8b)	CHCl ₃	2	8c , 83
17	5	Pivaloyltropine (8b)	<i>i</i> -PrOH	17	8c , 63
18	5	Pivaloyltropine (8b)	EtOAc/MeOH (9 : 1)	0.1	8c , 66
19	5	Pivaloyltropine (8b)	EtOAc/ <i>i</i> -PrOH (9 : 1)	0.1	8c , 63

^a 10 mL of solvent per 100 mg substrate at ambient temperature (measured to be 21 °C on average) under an open atmosphere. Reactions were stirred using a 12 mm magnetic bead at 750 RPM. ^b Isolated yield following column chromatography. ^c NMR of crude product mixture showed no evidence of any conversion of *N*-oxide starting material to *N*-nor product.

strate. Ester solvents (Table 2, entries 4, 6–8) afforded generally good results for the reaction with **4b**. Dimethyl carbonate (DMC) (Table 2, entry 5) proved to be the exception, with very low recovery of the product. Although DMC is known to be a methylating agent, its ability to alkylate is only evident under relatively harsh conditions. Therefore, we suspect that methylation of **4c** under the tested conditions is unlikely to occur. Rather, this solvent may simply not be amenable to this particular reaction. The effect of substituting *i*-PrOH for MeOH in these solvent mixtures was also explored. EtOAc/*i*-PrOH (Table 2, entry 8) gave higher yields compared to the EtOAc/MeOH mixture (Table 2, entry 7). Indeed, when used as the bulk solvent, *i*-PrOH gave surprisingly good results (Table 2, entry 3). Although reaction times were longer, the yields obtained were improved.

Following the demonstration of nZVI and $\text{Fe}_3(\text{CO})_{12}$ as effective catalysts for the demethylation of **4b**, we sought to establish whether the methodology could be applied to other biologically interesting alkaloids. We therefore investigated the demethylation of the *N*-oxide hydrochlorides of noscapine (**5a**), atropine (**6a**), tropine (**7a**), pivaloyltropine (**8a**), and benzoyltropine (**9a**) (Fig. 3) using nZVI and $\text{Fe}_3(\text{CO})_{12}$. Compound **5a** is interesting as a potential starting material for synthesis. Its complex array of carbocycles and heterocycles makes it an attractive starting point for more complex products. Furthermore, **5a** has gained interest as a starting material for the synthesis of potential anti-cancer agents.^{31,32} Previous studies in our group have already indicated the potential use of *N*-substituted noscapine analogues as more potent anti-cancer agents, which obviously necessitates the preparation of *N*-nornoscapine, **5c**, as an intermediate.³¹ Compound **6a**, like many opioids, has been a historically important drug, present in various plant sources, particularly *Atropa belladonna*, from which the drug gets its name. It is also used as a starting material for various pharmaceuticals; *N*-noratropine, **6c**, is an important intermediate for the synthesis of ipratropium bromide, a bronchodilator.³³ Improved *N*-demethylation

methods for both **5a** and **6a** could be utilized for rapid and easy access to the *N*-nor compounds. Compound **7a** was tested as an interesting synthon that may be included in various drugs (such as Granisetron, Hyoscyamine and Tropisetron), while **8a** and **9a** represent more “drug-like” compounds with increased organic solubility.

N-Demethylation of these alternative test substrates gave variable, but promising results (Table 1, entries 7–11, Table 2, entries 9–19). Compound **5b**, for example, failed to give increased yields of **5c** when $\text{Fe}_3(\text{CO})_{12}$ was used as the catalyst compared to previously established literature methods.³¹ However, the reaction did go to completion (Table 2, entries 9–11). Using *i*-PrOH, no product was observed when either nZVI or $\text{Fe}_3(\text{CO})_{12}$ were used (Table 1, entry 7 and Table 2, entry 12). Once again, we believe this to be due to the limited solubility of the substrate in the selected solvents. Furthermore, **5a** may be a particularly difficult substrate for this particular process as the *N*-methyl group is quite sterically hindered. Upon oxidation to **5b**, further steric hindrance may occur, preventing approach of the catalyst to the required site for the radical oxidation to occur.

Using **6b** as a test substrate, very good yields were obtained when nZVI was used in *i*-PrOH (Table 1, entry 8), while only moderate yields were observed when using $\text{Fe}_3(\text{CO})_{12}$ in EtOAc/*i*-PrOH (Table 2, entries 13 & 14). Lower yields were observed when using MeOH instead of *i*-PrOH in the mixture, which is consistent with previous results. Conversion of **7b** to *N*-nortropine proved unsuccessful under all tested conditions, including using *i*-PrOH as the solvent (Table 1, entry 9 & Table 2, entry 15).

The more soluble **8b** gave variable results compared to those previously obtained using nZVI or $\text{Fe}_3(\text{CO})_{12}$. Whereas previous substrates gave good yields in a mixture of 9 : 1 (v/v) EtOAc/*i*-PrOH, conversion to **8c** was suboptimal in this system compared to in CHCl_3 (Table 2, entry 16). Switching to **9b** did not result in any appreciable increase in yield when using nZVI (Table 1, entry 11). The yields are, nevertheless, comparable to those obtained for previous attempts at *N*-demethylation of tropane alkaloids, but with a significantly reduced reaction time.³³ Although some optimisation may be required, these results highlight the possibility of using greener solvent substitutes without a significant compromise in yield.

Reactions using nZVI and $\text{Fe}_3(\text{CO})_{12}$ were observed to proceed much faster in CHCl_3 than in greener solvents such as *i*-PrOH. Furthermore, these two iron sources seemed to considerably enhance the rate of the *N*-demethylation reactions to a far greater degree than other iron sources investigated earlier by our research group. For example, *N*-demethylation of **4b** appeared complete within 5 min when conducted using $\text{Fe}_3(\text{CO})_{12}$, and within 1 h when using nZVI in CHCl_3 . Hence, we endeavoured to measure the relative rates of conversion for each of the iron sources. In order to make direct comparisons and also to emphasize the compatibility of our systems in green solvent systems, the study of relative conversions of **4b** to **4c**, using the different iron catalysts, were conducted in

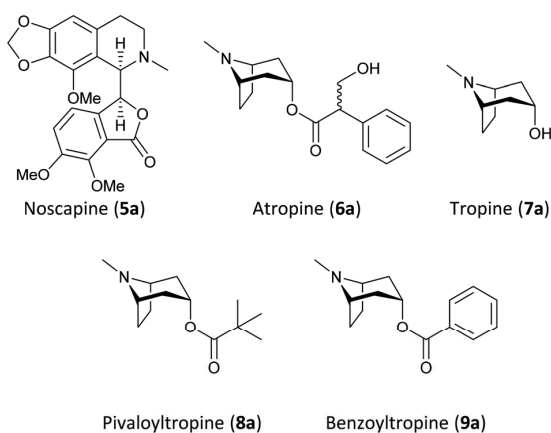


Fig. 3 Alternative alkaloid substrates for *N*-demethylations.

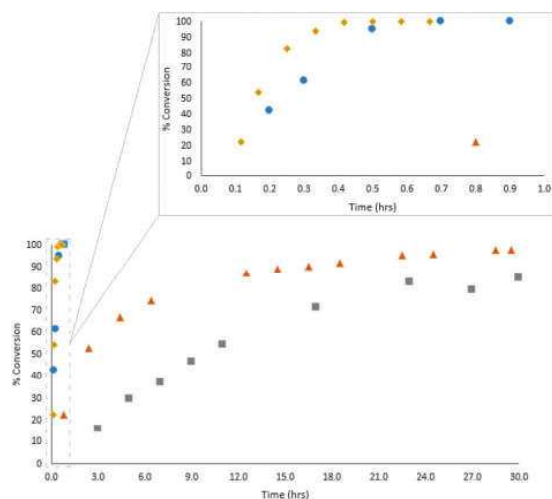


Fig. 4 Percentage conversion versus time for various iron catalysts. FeSO₄ (■), Fe(0) dust (▲), nZVI (●), Fe₃(CO)₁₂ (◆).

i-PrOH. Ferric sulfate did not give 100% conversion into nor-DXM, **4c**, even after 30 h (Fig. 4). As we reported earlier, the use of iron(0) dust improved this reaction and resulted in essentially 100% conversion after almost 30 h.¹⁵

As anticipated, the use of nZVI, with far greater surface area, afforded 100% conversion after only 40 min. Lastly, the use of Fe₃(CO)₁₂ as a catalyst affords even faster rates of conversion to demethylated, nor-alkaloid products. The solubility properties of this compound allow for genuinely catalytic amounts to be employed, while still permitting the use of *i*-PrOH. This methodology has been successfully applied to a number of *N*-methylated alkaloids, with the possibility of being further extended to the *N*-demethylation of opiates of social significance, used in the commercial preparation of naltrexone, naloxone and buprenorphine.

Conclusions

The green attributes of the modified Polonovski reaction, through which the *N*-demethylation of various alkaloids is achieved, have been significantly improved in comparison to previously reported methodologies. The use of nZVI as a green catalyst and *i*-PrOH as a green solvent afforded enhanced rates of conversion to nor-alkaloid products. Although less green, the use of Fe₃(CO)₁₂ as a catalyst affords even faster rates of conversion to demethylated, nor-alkaloid products. The solubility properties of this compound allow for genuinely catalytic amounts to be employed, while still permitting the use of *i*-PrOH. This methodology has been successfully applied to a number of *N*-methylated alkaloids, with the possibility of being further extended to the *N*-demethylation of opiates of social significance, used in the commercial preparation of naltrexone, naloxone and buprenorphine.

Experimental

All solvents were used as provided by the manufacturer (Fisher Scientific, Alfa Aesar, Sigma-Aldrich). TLC was performed using aluminium-backed silica plates (Merk, Silica gel 60 Å

f254), with compounds visualised using a UV lamp, or *via* poly-molybdate or KMnO₄ staining. ¹H and ¹³C NMR spectra were recorded at 400 and 101 MHz or 300 and 75 MHz (Bruker Avance Nanobay III 400 MHz Ultrashield Plus or Bruker Avance III HD), respectively. Chemical shifts were referenced to residual solvent peaks according to Gottlieb *et al.*³⁴ Alkaloids were purchased from the supplier and used as provided (Sigma-Aldrich, Alfa Aesar), except for dextromethorphan, which was washed with base (2 × 5% aqueous NaOH) to return the free base before *N*-oxidation according to literature procedure.¹⁴ Triirondodecacarbonyl and ferric sulfate heptahydrate were purchased from Sigma-Aldrich.

General procedure for *N*-oxidation of alkaloids using *m*CPBA

Alkaloid *N*-oxide hydrochloride salts were generated using variations of a literature procedure.¹⁴ The alkaloid free amine was dissolved in CHCl₃ and cooled to (−5–0 °C, typically 20 mL per gram of alkaloid). *m*CPBA (typically 1.2 eq.) was then added in a single portion and the reaction allowed to stir until reaction completion as determined by TLC analysis, after which time the mixture was worked up using one of the following procedures:

(A) The volume of CHCl₃ was doubled and *i*-PrOH was added to make the solution a 3 : 1 (v/v) mixture of CHCl₃/*i*-PrOH. This was then washed successively with 1 : 4 (v/v) 2 M NaOH/brine (5 × 5 mL), followed by 1 : 4 (v/v) 2 M HCl/brine (5 × 5 mL). The organic phase was dried over anhydrous Na₂SO₄, filtered, and the solvent removed *in vacuo* to give the alkaloid *N*-oxide hydrochloride salt.

(B) The reaction mixture was extracted with 1 M HCl (3 × 10 mL). The combined aqueous extracts were washed with CHCl₃ (2 × 10 mL) and the resulting aqueous phase reduced *in vacuo* to give the alkaloid *N*-oxide hydrochloride salt.

Procedure for *N*-oxidation of DXM using H₂O₂

DXM free amine (366 mg, 1.35 mmol, 1 eq.) was dissolved in MeOH (5 mL) and cooled to 0 °C. H₂O₂ (26% w/w in H₂O, 1.766 g, 13.5 mmol, 10 eq.) was then added dropwise and the reaction allowed to stir at room temperature for 18 h. The reaction was then diluted with MeOH and excess H₂O₂ deactivated with MnO₂. The reaction was filtered through Celite and the solvent removed *in vacuo*. Aqueous HCl (0.1 M, 50 mL) was then added, and the resulting solution freeze-dried to give **4b** as the hydrochloride salt (412 mg, 94%).

General procedure for *N*-demethylation of alkaloid *N*-oxides using nZVI

Following a modified procedure,²⁷ an appropriate amount of FeSO₄·7H₂O (see Table 1) was dissolved in aqueous methanol (two parts deionized water, one part methanol, 8 mL per 0.50 mmol FeSO₄·7H₂O) and stirred at 450 RPM using a mechanical stirrer in an appropriately sized round-bottom flask while a 0.12 M aqueous solution of NaBH₄ was added dropwise at a rate of approximately 1 drop every 5 s (0.8 mL per 0.50 mmol FeSO₄·7H₂O). As drops were added, the solution turned an increasingly darker green until finally a black pre-

precipitate was formed. The suspension of black precipitate was stirred for an additional 5 min before being transferred into a 15 mL centrifuge tube. The washing process next consisted of five repetitions of centrifugation (5 min each at 3200 RPM) and decantation of the supernatant fluid. Before each centrifugation, the tubes were shaken vigorously such that the iron particles were re-suspended in the solvent. After the initial centrifugation and decantation, the tube was filled to the 5 mL mark with 2 mL of water and 3 mL of methanol, centrifuged and decanted. The same washing process was then repeated. The tube was then filled with 5 mL of the solvent to be used in the *N*-demethylation reaction, centrifuged and decanted. The same washing process was repeated one more time. At this point the nZVI was suspended in the appropriate solvent (5 mL) and added to the *N*-demethylation reaction flask. The alkaloid *N*-oxide hydrochloride salt (0.50 mmol) was previously dissolved or partially dissolved in the selected solvent (10 mL) in the reaction flask, giving a total of 15 mL of solvent, along with the *N*-oxide hydrochloride salt and suspended nZVI. This mixture was stirred for the appropriate amount of time (see Table 1) at room temperature. Upon completion of reaction, the solvent was removed under reduced pressure and the residue dissolved in 3:1 (v/v) CHCl₃/i-PrOH (26 mL). The resulting organic phase was washed with 2 M NaOH (2 × 2 mL), dried over anhydrous Na₂SO₄, filtered, and the solvent removed *in vacuo*. The resulting residue was purified by silica column chromatography to give the corresponding *N*-nor compounds.

General procedure for *N*-demethylation of alkaloid *N*-oxides using Fe₃(CO)₁₂

The alkaloid *N*-oxide hydrochloride salt (100 mg) was dissolved or partially dissolved in the selected solvent (9 mL) and an appropriate amount of Fe₃(CO)₁₂ (see Table 2) was added as a solution/suspension in the solvent (1 mL). The reaction was allowed to stir until reaction completion (see Table 2). Where solvent mixtures with 10% MeOH or i-PrOH were used, the alkaloid was dissolved in the appropriate alcohol (1 mL) first, followed by the bulk solvent (8 mL). The iron species was then delivered as a suspension/solution in the bulk solvent (1 mL). Upon reaction completion, the solvent was removed *in vacuo* and the residue dissolved in 3:1 (v/v) CHCl₃/i-PrOH (26 mL). The resulting organic phase was washed with 2 M NaOH (2 × 2 mL), dried over anhydrous Na₂SO₄, filtered, and the solvent removed *in vacuo*. The resulting residue was purified by silica column chromatography and evaporated from DCM to give the corresponding *N*-nor compounds.

Acknowledgements

The authors wish to thank the Natural Sciences and Engineering Research Council of Canada (NSERC Discovery to R. D. S.) for financial support for this research. R. L. would like to acknowledge financial support from an Australian Government Research Training Program Scholarship.

Financial contributions from Saint Mary's University, Monash University and the University of Nottingham are also gratefully acknowledged.

Notes and references

- P. R. Blakemore and J. D. White, *Chem. Commun.*, 2002, **11**, 1159–1168.
- S. Berenyi, C. Csutoras and A. Sipos, *Curr. Med. Chem.*, 2009, **16**, 3215–3242.
- A. K. Clark, C. M. Wilder and E. L. Winstanley, *J. Addict. Med.*, 2014, **8**, 153–163.
- R. A. Rudd, N. Aleshire, J. E. Zibbell and R. M. Gladden, *Morb. Mortal. Wkly. Rep.*, 2016, **64**, 1378–1382.
- P. S. Portoghese, M. Sultana, H. Nagase and A. E. Takemori, *J. Med. Chem.*, 1988, **31**, 1986–1987.
- J. von Braun, *Ber. Dtsch. Chem. Ges.*, 1900, **33**, 1438–1452.
- J. H. Cooley and J. E. Evain, *Synthesis*, 1989, 1–7.
- W. E. Luttrell, *J. Chem. Health Saf.*, 2009, **16**, 29–30.
- A. Mary, D. Z. Renko, C. Guillou and C. Thal, *Tetrahedron Lett.*, 1997, **38**, 5151–5152.
- K. McCamley, J. A. Ripper, R. D. Singer and P. J. Scammells, *J. Org. Chem.*, 2003, **68**, 9847–9850.
- G. B. Kok and P. J. Scammells, *Aust. J. Chem.*, 2011, **64**, 1515–1521.
- Y. Nakano, G. P. Savage, S. Saubern, P. J. Scammells and A. Polyzos, *Aust. J. Chem.*, 2013, **66**, 178–182.
- S. Thavaneswaran and P. J. Scammells, *Bioorg. Med. Chem. Lett.*, 2006, **16**, 2868–2871.
- G. B. Kok, T. D. Ashton and P. J. Scammells, *Adv. Synth. Catal.*, 2009, **351**, 283–286.
- G. B. Kok, C. C. Pye, R. D. Singer and P. J. Scammells, *J. Org. Chem.*, 2010, **75**, 4806–4811.
- Toxicological Profile for Chloroform, <https://www.atsdr.cdc.gov/toxprofiles/tp.asp?id=53&tid=16>, (accessed January 2017).
- G. B. Kok and P. J. Scammells, *Org. Biomol. Chem.*, 2011, **9**, 1008–1011.
- Z. Dong and P. J. Scammells, *J. Org. Chem.*, 2007, **72**, 9881–9885.
- R. Dey, N. Mukherjee, S. Ahammed and B. C. Ranu, *Chem. Commun.*, 2012, **48**, 7982–7984.
- J. F. Sonnenberg, N. Coombs, P. A. Dube and R. H. Morris, *J. Am. Chem. Soc.*, 2012, **134**, 5893–5899.
- V. Kelsen, B. Wendt, S. Werkmeister, K. Junge, M. Beller and B. Chaudret, *Chem. Commun.*, 2013, **49**, 3416–3418.
- S. R. Kanel, B. Manning, L. Charlet and H. Choi, *Environ. Sci. Technol.*, 2005, **39**, 1291–1298.
- X. Q. Li, J. Cao and W. X. Zhang, *Ind. Eng. Chem. Res.*, 2008, **47**, 2131–2139.
- Z. Li, K. Greden, P. J. J. Alvarez, K. B. Gregory and G. V. Lowry, *Environ. Sci. Technol.*, 2010, **44**, 3462–3467.
- J. F. Sonnenberg, N. Coombs, P. A. Dube and R. H. Morris, *J. Am. Chem. Soc.*, 2012, **134**, 5893–5899.
- L. Tan, S. Lu, Z. Fang, W. Cheng and E. Tsang, *Appl. Catal., B*, 2017, **200**, 200–210.

[View Article Online](#)

Paper

Green Chemistry

- 27 C. M. Cirtiu, T. Raychoudhury, S. Ghoshal and A. Moores, *Colloids Surf., A*, 2011, **390**, 95–104.
- 28 E. Ye, B. Liu and W. Fan, *Chem. Mater.*, 2007, **3**, 3845–3849.
- 29 D. Amara, I. Felner, I. Nowik and S. Margel, *Colloids Surf., A*, 2009, **339**, 106–110.
- 30 R. K. Henderson, C. Jiménez-González, D. J. C. Constable, S. R. Alston, G. G. A. Inglis, G. Fisher, J. Sherwood, S. P. Binksa and A. D. Curzonsf, *Green Chem.*, 2011, **13**, 854–862.
- 31 A. Debono, J. Xie, S. Ventura, C. Pouton, B. Capuano and P. J. Scammells, *ChemMedChem*, 2012, **7**, 2122–2133.
- 32 A. DeBono, S. Mistry, J. Xie, D. Muthiah, J. Phillips, S. Ventura, R. Callaghan, C. Pouton, B. Capuano and P. J. Scammells, *ChemMedChem*, 2014, **9**, 399–410.
- 33 D. D. Do Pham, G. F. Kelso, Y. Yang and M. T. W. Hearn, *Green Chem.*, 2012, **14**, 1189–1195.
- 34 H. E. Gottlieb, V. Kotlyar and A. Nudelman, *J. Org. Chem.*, 1997, **62**, 7512–7515.

5.4.1 Additional Notes

Compound references here will refer directly to the numbering scheme in the paper, and should be viewed independently from the rest of this dissertation.

In addition to the published tests, various other conditions were trialled that gave interesting results. First, it was found that using chloroform as the solvent, compound **4b** could be demethylated using only 2 mol% loading of the catalyst, returning a yield of 88%. At 3 mol% loading, a slightly lowered yield of 87% was observed. These marginal improvements in yield were not considered to be significant, and were within the margin of error for recovery following flash chromatography. Furthermore, it was also found that such low catalytic loading was not consistent across the more polar solvents such as isopropanol or the ethyl acetate/alcohol mixtures. Hence, 5 mol% was chosen as our "standard" catalyst loading when solvent conditions were being optimized.

In addition to the described panel of solvents tested, methanol was also trialled. However, rapid poisoning of the catalyst was observed, with no reaction occurring prior to catalyst deactivation. In addition to this, an attempt at *N*-demethylating atropine *N*-oxide was also attempted using water as the solvent. However, this again gave no reaction. In this case, it was suspected that the catalyst simply wasn't soluble in water, and therefore wasn't available for interaction with the substrate. The catalyst is suspected to work via the loss of a single labile carbonyl ligand, therefore allowing access of the substrate to the active iron center. If the catalyst is not in solution, this may not be possible, hence the lack of reaction observed in water.

Tropine, one of the simplest alkaloids tested, failed to give any observable conversion to the *N*-nor compound under all tested conditions. Here, poor substrate solubility was found across all tested solvents, and therefore was not available for the reaction.

References

- (1) Abdel-Monem, M. M., and Portoghese, P. S., (1972). *N*-Demethylation of morphine and structurally related compounds with chloroformate esters. *J. Med. Chem.* *15*, 208–210.
- (2) Polonovski, M., and Polonovski, M., (1927). Amine oxides of the alkaloids. III. Action of organic acid chlorides and anhydrides. Preparation of the nor bases. *Bulletin de la Societe Chimique de France* *41*, 1190–1208.
- (3) Grierson, D., (1990). The Polonovski Reaction. *Org. React.* *39*, 85–295.
- (4) Mary, A., Renko, D. Z., Guillou, C., and Thal, C., (1997). Selective *N*-demethylation of galanthamine to norgalanthamine via a non classical Polonovski reaction. *Tetrahedron Lett.* *38*, 5151–5152.
- (5) McCamley, K., Ripper, J. A., Singer, R. D., and Scammells, P. J., (2003). Efficient *N*-demethylation of opiate alkaloids using a modified nonclassical Polonovski reaction. *J. Org. Chem.* *68*, 9847–9850.
- (6) Thavaneswaran, S., and Scammells, P. J., (2006). Further investigation of the *N*-demethylation of tertiary amine alkaloids using the non-classical Polonovski reaction. *Bioorg. Med. Chem. Lett.* *16*, 2868–2871.
- (7) Dong, Z., and Scammells, P. J., (2007). New methodology for the *N*-demethylation of opiate alkaloids. *J. Org. Chem.* *72*, 9881–9885.
- (8) Kok, G., Ashton, T. D., and Scammells, P. J., (2009). An improved process for the *N*-demethylation of opiate alkaloids using an iron(II) catalyst in acetate buffer. *Adv. Synth. Catal.* *351*, 283–286.
- (9) Kok, G. B., Pye, C. C., Singer, R. D., and Scammells, P. J., (2010). Two-step iron(0)-mediated *N*-demethylation of *N*-methyl alkaloids. *J. Org. Chem.* *75*, 4806–4811.
- (10) Kok, G. B., and Scammells, P. J., (2010). *N*-demethylation of *N*-methyl alkaloids with ferrocene. *Bioorganic Med. Chem. Lett.* *20*, 4499–4502.

- (11) Kok, G. B., and Scammells, P. J., (2011). Efficient iron-catalyzed *N*-demethylation of tertiary amine-*N*-oxides under oxidative conditions. *Aust. J. Chem.* *64*, 1515–1521.
- (12) Kok, G. B., and Scammells, P. J., (2011). Further investigations into the *N*-demethylation of oripavine using iron and stainless steel. *Org. Biomol. Chem.* *9*, 1008–1011.
- (13) Do Pham, D. D., Kelso, G. F., Yang, Y., and Hearn, M. T. W., (2012). One-pot oxidative *N*-demethylation of tropane alkaloids with hydrogen peroxide and a Fe(III)-TAML catalyst. *Green Chem.* *14*, 1189–1195.
- (14) Kok, G. B., and Scammells, P. J., (2012). Polonovski-type *N*-demethylation of *N*-methyl alkaloids using substituted ferrocene redox catalysts. *Synthesis* *44*, 2587–2594.
- (15) Nakano, Y., Savage, A. G. P., Saubern, A. S., Scammells, P. J., and Polyzos, A., (2013). A multi-step continuous flow process for the *N*-demethylation of alkaloids. *Aust. J. Chem.* *66*, 178–182.
- (16) Thavaneswaran, S., McCamley, K., and Scammells, P. J., (2006). *N*-Demethylation of alkaloids. *Nat. Prod. Commun.* *1*, 885–897.
- (17) Henderson, R. K., Jiménez-González, C., Constable, D. J. C., Alston, S. R., Inglis, G. G. a., Fisher, G., Sherwood, J., Binks, S. P., and Curzons, A. D., (2011). Expanding GSK's solvent selection guide - embedding sustainability into solvent selection starting at medicinal chemistry. *Green Chem.* *13*, 854–862.

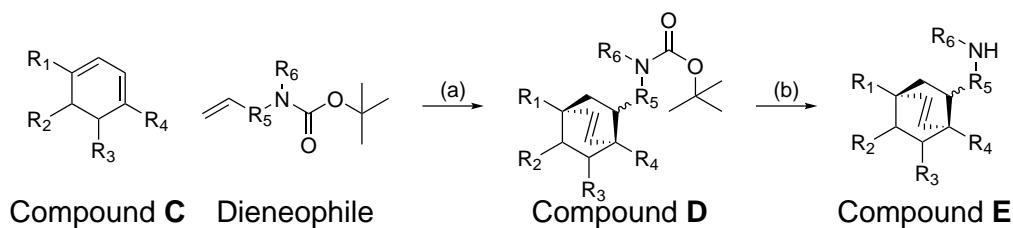
6 Industrial Placement at Sun Pharmaceutical Industries

As a part of this PhD, an industrial placement was conducted with Sun Pharmaceutical Industries Ltd. at their facility in Port Fairy for 5 weeks. The work done here involved the large-scale optimization of two reactions for the synthesis of a product, here named "compound **E**", which would be further elaborated at another facility. Due to the confidentiality of this project, specific details will not be revealed with regards to the compound structures or their intended use. However, more general discussions on the chemistry itself as well as the equipment used will be included.

6.1 Reaction Overview and Immediate Issues

A procedure for the synthesis of **E** was initially provided by a third party. Briefly, the diene starting material "compound **C**", was reacted with an *N*-Boc-protected dieneophile in xylenes at reflux for 19 h to give the Diels Alder product "compound **D**" (Scheme 14). On a small scale, purification involved addition of 10% hydrogen chloride in ethyl acetate to the Diels Alder mixture, followed by the addition of *tert*-butyl methyl ether (TBME) as an anti-solvent to effect the precipitation of compound **D** hydrochloride salt. This was then returned to the free-base by suspending the solid in ethyl acetate and washing with a basic aqueous phase, followed by evaporation of the organic layer to give compound **D** as the free-base foam. This Diels Alder adduct could then be deprotected using a 2:1 DCM/TFA mixture over 12 h to reveal the desired compound **E**. This was then isolated by neutralizing the reaction mixture with a basic aqueous solution and extracting the aqueous phase using DCM. The DCM extracts were then combined and the solvent removed *in vacuo* to give compound **E** as a foam at 74% yield and 89% purity. This provided procedure will herein be referred to as the "standard method".

Although the described method was successful in providing the compound on a relatively small scale, various factors limited its utility while trying to scale up. First, the Diels Alder reaction was conducted at relatively dilute concentrations, requiring the use of a large volume of solvent for a relatively small amount of substrate. Furthermore, heating at reflux for 19 h presented issues at scale, as careful heating and cooling were required in order to avoid damage to the reactors that would be used, adding additional time to the reaction. Ideally, shortening



Scheme 14. The "standard method" for the synthesis of compound **E** as provided by a third party. Reagents and Conditions: (a) xylenes, reflux; (b) TFA, DCM.

the reaction time to a reasonable time-frame was desired.

In addition to this, the workup required to isolate compound **D** necessitated the use of a large volume of additional solvent. Furthermore, the quantities of 10% hydrogen chloride in ethyl acetate required for this could not be acquired locally and had to be generated on site. This is typically done using one of two methods; bubbling hydrogen chloride gas through ethyl acetate, or reacting anhydrous ethanol with acetyl chloride in ethyl acetate at the desired concentration. With the quantities required at scale neither of these approaches was practical. A safety review of the fumehoods available revealed that the fumes generated could not be scrubbed sufficiently to prevent corrosion of the drive belt of the fan, as well as to ensure safety of the staff working in the surrounding areas.

The second Boc-deprotection step again presented several issues. First, the use of DCM on such a large scale was assessed and considered unsafe with the equipment available. Not only is this a toxic solvent that is also a hazard to the environment, but the high volatility of the solvent would have generated a large volume of gaseous DCM from various heating effects such as heat of dilution and the exothermic Boc-deprotection reaction. Although respiration equipment was available, the filters were not intended for use with such volatile solvents in addition to the fumes displacing O₂ to dangerously low levels. Furthermore, fumehood extraction would have spread these fumes into the immediate area, and depending on the direction of the wind could have negatively affected the health of staff working in the surrounding areas. This would have been particularly true of the workup, where the DCM was simply removed via rotary evaporation. Hence, elimination of DCM from this synthesis was desired. Compounding the

issue, TFA is an extremely hazardous and corrosive acid. Use on such a large scale would have presented an extreme hazard to not only the staff working on the project, but also to any staff in the area. Disposal of these two halogenated materials was also of concern, as the waste would have to be sent off-site for disposal, incurring a high cost. Therefore, the use of any halogenated material had to be eliminated from the procedure.

In addition to the issues with the solvent and reagents, anhydrous deprotection of the Boc protecting group liberates isobutylene gas and CO₂. While the CO₂ can be safely vented and diluted in a fumehood to avoid asphyxiation, the isobutylene gas presented a flammable gas hazard. As the drive belts of the fans were not isolated as in typical synthetic laboratory fumehoods, the motor presented a sparking hazard if the volume of gas generated built up to a sufficient concentration. The total volume of flammable isobutylene gas generated was calculated to be approximately 0.5 m³. This meant that the gas had to be diluted to a volume more than 50 m³ in order to be below the lower explosive limit. Although fumehood extraction into the atmosphere may have sufficiently diluted the flammable gas, spot concentrations between the explosive concentrations of 1.8-9.6% could occur, presenting an explosion hazard.

The final issue noted was that compound **E** tended to form a foam when the solvent was removed *in vacuo*. This would result in a large volume being occupied by a relatively small mass of material. Furthermore, this foam had to be manually scraped out of the flask in order to be compacted for shipping. This amount of manual labour would be time consuming on the desired scale, and hence a precipitation method for isolation was desired.

6.1.1 Project Aims and Objectives

This project aimed to synthesize compound **E** on a multi-kilogram scale in a manner that is both safe and practical using the equipment available. In keeping with this, a one-pot synthesis was desired with no workup between the Diels Alder reaction and the Boc-deprotection steps. This would be achieved using the following steps:

1. Optimization of the Diels Alder reaction for substrate loading and reaction time.

2. Identify alternatives for the Boc-deprotection that could be performed directly from the Diels Alder reaction mixture.
3. Optimize a workup for the isolation of a salt form of compound **E**.
4. Scale up the reaction to a multi-kilogram scale using a 20 L reactor.
5. Address all the safety concerns presented with the standard method.

This work was done in collaboration with the staff at Sun Pharmaceutical Industries in Port Fairy, including Dr Stuart Purcell, Elise Neff and Dr Paul Alexander.

Primarily these reactions were conducted using jacketed reactors which were heated using Huber Dynamic Temperature Control units circulating silicone oil. Previous experience from the group had demonstrated that a temperature difference of 60 °C between the reactor contents and the reactor jacket resulted in cracking of the vessel. Hence, careful control of the temperature was required. The vessels used ranged from 500 mL to the full scale 20 L reactor.

6.2 Optimization of the Diels Alder Reaction

In order to obtain the maximum turnover of the product, the maximum loading of the Diels Alder reaction needed to be achieved, as the extended reaction time precluded further work. An initial solubility experiment was conducted to determine the maximal loading of the least soluble substrate, the diene compound **C**. At reflux temperature, it was found that the loading could be tripled compared to the provided procedure, allowing for greater throughput.

In parallel, the Diels Alder reaction between compound **C** and the dieneophile was tested using the standard method as well as the modified method using three times the reactant concentration at a 500 mL scale. Using jacketed reactors, the reactions were allowed to heat at 120 °C for 16 h, after which UPLC samples were taken and analyzed. These results showed that conversion from compound **C** to compound **D** was successful, with > 99% conversion to the desired product. Furthermore, it was found that using the elevated concentrations, the reaction time could be reduced to just 12 h. These results remained consistent at the 2 L scale,

suggesting that the Diels Alder reaction was not affected by scale. It was also noted in all cases that while the jacket temperature reached 120 °C, the internal reactor temperature never exceeded 116 °C. Despite this lower temperature, the reaction proceeded without issue.

One serious issue was found when scaling up to the 2 L reactor. Due to the amount of material being added to the solvent, the volume of the reaction expanded significantly. With the amount of material being used, 1 L of solvent expanded to 2.1 L with all the substrates either suspended or dissolved. This was not found earlier during the 500 mL scale, as the expansion was not noticed due to the proportionally larger headspace allowed the mixture to be contained. Hence, although at full scale a 20 L reactor could be used, only 10 L of solvent could be used as this was calculated to expand to the full volume upon addition of all the substrates.

It was also found that following the reaction, compound **D** would remain in solution, where compound **C** was insoluble in xylenes. This suggested that this was a safe point for holding the reaction mixture until further processing could be performed on the mixture. Storing the reaction mixture at 4 °C for a prolonged period showed no change to the reaction mixture after 5 weeks. Although this reaction mixture was stable, one of the disadvantages of having such a concentrated reaction mixture was that it tended to be quite sticky. This necessitated careful cleaning of the work area to minimize exposure and contamination.

6.3 One-Pot Feasibility and Boc-Deprotection Optimization

As we wished to perform the Boc-deprotection of compound **D** without workup, small samples of the reaction mixture previously generated were taken to assess the feasibility of performing the deprotection directly in xylenes in a one-pot method. Acids that were commonly used on site were tested to assess which of them would be the most effective for this reaction. These included 98% sulfuric acid, 81% phosphoric acid, glacial acetic acid and 37% hydrochloric acid, using TFA as a control acid. Using two equivalents of these various acids, deprotection of compound **D** was performed directly from xylenes.

These acids gave a variety of results. Interestingly, TFA gave partial conversion to

compound **E**, but did not proceed to completion. Acetic acid gave no conversion to the product, even when heated to 50 °C. Sulfuric acid and phosphoric acid both gave partial conversion to compound **E**, but resulted in precipitation of both the starting material and the product before the reaction could be completed. In the case of sulfuric acid, the material precipitated as a hard solid, whilst with phosphoric acid it formed a gel-like substance. Hydrochloric acid gave the desired product after being allowed to stir overnight at room temperature with > 99% conversion to compound **E**. This demonstrated that Boc-deprotection directly from xylenes was feasible and could be done without any workup in between.

Heating the Boc-deprotection reaction at 50 °C dramatically increased the reaction rate, reducing the time to 1 h from the overnight reaction as previously required. Optimization of the mixing on a small scale further reduced this to 40 min. In addition to reducing the reaction time and eliminating the need for halogenated reagents, the use of an aqueous acid also eliminated the formation of isobutylene gas, as the *tert*-butyl carbocation that formed would simply react with water to produce *tert*-butanol. This also eliminated the need to generate hydrogen chloride gas for the generation of hydrogen chloride in ethyl acetate, as isolation of the Boc-protected material was no longer required. Of note for the scale-up, addition of 37% hydrochloric acid to the Diels Alder reaction mixture was an exothermic process, hence chilling the reaction to 0 °C was necessary to prevent thermal runaway. In addition, the exothermic process only occurred for the first half of the addition. The second half would either maintain temperature or would cool down, allowing the rate of titration of the acid to be increased.

Upon cooling of this mixture, it was found that the product formed a viscous liquid that settled to the bottom of the reaction mixture. This phase did not redissolve effectively into xylenes when diluted and no separate aqueous phase was observed. This phase was hypothesized to be a mixture of xylenes, compound **E** and the aqueous phase. This meant that the mixture could not be held at this point and had to be processed immediately to avoid formation of this viscous liquid.

When this procedure was tested on a 500 L scale, it was found that keeping the reaction mixture at 30 °C and maintaining stirring prevented the formation of this mixed phase. Various

workups were postulated in order to isolate the material. Simply removing the solvent *in vacuo* proved problematic, as it formed a foam that filled the vessel without completely removing the solvent. Releasing the vacuum resulted in the foam collapsing into a thick tar. Addition of TBME resulted in the tar hardening into a solid block, likely due to leaching of any residual xylenes left in the tar. It was found here that addition of ethanol allowed this solid block to be manually broken up into a fluffy white solid followed by washing gave compound **E** hydrochloride salt of >99% purity by HPLC in moderate yields. Although successful, this approach was not practical on larger scales, hence a better method was sought.

6.4 Extraction Workup of Compound **E**

Rather than removing the solvent *in vacuo*, it was decided that an extraction method could be used to wash the product into an aqueous phase, then back into a different organic phase following pH adjustment to allow for easier precipitation. On a small scale, various extraction methods were attempted. Simply using water as the aqueous phase was not sufficient to extract compound **E**. Addition of dilute aqueous HCl tended to also give a viscous tar that was difficult to work with. Switching acids, an equivolume of 10% v/v acetic acid was found to effectively partition the product into the aqueous phase. Here, it was found that three separate phases formed. On top was the organic xylenes layer, containing residual product as well as the majority of the impurities. In the middle was the aqueous phase, which was found to contain a significant amount of product with few impurities. Finally, a thicker, more viscous layer formed at the bottom, which was found to be a mixture of xylenes, the product and the aqueous phase. Both the bottom mixed phase and the aqueous phases were collected, and the remaining xylenes phase could be extracted again using 10% v/v acetic acid.

Addition of 10% w/v NaOH to the combined aqueous extracts to pH 12 resulted in precipitation of compound **E**, which could be partitioned into an ethyl acetate phase over two extractions. Expectedly, this acid-base neutralization was found to be exothermic, giving a temperature rise of around 10 °C depending on scale. This neutralization could also be achieved using 30% w/v NaOH in order to reduce the total volume. Using these ethyl acetate

extracts, oxalic acid and tartaric acid were trialled as counterions for the precipitation of the product. Neither acid precipitated the product initially, but upon addition of an alcohol such as isopropanol or ethanol a fine solid formed which could be collected by filtration. UPLC analysis revealed that oxalic acid more selectively precipitated the product over the impurities, so was the preferred agent. Precipitation could also be achieved by first dissolving oxalic acid in ethanol at 25% w/v before adding it to the ethyl acetate extracts. This purification method was trialled on a 1 L scale, altering it slightly to use five smaller ethyl acetate extractions rather than two larger ones for the purposes of minimizing volumes in the reactor. Oxalic acid (25% w/v in ethanol) was then gradually added and resulted in the precipitation of a white solid. This could then be filtered and washed with a 3:1 mixture of TBME/ethanol to remove any impurities. This successfully gave compound **E** oxylate salt at >99% purity and approximately 64% yield.

6.5 20 L Pilot Scale-Up

Scaling up to a 20 L jacketed reactor, a method based on the previous findings was developed. Due to the scale, various safety measures had to be implemented in order to protect the individuals performing the work. In addition to a full protective suit, the use of double gloves, sleeve guards and air hoods were all implemented to minimize exposure to both the materials and solvents being used. All the reactors, filtration equipment, peristaltic pumps and stands were all earthed inside a walk-in fumehood. All reaction vessels were purged with N₂ to lower the O₂ level below 2% before solvents were charged into or out of the vessel. Loading the reactor also presented a challenge, as compound **C** tended to form flammable dust clouds if handled improperly. Two methods of loading were trialled. First, the container was carefully lowered into the reactor and compound **C** gently tipped into the bottom one portion at a time. Although this method minimized the dust cloud, it proved difficult to suspend material into a slurry upon addition of xylenes. Alternatively, it was found that charging the reactor with xylenes first, sealing and purging the reactor, then adding compound **C** slowly via a port suspended the solid well. The *N*-Boc-protected dieneophile could then be charged through the port. In

keeping with the previous calculations, 10 L of xylenes was expanded to approximately 19 L upon addition of all the material. This mixture was easily mixed using an overhead agitator.

Heating was carefully controlled using a ramping method to ensure the reactor was not damaged. An initial ramp to 30 °C was held for 30 min. The temperature was then successively increased by 30 °C over 30 min and held at that temperature for a further 30 min to enable the reactor contents to catch up to the jacket and minimize the temperature difference. The reactor was then held at 120 °C for 12 hours. Monitoring an internal temperature probe showed that the reactor contents only reached a maximum of 112 °C. However, UPLC analysis showed that this was still sufficient to drive the reaction to >99% conversion to compound **D** over the prescribed time. Cooling was done in a linear fashion over 2 hours to room temperature.

Following this, half the reaction contents (approximately 10 L) had to be drained in order to make room for additional reagents. The other half-batch could then be processed at a later time in the same manner. The reactor and contents were then cooled to 0 °C, and 2 equivalents of 37% HCl at 0 °C was added over 30 min using a peristaltic pump. Over the course of the addition, the temperature was closely monitored to ensure no sudden temperature jumps occurred. If the reaction mixture rose above 18 °C, the addition was stopped and allowed to cool before continuing. The reaction mixture was then heated to 50 °C, which necessitated heating the reactor jacket to 55 °C. Although on a small scale it was found that this reaction proceeded to completion in 40 min under optimal conditions, at scale it was found that even with a 1.5 h reaction time, the conversion of compound **D** to **E** did not proceed to more than 98% completion. This was postulated to be due to the mixing not being optimal, as the agitator only permitted for relatively laminar flow of the reaction mixture, where turbulent flow generally gives better mixing. In addition to the usual safety precautions used, here the vent port which was connected to a nitrogen bubbler was opened in order to effectively vent any evolved gas, preventing the build-up of pressure within the reactor.

Following the deprotection to compound **E**, the reaction mixture was cooled to 30 °C, after which 5 L of 10% v/v acetic acid was added and mixed for 10 min. The layers were allowed to separate and the bottom two layers were collected. This initial extract was found to

contain 90% of the product, hence a reduced volume of 2.5 L was used for the second aqueous extraction, retrieving the remaining 10% of the product and leaving only the impurities in the xylenes phase, which could be discarded.

Recombining the aqueous extracts, neutralization proved difficult at this scale. Initially, 30% w/v NaOH at 10 °C was simply added gradually as previously done on a small scale. Upon reaching pH 12, a white solid suddenly precipitated. However, unlike the small scale experiments where the solid remained suspended, this solid settled to the bottom of the reactor and formed a solid mass that stopped the agitator from spinning and blocked of the draining valve in the bottom of the reactor. This was eventually rescued by removing the aqueous phase and washing the reactor with ethyl acetate to redissolve the material, but was not a practical method going forward.

In an alternative approach, 4 L of ethyl acetate was first added to the aqueous extracts to enable immediate dissolution of the free-base product upon neutralization. 30% w/v NaOH was then slowly added to pH 12, again resulting in rapid precipitation of the product. Unlike the previous attempt, the product tended to form sticky round solid bodies that did not settle upon cessation of agitation. Furthermore, there was no discernible separation between the aqueous and organic phases. It was noted that upon acidification using 10% v/v acetic acid, dissolution of these solids and phase separation was again observed.

Rather than directly adjust to pH 12, an extraction at an intermediate pH was tested. The acidic aqueous extracts were charged with 6 L of ethyl acetate, after which 30% w/v NaOH was gradually added until pH 5. Interestingly, the reaction mixture did not deviate from pH 5 despite the addition of increasing amounts of the basic solution. This was likely due to the formation of sodium acetate acting as a buffer. At this pH, 3 layers were again formed; a top organic layer containing some product, a middle aqueous phase, and a lower mixed phase. The top organic phase was separated, and an additional 2 L of ethyl acetate added. The aqueous phase was then adjusted to pH 12 as before with mixing. Using this method, the rapid precipitation of the product previously observed was localized entirely to the top organic phase, with no third phase being formed. Fortunately, this suspension could be separated from the

aqueous phase and mixed with the previous ethyl acetate extract.

Using this material, precipitation as the oxylate salt was not possible using the previously developed method using 25% w/v oxalic acid in ethanol. Here, it was found that the extraction at pH 5 had partitioned compound **E** acetate salt into the organic phase, which was relatively soluble in organic solvents despite being ionized. When a sufficiently large quantity of oxalic acid was added and given enough time, counterion exchange occurred and compound **E** oxylate salt eventually precipitated. However, this was time-inefficient and could not be consistently reproduced.

Moving back to a small scale, it was found that the combined ethyl acetate extracts could be washed with a 15% w/v NaOH solution. This washed out the residual acetic acid into the aqueous phase, as well as allowing the precipitate from the second ethyl acetate extract to redissolve and form a homogeneous organic phase. Furthermore, this second basic wash seemed to also remove some impurities. Interestingly, addition of 25% w/v oxalic acid in ethanol to the organic phase no longer caused precipitation of the product. The reason for this remains unclear.

Rather than having the oxalic acid pre-dissolved in ethanol, it was found that adding the two components separately gave more consistent and repeatable precipitation of the product. Furthermore, this allowed for more controlled precipitation such that a known amount of product could be precipitated by adding the oxalic acid in portions. The resulting precipitate could be filtered, then oxalic acid added to the mother liquor again to effect the precipitation of the next crop of product. Expectedly, it was found that the amount of product precipitated corresponded linearly with the amount of oxalic acid added, suggesting a stoichiometric precipitation. This procedure was further enhanced by first adding 3:1 TBME/ethanol to allow for better formation of an easily pumped slurry upon precipitation.

Returning to the large scale, the remaining 6 L of washed ethyl acetate extract was charged with 3:1 TBME/ethanol, an extra volume of ethanol and oxalic acid added in portions. The resulting precipitate was then filtered in portions, washed with 3:1 TBME/ethanol and allowed to dry to give compound **E** oxylate salt as a white solid at >99% purity and >62%

yield. Furthermore, oxalic acid could be added to the mother liquors to recover the remaining product as the oxylate salt, further increasing the overall yield.

6.6 Final 20 L Scale Procedure

With the conclusion of these experiments, a final protocol for the synthesis of compound **E** was established:

1. Xylenes (10 L), compound **C** and the *N*-Boc-protected dieneophile are loaded into the 20 L reactor in order.
2. The reactor is purged with N₂ and heated to 120 °C over 3.5 h using a step-wise ramping process, then held at temperature for 12 h.
3. The reaction is then cooled to room temperature, half the reaction contents drained (approximately 10 L), and the remaining half-batch cooled to 0 °C.
4. 2 equivalents of 37% HCl at 0 °C is then added to the reaction mixture over 30 min, carefully monitoring the temperature to ensure it does not rise over 18 °C.
5. The reaction mixture is heated to 50 °C over 30 min and held at temperature for 1.5 h.
6. The reaction mixture is then cooled to 30 °C and 5 L of 10% v/v acetic acid is charged into the reaction and mixed for 10 min.
7. The agitation is stopped, the layers separated and the bottom two layers collected.
8. The remaining organic phase is again extracted with 2.5 L of 10% v/v acetic acid.
9. The combined aqueous extracts are charged with 6 L of ethyl acetate, then neutralized to pH 5 using 30% w/v NaOH with stirring.
10. The organic layer is separated, 2 L of fresh ethyl acetate is charged back into the remaining aqueous layer and the pH adjusted to 12 with stirring.

11. The organic layer is again separated and combined with the previous ethyl acetate extract and washed with 15% w/v NaOH.
12. A 3:1 mixture of TBME/ethanol (2 L) and absolute ethanol (2 L) are added to the ethyl acetate extracts, followed by oxalic acid.
13. The resulting precipitate is then filtered via vacuum filtration, the filter cake washed with 3:1 TBME/ethanol and allowed to dry under vacuum to give the compound **E** oxylate salt as a white powder.
14. The mother liquors can then be recovered and oxalic acid added to precipitate any remaining product as the second crop and isolated as per Step 13.

This procedure is currently being used to manufacture the successive batches of compound **E**.

6.7 Conclusion

Throughout this 5 week project, a variety of safety and scale-up issues were addressed in order to devise a method for the large-scale synthesis of compound **E**. The standard method provided proved too complicated and hazardous to be conducted on a multi-kilogram scale. Optimization of the reaction concentration and conditions has significantly reduced the reaction times. The initial Diels Alder reaction from compound **C** to **D** was reduced by 7 h, while the Boc-deprotection reaction from compound **D** to **E** was reduced by 11 h. In addition to this, no workup was required between these two reactions, greatly reducing the labour time and reducing the total amount of solvent waste generated. The final workup was also simplified such that no evaporation steps were required, as the desired product was simply precipitated as the oxylate salt following several wash steps.

In addition to the simplification of the overall procedure, many of the more hazardous reagents that were used in the standard method were eliminated. Due to the modified Boc-deprotection, DCM and TFA were no longer necessary, as the deprotection could be effected in xylenes with 37% HCl. In addition to this, moving away from anhydrous conditions eliminated

flammable gas hazard, as the *tert*-butyl carbocation formed from the Boc-deprotection would react with water to form *tert*-butanol rather than isobutylene.

This work enabled the synthesis of compound **E** without the need for any additional equipment or retrofitting of the lab to accommodate for materials that previously have not been used on site. In summary, the following improvements were made to the process over the 5 week placement:

- Loading of the reactants in the solvent was tripled, allowing for higher throughput of raw material.
- Reduction of the Diels Alder reaction time from 19 h to 12 h to provide compound **D** at > 99% conversion, reducing the process timeframe.
- Removal of the workup step where compound **D** was precipitated as the hydrochloride salt via addition of hydrogen chloride in ethyl acetate and TBME, followed by redissolution in ethyl acetate and washing with NaOH to return the free base. This eliminated excessive solvent use and further reduced processing time.
- Boc-deprotection directly from the xylenes solution without the need for DCM, substituting TFA with 37% HCl. This eliminated the generation of flammable isobutylene gas.
- Boc-deprotection time was reduced from 12 h to 1 h via heating of the reaction mixture to give compound **E** at > 99% conversion, further reducing the process timeframe.
- Complete substitution of the original workup procedure which involved a wash stepped followed by rotary evaporation to give the product as a foam that had to be manually scraped out of the vessel. Instead, the product could be purified via several rounds of washing and extraction, followed by precipitation to give compound **E** oxylate salt as a fine white powder. This procedure eliminated the need for rotary evaporation, removed the need for manually scraping the product from a vessel, and gave a much denser product compared to the free-base foam making it easier to transport.

6.7 Conclusion

These improvements have been utilized for the efficient production of compound **E** oxylate salt, and has already enabled several kilograms of product to be delivered to the client in the weeks following the conclusion of the placement.

7 Thesis Outcomes and Future Directions

Throughout this work, various topics have been explored relating to the study of opioid receptor pharmacology, as well as general opioid chemistry. Specifically, the development and synthesis of a fluorescent probe for the MOR based on the clinically used partial agonist morphine has been described. Further to this, we have commenced work on the development of a novel imaging system based on AuNRs that we hope will add another tool for the study of GPCR pharmacology. Finally, work was done to explore greener alternatives for the *N*-demethylation of alkaloids, which is an important reaction for the discovery and synthesis of opioid analogues with clinically relevant outcomes.

Chapter 2: Molecular Modelling with the Opioid Receptors

This chapter primarily focused on the 6 week rotation done with Dr David Chalmers with regards to the molecular modelling of the opioid receptors. Here, we found that subtype selectivity studies based on the antagonist crystal structures could not be performed, as no rank-based correlation between the Glide docking score and the literature K_D value was consistently observed. However, a Spearman rank correlation of 0.77 was observed for the antagonist-bound MOR crystal structure,¹ suggesting the potential of using these for the discovery of new opioids. Indeed, using the more recently published agonist crystal structure,² a novel opioid agonist for the MOR lacking some of the classical opioid side effects was discovered by Manglik *et al.*³

Moving on, MD studies were conducted using the antagonist-bound crystal structure of the MOR in an attempt to generate an agonist homology,¹ which was unavailable at the time. Using the MD program DESMOND, the reconstructed MOR docked with morphine was simulated for 70 ns. Although this failed to produce an agonist homology as desired, some interesting observations were made. Compared to the crystal structure ligand β -FNA, morphine formed different water-mediated hydrogen-bonding network. Comparison of the generated structure shows that indeed, the simulation time was insufficient in order to generate the agonist homology.

Additional work prolonging the MD simulation time could provide interesting data, giving an insight to the transition between the antagonist and agonist state and the movement

of the TM helices. However, a large amount of computer time would be required for this, potentially using a supercomputer cluster or using a Monte-Carlo approach.

Chapter 3: Fluorescent Opioid Partial Agonist Probes for the μ -Opioid Receptor

Development of agonist probes for the MOR have always been desired. Historical development has only resulted in peptide-based fluorescent opioid agonist probes. Small molecule-based fluorescent probes have previously all resulted in antagonists. Here, utilizing the clinically used opiate morphine, a partial agonist probe was successfully synthesized and characterized. A variety of linkage methods were explored to find an appropriate modification that would enable conjugation of the fluorescent tag Sulfo-Cy5 without loss of partial agonist activity. From this, the model compound **5** was developed containing an ether linkage with a free acid for further spacer elongation. Using this method, the probe compound **21** was successfully developed (Figure 31).

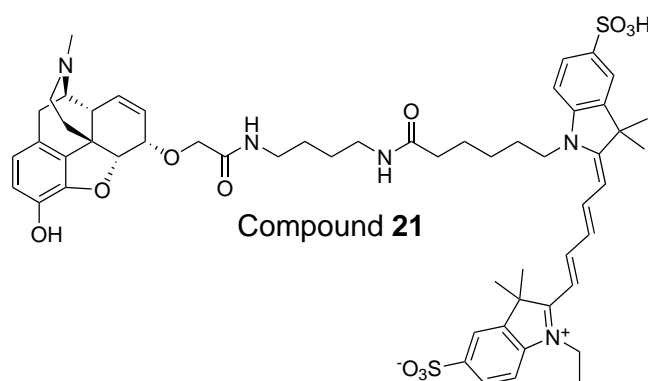


Figure 31. Compound **21**, the first morphine-Cy5 conjugate, retaining the partial agonist activity of morphine.

Although the probe was approximately an order of magnitude less potent than the parent compound, it maintained partial agonist activity, as well as specific binding to the MOR. Furthermore, little background fluorescence was observed during confocal microscopy, suggesting this compound may be a useful tool to simulate the behavior of morphine.

Currently, this probe is being used in further imaging experiments at the University of Nottingham, Queen's Medical Centre and at the Drug Discovery Biology theme of the Monash Institute of Pharmaceutical Sciences as a tool compound for visualizing the behavior of morphine under confocal microscopy. These results will aid in the understanding of MOR pharmacology, and the behavior of morphine at a cellular level. This probe could be used to explore the effects of morphine administration on receptor translocation on the cell surface, as well as to understand the trafficking pathways of the ligand upon MOR internalization. Furthermore, it may give insight into the behavior of the MOR when administered in the presence of other GPCRs that may form heterodimers. Although much fluorescence characterization of the MOR has been described in literature, no work has been done with regards to the trafficking of the ligand due to the historical lack of a suitable small-molecule fluorescent probe. This new probe may be used to fill this gap in knowledge.

Further exploration into different linkage methods and fluorophores may also lead to the development of a more potent morphine-based fluorescent probe. In addition, this method of development could be used design and synthesize other fluorescent probes based on clinically interesting MOR agonists, such as fentanyl or herkinorin. In combination with the literature data and other fluorescent probes, this could give a clearer indication as to the factors that are involved in MOR-mediated tolerance and dependence.

Chapter 4: Development of Gold Nanorod-based Imaging Systems

An exploration into the use of AuNRs as an imaging platform was conducted. Using clearly defined, discreet chemical entities, AuNRs were coated to give a variety of potential imaging tools. Utilizing morphine-based congeners based on prior data, AuNR@ZW(MorPEG 10%) was assembled. Furthermore, the DOR antagonist congener based on naltrindole was also synthesized and coated alongside MorPEG to give AuNR@ZW(MorPEG 5%, NaltPEG 5%). This multivalent AuNR system could potentially be used to image the MOR-DOR heterodimer, elucidating the mechanism by which MOR-DOR biased ligands exhibit their analgesic effects.

In order to demonstrate the robustness of this system, as well as to act as a "control"

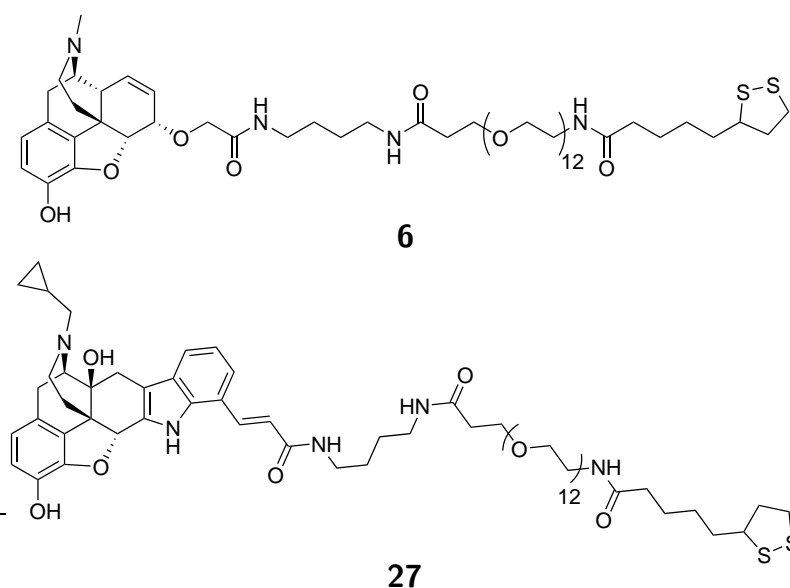


Figure 32. The two opioid-based congeners synthesized for attachment to AuNRs. Compound **6** was based on the clinically used opiate morphine, while **27** was based on the well known DOR antagonist naltrindole.

system, the adenosinergic ligand NECA was functionalized to give **34** (Figure 33), conjugated to AuNRs in the same fashion as the morphine congener to give AuNR@ZW(NECA-PEG 5 or 10%). This system is currently undergoing further study at the University of Nottingham, Queen's Medical Centre as a potential imaging agent for visualizing the adenosine receptors. Differences between it and the literature NECA-BODIPY conjugate could reveal differing pharmacologies when receptors act as single units compared to oligomers.⁴

Further work may be conducted in order to optimize the coating of these systems such that they may be used directly without the need to exchange buffers to something more biologically suitable. Full biological characterization of these nanoparticle systems, particularly of AuNR@ZW(MorPEG 5%, NaltPEG 5%), needs to be carried out. This could reveal previously unknown behaviors of MOR-DOR heterodimer trafficking, giving a better understanding of the dimer biases involved in these drugs. Other clinically interesting ligands such as fentanyl or oxycodone could also be integrated into this approach, giving more insight into the receptor trafficking behavior of these drugs in a heterodimer paradigm. Critical to all of this

is the development of an imaging approach that enables visualization of both the AuNR using a multi-photon luminescence method, as well as seeing organic or biological fluorophores using a standard confocal microscopy approach. While this is still under development, other approaches may be used in the interim to utilize the currently available facilities, such as switching out the AuNRs for QDs.

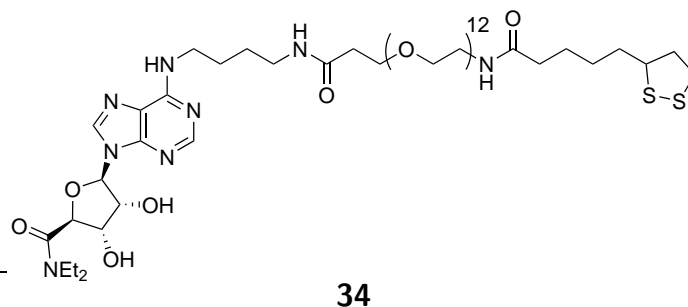


Figure 33. A congener based on the previously used adenosinergic ligand NECA, which was synthesized to act as a control system for comparison to previously established literature NECA-based organic fluorescent probes.

Further experiments need to be done in order to develop an imaging protocol for the visualization of both the nanoparticle tag in conjunction with the organic fluorophores that are typically used to visualize proteins and other small molecules. The development of such a method would allow a variety of imaging tags to be used together without interference. Should these be successful, imaging studies using AuNRs decorated with multiple ligands could be done in order to determine the effect the formation of heterodimers has on receptor trafficking.

Chapter 5: Alternative Catalysts for Non-Classical Polonovski

N-Demethylation of Alkaloids

$\text{Fe}_3(\text{CO})_{12}$ was explored as an alternative catalyst for the *N*-demethylation of alkaloids. This organic soluble iron(0)-carbonyl complex was found to rapidly catalyse this reaction in a variety of green solvents such as isopropanol and ethyl acetate as suggested by the GSK guide to solvent selection.⁵ Although the majority of the alkaloids tested proceeded to completion with good

to reasonable yields, further optimization of each alkaloid may be required to achieve optimal yield using this solution-phase catalyst. Further to this, it was found that a mixture of 9:1 ethyl acetate/isopropanol was an ideal solvent to facilitate this reaction with a variety of alkaloids, although optimization of this may further increase the yield. Further to this work, optimization of the precursor *N*-oxidation step was performed using a green chemistry methodology. Using hydrogen peroxide and methanol instead of the typical *m*CPBA in chloroform, a method for generating DXM *N*-oxide was developed that did not require further use of any solvents and produced minimal waste.

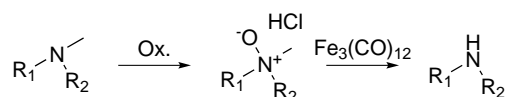


Figure 34. The non-classical Polonovski reaction utilizing $\text{Fe}_3(\text{CO})_{12}$ as the catalytic species. Oxidation can be achieved using a variety of methods. The *N*-demethylation could be carried out in a variety of solvents, with optimal conditions depending on the alkaloid.

Further exploration of green chemistry methodologies for this reaction could be done in order to reduce the environmental impact and waste produced from this clinically important reaction. Catalyst exploration and solvent substitution could be done in order to further explore the scope of this reaction. One possible alternative catalyst could be iron pentacarbonyl ($\text{Fe}(\text{CO})_5$), a liquid iron complex that is cheaper compared to $\text{Fe}_3(\text{CO})_{12}$ and can potentially be recovered via distillation. Other directions may be to explore iron complexes that may be amenable to solid support to be used in continuous flow processes, or to explore solvent-free methods.

Chapter 6: Industrial Placement at Sun Pharmaceutical Industries

A five week placement at Sun Pharmaceutical Industries was conducted working on the optimization of two reactions for the synthesis of compound **E**. As a part of this optimization, hazardous reagents and issues with scale were addressed to ensure the synthesis could be carried out in a safe manner. For this work, a procedure provided by a third party was modified to

reduce the turnover time and to improve the safety of the procedure.

The procedure was modified to remove the intermediate workup step, as well as drastically reducing the reaction and processing times. The total reaction time was reduced by 21 h overall in addition eliminating more than half of the workup time. Furthermore, the modified procedure eliminated the need for any halogenated solvents and reagents, making the process much safer for both the staff working on the project and for the staff on site, as the safety equipment available was not rated to handle these types of materials. Finally, the procedure was modified to eliminate the need to evaporate solvents, giving the final product compound **E** by extraction and precipitation as an oxylate salt.

References

- (1) Manglik, A., Kruse, A. C., Kobilka, T. S., Thian, F. S., Mathiesen, J. M., Sunahara, R. K., Pardo, L., Weis, W. I., Kobilka, B. K., and Granier, S., (2012). Crystal structure of the μ -opioid receptor bound to a morphinan antagonist. *Nature* 485, 321–326.
- (2) Huang, W., Manglik, A., Venkatakrisnan, A. J., Laeremans, T., Feinberg, E. N., Sanborn, A. L., Kato, H. E., Livingston, K. E., Thorsen, T. S., Kling, R. C., Granier, S., Gmeiner, P., Husbands, S. M., Traynor, J. R., Weis, W. I., Steyaert, J., Dror, R. O., and Kobilka, B. K., (2015). Structural insights into μ -opioid receptor activation. *Nature* 524, 315–321.
- (3) Manglik, A., Lin, H., Aryal, D. K., McCorvy, J. D., Dengler, D., Corder, G., Levit, A., Kling, R. C., Bernat, V., Hübner, H., Huang, X.-P., Sassano, M. F., Giguère, P. M., Löber, S., Duan, D., Scherrer, G., Kobilka, B. K., Gmeiner, P., Roth, B. L., and Shoichet, B. K., (2016). Structure-based discovery of opioid analgesics with reduced side effects. *Nature* 537, 185–190.
- (4) Middleton, R. J., Briddon, S. J., Cordeaux, Y., Yates, A. S., Dale, L., George, M. W., Baker, J. G., Hill, S. J., and Kellam, B., (2007). New fluorescent adenosine A₁-receptor agonists that allow quantification of ligand - receptor interactions in microdomains of single living cells. *J. Med. Chem.* 50, 782–793.
- (5) Henderson, R. K., Jiménez-González, C., Constable, D. J. C., Alston, S. R., Inglis, G. G. a., Fisher, G., Sherwood, J., Binks, S. P., and Curzons, A. D., (2011). Expanding GSK's solvent selection guide - embedding sustainability into solvent selection starting at medicinal chemistry. *Green Chem.* 13, 854–862.

8 Appendix

8.1 Molecular Modelling Compounds

The compound libraries used throughout the molecular modelling studies (Chapter 2) are shown here. Where compounds have a common or clinically used name, these have been used. For novel compounds the author, year and compound number are listed. The following references were used to assemble the subtype selectivity, training and test libraries.

Carroll, F. I.; Zhang, L.; Mascarella, S. W.; Cantrell, B. E.; Zimmerman, D. M.; Thomas, J. B. Discovery of the First *N*-Substituted 4 β -Methyl-5-(3-Hydroxyphenyl)morphinan to Possess Highly Potent and Selective Opioid δ Receptor Antagonist Activity. *J. Med. Chem.* **2004**, *47* (2), 2-5.

Coop, A.; Rothman, R. B.; Dersch, C.; Partilla, J.; Porreca, F.; Davis, P.; Jacobson, A. E.; Rice, K. C. δ Opioid Affinity and Selectivity of 4-Hydroxy-3-Methoxyindolomorphinan Analogues Related to Naltrindole. *J. Med. Chem.* **1999**, *42* (9), 1673-1679.

Fujii, H.; Hayashida, K.; Saitoh, A.; Yokoyama, A.; Hirayama, S.; Iwai, T.; Nakata, E.; Nemoto, T.; Sudo, Y.; Uezono, Y.; Yamada, M.; Nagase, H. Novel Delta Opioid Receptor Agonists with Oxazatricyclodecane Structure. *ACS Med. Chem. Lett.* **2014**, *5* (4), 368-372.

Grundt, P.; Jales, A. R.; Traynor, J. R.; Lewis, J. W.; Husbands, S. M. 14-Amino, 14-Alkylamino, and 14-Acylamino Analogues of Oxymorphone. Differential Effects on Opioid Receptor Binding and Functional Profiles. *J. Med. Chem.* **2003**, *46* (8), 1563-1566.

Healy, J. R.; Bezawada, P.; Shim, J.; Jones, J. W.; Kane, M. A.; MacKerell, A. D.; Coop, A.; Matsumoto, R. R. Synthesis, Modeling, and Pharmacological Evaluation of UMB 425, a Mixed μ Agonist/ δ Antagonist Opioid Analgesic with Reduced Tolerance Liabilities. *ACS Chem. Neurosci.* **2013**, *4* (9), 1256-1266.

Li, G.; Aschenbach, L. C.; Chen, J.; Cassidy, M. P.; Stevens, D. L.; Gabra, B. H.; Selley, D. E.; Dewey, W. L.; Westkaemper, R. B.; Zhang, Y. Design, Synthesis, and Biological Evaluation of 6 α - and 6 β -*N*-Heterocyclic Substituted Naltrexamine Derivatives as μ Opioid Receptor Selective Antagonists. *J. Med. Chem.* **2009**, *52* (5), 1416-1427.

Mclamore, S.; Ullrich, T.; Rothman, R. B.; Xu, H.; Dersch, C.; Coop, A.; Davis, P.; Porreca, F.; Jacobson, A. E.; Rice, K. C. Effect of *N*-Alkyl and *N*-Alkenyl Substituents in Noroxymorphindole, 17-Substituted-6,7-Dehydro-4,5 α -Epoxy-3,14-Dihydroxy-6,7:2'3'-indolomorphinans, on Opioid Receptor Affinity, Selectivity, and Efficacy. *J. Med. Chem.* **2001**, *44* (9), 1471-1474.

Yuan, Y.; Zaidi, S. A.; Elbegdorj, O.; Aschenbach, L. C. K.; Li, G.; Stevens, D. L.; Scoggins, K. L.; Dewey, W. L.; Selley, D. E.; Zhang, Y. Design, Synthesis, and Biological Evaluation of 14-Heteroaromatic-Substituted Naltrexone Derivatives: Pharmacological Profile Switch from Mu Opioid Receptor Selectivity to Mu/kappa Opioid Receptor Dual Selectivity. *J. Med. Chem.* **2013**, *56* (22), 9156-9169.

Li, F.; Gaob, L.; Yin, C.; Chen, J.; Liu, J.; Xie, X.; Zhang, A. Synthesis and Opioid Receptor Activity of Indolopropellanes. *Bioorg. Med. Chem. Lett.* **2009**, *19* (16), 4603-4606.

Portoghese, P. S.; Moe, S. T.; Takemori, A. E. A Selective δ_1 Opioid Receptor Agonist Derived from Oxymorphone. Evidence for Separate Recognition Sites for δ_1 Opioid Receptor Agonists and Antagonists. *J. Med. Chem.* **1993**, *36* (17), 2572-2574.

Spetea, M.; Greiner, E.; Aceto, M. D.; Harris, L. S.; Coop, A.; Schmidhammer, H. Effect of a 6-Cyano Substituent in 14-Oxygenated *N*-Methylmorphinans on Opioid Receptor Binding and Antinociceptive Potency. *J. Med. Chem.* **2005**, *48* (15), 5052-5055.

Thomas, J. B.; Herault, X. M.; Rothman, R. B.; Atkinson, R. N.; Burgess, J. P.; Mascarella, S. W.; Dersch, C. M.; Xu, H.; Flippen-Anderson, J. L.; George, C. F.; Carroll, F. I. Factors Influencing Agonist Potency and Selectivity for the Opioid δ Receptor Are Revealed in Structure-Activity Relationship Studies of the 4-[(*N*-Substituted-4-Piperidinyl)arylamino]-*N,N*-Diethylbenzamides. *J. Med. Chem.* **2001**, *44* (6), 972-987.

Wu, H.; Smith, T. A.; Huang, H.; Wang, J. B.; Deschamps, J. R.; Coop, A. Functionalization of the 6,14-Bridge of the Orvinols. Part 3: Preparation and Pharmacological Evaluation of 18- and 19-Hydroxyl Substituted Orvinols. *Bioorg. Med. Chem. Lett.* **2007**, *17* (17), 4829-4831.

Zhang, Y.; Lee, Y. S.; Rothman, R. B.; Dersch, C. M.; Deschamps, J. R.; Jacobson, A. E.; Rice, K. C. Probes for Narcotic Receptor Mediated Phenomena. 39. Enantiomeric *N*-Substituted benzofuro[2,3-*c*]pyridin-6-ols: Synthesis and Topological Relationship to Oxide-Bridged Phenylmorphans. *J. Med. Chem.* **2009**, *52* (23), 7570-7579.

Chen, Z.; Davies, E.; Miller, W. S.; Shan, S.; Valenzano, K. J.; Kyle, D. J. Design and Synthesis of 4-Phenyl Piperidine Compounds Targeting the Mu Receptor. *Bioorg. Med. Chem. Lett.* **2004**, *14*, 5275-5279.

Goehring, R. R.; Whitehead, J. F. W.; Brown, K.; Islam, K.; Wen, X.; Zhou, X.; Chen, Z.; Valenzano, K. J.; Miller, W. S.; Shan, S.; Kyle, D. J. 1,3-Dihydro-2,1,3-Benzothiadiazol-2,2-Diones and 3,4-Dihydro-1*H*-2,1,3-Benzothidiazin-2,2-Diones as Ligands for the NOP Receptor. *Bioorg. Med. Chem. Lett.* **2004**, *14*, 5045-5050.

Hayashi, S.; Hirao, A.; Imai, A.; Nakamura, H.; Murata, Y.; Ohashi, K.; Nakata, E. Novel

Non-Peptide Nociceptin/orphanin FQ Receptor Agonist,
1-[1-(1-Methylcyclooctyl)-4-Piperidinyl]-2-[(3*R*)-3-Piperidinyl]-1*H*-Benzimidazole: Design,
Synthesis, and Structure-Activity Relationship of Oral Receptor Occupancy in the Brain for
Orally Potent Antianxiety Drug. *J. Med. Chem.* **2009**, *52* (3), 610-625.

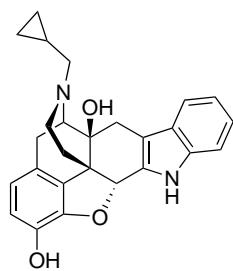
Jong, L.; Zaveri, N.; Toll, L. The Design and Synthesis of a Novel Quinolizidine Template for
Potent Opioid and Opioid Receptor-like (ORL1, NOP) Receptor Ligands. *Bioorg. Med.
Chem. Lett.* **2004**, *14* (1), 181-185.

Lattanzi, R.; Spetea, M.; SchÄijllner, F.; Rief, S. B.; Krassnig, R.; Negri, L.; Schmidhammer,
H. Synthesis and Biological Evaluation of 14-Alkoxymorphinans. 22. Influence of the
14-Alkoxy Group and the Substitution in Position 5 in 14-Alkoxymorphinan-6-ones on in
Vitro and in Vivo Activities. *J. Med. Chem.* **2005**, *48* (9), 3372-3378.

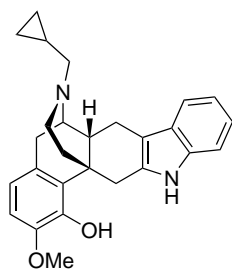
Wentland, M. P.; Duan, W.; Cohen, D. J.; Bidlack, J. M. Selective Protection and
Functionalization of Morphine: Synthesis and Opioid Receptor Binding Properties of
3-Amino-3-Desoxymorphine Derivatives. *J. Med. Chem.* **2000**, *43* (19), 3558-3565.

Renton, P.; Green, B.; Maddaford, S.; Rakhit, S.; Andrews, J. S. NOpiates: Novel Dual
Action Neuronal Nitric Oxide Synthase Inhibitors with μ -Opioid Agonist Activity. *ACS Med.
Chem. Lett.* **2012**, *3* (3), 227-231.

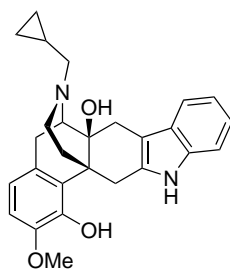
8.1.1 Subtype Selectivity Ligands



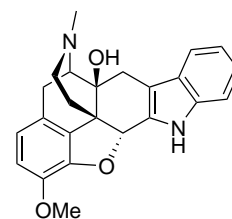
Carrol_2004_NT1



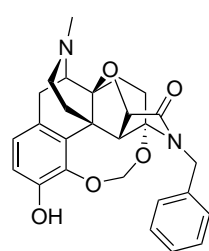
Coop_1999_13



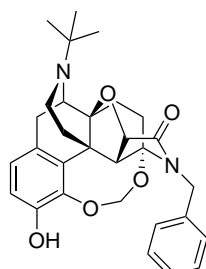
Coop_1999_23



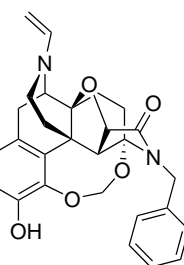
Coop_1999_OMI



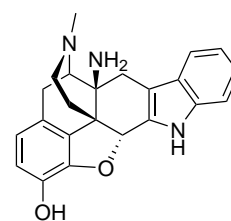
Fujii_2014_4c



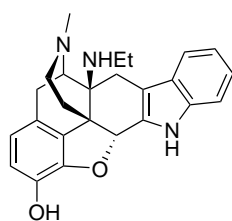
Fujii_2014_4d



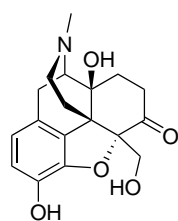
Fujii_2014_4e



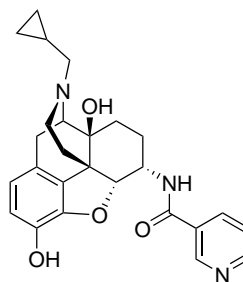
Grundt_2003_4



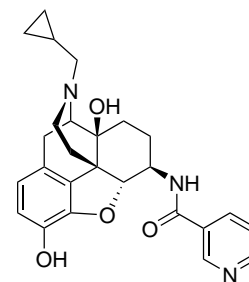
Grundt_2003_5a



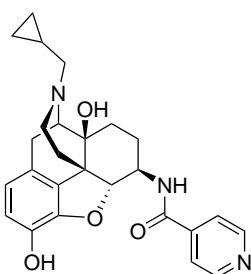
Healy_2013_UMB425



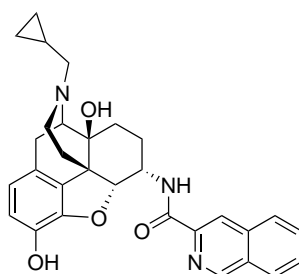
Li_2009_3



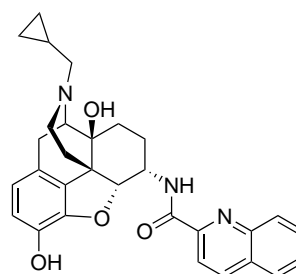
Li_2009_4



Li_2009_6

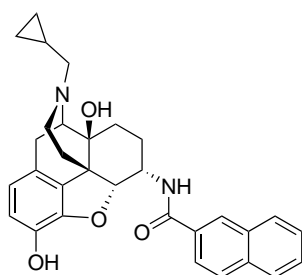


Li_2009_9

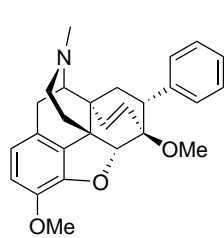


Li_2009_11

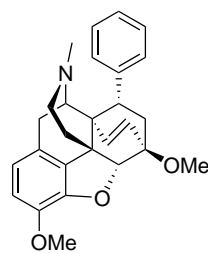
8.1 Molecular Modelling Compounds



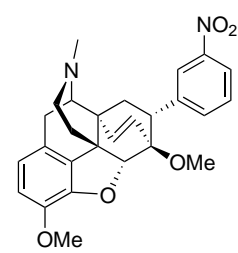
Li_2009_15



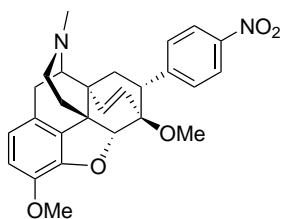
Li_2010_1



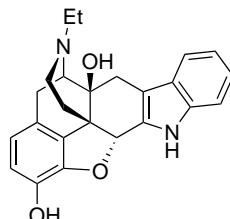
Li_2010_2



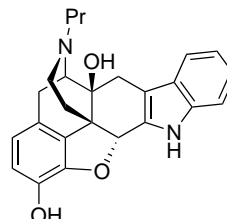
Li_2010_4



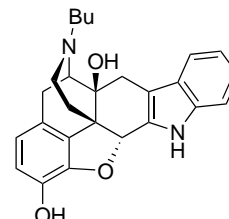
Li_2010_6



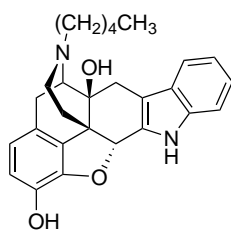
Mclamore_2001_2



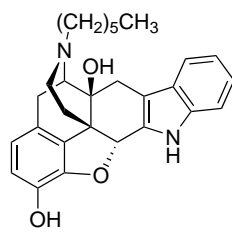
Mclamore_2001_3



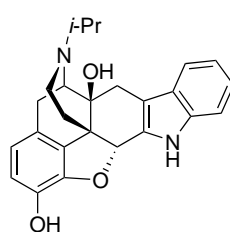
Mclamore_2001_4



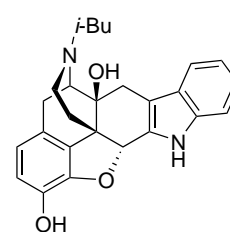
Mclamore_2001_5



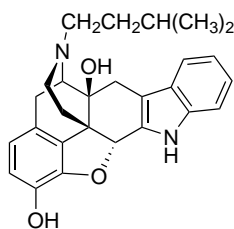
Mclamore_2001_6



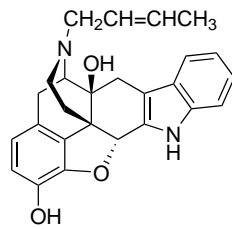
Mclamore_2001_8



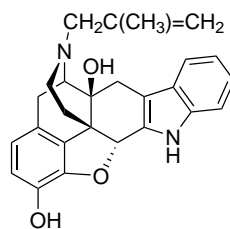
Mclamore_2001_9



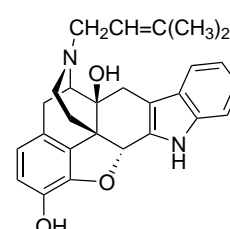
Mclamore_2001_10



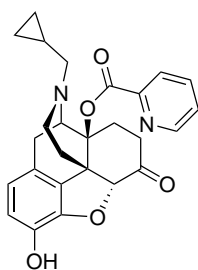
Mclamore_2001_11



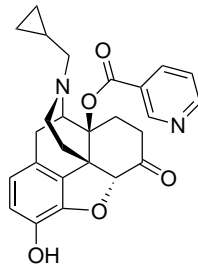
Mclamore_2001_12



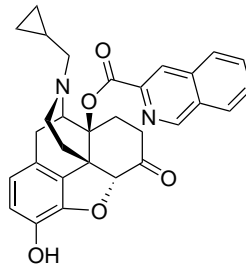
Mclamore_2001_13



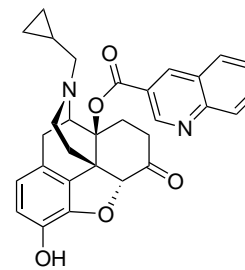
Yuan_2013_2



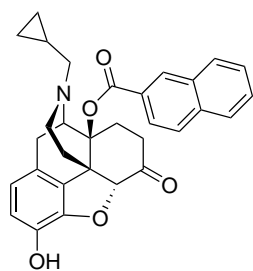
Yuan_2013_3



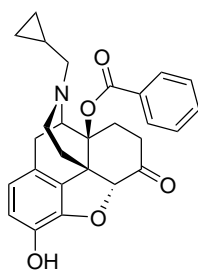
Yuan_2013_6



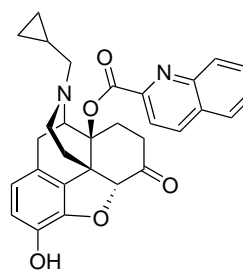
Yuan_2013_8



Yuan_2013_9

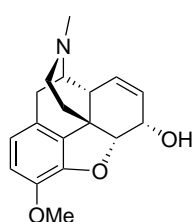


Yuan_2013_13

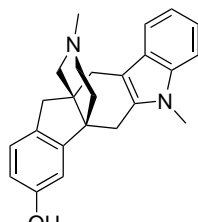


Yuan_2013_15

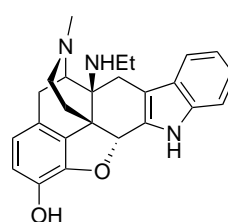
8.1.2 Training Set Compounds



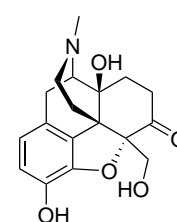
Codeine



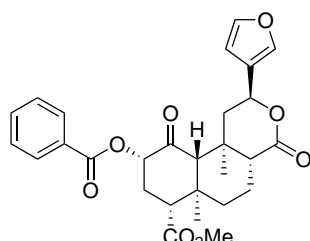
Fuying_2009_7b



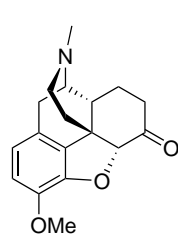
Grundt_2003_5a



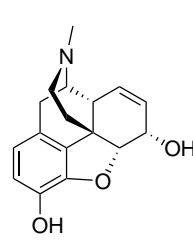
Healy_2013_UMB425



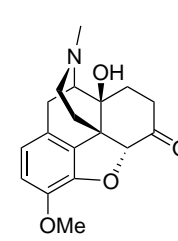
Herkinorin



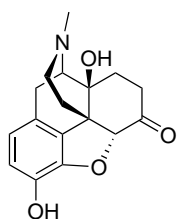
Hydrocodone



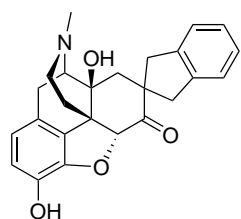
Morphine



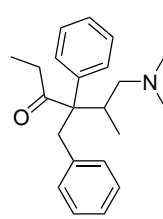
Oxycodone



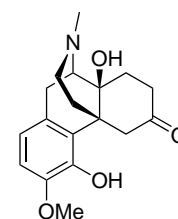
Oxymorphone



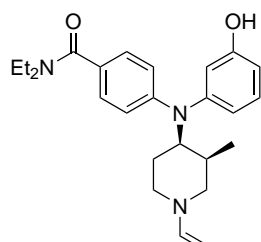
Portoghese_1993_SIOM



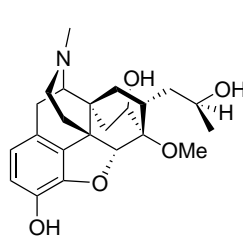
Propoxyphene



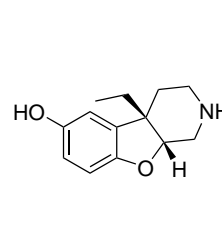
Spetea_2005_4



Thomas_2001_21

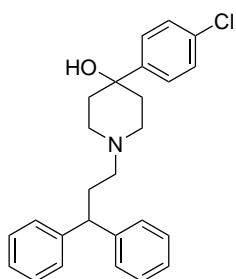


Wu_2007_UMB95

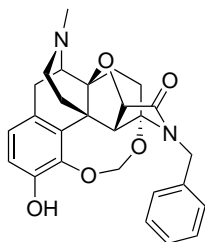


Zhang_2009_20

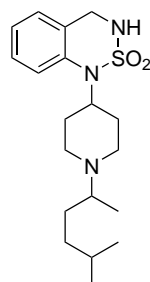
8.1.3 Test Set compounds



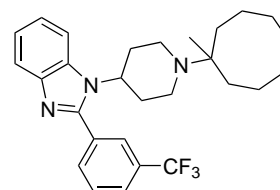
Chen_2004_1b



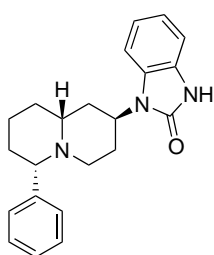
Fujii_2014_4c



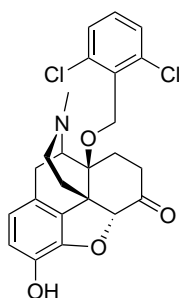
Goehring_2004_20j



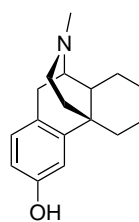
Hayashi_2009_36



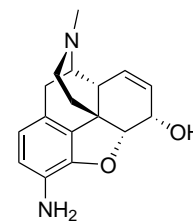
Jong_2004_14135



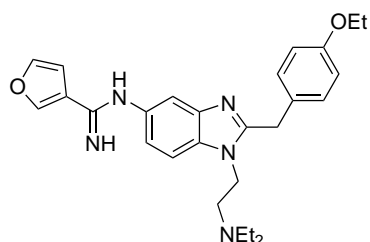
Lattanzi_2005_10



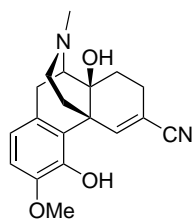
Levorphanol



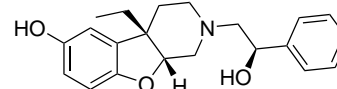
Wentland_2000_16



Renton_2012_30



Spetea_2005_1



Zhang_2009_24

8.2 Characterization of Nitro vs Nitroso Derivatives of Naltrindole

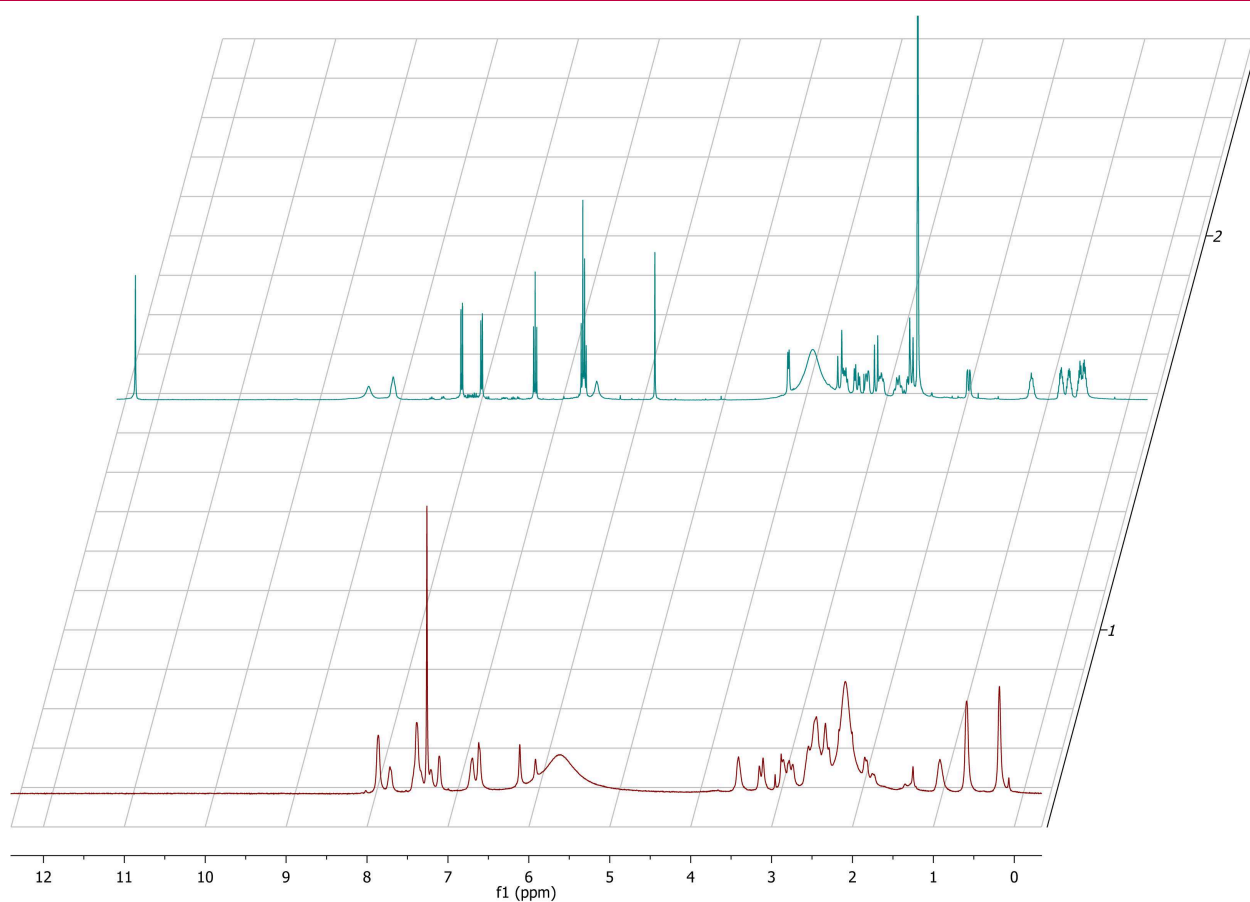


Figure 35. NMR spectra of the apparent 7'-nitroso naltrindole (CDCl₃, spectra 1, red) compared to the starting material **18** (DMSO-d₆, spectra 2, turquoise). Although the general features of the structure are evident (such as the cyclopropyl methyl group (0 - 1 ppm) and the aromatic signals, no fine splitting was observed. Deconvolution of the alkyl region was also not possible due to signal overlap.

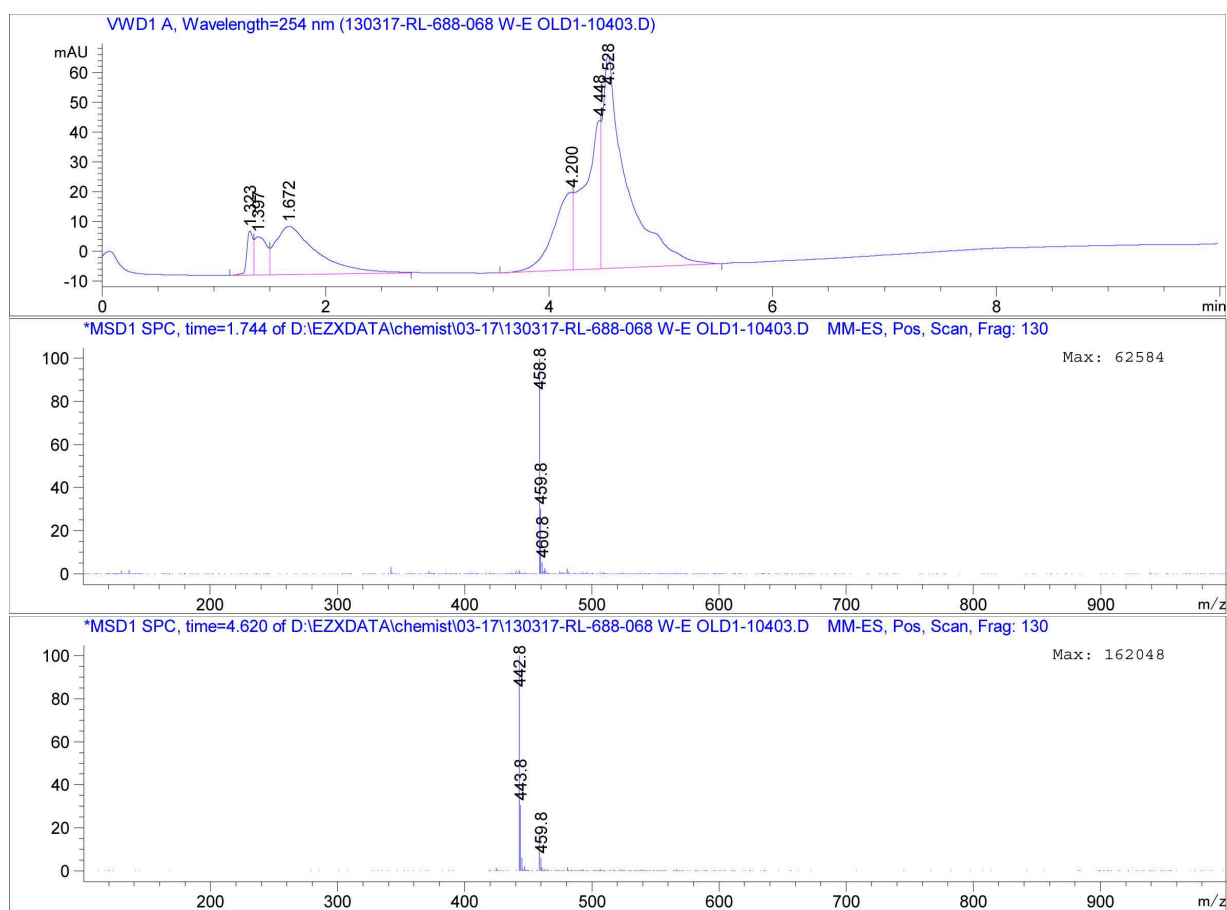


Figure 36. LC-MS spectra of the reduction of **18** using Pd/C in an H₂ atmosphere (60 PSI). The 459 mass corresponds to the starting material, whilst the 443 mass suggests reduction to the nitroso compound.

8.3 Characterization of Attempted 2-Aminophenylhydrazine Synthesis

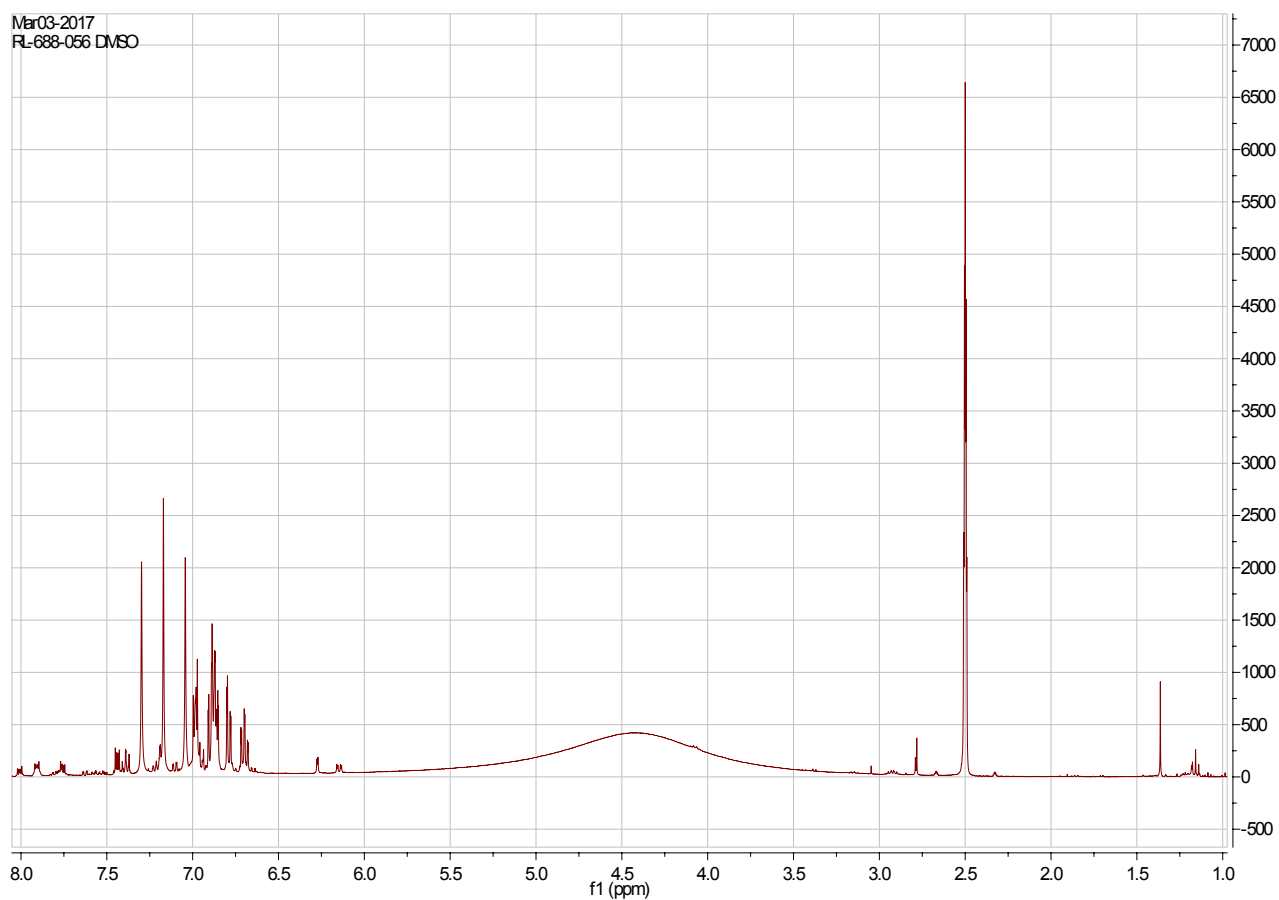


Figure 37. Crude NMR of the attempted synthesis of 2-aminophenylhydrazine (DMSO- d_6 , 401 MHz). Compound **28** was reduced using Pd/C under an H_2 atmosphere, followed by deprotection using TFA, after which this crude spectra was acquired. This spectra suggests degradation of the sample, with no clear evidence of product formation.

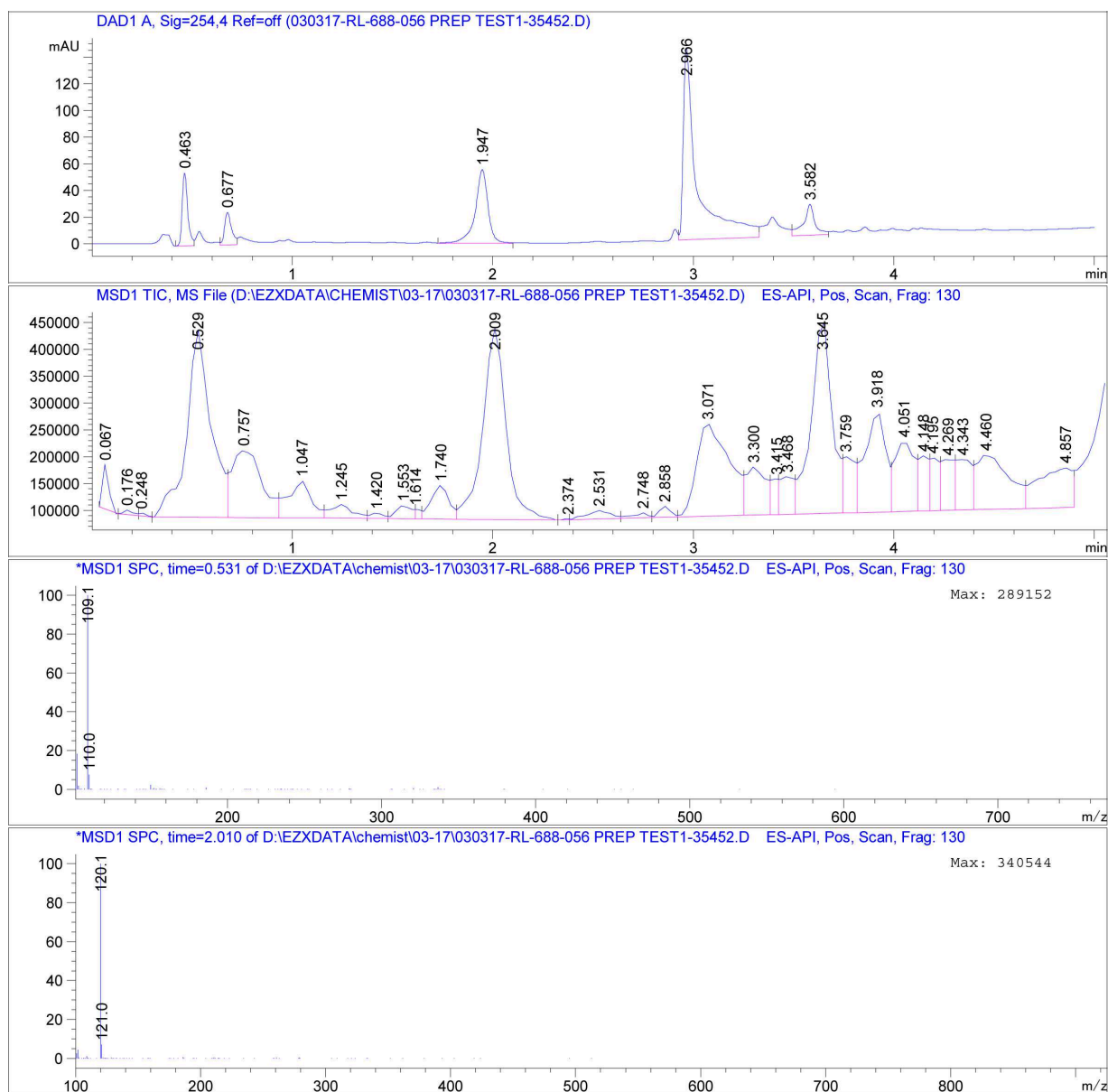


Figure 38. LC-MS data of the attempted synthesis of 2-aminophenylhydrazine. Here, 4 clear peaks were observed by UV-Vis absorbance, corresponding to 4 different byproducts. Two of these were identified by mass as being 1,2-phenylenediamine (109 m/z) and benzotriazole (120 m/z). No indication of the desired hydrazine was observed.

8.4 Zwitterionic Modification of Ultrasmall Iron Oxide Nanoparticles for Reduced Protein Corona Formation (Paper)

Karina Pombo-García ^{+, [a]}, Carmen L. Rühl ^{+, [c]}, Raymond Lam ^[b], José A. Barreto ^[d], Ching-Seng Ang ^[e], Peter J. Scammells ^[b], Peter Comba ^[c], Leone Spiccia†^[d], Bim Graham ^{*[b]}, Tanmaya Joshi ^{*[a]} and Holger Stephan ^{*[a]}

In memory of Leone Spiccia

⁺ These authors contributed equally to this work.

^[a] Institute of Radiopharmaceutical Cancer Research, Helmholtz-Zentrum

Dresden-Rossendorf, 01328 Dresden, Germany. Email:h.stephan@hzdr.de, t.joshi@hzdr.de.

^[b] Monash Institute of Pharmaceutical Sciences, Monash University, Parkville, Victoria 3052, Australia. Email:Bim.Graham@monash.edu.

^[c] Institute of Inorganic Chemistry and Interdisciplinary Centre for Scientific Computing, Heidelberg University, Im Neuenhimer Feld 270, 69120 Heidelberg, Germany.

^[d] School of Chemistry, Monash University, Clayton, Victoria 3800, Australia.

^[e] BIO21 Molecular Science and Biotechnology Institute, The University of Melbourne, Melbourne, Victoria 3010, Australia.

This work was performed by Karina Pombo-García and Carmen L. Rühl investigating utility of zwitterionic coatings on nanoparticles and their resistance to protein-corona formation. The zwitterionic ligand "ZW-L1" was synthesized as the contribution to this work. Screening against a selection of model proteins showed this particular coating performed well, adhering to the fewest number of proteins of the coatings tested, as well as having low protein adsorption.



Zwitterionic Modification of Ultrasmall Iron Oxide Nanoparticles for Reduced Protein Corona Formation

Karina Pombo-García^{+, [a]} Carmen L. Rühl^{+, [c]} Raymond Lam,^[b] José A. Barreto,^[d] Ching-Seng Ang,^[e] Peter J. Scammells,^[b] Peter Comba,^[c] Leone Spiccia†,^[d] Bim Graham,^{*, [b]} Tanmaya Joshi,^{*, [a]} and Holger Stephan^{*, [a]}

In memory of Leone Spiccia

Polyacrylic-acid-coated ultra-small super-paramagnetic iron oxide nanoparticles were surface-modified with low-molecular-weight sulfobetaines or 3-(diethylamino)propylamine in order to generate nanoparticles with zwitterionic character (ZW-NPs). The ZW-NPs proved highly resistant to serum protein corona formation in vitro, as revealed by atomic force microscopy, SDS-PAGE and proteomics analysis, and exhibited low cytotoxicity towards A431 and HEK293 cells. The presence of unreacted carboxylic acid groups enabled additional functionalization with fluorescent (Cy5) and radioactive [⁶⁴Cu-dmptacn; dmptacn = 1,4-bis(2-pyridinylmethyl)-1,4,7-triazacyclononane] moieties. Overall, the ZW-NPs represent promising platforms for the development of new multimodal diagnostic/therapeutic agents possessing "stealth" properties.

icity towards A431 and HEK293 cells. The presence of unreacted carboxylic acid groups enabled additional functionalization with fluorescent (Cy5) and radioactive [⁶⁴Cu-dmptacn; dmptacn = 1,4-bis(2-pyridinylmethyl)-1,4,7-triazacyclononane] moieties. Overall, the ZW-NPs represent promising platforms for the development of new multimodal diagnostic/therapeutic agents possessing "stealth" properties.

Introduction

The success of ultrasmall superparamagnetic iron oxide nanoparticles (USPIONS) in in vivo biomedical applications, such as magnetic resonance imaging (MRI), relies on chemical modifications that lead to controlled biodistribution, reduced toxicity and extended circulation times of these particles within the

bloodstream.^[1–8] Appropriate surface modification of USPIONS so as to fulfill these pharmacokinetic requirements presents a key challenge. It is particularly important that USPIONS are able to resist extensive nonspecific adsorption of proteins (formation of a "protein corona") and opsonization, so as to avoid rapid scavenging by the mononuclear phagocyte system.^[1,2,6–10] One way to achieve this is through the introduction of zwitterionic species onto the nanoparticle (NP) surface.^[1,2,6,10–27] Zwitterionic surfaces confer antifouling properties similar to poly(ethylene glycol) (PEG) coatings, but without adding substantially to the hydrodynamic size of the coated NPs. Zwitterionic NPs (ZW-NPs) are also less prone to aggregation under high ionic strength conditions.^[1,17,21,24–32]

Recently, we reported a detailed in vitro investigation of the "stealth" properties of USPIONS coated with a 3-(dimethylamino)propylamine derivative of poly(maleic anhydride-alt-1-decene) (PMAL), an amphiphilic zwitterionic polymer.^[15,33] The PMAL-USPIONS proved superior to USPIONS coated with octylamine-modified polyacrylic acid, a negatively charged polymer, in terms of their ability to resist protein corona formation.^[15] Encouraging results from that study, along with a continued interest in developing NP-based multimodal imaging agents for in vivo use, have now led us to investigate the effect of zwitterionic modifications on the properties of polyacrylic-acid-coated USPIONS (PAA-USPIONS). Herein, we present the results of a study examining the serum protein adsorption characteristics, cellular uptake and cytotoxicity of PAA-USPIONS functionalized with three low-molecular-weight compounds that impart zwitterionic character to the NP surface. Given that previous studies have shown that the interactions of NPs with proteins and cells are nanomaterial-specific and dictate their ultimate metabolic fate,^[10,14,16,21–23,27,30,34–38] examination of such

[a] Dr. K. Pombo-García,⁺ Dr. T. Joshi, Dr. H. Stephan
Institute of Radiopharmaceutical Cancer Research
Helmholtz-Zentrum Dresden-Rossendorf
01328 Dresden (Germany)
E-mail: h.stephan@hzdr.de
t.joshi@hzdr.de

[b] R. Lam, Prof. P. J. Scammells, Assoc. Prof. B. Graham
Monash Institute of Pharmaceutical Sciences
Monash University
Parkville, VIC 3052 (Australia)
E-mail: bim.graham@monash.edu

[c] C. L. Rühl,⁺ Prof. P. Comba
Heidelberg University
Institute of Inorganic Chemistry and Interdisciplinary Centre for Scientific Computing
Im Neuenheimer Feld 270, 69120 Heidelberg (Germany)

[d] Dr. J. A. Barreto, Prof. L. Spiccia†
School of Chemistry
Monash University
Clayton, VIC 3800 (Australia)

[e] Dr. C.-S. Ang
BIO21 Molecular Science and Biotechnology Institute
The University of Melbourne
Melbourne, VIC 3010 (Australia)

[*] These authors contributed equally to this work.

Supporting information and the ORCID identification number(s) for the author(s) of this article can be found under <http://dx.doi.org/10.1002/cplu.201700052>.



This article is part of the "Biofest" Special Issue. To view the complete issue, visit: <https://doi.org/10.1002/cplu.v82.4>.

8.4 Zwitterionic Modification of Ultrasmall Iron Oxide Nanoparticles for Reduced Protein Corona Formation (Paper)

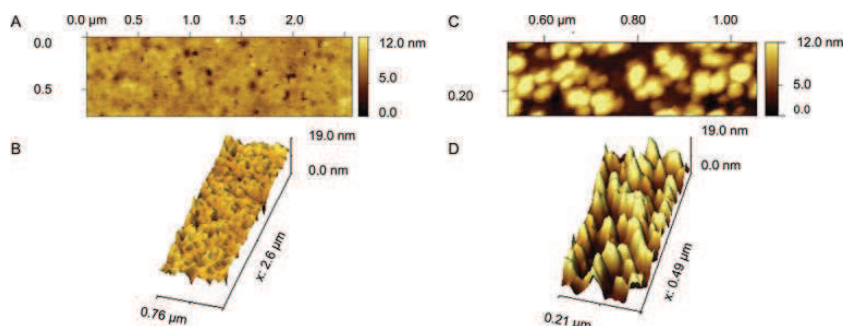


Figure 3. AFM micrographs of ZW-L1 (A and B) and PAA-USPIONs (C and D) after incubation with 80% HS for 30 min. Panels A and C show height images (scan size = 2.6×0.76 nm); B and D show 3D images (scan size = 0.21×0.49 nm).

would decrease the amount of free carboxylic acid groups in ZW-NPs, the relative intensities of these bands are lower in the spectra of ZW-L1, ZW-L2, and ZW-L3. Prominent bands in the region of $1100\text{--}850\text{ cm}^{-1}$ correspond to C-H_{bend} , $\text{S=O}_{\text{stretch}}$, and $\text{S-O}_{\text{stretch}}$ vibrations. Amide I and II bands are visible between 1500 and 1600 cm^{-1} , as is an $\text{Fe-O}_{\text{stretch}}$ vibration band at 580 cm^{-1} .^[2]

The ZW-NPs displayed good colloidal stability under physiological conditions, with no signs of aggregation in response to pH changes in the range of 6–10 after 24 h incubation. Figure 2E shows representative photographs of aqueous dispersions of ZW-L1 at different pH, thus demonstrating their stability.

Analysis of serum protein–nanoparticle interactions

The ability of the ZW-NPs to resist serum protein adsorption was evaluated using a combination of atomic force microscopy (AFM), sodium dodecyl sulfate polyacrylamide gel electrophoresis (SDS-PAGE) and proteomics analysis.

Figure 3A and B show representative AFM images of ZW-L1 after 30 min of exposure to 80% human serum (HS). The NPs remained well dispersed and did not increase beyond about 12 nm in diameter. In contrast, PAA-USPIONs formed large aggregates (≈ 100 nm diameter) upon exposure to HS (Figure 3C and D).

The absence of significant protein corona formation for ZW-L1, ZW-L2, and ZW-L3 was further confirmed through SDS-PAGE analysis of adsorbed serum proteins (removed by denaturation and heating to 95°C with $2\times$ Laemmli sample buffer containing 2-mercaptoethanol). As shown in Figure 4A, only very faint protein bands were observed compared to those found for PAA-USPIONs exposed to 80% HS.

The identity of the NP-binding proteins was established using MS-based proteomics techniques. The relative quantification of the amounts of individual proteins within the coronas of the serum-exposed ZW-NPs versus that of the PAA-USPIONs was performed using isotope dimethyl labeling.^[15,43,44] This involved detachment of the adsorbed proteins using a denaturant containing 8 M urea, followed by reduction, digestion with trypsin, and labeling with non-deuterated (“light”) formalde-

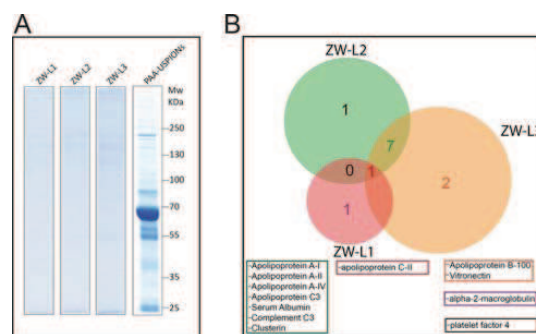


Figure 4. Analysis of HS proteins adsorbed by ZW-NPs and PAA-USPIONs. A) Coomassie-stained 12% SDS polyacrylamide gel of adsorbed proteins. B) Venn diagram of all proteins identified by proteomic analysis within the protein coronas of the HS-exposed ZW-NPs (refer to Tables S1–S4 for a detailed list of the proteins identified).

hyde in the case of the PAA-USPIONs and deuterated (“heavy”) formaldehyde in the case of the ZW-NPs. The labeled tryptic digests were then mixed in equal amounts for each combination of PAA-USPIONs/ZW-NPs and analyzed by LC–MS/MS in order to determine the identity and relative quantity of adsorbed proteins.^[15,44] Only two, nine and ten serum proteins were identified with a high degree of confidence in the coronas of ZW-L1, ZW-L2, and ZW-L3, respectively (Figure 4B). One of these proteins was common to all three protein coronas, and a further seven to the coronas of ZW-L2 and ZW-L3. The majority of the identified proteins were vastly enriched in the corona of the PAA-USPIONs relative to those of the ZW-NPs (Tables S1–S4 in the Supporting Information).

Collectively, these data suggest that the imidazolium-containing sulfobetaine derivative L1 is the most effective in reducing protein corona formation, and provide further evidence of the general ability of zwitterionic surfaces to limit formation of a protein corona and enhance the stability of NPs within biological fluids.^[3,4,8,27,37,45,46] Reduced protein adsorption in serum has previously been observed for Au NPs featuring zwitterionic sulfobetaine groups,^[11] and we have recently reported

the similar behavior of other zwitterionic polymer-coated US-PIONS.^[15]

Cellular uptake and cytotoxicity of nanoparticles

Next, we investigated the cellular uptake properties of the ZW-NPs. A431 cancer cells were exposed to ZW-NPs in serum-free media as well as cell media supplemented with 10% and 100% fetal bovine serum (FBS) for 24 h. This was followed by ICP-MS analysis to quantify the concentration of Fe arising from the magnetite core of the NPs (prior experiments performed in the absence of NPs confirmed that the cells were able to grow under all conditions examined). A control experiment without NPs was performed to quantify the endogenous

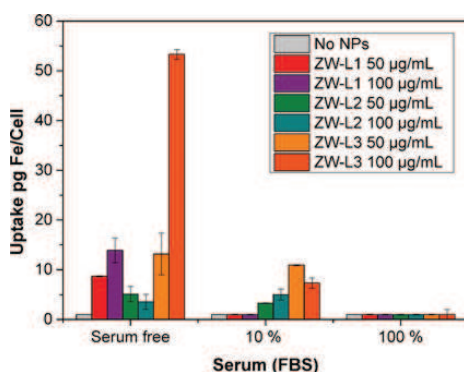


Figure 5. Degree of uptake of ZW-NPs into A431 cells in the absence or presence of 10% or 100% FBS. Cells were incubated with 50 or 100 $\mu\text{g mL}^{-1}$ of ZW-NPs for 24 h before digestion.

cellular iron concentration. As shown in Figure 5, low cellular uptake was observed for all three of the ZW-NPs, with values ranging from 1 to 10 pg Fe per cell.^[47] Furthermore, the uptake decreased with increasing serum concentration, that is, little uptake was detected in 100% FBS. In the presence of an excess of proteins, NPs that do not possess a protein corona have a lower probability of interacting with the cellular membrane, thus slowing down their endocytic uptake by the cell, which is concordant with our findings for other NPs.^[15,33] A notable observation is the approximately fivefold greater uptake of ZW-L3 versus ZW-L1 and ZW-L2, which is in accordance with the differing degrees of protein corona formation for these ZW-NPs.

We speculate that the lower protein adsorption and decreased cellular uptake of ZW-L1 is attributable to its higher surface hydrophilicity. The predicted distribution coefficient values at pH 7.4 please define $D_{7.4}$ ($\log D_{7.4}$) of -6.2 , -5.5 and -2.0 for amide derivatives of the zwitterionic headgroups L1, L2, and L3, respectively (calculated using the ACD Labs 2016 software program), suggest that ZW-L1 is more hydrophilic compared to ZW-L2 and ZW-L3. The results are in agreement with previous studies, in which greater NP-protein interactions and enhanced cellular uptake of NPs were observed with increasing surface hydrophobicity.^[11]

To assess cell viability following exposure to the ZW-NPs, the metabolic activities of both cancerous (A431) and non-cancerous cells (HEK293) cells were measured using a 3-(4,5-dimethylthiazol-2-yl)-5-(3-carboxymethoxyphenyl)-2-(4-sulfophenyl)-2H-tetrazolium (MTS) based cell proliferation assay (Figure 6A and B). In addition, membrane integrity was assessed as a measure of viability and necrosis by monitoring the NP-induced leakage of active lactate dehydrogenase (LDH) into the cell cul-

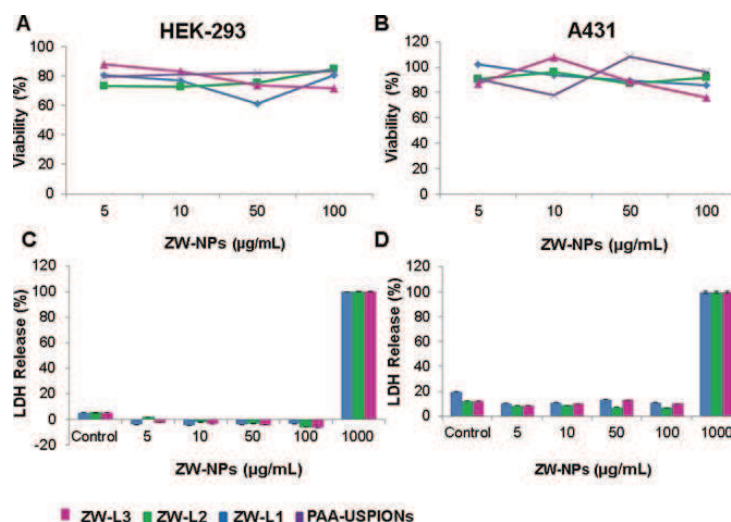


Figure 6. Nanotoxicity of ZW-NPs and PAA-USPIONS. A) and B) Viability of A431 and HEK293 cells measured after 24 h exposure to increasing concentrations of NPs, expressed as a percentage with respect to the negative control (cells without NPs). C) and D) LDH release from A431 and HEK293 cells measured after 24 h exposure to increasing concentrations of NPs. Cells were incubated with supplied lysis buffer to obtain maximum LDH release (positive control). All experiments were independently repeated three times, with triplicate determinations for each NP concentration.

8.4 Zwitterionic Modification of Ultrasmall Iron Oxide Nanoparticles for Reduced Protein Corona Formation (Paper)

ture media (Figure 6C and D). The ZW-NPs showed low and comparable cytotoxicity up to their highest dosed concentrations (100 ng mL^{-1}), indicating no major damage to the mitochondria (MTS assay) or lysis of the cell membrane upon incubation (LDH assay).

Generation of bimodal imaging agents

The availability of unreacted carboxylate functionalities prompted us to investigate the possibility of conjugating additional moieties to the surface of the ZW-NPs, thereby providing a facile route to bimodal or multimodal imaging agents. In the first instance, covalent attachment of a near-infrared fluorescent dye (Cy5) to ZW-L1 was investigated, with the aim of installing an optical imaging capability. Using conventional EDC/sulfo-NHS-mediated coupling conditions,^{15,33} an amine-bearing derivative of Cy5 was successfully linked to the NPs (Figure 7), as verified by UV/Vis absorption and photoluminescence spectroscopic measurements (Figure 8), performed following SEC

purification to remove low-molecular-weight material. The spectra displayed the characteristic absorption and emission bands of Cy5, with the I_{max} values (≈ 650 and 655 nm , respectively) slightly red-shifted relative to those of unincorporated Cy5 itself, as already reported for other dye-NP interfaces.⁴⁸ A fluorescence quantum yield of 0.18 was calculated, which is about two-thirds that of free Cy5,⁴⁹ presumably due to self-quenching effects or quenching by the iron oxide core of the NPs.

To generate a potential design for dual imaging by MRI and positron emission tomography (PET), a preformed ^{64}Cu complex ($[^{64}\text{Cu}]\text{Cu-dmptacn}$; dmptacn = 1,4-bis(2-pyridinylmethyl)-1,4,7-triazacyclononane)³³ was coupled to ZW-L2, also by using EDC/sulfo-NHS-mediated coupling (Figure 7). Radio-SEC was used to remove unreacted complex and confirm successful radiolabeling of the NPs (Figure 9A). The ^{64}Cu -labeled NPs were found to be resistant to metal ion leakage when challenged with EDTA for a 24 h period, as indicated by radio-TLC analysis (Figure 9B). It should be noted that a post-labeling

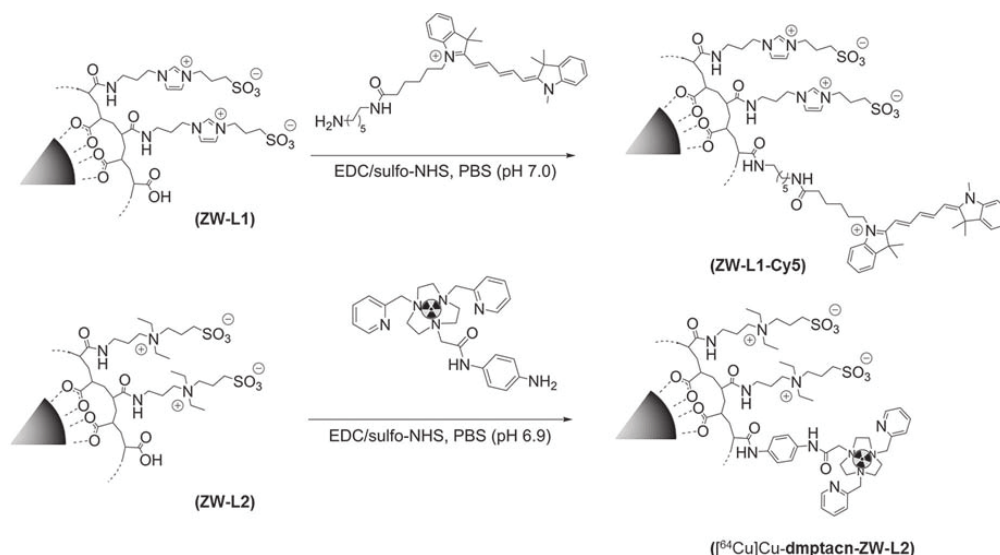


Figure 7. Conjugation of a near-IR fluorophore (Cy5) and a radiochelate ($[^{64}\text{Cu}]\text{Cu-dmptacn}$) to ZW-NPs to generate potential bimodal MRI/optical imaging and MRI/PET imaging agents.

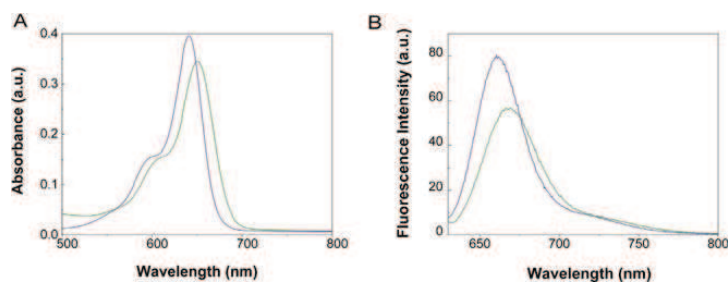


Figure 8. A) Electronic absorbance and B) emission spectra of Cy5-functionalized ZW-L1 (green) and free Cy5 (blue).

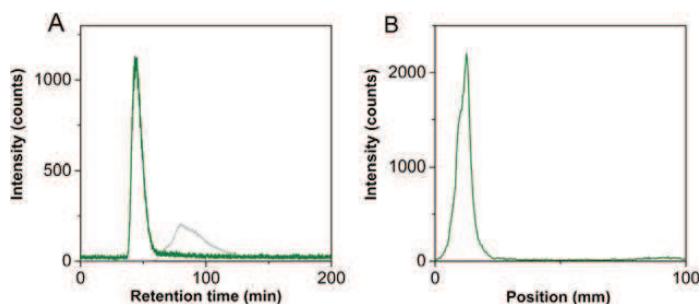


Figure 9. Analysis of $[^{64}\text{Cu}]\text{Cu}$ -dmptacn-labeled ZW-L2. A) Radio-SEC of $[^{64}\text{Cu}]\text{Cu}$ -dmptacn-labeled ZW-L2 (green) and $[^{64}\text{Cu}]\text{Cu}$ -dmptacn (gray). B) Radio-TLC of EDTA-challenged $[^{64}\text{Cu}]\text{Cu}$ -dmptacn-labeled ZW-L2 ($R_f = 0$ versus 0.8 for $[^{64}\text{Cu}]\text{Cu}$ -EDTA) recorded using a neutral Al_2O_3 stationary phase and a mobile phase of 2 M $\text{NH}_4\text{OAc}/\text{MeOH}$ (1:1, v/v).

strategy was also attempted, in which the dmptacn chelator was first attached to the NPs and then complexation of $^{64}\text{Cu}^{2+}$ ions was attempted. However, the results were not promising, with a very low radiochemical yield obtained.

Overall, these results clearly demonstrate that tethering additional groups to the ZW-NPs is feasible, despite them having a reduced number of carboxylate functionalities on their surface after zwitterionic modification.

Conclusion

The studies reported herein demonstrate that modifying the surface of PAA-USPIONS with sulfobetaines or 3-(diethylamino)propylamine is an effective strategy for limiting protein corona formation. AFM, SDS-PAGE and proteomics analysis all showed that adsorption of serum proteins was greatly reduced by imparting a degree of zwitterionic character to the NP surface. The ZW-NPs exhibit minimal cytotoxicity (A431 cells) and only low levels of cellular uptake (A431 and HEK293 cells). We have shown that a fluorophore and a radiochelate can be readily coupled to the NPs. Collectively, these results indicate that the ZW-NPs provide an attractive foundation for the development of stealth multimodal imaging and theranostic agents. Our future research will focus on investigating the *in vivo* behavior of the NPs, as well as the development of more sophisticated designs featuring a combination of bifunctional chelators, dye molecules, active targeting agents (e.g., peptides, antibodies) and/or therapeutic agents attached to the NP surface.

Experimental Section

Materials

All chemicals and solvents were purchased from reputable commercial suppliers and used as received without further purification. Compound L2 and the $[^{64}\text{Cu}]\text{Cu}$ -dmptacn radiochelate were synthesized by adapting the procedures described by Kim et al.^[50] and Pombo-Garcia et al.^[33] respectively. Ultrapure water with resistivity of 18 MWcm was obtained from an inline Millipore RiOs/Origin System (Millipore Corporation).

Instrumentation and methods

^1H and ^{13}C NMR spectra were recorded at 400.13 and 100.61 MHz, respectively, using a Bruker Avance III Nanobay 400 MHz spectrometer coupled to a BACS 60 automatic sample changer. Data acquisition and processing was managed using Topspin software package version 3. Additional processing was handled with MestReNova software (PC). Chemical shifts (δ) were measured in parts per million (ppm), referenced to an internal standard of residual solvent.^[51] Spectroscopic data are given using the following abbreviations: s, singlet; d, doublet; dd, doublet of doublets; dt, doublet of triplets; t, triplet; app p, apparent pentet; m, multiplet; J, coupling constant [Hz]. MS was performed using an Agilent 6100 Series Single Quad LC/MS instrument coupled to an Agilent 1200 Series HPLC system with the following mass spectrometer conditions: multi-mode ESI mode, 300°C drying gas temperature, 200°C vaporizing temperature, capillary voltage 2000 V (positive), capillary voltage of 4000 V (negative), scan range between m/z 100–1000 with an 0.1 s step size and a 10 min acquisition time. Absorbance spectra were recorded on a Varian Cary 50 Bio UV/Vis spectrophotometer. Fluorescence emission spectra were acquired using a Varian Cary Eclipse fluorescence spectrophotometer.

Synthesis of L1

N-(3-Phthalimidopropyl)imidazol(1): A mixture of imidazole (2.96 g, 44.8 mmol), N-(3-bromopropyl)phthalimide (4.00 g, 14.9 mmol) and K_2CO_3 (2.06 g, 14.9 mmol) in MeCN (30 mL) was heated at reflux for 17 h. The reaction mixture was allowed to cool to RT and filtered. The filtrate was evaporated and the remaining residue purified by flash chromatography ($\text{CHCl}_3/\text{MeOH}$, 9:1 v/v, on silica) to afford 1 as an off-white solid (1.81 g, 48%). ^1H NMR (400 MHz, CDCl_3): δ = 7.85–7.78 (m, 2H), 7.75–7.66 (m, 2H), 7.58 (s, 1H), 7.02 (s, 1H), 6.98 (t, $J = 1.2$ Hz, 1H), 4.00 (t, $J = 7.0$ Hz, 2H), 3.71 (t, $J = 6.6$ Hz, 2H), 3.44 (s, 1H), 2.17 ppm (app p, $J = 6.8$ Hz, 2H); ^{13}C NMR (101 MHz, CDCl_3): δ = 168.4, 137.2, 134.3, 131.9, 129.4, 123.5, 118.9, 50.5, 44.6, 35.2, 30.2 ppm; MS (ESI): m/z : calcd for $\text{C}_{14}\text{H}_{14}\text{N}_3\text{O}_2$: 256.11 [$M+H$] $^+$; found: 256.2.

1-(3-Phthalimidopropyl)-3-(3-sulfonatopropyl)imidazolium(2): Compound 1 (1.79 g, 7.03 mmol) and 1,3-propanesultone (0.944 g, 7.73 mmol) were added to anhydrous MeCN (40 mL) and the mixture was heated at reflux for 3 h. The reaction mixture was allowed to cool to RT, the formed precipitate was collected by filtration, washed with CHCl_3 and air-dried to afford 2 as a white solid (2.26 g, 85%). ^1H NMR (400 MHz, $[\text{D}_6]\text{DMSO}$): δ = 9.19–9.11 (m, 1H),

7.93–7.81 (m, 4H), 7.79 (dd, $J = 3.3, 1.6$ Hz, 2H), 4.29 (t, $J = 6.9$ Hz, 2H), 4.22 (t, $J = 7.3$ Hz, 2H), 3.61 (t, $J = 6.3$ Hz, 2H), 2.42 (t, $J = 7.1$ Hz, 2H), 2.17 (dt, $J = 13.5, 6.8$ Hz, 2H), 2.13–2.04 ppm (m, 2H); ^{13}C NMR (101 MHz, $[\text{D}_6]\text{DMSO}$): $\delta = 168.1, 136.4, 134.4, 131.9, 123.1, 122.5, 122.3, 47.9, 47.3, 46.6, 34.4, 28.5, 26.2$ ppm; MS (ESI): m/z : calcd for $\text{C}_{17}\text{H}_{20}\text{N}_3\text{O}_5\text{S}$: 378.11 $[\text{M}+\text{H}]^+$; found: 378.2.

1-(3-Aminopropyl)-3-(3-sulfonatopropyl)imidazolium trifluoroacetate (L1-TFA): $\text{N}_2\text{H}_4\cdot\text{H}_2\text{O}$ (2.88 mL) was added to a suspension of compound 2 (2.24 g, 5.94 mmol) in MeOH (50 mL) and the mixture was heated at reflux for 2 h, during which time a white precipitate formed. The reaction mixture was allowed to cool to RT and filtered. The filtrate was concentrated under reduced pressure and the resulting crude residue purified by reversed-phase chromatography (0.1% TFA in water on C_{18} silica) to obtain L1 as a yellow oil, isolated as a TFA salt (1.86 g, 86%). ^1H NMR (400 MHz, $[\text{D}_6]\text{DMSO}$): $\delta = 9.20$ (s, 1H), 7.81 (dt, $J = 20.1, 1.7$ Hz, 2H), 4.29 (dt, $J = 16.8, 6.9$ Hz, 4H), 2.85–2.76 (m, 2H), 2.46 (t, $J = 7.2$ Hz, 2H), 2.17–2.03 ppm (m, 4H); ^{13}C NMR (101 MHz, $[\text{D}_6]\text{DMSO}$): $\delta = 136.5, 122.8, 122.4, 47.9, 47.4, 46.0, 35.9, 27.7, 26.0$ ppm; MS (ESI): m/z : calcd for $\text{C}_9\text{H}_{18}\text{N}_3\text{O}_5\text{S}$: 248.11 $[\text{M}+\text{H}]^+$; found: 248.2.

General procedure for the synthesis of zwitterionic nanoparticles

Polyacrylic-acid-coated USPIOs were prepared using the co-precipitation method reported by Li and co-workers.^[39] For the coupling reactions, EDC (5.2 mg, 27 mmol) and sulfo-NHS (5.8 mg, 27 mmol) in 50 mm phosphate buffer (pH 6.0) were added to the PAA-USPIOs (5 mg). A solution (0.5 mL) of L1, L2, or L3 (13.5 mmol), note: DEAPA = L3, in 300 mm phosphate buffer (pH 7.5) was then added to the activated PAA-USPIOs. The pH of the mixture was adjusted to 7.5 by addition of phosphate buffer (300 mm, pH 7.5, 3 mL), and the reaction solution was stirred for 24 h at 37°C. After purification by size-exclusion chromatography (Sephadex G-25 fine, eluting with 100 mm phosphate buffer, pH 7.5) and subsequent filtration through a 0.2 μm membrane, ZW-L1, ZW-L2 and ZW-L3 were stored at 4°C until required. The concentrations of Fe were measured by inductively coupled plasma mass spectrometry (ICP-MS; ELAN 9000, PerkinElmer) and used to calculate the final concentrations of the NPs. The measurements were performed with an internal rhodium standard and a standard curve constructed using ICP standard solutions, for example, Fe in HNO_3 (0.5 M; Bernd Kraft GmbH, Duisburg, Germany).

Cy5-labeled ZW-L1 and ^{64}Cu -dmptacn-labeled ZW-L2 were prepared and characterized according to previously described methods.^[15,33]

Particle characterization techniques

TEM images of the NPs were recorded on a FEI Tecnai G2 T20 transmission electron microscope with an accelerating voltage of 200 kV and a lanthanum hexaboride (LaB_6) thermal emitter. Images were acquired with a Gatan Orius SC camera and edited using the Gatan Digital Micrograph program. Samples were prepared by dipping an ultrathin carbon-copper grid in a diluted solution of NPs in Milli-Q water. The HD of the NPs in the presence of NaCl (10 mM) was determined by DLS, and zeta potentials were determined by laser Doppler velocimetry (Zetasizer Nano ZS Malvern Instruments, Malvern, UK). Infrared spectra (4000–550 cm^{-1}) were recorded on solid samples of the NPs with a ThermoFisher Scientific (Waltham, MA) FTIR spectrometer using the attenuated total reflection

technique. Elemental analyses were performed on a EuroEA 3000 instrument from EuroVector (Milan, Italy).

Atomic force microscopy

AFM was performed using a Multimode 8 scanning probe microscope (Bruker) and PPP-NCLR cantilevers from Nanosensors (nominal force constant 48 N m^{-1} , tip radius < 10 nm). Images were processed using Gwyddion open source software. Samples were prepared by adding a stock solution of NPs (30 mg mL^{-1} , 20 mL) that had been incubated for 30 min at 37°C with water or HS to a freshly cleaved mica surface and air-drying before imaging.

Isolation of proteins from nanoparticles and SDS-PAGE

NP samples were incubated in HS at different concentrations for 30 min at 37°C. After incubation, serum-NP mixtures were centrifuged (20000 $\times g$, 4 h). In each case, the supernatant was carefully removed and the pellet washed four times with phosphate-buffered saline (PBS, pH 7.4, 1 mL) by suspension followed by pelleting and removal of the supernatant (a serum-only sample showed no sedimentation of free proteins under such conditions). Proteins were eluted from the NP surfaces by adding 2 \times Laemmli sample buffer (Bio-Rad) containing 2-mercaptoethanol (350 mM) to the final pellets and subsequent incubation at 95°C for 5 min. For SDS-PAGE analysis, recovered proteins in sample buffer (20 mL) were separated on a 4–12% SDS-PAGE gel (NuPAGE, Invitrogen). PageRuler Plus prestained protein ladder (Thermo Scientific) was used as a marker and 1 \times 3-(N-morpholino)propanesulfonic acid (MOPS; Invitrogen) as a running buffer. Gels were run at 120 V for 1.3 h and Coomassie staining (InstantBlue, Expedeon, San Diego, USA) was performed to visualize the bands.

Identification and relative quantification of proteins by dimethyl labeling

For the quantitative proteomics analysis, NPs were incubated in triplicate with 50% HS for 30 min at 37°C. Washing of the NPs was performed in the same way as described for the SDS-PAGE. Detachment of the bound proteins from the corona of the NPs was achieved using urea (8 M) in aqueous tetraethylammonium bromide (25 mM). The proteins were then reduced, alkylated and digested using sequencing-grade trypsin, and labeled with formaldehyde (CH_2O for PAA-USPIOs and CD_2O for either ZW-L1, ZW-L2, and ZW-L3) by following the protocol published by Boersema and co-workers.^[44] Finally, both labeled samples (for each single experiment) were mixed and analyzed by LC-MS/MS as described below.

Mass spectrometry and data analysis

Tryptic digests were analyzed by LC-MS/MS using an LTQ Orbitrap Elite instrument (Thermo Scientific) with a nanoelectrospray interface coupled to an Ultimate 300 RSLC nanosystem (Dionex). The nanoLC system was equipped with an Acclaim Pepmap Nanotrap column (Dionex C18, 100 \AA , 75 $\text{mm} \times 2$ cm) and an Acclaim Pepmap analytical column (Dionex C18, 2 mm, 100 \AA , 75 $\text{mm} \times 15$ cm). An aliquot of the digestion mix (2 mL) was loaded onto the trap column with an isocratic flow of 4 mL min^{-1} of 3% CH_3CN containing 0.1% formic acid for 5 min before the enrichment column was switched in-line with the analytical column. The eluents used for the liquid chromatography were 0.1% (v/v) formic acid (solvent A) and 100% $\text{CH}_3\text{CN}/0.1\%$ formic acid (v/v) (solvent B). The following gradient

was used: 3–12% B for 1 min, 12–35% B for 20 min, 35–80% B for 2 min, and then constant 80% B for 2 min, followed by equilibration at 3% B for 7 min before the next sample injection. The mass spectrometer was operated in the data-dependent mode with a nano-ESI spray voltage of +2.0 kV, a capillary temperature of 250°C, and an S-lens RF value of 60%. Spectra were acquired first in positive-ion mode with a full scan, scanning from *m/z* 300 to 1650 in the FT mode at 240 000 resolution, followed by collision-induced dissociation in the linear ion trap with the 10 most intense peptide ions with charge states ≥ 2 isolated and fragmented using a normalized collision energy of 35 and an activation Q value of 0.25.

Data analysis was performed using Proteome Discoverer (Thermo Scientific, version 1.4) with Mascot search engine (Matrix Science version 2.4) against the Uniprot database of the human genome. The search parameters included a precursor mass tolerance of 20 ppm, a fragment mass tolerance of 0.6 Da, carbamidomethylation of cysteine as a fixed modification, and dimethyl labeling (CH_2O , +28.031 Da; CD_2O , +32.056 Da) at the peptide N terminus and lysine set as variable modifications. Trypsin was used as the cleavage enzyme, with no missed cleavages. Search results were set to a maximum of 1% false discovery rate and at least two unique peptides required for positive identification.^[23] Quantification of the dimethyl-labeled peptides was conducted using the Quant node on Proteome Discoverer, which works by extracting and comparing the areas corresponding to the light and heavy labeled peptides. To add further confidence, proteins were filtered against the human plasma proteome database.^[52]

Cell culture

Cell culture flasks, dishes and plates (CELLSTAR) were supplied by Greiner Bio-One GmbH (Frickenhausen, Germany). The epidermoid human cancer cell line A431 (ATCC number: CRL-1555) and the human embryonic kidney cell line HEK293 (DMSZ number: ACC 305) were cultured as previously reported.^[15,53] All cell lines were confirmed to be mycoplasma-free using the LookOut mycoplasma PCR detection kit (Sigma-Aldrich) and were tested monthly.

Quantification of uptake by A431 cells

A total of 200 000 A431 cells per well in 12-well plates (CELLSTAR, Greiner Bio-One GmbH) were cultivated for 24 h before exposure to NPs. After 24 h, media was replaced with NP dispersions (final concentration of 100 ng mL^{-1}), freshly prepared by diluting NP stocks in serum-free Dulbecco's modified Eagle's medium (DMEM), or DMEM supplemented with different concentrations of FBS. Following exposure to NPs for a period of 24 h, cells were washed three times with PBS in order to ensure removal of loosely attached NPs from the cell membrane. To determine cell numbers, cells were harvested by trypsinization and counted using a CASY cell counter (Roche Diagnostics) according to the manufacturer's protocol. To measure the cellular iron content by ICP-MS, cells were lysed by adding 0.1% NaOH (500 μL), dissolved by adding 65% HNO_3 (100 μL) and finally diluted to 2 mL with distilled H_2O prior to analysis. The iron content was expressed in picograms per cell. Cells without NP treatment served as controls for calculations.

In vitro assessment of nanotoxicity

To assess cell viability following NP exposure, the A431 and HEK293 cells were seeded in 96-well plates at a density of 40 000

and 60 000 cells per 0.1 mL per well, respectively, and grown for 24 h prior to addition of NPs, which were freshly diluted to different final concentrations (0, 5, 10, 50, 100, 1000 ng mL^{-1}) in DMEM supplemented with 10% FBS. After 24 h incubation, the CellTiter 96 Aqueous One Solution cell proliferation assay (Promega) and CytoScan LDH cytotoxicity assay (G-Biosciences, St. Louis, USA/MO) were performed according to the manufacturer's instructions. For the latter assay, a triplicate set of wells was incubated with the supplied lysis buffer to obtain a maximum LDH release (positive control). NP-dependent LDH release was calculated relative to this value. In the proliferation assay, a triplicate set of wells containing untreated cells served as a negative control. Cell viability upon NP exposure was expressed as a percentage relative to this negative control. All experiments were performed three times.

Acknowledgements

We acknowledge use of facilities within the Monash Centre for Electron Microscopy. We also thank Dr. Avinash Patel for support with protein-based techniques, Bezu Teschome for instrumental help with AFM, Stephan Weiss for support with zeta potential measurements, Utta Herzog for technical support during the cell culture work, and Karin Landrock for the elemental analyses. KPG also thanks the Max Planck Institute of Molecular Cell Biology and Genetics for providing office space. This study was supported by the Helmholtz Initiative and Networking Fund (Functional Nanomaterials for Multimodality Cancer Imaging (NanoTracking), project ID: VH-VI-421), the Australian Research Council through a Future Fellowship to B.G. (FT130100838), a Discovery Outstanding Researcher Award and Discovery Grant to L.S. (DP130100816), and by an Alexander von Humboldt Foundation research fellowship to T.J. This article is dedicated to the memory of our friend, colleague and mentor, Prof. Leone Spiccia, who passed away on the 18th December 2016.

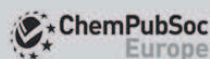
Conflict of interest

The authors declare no conflict of interest.

Keywords: iron oxide nanoparticles · multimodal imaging · protein corona · proteomics · zwitterions

- [1] K. Pombo García, K. Zarschler, L. Barbaro, J. A. Barreto, W. O'Malley, L. Spiccia, H. Stephan, B. Graham, *Small* 2014, 10, 2516–2529.
- [2] K. Zarschler, L. Rocks, N. Licciardello, L. Boselli, E. Polo, K. P. Garcia, L. De Cola, H. Stephan, K. A. Dawson, *Nanomed. Nanotech. Biol. Med* 2016, 12, 1663–1701.
- [3] B. Pelaz, G. Charron, C. Pfeiffer, Y. Zhao, J. M. de la Fuente, X. J. Liang, W. J. Parak, P. Del Pino, *Small* 2013, 9, 1573–1584.
- [4] C. D. Walkey, W. C. Chan, *Chem. Soc. Rev.* 2012, 41, 2780–2799.
- [5] J. Feng, H. Liu, K. K. Bhakoo, L. Lu, Z. Chen, *Biomaterials* 2011, 32, 6558–6569.
- [6] R. R. Arvizo, O. R. Miranda, D. F. Moyano, C. A. Walden, K. Giri, R. Bhattacharya, J. D. Robertson, V. M. Rotello, J. M. Reid, P. Mukherjee, *PLoS One* 2011, 6, e24374.
- [7] S. T. Kim, K. Saha, C. Kim, V. M. Rotello, *Acc. Chem. Res.* 2013, 46, 681–691.
- [8] D. F. Moyano, M. Goldsmith, D. J. Solfield, D. Landesman-Milo, O. R. Miranda, D. Peer, V. M. Rotello, *J. Am. Chem. Soc.* 2012, 134, 3965–3967.
- [9] A. Lesniak, F. Fenaroli, M. R. Monopoli, C. Aberg, K. A. Dawson, A. Salvati, *ACS Nano* 2012, 6, 5845–5857.

8.4 Zwitterionic Modification of Ultrasmall Iron Oxide Nanoparticles for Reduced Protein Corona Formation (Paper)



- [10] A. Jedlovsky-Hajdú, F. B. Bombelli, M. P. Monopoli, E. Tombácz, K. A. Dawson, *Langmuir* 2012, 28, 14983–14991.
- [11] D. F. Moyano, K. Saha, G. Prakash, B. Yan, H. Kong, M. Yazdani, V. M. Rotello, *ACS Nano* 2014, 8, 6748–6755.
- [12] K. Saha, D. F. Moyano, V. M. Rotello, *Mater. Horiz.* 2014, 1, 102–105.
- [13] C. C. Fleischer, U. Kumar, C. K. Payne, *Biomater. Sci.* 2013, 1, 975–982.
- [14] C. C. Fleischer, C. K. Payne, *Acc. Chem. Res.* 2014, 47, 2651–2659.
- [15] K. Pombo-García, S. Weiss, K. Zarschler, C.-S. Ang, R. Hübner, J. Pufe, S. Meister, J. Seidel, J. Pietzsch, L. Spiccia, H. Stephan, B. Graham, *ChemNanoMat* 2016, 2, 959–971.
- [16] U. Sakulkhu, M. Mahmoudi, L. Maurizi, J. Salaklang, H. Hofmann, *Sci. Rep.* 2014, 4, 5020.
- [17] Z. Estephan, P. Schlenoff, J. Schlenoff, *Langmuir* 2011, 27, 6794–6800.
- [18] S. Mondini, M. Leonzino, C. Drago, A. M. Ferretti, S. Usseglio, D. Maggioni, P. Tornese, B. Chini, A. Ponti, *Langmuir* 2015, 31, 7381–7390.
- [19] D. Kim, M. K. Chae, H. J. Joo, I.-H. Jeong, J.-H. Cho, C. Lee, *Langmuir* 2012, 28, 9634–9639.
- [20] Z. Zhou, H. Liu, X. Chi, J. Chen, L. Wang, C. Sun, Z. Chen, J. Gao, *ACS Appl. Mater. Interfaces* 2015, 7, 28286–28293.
- [21] W. Xiao, J. Lin, M. Li, Y. Ma, Y. Chen, C. Zhang, D. Li, H. Gu, *Contrast Media Mol. Imaging* 2012, 7, 320–327.
- [22] M. P. Monopoli, D. Walczyk, A. Campbell, G. Elia, I. Lynch, F. B. Bombelli, K. A. Dawson, *J. Am. Chem. Soc.* 2011, 133, 2525–2534.
- [23] Y. Yan, K. T. Gause, M. M. J. Kamphuis, C.-S. Ang, N. M. O'Brien-Simpson, J. C. Lenzo, E. C. Reynolds, E. C. Nice, F. Caruso, *ACS Nano* 2013, 7, 10960–10970.
- [24] J. Liu, M. Yu, X. Ning, C. Zhou, S. Yang, J. Zheng, *Angew. Chem. Int. Ed.* 2013, 52, 12572–12576; *Angew. Chem.* 2013, 125, 12804–12808.
- [25] D. E. Owens, III, N. A. Peppas, *Int. J. Pharm.* 2006, 307, 93–102.
- [26] K. Susumu, E. Oh, J. B. Delehanty, J. B. Blanco-Canosa, B. J. Johnson, V. Jain, W. J. Hervey IV, W. R. Algar, K. Boeneman, P. E. Dawson, I. L. Medintz, *J. Am. Chem. Soc.* 2011, 133, 9480–9496.
- [27] S. Ashraf, J. Park, M. A. Bichelberger, K. Kantner, R. Hartmann, P. Maffre, A. H. Said, N. Feliu, J. Lee, D. Lee, G. U. Nienhaus, S. Kim, W. J. Parak, *Nanoscale* 2016, 8, 17794–17800.
- [28] Q. Dai, C. Walkey, W. C. Chan, *Angew. Chem. Int. Ed.* 2014, 53, 5093–5096; *Angew. Chem.* 2014, 126, 5193–5196.
- [29] K. Knop, R. Hoogenboom, D. Fischer, U. S. Schubert, *Angew. Chem. Int. Ed.* 2010, 49, 6288–6308; *Angew. Chem.* 2010, 122, 6430–6452.
- [30] J. S. Gebauer, M. Malissek, S. Simon, S. K. Knauer, M. Maskos, R. H. Stauber, W. Peukert, L. Treuel, *Langmuir* 2012, 28, 9673–9679.
- [31] E. L. Foster, Z. Xue, C. M. Roach, E. S. Larsen, C. W. Bielawski, K. P. Johnston, *ACS Macro Lett.* 2014, 3, 867–871.
- [32] H. Wei, O. T. Bruns, O. Chen, M. G. Bawendi, *Integr. Biol.* 2013, 5, 108–114.
- [33] K. Pombo-García, K. Zarschler, J. A. Barreto, J. Hesse, L. Spiccia, B. Graham, H. Stephan, *RSC Adv.* 2013, 3, 22443–22454.
- [34] D. Docter, U. Distler, W. Storch, J. Kuharev, D. Wunsch, A. Hahlbrock, S. K. Knauer, S. Tenzer, R. H. Stauber, *Nat. Protoc.* 2014, 9, 2030–2044.
- [35] C. C. Fleischer, C. K. Payne, *J. Phys. Chem. B* 2014, 118, 14017–14026.
- [36] W. Liu, J. Rose, S. Plantevin, M. Auffan, J. Y. Bottero, C. Vidaud, *Nanoscale* 2013, 5, 1658–1668.
- [37] M. P. Monopoli, C. Aberg, A. Salvati, K. A. Dawson, *Nat. Nanotechnol.* 2012, 7, 779–786.
- [38] S. Tenzer, D. Docter, J. Kuharev, A. Musyanovych, V. Fetz, R. Hecht, F. Schlenk, D. Fischer, K. Kiouptsi, C. Reinhardt, K. Landfester, H. Schild, M. Maskos, S. K. Knauer, R. H. Stauber, *Nat. Nanotechnol.* 2013, 8, 772–U1000.
- [39] Z. Li, B. Tan, M. Allix, A. I. Cooper, M. J. Rosseinsky, *Small* 2008, 4, 231–239.
- [40] Y. Chang, S. Chen, Q. Yu, Z. Zhang, M. Bernards, S. Jiang, *Biomacromolecules* 2007, 8, 122–127.
- [41] R. Hu, G. Li, Y. Jiang, Y. Zhang, J. J. Zou, L. Wang, X. Zhang, *Langmuir* 2013, 29, 3773–3779.
- [42] C. J. Huang, Y. Li, S. Jiang, *Anal. Chem.* 2012, 84, 3440–3445.
- [43] Q. Dai, Y. Yan, C. S. Ang, K. Kempe, M. M. Kamphuis, S. J. Dodds, F. Caruso, *ACS Nano* 2015, 9, 2876–2885.
- [44] P. J. Boersema, R. Rajmakers, S. Lemeer, S. Mohammed, A. J. R. Heck, *Nat. Protoc.* 2009, 4, 484–494.
- [45] S. R. Saptarshi, A. Duschl, A. L. Lopata, *J. Nanobiotechnol.* 2013, 11, 26.
- [46] J. Wang, U. B. Jensen, G. V. Jensen, S. Shipovskov, V. S. Balakrishnan, D. Otzen, J. S. Pedersen, F. Besenbacher, D. S. Sutherland, *Nano Lett.* 2011, 11, 4985–4991.
- [47] High levels of cellular uptake of PAA-USPIONS have been previously reported by Gu and co-workers (Ref. [21]). Similar to this, we have also recently reported that USPIONS featuring a carboxylate coating (OPA-USPIONS) show significantly higher levels of cellular uptake relative to zwitterion-coated particles (Ref. [15]).
- [48] E. Dulkeith, M. Ringler, T. A. Klar, J. Feldmann, A. Munoz Javier, W. J. Parak, *Nano Lett.* 2005, 5, 585–589.
- [49] R. B. Mujumdar, L. A. Ernst, S. R. Mujumdar, C. J. Lewis, A. S. Waggoner, *Bioconjugate Chem.* 1993, 4, 105–111.
- [50] G. Kim, C. E. Yoo, M. Kim, H. J. Kang, D. Park, M. Lee, N. Huh, *Bioconjugate Chem.* 2012, 23, 2114–2120.
- [51] G. R. Fulmer, A. J. M. Miller, N. H. Sherden, H. E. Gottlieb, A. Nudelman, B. M. Stoltz, J. E. Bercaw, K. I. Goldberg, *Organometallics* 2010, 29, 2176–2179.
- [52] V. Nanjappa, J. K. Thomas, A. Marimuthu, B. Muthusamy, A. Radhakrishnan, R. Sharma, A. Ahmad Khan, L. Balakrishnan, N. A. Sahasrabudde, S. Kumar, B. N. Jhaveri, K. V. Sheth, R. Kumar Khatana, P. G. Shaw, S. M. Srikanth, P. P. Mathur, S. Shankar, D. Nagaraja, R. Christopher, S. Mathivanan, R. Raju, R. Sirdeshmukh, A. Chatterjee, R. J. Simpson, H. C. Harsha, A. Pandey, T. S. Prasad, *Nucleic Acids Res.* 2014, 42, D959–D965.
- [53] K. Zarschler, K. Prapainop, E. Mahon, L. Rocks, M. Bramini, P. M. Kelly, H. Stephan, K. A. Dawson, *Nanoscale* 2014, 6, 6046–6056.

Manuscript received: February 1, 2017
Accepted Article published: March 6, 2017
Final Article published: March 27, 2017

8.5

Curriculum Vitae

Name: Raymond Lam
Nationality: Australian
ORCID no.: 0000-0001-6234-2792

Education

Mar 2014 – Mar 2018 PhD in Medicinal Chemistry at the Monash Institute of Pharmaceutical Sciences, Monash University
Monash-Nottingham Joint Doctoral Training Program
Jan 2013 – Dec 2013 Honours in Bachelor in Pharmaceutical Sciences (Medicinal Chemistry)
Mar 2010 – Dec 2012 Bachelor in Pharmaceutical Sciences (Medicinal Chemistry)
Feb 2006 – Dec 2009 Melbourne High School, ATAR: 96.25

Industrial Experience

Jan 2018 – Feb 2018 Sun Pharmaceutical Industries Ltd.
Safety modification and scale-up of a process for the synthesis of an alkaloid derivative.

Theses

Apr 2018 Design and Synthesis of Fluorescent Opioids for Bioimaging (PhD)
Dec 2013 Fragment-Based Drug Discovery Against the Malarial Surface Antigen AMA1 (Hons.)

Awards and Scholarships

2014 - 2018 Australian Research Training Scheme
2012 Summer Research Scholarship
2011 Summer Research Scholarship

Papers

Lam, R.; Gondin, A. B.; Canals, M.; Kellam, B.; Briddon, S. J.; Graham, B.; Scammells, P. J. Fluorescently Labelled Morphine Derivatives for Bioimaging Studies. *J. Med. Chem.* **2018**, *61* (3), 1316–1329.

Awalt, J. K. and Lam, R.; Kellam, B.; Graham, B.; Scammells, P. J.; Singer, R. D. Utility of Iron Nanoparticles and a Solution-Phase Iron Species for the N-Demethylation of Alkaloids. *Green Chem.* **2017**, *19* (11), 2587–2594.

Pombo-García, K. and Rühl, C. L.; Lam, R.; Barreto, J. A.; Ang, C. S.; Scammells, P. J.; Comba, P.; Spiccia†, L.; Graham, B.; Joshi, T.; Stephan, H. Zwitterionic Modification of Ultrasmall Iron Oxide Nanoparticles for Reduced Protein Corona Formation. *Chempluschem* **2017**, *82* (4), 638–646.

Krishnarajuna, B.; Lim, S. S.; Devine, S. M.; Debono, C. O.; Lam, R.; Chandrashekar, I. R.; Jaipuria, G.; Yagi, H.; Atreya, H. S.; Scanlon, M. J.; MacRaild, C. A.; Scammells, P. J.; Norton, R. S. Solution NMR Characterization of Apical Membrane Antigen 1 and Small Molecule Interactions as a Basis for Designing New Antimalarials. *J. Mol. Recognit.* **2016**, *29* (6), 281–291.

Devine, S. M.; Lim, S. S.; Chandrashekar, I. R.; MacRaild, C. A.; Drew, D. R.; Debono, C. O.; Lam, R.; Anders, R. F.; Beeson, J. G.; Scanlon, M. J.; Scammells, P. J.; Norton, R. S. A Critical Evaluation of pyrrolo[2,3-D]pyrimidine-4-Amines as Plasmodium Falciparum Apical Membrane Antigen 1 (AMA1) Inhibitors. *Med. Chem. Commun.* **2014**, *5*, 1500–1506.

Conferences and Symposiums

Oct 2017	Annual Postgraduate Research Symposium (Monash Institute of Pharmaceutical Sciences, Australia), Oral communication
July 2017	Royal Australian Chemical Institute Centenary Congress (Melbourne, Australia), Poster
Aug 2016	European Federation of Medicinal Chemistry - International Symposium on Medicinal Chemistry (Manchester, U.K.), Poster
July 2016	International Narcotics Research Conference (Bath, U.K.), Poster
June 2016	Centre for Biomolecular Sciences Researcher Symposium (Nottingham, U.K.), Oral communication

Society Membership

2015 – Present	Royal Society of Chemistry
----------------	----------------------------

Technical

Synthesis	Organic chemistry, nanoparticle synthesis and functionalization
Analytics	NMR, LCMS, HPLC, TLC, prep-TLC, IR, Optical rotation
Computer	MS Office (Word, Powerpoint, Excel, Publisher, Project), LaTeX, Adobe Suite (Illustrator, Photoshop)

Teaching

Mar 2014 – Nov 2017	Teaching Associate, Monash University (Practicals and tutorials, 1 st to 3 rd year) Units PSC1021 Organic Chemistry I PSC1022 Organic Chemistry II PSC2171 Basis of Drug Action I PSC2021 Structural Organic Chemistry PSC2132 Introduction to Spectroscopy PSC3121 Synthetic Medicinal Chemistry
Jan 2011 – Mar 2013	NQT Education, tutor for years 4 – 12

Other Activities

2013	Music @ Parkville Events organizer
2012	Music @ Parkville Vice-President
2011	Music @ Parkville President
Feb 2007 – Dec 2009	Melbourne High School Debating team